



**DEVELOPMENT OF A REAL-TIME TESTBED FOR RENEWABLE ENERGY INTEGRATION STUDIES**

**by**

**GIDEON DANIEL JOUBERT** Student no. 212274872

**Thesis submitted in fulfilment of the requirements for the degree**

**Doctor of Engineering in Electrical Engineering**

**in the Faculty of Engineering and the Built Environment**

**at the Cape Peninsula University of Technology**

**Supervisor: Prof. Atanda Raji**

**Bellville Campus**

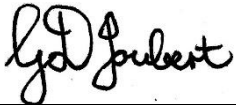
**October 2022**

**CPUT copyright information**

The dissertation/thesis may not be published either in part (in scholarly, scientific or technical journals), or as a whole (as a monograph), unless permission has been obtained from the University

## DECLARATION

I, Gideon Daniel Joubert, declare that the contents of this dissertation represent my own unaided work, and that the dissertation has not previously been submitted for academic examination towards any qualification. Furthermore, it represents my own opinions and not necessarily those of the Cape Peninsula University of Technology.



---

Signed G.D. Joubert

02/10/2022

---

Date

## ABSTRACT

Joining the global energy movement, South Africa has, in recent, years seen a steady increase in the number of grid-connected renewables. This follows an interest to include renewable energy in its generation mix as early as 1998, supported by initiatives such as the updated 2030 IRP (Integrated Resource Plan) today. South Africa's electrical energy demand is, however, still predominantly supplied by coal, which the 2030 IRP plans to change through a significant increase in the amount of grid-connected renewables, to the extent where renewable generation is set to almost match that of coal by 2030. Such a shift from synchronous inertia-providing fossil-fuel generation, to largely asynchronously natured renewables, is bound to bring about significant changes to South Africa's electrical grid, and consequently, new challenges given South Africa's still-limited renewable-generation experience. These challenges largely relate to grid stability and supply reliability concerns, noted by studies of countries with similar renewable-integration goals. It is often also observed that these effects tend to be more prominent for weaker grids, raising concerns over the effect South Africa's planned renewable integration could have, given the ongoing struggle to supply the current electrical demand reliably. Perspective is, however, provided by the motivation behind South Africa's integration goals which, contrary to displacing fossil-fuel generation, is intended in South Africa as a means of adding much-needed grid-connected generation capacity. This places immense pressure on the success of South Africa's renewable-generation integration goals, necessitating comprehensive integration studies to determine grid-connected RPP (Renewable Power Plant) behaviour if this desired outcome is to be achieved.

From what is known, no tailored South African simulation tools promoting RPP grid-integration behavioural studies yet existed for South Africa. The aim of the research is therefore to develop a tailored South African real-time RPP grid-integration behavioural studies testbed, promoting the necessary renewable-integration studies needed in support of the successful integration of South Africa's renewable-integration goals.

This work follows the development of the real-time testbed, which first sees the implementation of a MATLAB live script to select RPP grid-code requirements, according to which simulated RPPs are operated. MATLAB Simulink is then used to develop the testbed's main circuit sections, which incorporate a means of importing external grid data to allow simplified recreation of test conditions. The testbed furthermore includes a voltage- and frequency-validation subsystem, responsible for active grid-code compliance monitoring and RPP control, allowing the strains imposed by grid-code requirements on RPPs to be studied. The MATLAB-developed testbed is then integrated

with RT-LAB of OPAL-RT, adhering to the necessary real-time execution requirements, allowing the model to be simulated in real-time.

To assess the accuracy and success of the developed testbed, while showing its worth as an RPP grid-integration behavioural studies tool, a testing procedure was developed involving high- and low-voltage and frequency, short-circuit, and real-world data simulations, operating the test RPP within its continuous, fault ride-through, and trip regions of operation. Results produced support the selected simulation data-import method as an effective and efficient means of replaying and recreating simulation conditions. Results furthermore support the testbed's ability to assess and track POC conditions effectively, operating the RPP in line with voltage- and frequency grid-code requirements. Finally, results support the testbed's design as an effective tool for assessing RPP response and behaviour in line with grid-code requirements, allowing the support abilities of the RPP, its limitations, and grid-code-imposed strains to become apparent. Then, through the design and testing of the developed testbed, the research achieved its goal of developing a real-time tailored South African RPP grid-integration behavioural studies tool, in support of the renewable grid-integration studies needed for the successful integration of South Africa's renewable-integration goals.

## **ACKNOWLEDGMENTS**

### **I wish to thank:**

- My supervisor and mentor, Prof. Atanda Raji, at the Cape Peninsula University of Technology for always being available and for the encouragement and support throughout this thesis
- My family members and friends for their support
- The Cape Peninsula University of Technology for the use of their facilities and OPAL-RT real-time simulator
- My editor Ms. Woods for editing of this document
- My Lord and Saviour, Jesus Christ

# TABLE OF CONTENTS

Declaration .....	ii
Abstract .....	iii
Acknowledgments .....	v
List of Tables .....	ix
List of Figures .....	xi
Acronyms and Abbreviations .....	xiv
Chapter One .....	1
General concept of the study .....	1
1.1 Background and introduction .....	1
1.2 Problem statement .....	1
1.3 Research objectives .....	3
1.4 Research methodology .....	3
1.5 Delineation of the study .....	5
1.6 Study limitations .....	5
1.7 Literature study .....	5
1.8 Modelling and simulation .....	6
1.9 Thesis outline .....	7
Chapter Two .....	9
Literature review .....	9
2.1 Introduction .....	9
2.2 State of renewable integration in South Africa .....	9
2.3 Grid strength and renewable suitability studies .....	10
2.4 Renewable suitability studies in South Africa .....	15
2.5 Grid codes (General) .....	19
2.6 South African grid-code requirements for renewable power plants .....	26
2.6.1 Normal operating conditions .....	26
2.6.2 Abnormal operating conditions .....	27
2.6.3 Reactive power requirements .....	29
2.6.4 Reactive power and voltage control requirements .....	30
2.6.5 Power quality and protection requirements .....	30
2.6.6 Active power constraint requirements .....	31
2.6.7 RPP control requirements .....	32

2.6.8 RPP data and control signal requirements.....	33
2.6.9 Signal and data requirements from RPPs to SO.....	33
2.6.10 Signal and data requirements from so to RPPs.....	36
2.6.11 Communication specifications and requirements .....	37
2.7 Faults and disturbances on South Africa’s electrical network: .....	37
2.8 South Africa’s grid infrastructure .....	38
2.9 South Africa’s energy future .....	42
2.10 Cost of renewables in South Africa .....	43
2.11 Maximum renewable penetration and simulation of fault conditions on the Indian grid .....	44
2.12 Wind turbine background .....	47
2.13 Solar technology.....	51
2.14 OPAL-RT real-time simulator.....	53
2.15 Summary .....	60
Chapter Three .....	61
Literature analysis and testbed development theory.....	61
3.1 Introduction.....	61
3.2 South Africa’s current and future generation mix: .....	61
3.3 South African renewable grid-code requirements summary.....	65
3.3.1 Voltage requirements set for RPPs in South Africa.....	65
3.4.1 Reactive power requirements set for RPPs in South Africa .....	70
3.4.2 Frequency response requirements set for RPPs in South Africa.....	74
3.4.3 Grid-code compliance and testing procedures .....	76
3.4.4 RPP testing specifications for South Africa .....	78
3.5 Analysing the effects of the changing generation mix on the South African grid .....	82
3.6 Test wind turbine .....	85
3.7 Summary: .....	88
Chapter Four .....	90
Research results/Deliverables.....	90
4.1 Introduction.....	90
4.2 Development of the MATLAB live script .....	90
4.3 MATLAB circuit setup for real-time simulation.....	93
4.4 SM_Target subsystem .....	94
4.4.1 Data imports.....	95
4.4.2 Circuit components .....	96

4.4.3 Grid-code validation subsystems .....	98
4.4.4 Wind turbine data acquisition subsystem.....	105
4.5 SC_Local subsystem .....	107
4.5.1 Measurements and outputs.....	107
4.6 Experimental setup .....	109
4.7 Testing strategy .....	110
4.7.1 High-and low-voltage ride-through tests.....	110
4.7.2 High-and low-frequency ride-through tests.....	111
4.7.3 Short-circuit tests .....	111
4.7.4 Real-world data tests .....	112
4.8 Summary .....	112
Chapter Five .....	114
Case studies.....	114
5.1 Introduction.....	114
5.2 Voltage subsystem validation studies.....	114
5.2.1 Case study 1 .....	115
5.2.2 Case study 2 .....	118
5.2.3 Case study 3 .....	121
5.3 Frequency subsystem validation studies .....	127
5.3.1 Case study 4 .....	127
5.3.2 Case study 5 .....	130
5.3.3 Case study 6 .....	132
5.4 Short-circuit studies .....	136
5.4.1 Case study 7 .....	138
5.5 Real-world event data studies.....	143
5.5.1 Case study 8 .....	143
5.5.2 Case study 9 .....	147
5.6 Summary .....	150
Chapter Six .....	151
Analysis and summary of results.....	151
6.1 Introduction.....	151
6.2 Research findings summary .....	151
6.3 How this study compares to existing work .....	155
6.4 Simulation results analysis and findings.....	157



6.5 Voltage case studies .....	157
6.5.1 Frequency case studies .....	162
6.5.2 Short-circuit case study .....	165
6.5.3 Real-world data case studies.....	169
6.6 Simulation summary .....	172
6.7 Summary .....	174
Chapter Seven .....	175
Conclusion .....	175
1.1 Introduction.....	175
7.3 Study contributions.....	177
7.4 Limitations of the study .....	177
7.5 Recommendations for future work.....	177
7.6 Closing summary .....	178
References.....	179
Appendices.....	186
Appendix A: Grid-code frequency requirements .....	186
Appendix B: Grid-code voltage requirements.....	187
Appendix C: Grid-code power requirements .....	190
Appendix D: Grid-code reactive power requirements .....	192
Appendix E: Grid-code reactive power control requirements .....	195
Appendix F: South African electrical grid map .....	196
Appendix G: MATLAB Live script code .....	197
Appendix H: Editing Certificate .....	199

## LIST OF TABLES

Table 2.1: Normal operating range for category B and C RPPs in South Africa .....	26
Table 2.2: RPP control requirements .....	33
Table 2.3: Eskom-owned and operated power plants .....	39
Table 2.4: Share of renewables connected to the South African grid .....	41
Table 3.1: Category A1 and A2 RPP disconnect times .....	66
Table 3.2: Default frequency values set for frequency support requirements.....	75
Table 3.3: Grid assessment data .....	82
Table 3.4: Siemens SWT-2.3-108 key specifications .....	86
Table 4.1: 20% POC voltage short-circuit example sheet .....	112

Table 5.1: Case study 7: 20% short-circuit test data .....	138
Table 5.2: Case study 7: 30% short-circuit test data .....	139
Table 5.3: Case study 7: 50% short-circuit test data .....	141
Table 5.4: Case study 7: 80% short-circuit test data .....	142
Table 6.1: Summary of comparable studies .....	155
Table 6.2: Case study 1: simulation data summary .....	158
Table 6.3: Case study 2, simulation data summary .....	159
Table 6.4: Case study 3, high-voltage event simulation data summary .....	160
Table 6.5: Case study 3, low-voltage event simulation data summary .....	160
Table 6.6: Case study 4: simulation data summary .....	163
Table 6.7: Case study 5: simulation data summary .....	163
Table 6.8: Case study 6, high-frequency event simulation data summary .....	164
Table 6.9: Case study 6, low-frequency event simulation data summary .....	165
Table 6.10: Case study 4, 80% voltage drop at POC data summary .....	167
Table 6.11: Case study 8: noteworthy events summary .....	169
Table 6.12: Case study 9: noteworthy events summary .....	170
Table 6.13: Voltage and Frequency-validation subsystem case study test results .....	172
Table 8.1: Maximum disconnection times set for Categories A1 and A2 RPPs .....	187
Table 8.2: Default frequency settings .....	191

## LIST OF FIGURES

Figure 2.1: LVRT requirements set by different grid codes of different countries .....	21
Figure 2.2: Mode 1 of active power control.....	22
Figure 2.3: Mode 2 of active power control.....	22
Figure 2.4: Mode 3 of active power control.....	23
Figure 2.5: Operating frequency limits set by different grid codes .....	24
Figure 2.6: RMS voltage variation for grid-code compliance test.....	25
Figure 2.7: Active power control functions.....	32
Figure 2.8: Process of real-time modelling using OPAL-RT .....	56
Figure 3.2: SA's grid-integrated renewable generation mix .....	62
Figure 3.1: SA's current generation mix.....	62
Figure 3.3: SA's operational renewable-generation mix.....	63
Figure 3.4: REIPPPP renewable generation mix target .....	63
Figure 3.5: 2030 IRP renewable generation mix target .....	63
Figure 3.7: 2030 forecasted % annual energy contribution by generation type .....	64
Figure 3.6: SA's future generation mix as per the 2030 IRP.....	64
Figure 3.8: Category A1 and A2 voltage ride-through requirements.....	66
Figure 3.9: Non-synchronous Category A3, B and C voltage ride-through requirements .....	67
Figure 3.10: Synchronous Category A3, B and C voltage ride-through requirements.....	68
Figure 3.11: Synchronous Category A3 and B voltage ride-through requirements in the event of 3-ph faults.....	68
Figure 3.12: Reactive-power support requirements during voltage drops or spikes .....	70
Figure 3.14: Category B reactive power and voltage range requirements .....	72
Figure 3.13: Category B reactive power support requirements .....	72
Figure 3.15: Category B reactive power support requirements at normal POC voltage .....	72
Figure 3.17: Category C reactive power and voltage range requirements .....	73
Figure 3.16: Category C reactive power support requirements .....	73
Figure 3.18: Category C reactive-power support requirements at normal POC voltage .....	74
Figure 3.19: Power curtailment requirements during over-frequency events.....	74
Figure 3.20: Category C frequency response requirements .....	75
Figure 3.21: Short-circuit testing table, 20% reduction in voltage .....	79
Figure 3.22: Example test network .....	81
Figure 3.23: Example test network combined and reduced .....	81
Figure 3.24: Adapted voltage ride-through and recovery requirements by country .....	85
Figure 3.25: Siemens SWT-2.3-108 turbine component layout .....	87
Figure 3.26: Siemens SWT-2.3-108 power vs wind speed characteristic curve.....	88
Figure 4.1: Process of selecting Vnu and Vnl voltage boundaries based on user input .....	91
Figure 4.2: Process of selecting HVRT, and LVRT boundaries based on user input .....	91
Figure 4.3: MATLAB live script user inputs.....	91
Figure 4.4: Normal and fault ride-through boundaries output based on user input.....	93
Figure 4.5: Grouped MATLAB testbed design .....	94
Figure 4.6: SM_Target subsystem, testbed model circuit design .....	95
Figure 4.7: Logic operation and circuit of the 'Detect Event' subsystem.....	99
Figure 4.8: Logic operation and circuit of the 'Measure Event Time' subsystem .....	100
Figure 4.9: Logic operation and circuit of 'Check Voltage Violation' subsystem .....	101
Figure 4.10: Voltage-validation subsystem flow diagram.....	102

Figure 4.11: Logic operation and circuit of 'Frequency Violation' subsystem .....	103
Figure 4.12: Adapted 'Calculate frequency' MATLAB block.....	104
Figure 4.13: Frequency-validation subsystem flow diagram .....	105
Figure 4.14: Wind turbine data acquisition subsystem .....	106
Figure 4.15: Simulator measurements scopes .....	108
Figure 4.16: Lab equipment setup diagram .....	109
Figure 4.17: Host computer .....	110
Figure 4.18: OPAL-RT OP4510 real-time simulator .....	110
Figure 5.1: Real-time simulation testbed circuit, SM_Target subsystem .....	115
Figure 5.2: Real-time simulation inputs and outputs/measurements, SC_Local subsystem.....	115
Figure 5.3: Case study 1: testbed voltage event response.....	116
Figure 5.4: Case study 1: RPP voltage event response.....	118
Figure 5.5: Case study 2: testbed voltage event response.....	119
Figure 5.6: Case study 2: RPP voltage event response.....	121
Figure 5.7: Case study 3: testbed high-voltage event response .....	122
Figure 5.8: Case study 3: testbed low-voltage event response .....	123
Figure 5.9: Case study 3: RPP high-voltage event response .....	125
Figure 5.10: Case study 3: RPP low-voltage event response .....	126
Figure 5.11: Real-time simulation test circuit: frequency validation.....	127
Figure 5.12: Case study 4: testbed frequency event response .....	128
Figure 5.13: Case study 4: RPP frequency event response .....	129
Figure 5.14: Case study 5: testbed frequency event response .....	130
Figure 5.15: Case study 5: RPP frequency event response .....	132
Figure 5.16: Case study 6: testbed high-frequency event response.....	133
Figure 5.17: Case study 6: testbed low-frequency event response .....	134
Figure 5.18: Case study 6: RPP high-frequency event response .....	135
Figure 5.19: Case study 6: RPP low-frequency event response .....	136
Figure 5.20: Case study 7: RPP 20% short circuit at POC response.....	138
Figure 5.21: Case study 7: RPP 30% short circuit at POC response.....	139
Figure 5.22: Case study 7: RPP 50% short circuit at POC response.....	140
Figure 5.23: Case study 7: RPP 80% short circuit at POC response.....	141
Figure 5.24: Case study 8: testbed voltage response.....	144
Figure 5.25: Case study 8: testbed frequency response .....	145
Figure 5.26: Case study 8: RPP response .....	146
Figure 5.27: Case study 9: testbed voltage response.....	147
Figure 5.28: Case study 9: testbed frequency response .....	148
Figure 5.29: Case study 9: RPP response .....	149
Figure 6.1: Current vs 2030 IRP predicted generation contribution.....	152
Figure 6.2: Grid-code-specified test circuit vs developed test circuit.....	154
Figure 6.3: Voltage ride-through requirements set for test RPP as per SA grid codes .....	158
Figure 6.4: Frequency ride-through requirements set for all RPPs during a disturbance .....	162
Figure 6.5: Case study 7 RPP response to 20% POC voltage drop .....	166
Figure 6.6: Case study 7 RPP response to 30% POC voltage drop .....	166
Figure 6.7: Case study 7 RPP response to 50% voltage drop .....	166
Figure 6.8: Case study 7 RPP response to 80% POC voltage drop .....	166
Figure 6.9: Case study 7 active current generated during respective POC voltage drops.....	168

Figure 6.10: Case study 7 reactive power generated during respective POC voltage drops .....168

Figure 6.11: Case study 7 peak-current generated during respective POC voltage drops .....168

Figure 8.1: Minimum cumulative frequency operating range over a RPPs lifespan .....186

Figure 8.2: Minimum frequency operating range of a RPP during a frequency disturbance .....186

Figure 8.3: Voltage ride through requirements for Categories A1 and A2 RPPs .....187

Figure 8.4: Voltage ride-through limits for non-synchronous machines of Categories A3, B, and C.....188

Figure 8.5: Voltage ride-through limits for synchronous machines of Categories B and C .....188

Figure 8.6: Voltage ride-through limits for synchronous machines of Category B during 3-phase faults .189

Figure 8.7: Reactive power (IQ) support requirements during voltage drops or peaks at the POC.....189

Figure 8.8: Power curtailment requirements for RPPs during over-frequency events.....190

Figure 8.9: Category C RPP frequency response requirements .....190

Figure 8.10: Category B RPP reactive power requirements at the POC.....192

Figure 8.11: Category B RPP reactive power requirements at nominal voltage at POC.....192

Figure 8.12: Reactive power and voltage control range requirements for Category B RPPs .....193

Figure 8.13: Category C reactive power requirements at POC .....193

Figure 8.14: Reactive power and voltage control range for Category C RPPs .....194

Figure 8.15: RPP reactive power control function requirements .....195

Figure 8.16: RPP voltage control requirements .....195

Figure 8.17: South Africa's existing and planned electrical network .....196

## ACRONYMS AND ABBREVIATIONS

AC	Alternating Current
CSP	Concentrated Solar Power
DC	Direct Current
DFIG	Doubly Fed Induction Generator
DNI	Direct Normal Irradiance
DSG	Direct Stream Generation
FRT	Fault Ride-Through
HFRT	High-Frequency Ride-Through
HIL	Hardware-in-the-Loop
HVDC	High-Voltage Direct Current
HVRT	High-Voltage Ride-Through
IEC	International Electrotechnical Commission
IEEE	Institute of Electrical and Electronics Engineers
KW	Kilowatt
LFRT	Low-Frequency Ride-Through
LV	Low Voltage
LVRT	Low-Voltage Ride-Through
MV	Medium Voltage
MW	Megawatt
NIPS	National Integrated Power System
PF	Power Factor
PMSG	Permanent-Magnet Synchronous Generator
POC	Point of Connection
PV	Photovoltaic
REIPPPP	Renewable Energy Independent Power Producer Procurement Program
RPP	Renewable Power Plant
SIL	Software in the Loop
SO	Systems Operator
TANGEDCO	Tamil Nadu Generation and Distribution Corporation Limited

# **CHAPTER ONE**

## **GENERAL CONCEPT OF THE STUDY**

### **1.1 Background and introduction**

Following the global movement, South Africa plans to increase its use of renewable energy substantially going forward, giving rise to a need for comprehensive RPP grid-integration behavioural studies, on account of the differences between renewable generation, and the synchronous generation it is set to replace (Department of Energy, 2011). Considering South Africa's installed generation capacity, and profuse synchronous power plant history, extensive experience and knowledge have been gained over the years operating synchronous power plants, with its behaviour in the event of abnormal and fault conditions having become well known and understood by operators (Sreedevi *et al.*, 2016). However, the same cannot yet be said about the relatively recent introduction of renewables into the South African grid, which still make up a negligible percentage of the current generation in terms of its effect on grid behaviour. However, as this percentage of grid-connected renewables increases with the completion of ongoing and planned renewable energy integration projects, there are bound to be major changes to the workings of the South African grid, transforming the still largely passive network into a multi-directional active network driven by the asynchronous power electronic nature of renewable generation.

The push to integrate increasing amounts of renewable generation into the South African grid is driven not only by global pressure to reduce both emissions and reliance on fossil-fuel generation reserves, but also because it forms part of the solution to the country's ongoing energy crisis, stemming from an aging unreliable generation infrastructure which has led to an ongoing failure to keep up with demand. This sets South Africa apart from most countries, in that renewables are integrated into an already strained electrical grid, placing increased pressure on RPPs to support grid conditions sufficiently in line with grid-code requirements during disturbances. From what is known, no real-time simulation tool specific to South Africa's grid-code requirements yet existed for performing RPP grid-integration behavioural studies. Seeing the value and necessity for South African-tailored simulation tools to assist and promote the successful integration of planned renewable generation in the country, the study set out to address this issue by developing a real-time RPP grid-integration behavioural studies testbed, tailored to South African RPP grid-code requirements.

### **1.2 Problem statement**

The behaviour of an electrical network and its ability to recover from disturbances and faults is influenced by a wide range of factors, among which the generation mix has a profuse influence.

This behaviour and response to everyday load fluctuations, and abnormal fault conditions is ultimately a major contributing factor to the stability and reliability of a network. Older types of synchronous generation are often synonymous with large rotating masses and moving components resisting sudden speed changes, consequently resulting in voltage and frequency fluctuations. This short-term energy reserve and mechanical reluctance to sudden changes is what is referred to as the inertia of a system and is among the key attributes lost in shifting from conventional synchronous generation to inverter-based asynchronous generation.

South Africa, like many other countries, through initiatives such as the 2030 IRP, has revealed its goal of increasing grid-connected renewables by about 33%, an addition of 14 725 MW, by 2030. However, South Africa is unique in that, amidst the push towards an increased grid-integrated renewable future, the country is in an ongoing struggle to supply its current electrical demands reliably. This follows years of infrastructure neglect and lack of maintenance which have led to a dwindling energy availability factor nearing 62% by early 2022, as the country struggles to keep unplanned breakdowns below the point where planned load shedding is needed to maintain grid stability. This sets South Africa apart from most countries, in that renewables are being integrated into an already strained electrical grid to increase generation capacity, and thereby improve reliability of supply.

Considering renewable grid-integration studies conducted elsewhere, increased voltage levels, increased short-circuited currents, and deterioration in the reliability and quality of supply are among the noted effects of large-scale renewable grid integration, especially for countries with weaker grids, while increasing rotational load shedding like that experienced in South Africa has led to chronic supply interruptions and large-scale outages for comparable scenarios. This is reason for concern about the outcome and feasibility of South Africa's renewable-integration goals. No two networks are the same, and the effect that increasing renewable generation has on a grid will differ based upon the unique conditions of a country or region. Comprehensive South African-tailored renewable grid-integration studies therefore need to be performed, to determine how the planned renewable generation will affect the South African grid, since failure to do so could lead to renewable generation crippling South Africa's already volatile grid.

From what is known, no simulation tool existed tailored to South African grid-code requirements for performing such studies. Consequently, this study addressed the matter through the testbed developed in support of the successful integration of South Africa's renewable-integration goals.



### **1.3 Research objectives**

The aim of the research is to develop an OPAL-RT real-time renewable energy grid-integration behavioural studies testbed which is grid-code-tailored, and MATLAB-integrated for South Africa. The research objectives which the research aims to address and achieve, are as follows:

- To investigate, assess, and give perspective on South Africa's planned renewable-integration future.
- To develop a testbed capable of operating simulated RPPs accurately in line with South African RPP grid-code requirements, providing an efficient and accessible way of studying grid-integrated RPP behaviour.
- To test and corroborate the design of the testbed's grid-code validation subsystems.
- To illustrate the worth and abilities of the testbed as an RPP grid-integration behavioural studies tool.
- To contribute to the field of research needed in support of the successful integration of South Africa's renewable-integration goals.
- To identify limitations and obstacles associated with the planned integration of renewable generation.

### **1.4 Research methodology**

The objective of the thesis is to develop a real-time RPP grid-integration behavioural studies testbed tailored for South African to assist with the renewable grid-integration studies needed for the successful integration of South Africa's planned renewable energy additions. Accordingly, the testbed needs to incorporate South African grid-code requirements, in line with which the connected RPP could be operated, allowing the behaviour of the RPP to be studied given the imposed strain of ride-through and support requirements imposed by grid codes.

As a starting point, the research examines the relevant South African RPP grid-code document, which sets requirements for renewable generation connected to the South African grid. Research furthermore considers challenging areas for RPPs, which emerges largely in the form of support concerns and limitations, essential for maintaining grid stability during disturbances. Given the various RPP grid-code requirements and the aim to develop a testbed for studying RPP behaviour, it was decided that the testbed would perform active POC monitoring and RPP adherence of two key grid-code parameters, namely POC voltage and frequency. This is because grid-code voltage and frequency requirements play an important role in governing when an RPP is allowed to disconnect from the grid which, if not done in line with grid-code requirements, could have repercussions such as cascade tripping, affecting grid stability negatively. The testbed, therefore, needs to operate the simulated RPP in line with South African RPP grid-code requirements,

according to which it will determine when it is appropriate to disconnect the RPP from the rest of the network. Operating the RPP in this way, then through simulation measurements, allows the strain imposed by the requirements to be determined and studied, forming part of the testbed's ability to perform grid-integration behavioural studies.

A MATLAB live script is developed, containing all voltage and frequency grid-code requirements. The live script then requires the user to input basic RPP details, according to which it will select the appropriate grid-code requirements for the simulated RPP. Most of the testbed will then be developed using MATLAB's Simulink environment, grouped into subsystems according to their respective functions and tasks. The main Simulink circuit consists of a grid-representing section which, instead of a generic static layout, implements a data-import block allowing effective recreation of simulated conditions. This is included as a means of increasing the controllability, widening the testbed's abilities and application while producing more accurate results on account of its ability to replay previously recorded events. On the opposing side of the model is the simulated renewable power plant (RPP), which can be of any type and size. The trip input of the simulated RPP is controlled by the voltage and frequency-validation subsystems, using the MATLAB live script grid-code import data, and RPP POC circuit measurements, to determine and govern conditions during which the RPP is required to operate, and disconnect. The model is consequently designed with simplicity and versatility in mind, in that its design conforms to grid-code test-circuit requirements, while the MATLAB live script allows it to accommodate any RPP for a wide range of simulation conditions.

To test both the developed testbed and simulated RPP, a testing strategy is developed, focusing on testing of specific circuit sections under certain conditions, while also monitoring RPP response to show the worth of the testbed as an RPP grid-integration behavioural studies tool. The study therefore includes case studies simulating High-Voltage Ride-Through (HVRT), Low-Voltage Ride-Through (LVRT), High-Frequency Ride-Through (HFRT), Low-Frequency Ride-Through (LFRT), short-circuit, and replays real-world data events, varying in intensity to test different operating regions of the RPP grid-code requirements. For the case studies, the chosen RPP will be modelled after Eskom's Sere wind farm, chosen in response to the literature reviewed, showing wind energy playing a substantial role in the future integration of renewables in the country, while the Sere wind farm specifically was identified as Eskom's only operating grid-connected wind farm at the time.

The completed MATLAB model is then integrated with OPAL-RT's RT-LAB software, allowing the model to be simulated using the OP4510 real-time simulator. The generated case study results will first be analysed based on initial observations, followed by a detailed review of the logged

result data. The noted events are then given thorough consideration, allowing both the testbed and RPP behaviour and response to be analysed and assessed. This allows the success of the developed testbed to be determined based on the case study results, while also showing how the results produced can aid in performing RPP grid-integration behavioural studies, for which the testbed is developed.

### **1.5 Delineation of the study**

This study, generated from the research topic entitled 'Development of a real-time testbed for renewable energy integration studies', is focused on the following:

- South Africa's future renewable energy integration goals;
- the effect that large-scale grid-integrated renewables have on stability and security of supply;
- the integration of renewable generation into South Africa's electrical grid;
- renewable energy-specific grid-code requirements in South Africa;
- RPP support, behavioural, and testing requirements prior to grid connection;
- the identified lack of convenient, reliable, and accurate simulation-based RPP grid-integration behavioural study tools in South Africa;
- the development of a real-time testbed in response;
- testing of the testbed's abilities and accuracy through case studies; and
- illustrating the worth of the developed testbed as a tool to assist with and promote RPP grid-integration behavioural studies.

### **1.6 Study limitations**

Although mentioned, detailed research about the following fell outside the scope of the study and is not covered by this research:

- Grid-code requirements set for non-renewable-generation technologies;
- RPP testing beyond simulation, such as on-site testing;
- Although designed for implementation with any type and size of RPP, case study testing is limited to that of a wind farm for the thesis.

### **1.7 Literature study**

The literature study and research forming part of the testbed's development is housed in Chapters Two and Three of the thesis. Chapter Two starts by reviewing the current state of renewables in South Africa. It then continues to consider how a country's grid strength and unique geological conditions affect the renewable generation chosen for a specific region, important considerations also used to identify renewables best suited for South Africa. Grid codes are considered, both in

general as well as those specifically applicable to renewable generation in South Africa. The study then considers South Africa's current grid infrastructure, generation mix, and common types of network faults, as a representation of the conditions which present when renewables are integrated in South Africa. Bearing in mind the review of South Africa's electrical network and generation mix, future integration targets for renewable generation are examined and assessed. Literature then considers the associated challenges of renewable integration noted by other countries, recognising the fact that a limit still exists to the number of renewables that can be integrated soundly into an existing electrical grid, without sacrificing stability. Research ultimately shows wind and solar technologies to be a combination favoured for South African conditions, backed up by a further review of the details of these technologies.

Finally, Chapter Two shows South Africa to have limited experience with grid-integrated renewables, while initiatives illustrate the country's intention to integrate significant amounts going forward. Research and revision of existing literature failed to identify efficient and effective simulation tools to promote renewable-integration studies needed for the successful integration of renewable generation in the country. This supports the need for a real-time RPP grid-integration behavioural studies tool, tailored to South African grid-code requirements, which the study develops using a MATLAB-integrated OPAL-RT testbed. The process of developing an OPAL-RT real-time model is reviewed, followed by studies from other countries implementing real-time simulators for similar purposes, in support of the South African real-time RPP grid-integration behavioural studies testbed developed.

The literature in Chapter Three expands on important topics in support of the testbed's successful development, which includes analysing the goals set for renewable integration in South Africa, particularly focusing on more recent policies and goals such as that of the updated 2030 IRP. South Africa's RPP grid-code requirements are reviewed in greater detail, focusing on POC voltage and frequency requirements, having identified these as the actively monitored parameters against which the testbed's simulated RPPs will be operated. Grid codes furthermore specify RPP test-circuit requirements, and testing procedures, reviewed in greater detail as these requirements guided both the design of the testbed and the testing procedures developed.

## **1.8 Modelling and simulation**

The objective of this study was to develop a real-time RPP grid-integration behavioural studies testbed and accompanying testbed testing procedures to corroborate its accuracy and abilities. The development process can essentially be divided into three sections, the first being the development of the MATLAB model, followed by its integration with OPAL-RT's RT-LAB software, and finally, the execution of the model using the OPAL-RT OP4510 real-time simulator.

Similarly, the MATLAB model can further be broken down into the development of the grid code containing MATLAB live script, and the testbed circuit developed using MATLAB's Simulink environment. Finally, the Simulink model can also be viewed as two parts, the first being the grid-representing side using imported data to replay and recreate simulation conditions, connected to the renewable-generation side under study. The MATLAB model and all its contained sections are integrated with RT-LAB software, forming part of OPAL-RT's integrated eMEGAsim environment. This involves RT-LAB automatically converting the model to C++ code during compilation, after which it assigns the MATLAB subsystems in line with their prior groupings, to their respective cores for execution. If overruns occur at this stage, the model subsystems will have to be re-divided, and the process started again. Once successfully compiled, OPAL-RT's OP4510 real-time simulator is used to simulate the model in real time, using MATLAB scopes to log simulation result data for analysis.

Case studies performed as part of the thesis will make use of a wind farm as test RPP, representing Eskom Sere wind farm currently in operation in South Africa, though the testbed is not limited to any type or size of RPP. Case study testing conditions will make use of both fabricated test data, as well as measured grid data to test both the testbed and simulated RPP. Testing conditions will focus on operating the test RPP within its respective continuous, fault ride-through, and trip regions of operation, evaluating the response of both the testbed and RPP. In addition to measurements forming part of the active POC voltage and frequency monitoring, the testbed will also include additional measurements allowing the strains imposed by grid codes on RPPs to be studied. This allows passive monitoring of an RPP during simulated conditions, and consequently grid-integration behavioural studies to be performed.

### **1.9 Thesis outline**

- Chapter Two presents a review of literature of the current and planned state of renewables in South Africa, as well as renewable suitability studies, grid strength, renewable penetration limits, grid codes, local grid infrastructure, South Africa's generation mix, renewable-generation costs, wind turbines, solar technology, and OPAL-RT as the real-time simulator of choice.
- Chapter Three interprets the literature of Chapter Two, while expanding on the grid-code requirement details set for RPPs in South Africa, as well as the grid-code testing, and test-circuit requirements, before introducing the RPP selected for the forthcoming case studies.
- Chapter Four follows the testbed's development, which includes the MATLAB live script, grouping of the Simulink model, discussion of the Simulink model sections and subsections, model measurements, and testing strategy.

- Chapter Five executes the testing strategy developed in Chapter Four, implementing the developed model to showcase its abilities through the case studies performed.
- Chapter Six analyses thoroughly the case study results and occurrences noted in Chapter Five, summarising the findings to produce a verdict on the success of the developed real-time testbed, as a real-time RPP grid-integration behavioural studies tool.
- Chapter Seven presents the thesis conclusion, and recommendations for future work.

## **CHAPTER TWO**

### **LITERATURE REVIEW**

#### **2.1 Introduction**

With the objective of the thesis being to develop a tailored South African real-time RPP grid-integration behavioural studies testbed, this chapter was aimed at reviewing existing literature surrounding South Africa's current and future generation mix, grid codes, grid infrastructure, viable renewable technologies, and the process of developing a real-time simulation model. The purpose of this chapter is then to give motive and show the need which emerged for tools to perform renewable grid-integration studies, given South Africa's ambiguous renewable-integration goals. Revision of grid codes aims to show through their RPP-support requirements how they plan to mitigate potential RPP-support concerns, giving rise to the realisation that these requirements will also impose added strain on the already limited support capabilities of an RPP. Providing a means for studying these grid-code-imposed strains, support abilities, and RPP behaviour, when presented with grid disturbances, is ultimately what the testbed aims to achieve, starting with the comprehensive literature review of Chapter Two.

#### **2.2 State of renewable integration in South Africa**

Like many other countries, South Africa has, in recent years, added to its generation capacity in the form of renewable energy, commonly defined as energy produced from inexhaustible natural resources (Huang, Kittner and Kammen, 2019). By the year 2017, 539.123 GW of wind energy was already installed globally, with South Africa's capacity contributing 2 085 MW at the time (Global Wind Energy Council, 2017; CSIR Energy Centre, 2018). Also by 2017, globally installed PV reached close to 398 GW, with South Africa having 1 474 MW of solar PV, and 300 MW of concentrated solar power (CSP) installed at the time (International Energy Agency, 2017; CSIR Energy Centre, 2018). Although renewable penetration in South Africa is still considered minimal when compared to other countries such as Denmark or Spain, South Africa's revised 2018 IRP aims to change this by planning new wind, solar, and gas generation accounting for 42% of the country's energy needs by the year 2030, and penetration even beyond this in the years to follow, replacing the predominantly coal-based generation currently in use. As a result of programmes such as the REIPPPP, South Africa, with its abundance of sun and wind resources, has now been rated as the 12th most attractive country globally for renewable investments. This resulted in renewable investments to the value of R201.8 billion, of which 24% accounts for foreign investments, helping to drive the transition from fossil fuels to renewables in the country (D'Sa, 2005; Cochran *et al.*, 2012; Sewchurran and Davidson, 2016; Campbell, 2018; Department of Energy, 2018; RSA Department of Energy, 2018).

South Africa is currently, however, still heavily reliant on coal for supplying its electrical needs, as it generates approximately 77% of its power from coal. The main driving factor behind this is South Africa's abundance of coal, having the 5th largest recoverable coal resources globally, estimated at 66.7 billion tons, enabling coal-fired power plants to supply low-cost baseload electricity (RSA Department of Energy, 2018). This makes South Africa the 6th largest producer of electricity using coal, leading to its having the highest greenhouse gas emissions in Africa (Jain and Jain, 2017). Globally, it is forecast by the International Energy Agency (IEA) (2017) that the capacity of renewable energy sources will increase by as much as 43% between 2017 and 2022 (Bertrand-Vasseur and Berthelot, 2017). Renewable energies do not, however, come without their challenges, since they are often required to act and adhere to grid codes like conventional generation would, which can present quite a challenge (Wright, Tuson and Van Coller, 2012; Knorr *et al.*, 2016; Oyewo *et al.*, 2019).

### **2.3 Grid strength and renewable suitability studies**

Considering different studies regarding the grid integration of renewable energies, most address the issue of what the maximum renewable penetration can be before jeopardising the stability and reliability of supply. Making this such a common consideration is the fact that no two networks are the same, with the maximum penetration level varying greatly depending on grid characteristics surrounding the transmission network, power system flexibility, and system inertia. It is therefore deemed important to consider South Africa's grid reliability, stability, and most importantly, flexibility, which refers to a grid's ability to maintain a balance between supply and demand with change, as well as its ability to respond efficiently to these changes given the added challenge of variable output generation sources such as renewables, since the strength of a grid can be seen as an initial indicator of its suitability for renewable integration (Wright *et al.*, 2012; Gu, 2016; Mararakanye and Bekker, 2019).

An important transmission network characteristic would therefore be to have enough dispatchable reserve capacity when required. This would require the elimination of any possible bottlenecks in the system, while having a broad range of balancing resources at its disposal, including connections to neighbouring power systems. One way to measure and quantify transmission network strength is through impedance. As a rule of thumb, it can be said that a network with a high impedance is generally considered to be weak, having low fault levels. To determine the strength at a specific point in a network, consideration is required of the short circuit and reactance to resistance ratios at that point. If the impedance to resistance ratio is less than 0.5, or the short-circuit ratio is below 10, the network at that point is considered weak. Other indications of a weak grid considering local grid codes, would be a wider power factor operating range and strict fault



ride-through and fault-recovery time requirements. A weak transmission network will consequently result in small disturbances having a significant effect, resulting in voltage and power regulation limits being exceeded during what are normally considered minor disturbances. A high impedance value furthermore increases losses, brought about by a lack of transmission capacity (Mararakanye and Bekker, 2019).

A study, which set out to quantify and compare the grid strength of ASEAN member nations, considered an alternative method to determine their preparedness for the planned increase to 23% renewables by the year 2025 using what is known as a scorecard method. The method considers six criteria, namely grid reliability, load profile ramp, electricity market access, forecasting systems, the proportion of natural gas generation to other generation, and renewable energy diversity, to which the grid of each member country was rated, in order ultimately to calculate its grid strength as a single value. Some rating criteria, for example, forecasting systems, were simply noted in terms of whether the country was already using forecasting to predict energy generation, while others were more complex and required some calculation. As an example of these, (2.1) and (2.2) can be considered, used to calculate the load profile ramp, which are among the rating criteria for the countries (Barrows *et al.*, 2018; Huang *et al.*, 2019).

$$\text{Load profile ramp} = \frac{\text{Worst case load profile ramp}}{\sum \text{Flexible Installed Capacity}} \quad (2.1)$$

$$\begin{aligned} \text{Worst case load profile ramp} = \\ \frac{\text{Maximum demand of steepest slope (MW)} - \text{Minimum demand of steepest slope (MW)}}{\text{Time taken (hours)}} \end{aligned} \quad (2.2)$$

The flexibility of a power system is another important consideration, referring to the system's ability to respond to demand changes. To achieve a high level of flexibility, a system needs to be composed of elements able to respond efficiently and effectively during demand changes. This would require real-time decision-making capabilities of control equipment, power reserve, and storage incorporated into the system. One way to achieve this would be to operate power plants at a reduced capacity, which would lower efficiency, but would provide the ability to respond quickly to load changes in the system. The importance of system flexibility to the successful integration of renewables is supported by the fact that most regions with a high integration percentage of renewables have strategies in place, such as combined cycle gas turbine plants, pumped storage, or strong interconnections to other regions to ensure supply flexibility (Mararakanye and Bekker, 2019).

An important consideration, especially as the penetration of renewables increases, is that of system inertia, which refers to the spinning reserve of a large rotating mass inherently part of a

power plant using large synchronous machines. These spinning masses resist changes in speed provoked by demand changes and imbalances, and are essential to minimise the rate of change in system frequency. Spinning reserves in a network are for this reason classified as a primary reserve measure. When these are replaced by converter-based power sources such as renewable power plants, the reserve and resistance to system frequency change is lost, as renewable generation tends to contribute very limited to no inertia nor governor response as a result of their decoupled nature of connection, which can have devastating consequences (Yan *et al.*, 2015; Gu, 2016; Mararakanye and Bekker, 2019). The percentage of renewables which can safely be incorporated into a grid is therefore highly dependent on the inertia provided by conventional generators if stability and security of supply are to be maintained. For this reason, Gu (2016) developed (2.3) for calculating the allowable renewable penetration based on system inertia.

$$P_{re} = P_{load} - P_{sync} = P_{load} - (\alpha_{min} - P_{prim}) \quad (2.3)$$

Example calculations, explanation of values and an extended derivation of this formula can be found in Gu (2016), which should allow the theoretical calculation of allowable renewables for any network based on system inertia.

A grid that has received much attention in terms of the possible dangers resulting from a high penetration of non-synchronous generation renewables, leading to low inertia, is that of South Australia. The concerns associated with the network at the time of a study, included that grid codes allowed for a frequency deviation of 2% before implementing UFLS, while many of their PV units were set to trip following a deviation of more than 1% (Yan *et al.*, 2015). Therefore, it appeared that such a system would be relatively unstable because of the high penetration of renewables not being able to resist frequency deviations, while some PV units are set to trip before UFLS is implemented, contributing to the worsening situation during a low-frequency causing event. Among other things, the study set out to determine the effects in terms of the percentage load shedding required to maintain stability during a frequency disturbance, comparing the load shedding values for when PV units are allowed to trip before UFLS, to those when they are not allowed to trip before UFLS is applied. The study conducted the simulations using the Power System Simulator for Engineering software, for a network like that of South Australia. The scenarios simulated included the tripping of an interconnection during both day and night, and when power generated from PV units is respectively at its maximum and minimum. Next, the simulation included tripping of the network's largest synchronous generating unit, again for a day-and night-time scenario. Details of the total demand and power supplied by wind, PV units, the interconnection, and synchronous generators for the respective scenarios, are available in Yan *et al.* (2015).

Summarising the results, the study concluded that between 6% and 12% more load shedding is required to maintain stability if some of the PV generation is set to trip before under-frequency protection is activated. Importantly, the study also concluded that wind turbines of types 1 and 2 contribute to system inertia, and therefore cannot simply be disregarded in terms of system inertia considerations (Yan *et al.*, 2015). Curiously, during the year after publication of the above study, which raised concerns about the limited system inertia of the South Australian network, an event occurred which might not have mirrored those simulated in the study exactly, but did indeed have a resemblance to the concerns raised surrounding system inertia (Yan *et al.*, 2015).

This event, now known as the South Australian blackout of 2016 during which 850 000 customers lost their electricity supply, is widely considered to be a good example of the possible consequences of having limited system inertia available on a network. It stands out as the first blackout of a modern network incorporating a high share of renewables, leading to the system having limited inertia. The event has since sparked heated debates surrounding the role played by the almost 50% renewable energy generated at the time of the blackout, and whether the use of conventional power plants in the same scenario would have resulted in a different outcome. Although it cannot be argued that system inertia is lower when making use of renewable converter-based power sources, especially at high penetration levels, and that this indeed contributed to the cause of the blackout, renewables cannot solely be to blame. This becomes more evident considering the findings of the official report, revised reports, studies on the blackout, and simulations following the event. To obtain a better understanding of how this occurred, it is worth considering the circumstances leading up to the blackout (Australian Energy Market Operator, 2017; Lucas, 2017; Yan, Saha and Member, 2018; Mararakanye and Bekker, 2019).

It is said that problems began when a local thunderstorm led to two tornadoes almost simultaneously damaging a single 275 kV, and a double 275 kV line situated 170 km apart, causing the three lines to trip. Six voltage dips were recorded in quick succession during the two-minute period to follow, of which those that were not cleared were situated far from load centres, and therefore did not affect the network integrity significantly. Data showed that the online wind turbines managed to ride through these initial faults, but then reached a point where most unexpectedly tripped, resulting in a sustained generation reduction of 456MW in less than seven seconds. The loss of generation resulted in a significant increase in demand from the power imported through an interconnector, exceeding the limits set by protection equipment, and causing it to trip shortly afterwards. This caused the South Australian network to become islanded. The remaining generation could not sustain the network voltage and frequency, as the under-frequency load shedding protection was unsuccessful in shedding some of the load owing to the rate of

change in frequency being too high to be recognised by the protection equipment. This inevitably led to a system collapse, following a recorded frequency rate of change of 6 Hz/s, causing it to drop below the synchronous generator tripping threshold of 47 Hz (Australian Energy Market Operator, 2017; Yan *et al.*, 2018).

Although detailed reports following the event raised several concerns surrounding unexpected equipment behaviour, the one which stands out regarding the question of whether the high percentage of renewables is to blame, was the unexpected tripping of the wind turbines following the loss of the three 275 kV lines. Official findings concluded that the wind turbines did not trip because of their inability to ride through the network faults caused by high wind speeds, or because of an inability to provide services such as voltage and frequency control, but were rather the result of a protection setting only allowing a predetermined number of fault ride-through events within a two-minute time frame before disconnecting. The official AEMO report, therefore, blamed the collapse of the network, although there were several contributing factors, on the wind farm protection settings, and not directly on the high network penetration of renewables (Australian Energy Market Operator, 2017; Yan *et al.*, 2018).

Significantly, there were also some unanswered questions and network behaviour concerns raised following the initial report, which should be noted as factors to keep an eye out for when simulating different scenarios using the real-time testbed which this study aims to develop for the integration of renewable energies on the South African grid. The first is the presence of bottlenecks in the system resulting from different faults and generation-loss scenarios, and how this can be addressed. Overvoltage spikes following disconnections can, in turn, lead to the unnecessary disconnection of synchronous generators, as in the case of the South Australian blackout, contributing to the severity of a situation. The presence of pole slip which follows high rates of change in frequency. And finally, the malfunction of under-frequency load shedding protection during high rates of frequency change and frequency instability, which is the root cause of disconnecting generation units during abnormal events (Yan *et al.*, 2018).

The final AEMO report following the incident suggests that an extended number of improvements and changes should be made to the South Australian network to ensure that such an event is never to occur again. Some of the important suggestions can be highlighted. The first and most important was a change in the protection settings of the renewables, allowing an increased number of fault ride-through events per two-minute period, to prevent unnecessary disconnection. Improvement of load shedding equipment performance will allow the load shedding protection to stabilise the system within a few seconds once islanded. An increase in system inertia will slow down frequency change rates during disturbances, by requiring a minimum number of online

synchronous generators at any given moment. Most importantly, the report also suggests more rigorous and thorough testing of the wider network for a wider range of scenarios, using simulators and real-time testbeds such as the one this study developed for South Africa (Australian Energy Market Operator, 2017).

It is also ironic that, following the incident, South Australia was referred to by some as having an energy crisis, resulting from trying to better their network by incorporating a high percentage of renewables, which is often seen as the future solution and alternative to fossil-fuels-based generation methods. Nevertheless, this can still be considered as an isolated incident initiated by extreme weather events, and described by the labour premier of South Australia as circumstances which no other electricity network on earth would have been able to survive, whether making use of renewable or conventional generation methods. It is worth learning from the gaps noted in the integration studies of renewables, such as the settings limiting the number of fault ride-throughs during a two-minute period, which were not included in simulations, since this can assist in developing a better real-time testbed for renewable-integration studies (Australian Energy Market Operator, 2017; Lucas, 2017).

#### **2.4 Renewable suitability studies in South Africa**

South Africa has long shown an interest in the promotion of renewable energy, releasing its first policy documents including renewable energy integration plans in 1998, known as the White Paper on Energy Policy (WPEP) (Department of Minerals and Energy, 1998). Following this initial release, several other policy documents were also released in subsequent years, including the 2003 White Paper on Renewable Energy (WPRE) (Department of Minerals and Energy, 2003), the 2008 National Energy Act, the 2011 White Paper on National Climate Change Response Policy (WPNCCRP) (Department of Minerals and Energy, 2011), the 2011 National Development Plan (National Planning Commission, 2011), and the Integrated Energy Plan (IEP), approved for publication November 2016, which showed the South African government's commitment to increase the use of renewables (RSA Department of Energy, 2018). This also led to the establishment of what is now known as the Renewable Energy Independent Power Producers Procurement Program (REIPPPP), which replaced the Renewable Energy Feed-in Tariff (REFIT), originally released in 2009 by the National Energy Regulator of South Africa (NERSA), and aimed at increasing the percentage of renewables in the South African grid network. South Africa became the fourth largest renewable energy investor in 2012, with plans to install 6 300MW of renewable energy production by the end of 2014 through the REIPPPP. Unfortunately, most project allocations were not made by the Department of Energy, resulting in only 1 860MW being installed by 2015 (Bello *et al.*, 2013; Jain and Jain, 2017; Grobbelaar and Uriona, 2018).

South Africa has, nevertheless, seen several renewable suitability studies being performed over the years, revealing the wind, solar, biomass, geothermal, waste to energy, hydropower, and tidal energy production potential in the country. Of these, solar energy ranked first, having the highest potential in seven provinces, followed by wind in second place having the highest potential in the three Cape provinces, and biomass third, proving to be ideal for KwaZulu-Natal and Mpumalanga. The superiority of solar PVs is obvious because most regions in South Africa receive 8 to 10 hours of sunshine with radiation levels between 4.5 and 6.6 kWh/m<sup>2</sup> per day, adding up to 2 500 hours per year nationally. Wind power followed closely in second place, with 80% of South Africa's land surface being considered suitable for wind power generation, having an annual load factor greater than 30%. This adds up to a wind power potential of 6 700 GW which, in theory, shows South Africa to be able to generate its current energy requirement of 250 TWh/y from wind farms with a combined capacity of 75 GW, using only about 0.6% of the country's total land surface (Jain and Jain, 2017; Grobbelaar and Uriona, 2018; Oyewo *et al.*, 2019).

A study taking another approach to determine the ideal renewable energy sources for the South African energy mix of the future, is that of Naicker and Thopil (2019). Their approach rates the viable technologies, namely solar PV, wind, CSP, hydro, biomass, and biogas, according to 15 sub-criteria forming the technical, economic, environmental, social, and political considerations. After rating and normalising the values according to the method described extensively in the study, the following results were produced (Naicker and Thopil, 2019).

Concerning technical considerations, solar PV came out on top with a score of 0.83, followed by wind with a score of 0.8. This is largely because of the knowledge and experience South Africa has already gained in implementing and using these technologies. The conclusion for the technical considerations indicated that there is still room for improvement in terms of technical capabilities and maintenance of these technologies in South Africa; however, the country is well-enough equipped to implement and make use of solar PV and wind technology successfully. CSP technology, on the other hand, scored lowest in terms of technical considerations, with a score of 0.55. Concerning economic considerations, hydro energy scored the highest with 0.81, followed by CSP with 0.52. This results from having a low-levelised electricity cost, especially considering hydropower. Biogas technology, on the other hand, came last with a score of 0.35. Regarding environmental considerations, wind came out on top with a score of 1.06, followed by biogas with a score of 0.97. This is largely because of the low greenhouse gas emissions associated with these technologies. Biomass technology came last, having a score of 0.46. In terms of the social factor component, CSP scored highest with 0.94, followed by solar PV with 0.89. This outcome is largely based on the number of jobs created when making use of these technologies. Taking this

into consideration, biogas scored the lowest with 0.43. Lastly, looking at political considerations, wind scored highest with 1.10, followed by solar PV with 0.92. These were based on the financial support offered for each type of project, and how these technologies aligned with existing national energy plans. Hydro and biogas came last with 0.13 (Naicker and Thopil, 2019).

Depending on the weights and importance allocated to each of these categories and considerations, different outcomes can be reached on what the best technology is for South Africa going forward. The study also ultimately concludes that, given the results, and considering everything, solar PV and wind energy are the two best choices for implementation in South Africa. The maturity and technological advances made in terms of these technologies have also resulted in better financier participation compared to other technologies, making them safer and more attractive investment options for new investors to keep growing their implementation going forward (Naicker and Thopil, 2019).

A study that supports the significant availability of wind and solar irradiation resources in South Africa, is that of Knorr *et al.* (2016), which for the first time set out to quantify the wind and solar PV potential of the entire country and to determine whether this would be sufficient to supply future generation needs. It is established that the annual electricity demand in South Africa, based on averages from 2010 to 2012, is currently around 225 TWh, as mentioned previously and, given the average increases in demand, will reach 500 TWh in the future. The study considered a wide range of conditions and options for the increased integration of renewables, some realistic, and others purely theoretical. These include the distribution of wind and solar technologies uniformly across the entire country, or only in areas already designated as suitable for future renewable projects, or situated close to the current and planned grid, or all in one spot to minimise its footprint, or in areas with the highest availability of wind and irradiation (Knorr *et al.*, 2016; Oyewo *et al.*, 2019).

Findings from the study include that solar PV varies minimally with season and that the seasonal performance of wind matches that of the South African demand. This has the advantage of not requiring seasonal storage, which other countries may require. Considering a time scale of 24 hours, it is further noted that, when wind performance reaches a minimum at noon, solar PV reaches its peak, supporting the opinion that a combination of the two will complement each other well for South Africa, as compared to the rest of the world. This is recognised, considering the South African Department of Energy's original and the 2018 updated Integrated Resource Plan, indicating the country's intention to increase the percentage of renewables between 2010 and 2030, but also beyond this largely through the increased use of wind and solar technologies (Department of Energy, 2011, 2018; Knorr *et al.*, 2016). It is further found that, in terms of

generation stability, the best scenario is achieved when wind and solar PV are distributed across South Africa as widely and evenly as possible, although this might not always be ideal in terms of other considerations such as cost. Significantly, the advantages of widespread renewable generation do, however, include minimising generation fluctuation. For example, when widespread, the generation fluctuation of wind turbines commonly varies up to  $\pm 4\%$  per 15-minute time frame, compared to fluctuations of  $\pm 90\%$  considering a single wind turbine for the same period. Widespread distribution also leads to improved predictability and forecasting of renewable generation, which is essential to maintain stability and operating efficiency (Knorr *et al.*, 2016).

Since it has been established that solar PV is a viable option for South Africa, focus can shift to the most appropriate installation locations. A study that set out to determine the most appropriate provinces for PV installations in South Africa, is that of Mulaudzi and Bull (2016). The method used assessed the suitability of Limpopo, Mpumalanga, Gauteng, KwaZulu-Natal, Eastern Cape, Western Cape, Northern Cape, Free State, and Northwest provinces for PV installations, according to the criteria of solar radiation available, electricity tariff, available land space, population, electrification backlog, and electricity consumption. The study then considered three scenarios, with the difference being the weights allocated to the rating criteria (Mulaudzi and Bull, 2016).

The first considered all criteria, during which the highest consideration was given to the available solar irradiation and land space. The results of scenario 1 showed the Northern Cape province to have the highest PV potential, followed by the Eastern Cape and then KwaZulu-Natal. For scenario 2, the highest consideration was given successively to solar irradiation, available land space, and population, while minimal consideration was given to electrification backlog and consumption. For this scenario, the electricity tariff was not considered. Similar results were obtained from scenario 2, showing the Northern Cape province to have the highest potential for solar PV installations, followed by the Eastern Cape and KwaZulu-Natal. For scenario 3, the highest consideration was given to solar irradiation, followed by electricity consumption and available land space. All other criteria were excluded. Results from scenario 3 interestingly then showed Gauteng province to have the most potential for PV installations, even though this is one of the provinces with the least available land space. This result can be explained by the fact that Gauteng, on average, consumes more than a quarter of the electricity produced in the country, meaning that the electricity produced there will be consumed locally, and will not have to be transported for long distances using expensive transmission lines. Additionally, the solar radiation received in the province is at a good level, making solar PV an ideal option. Following Gauteng



province in first place for scenario 3, was KwaZulu-Natal in second, and the Northern Cape in third (Mulaudzi and Bull, 2016; Eskom, 2019b).

The best options for choosing a location are therefore to construct the PV plants in locations with abundant land space, and high levels of solar radiation, such as for scenarios 1 and 2. This would yield the highest electricity production; however, these are also often the areas with the lowest consumption of electricity. Extensive upgrades to the grid will therefore be required to transport the electricity produced, which will be expensive and may ultimately not make it worth the investment. The second option would be to construct solar PV plants as close to high-consumption areas as possible, where solar radiation may not be at a maximum, but still sufficient. The amount of electricity produced may then be limited by available land, and solar radiation levels; however, minimal upgrades to the network will be required, significantly cutting down on installation and maintenance costs (Mulaudzi and Bull, 2016).

Carefully planned distribution and an appropriate balance between wind and solar PV generation are important, as this increases the percentage of renewables that can be incorporated into the South African grid, without causing instabilities or requiring major changes. Nevertheless, there are other considerations, such as system inertia when making use of a high share of renewables. However, compared to most countries, South Africa is ideal for the use of renewables, and when appropriately planned, studied, and simulated, will play an important and reliable role in the future energy mix (Knorr *et al.*, 2016). Reaching the renewable-integration goals set for South Africa is still a mammoth task and will include hundreds of projects which first need to be discussed, analysed, simulated, and tested by Eskom engineers before being applied, constructed, and ultimately integrated into the grid. The study of Bello *et al.* (2013), highlights a need for proper models, data, skills, and tools to assess these projects efficiently before construction and integration. It is this need that the proposed study aims to address, developing a real-time testbed for renewable-integration studies, which will assist in assessing new renewable energy additions to the South African grid, accurately and efficiently, accelerating the approval and integration process (Wright *et al.*, 2012).

## **2.5 Grid codes (General)**

Grid codes, which are updated continually and adapted accordingly following the experience gained from integrating and introducing new-generation technologies into a power system, are essential to ensure the reliable, safe, and economic operation of a utility grid. Grid codes also have the essential role of ensuring power system uniformity and, although they may vary slightly in different regions based on the operating utility and local conditions, overall, they are very similar, since they support the same goal. Grid codes are also used by companies developing and

producing new power equipment, as these codes provide a point of reference according to which they need to develop their equipment and products (Wu *et al.*, 2011).

The introduction of renewable energy to the grid following its rapid development in recent years, required countries to adapt grid codes to be able to address new challenges and problems associated with the increased use of renewables. These mainly require renewable-generation plants to operate like conventional generation, in terms of fault ride-through capabilities, control of active power, reactive power, power factor, and frequency. This increased controllability is ultimately aimed at limiting losses during and following grid disturbances, stabilising renewable-generation behaviour to increase overall efficiency. The power output quality and protection capabilities of renewable-generation plants should therefore equal that of conventional plants during a variety of conditions, leading to some of the greatest challenges faced by equipment manufacturers, and plant and grid operators, forming the basis of this study to develop a real-time testbed for renewable-integration studies (Papathanassiou and Tsili, 2009; Wu *et al.*, 2011).

A basic requirement set by most grid codes of different countries and regions often includes that wind turbines, among other renewable technologies, need to remain connected during and following a variety of severe grid disturbances, such as short-circuit events. During this time, it is often required of wind turbines to feed reactive power to the grid, aiding in its recovery during fault conditions. A widely used industry standard for short-circuit testing of renewables is that of IEC 60909. This somewhat conservative standard introduced a precise procedure yielding results of acceptable accuracy for calculating primarily steady-state short-circuit currents. Calculations for this standard are done by introducing an equivalent voltage source at the short-circuit location, producing a graph illustrating short-circuit currents as a function of time corresponding to the voltage value before initiation of the short circuit, from initiation until it is cleared. As mentioned, grid codes also often require renewable power plants to inject reactive current during short-circuit events, during which time the modelled power station will act as a regulated current source assisting in raising grid POC voltage. During such an event, the level of reactive power required and supplied is determined by the depth of voltage drop. In steady state, the voltage magnitude is required to be kept fixed, and therefore the reactive power injected is dependent on the network reactance and AC phase angle (Liu *et al.*, 2018).

Following the occurrence of a fault, it is expected that the active power generated by the wind turbine should be restored to pre-fault levels, within a time limit specified by local grid codes. A common example of such a disturbance would be a short circuit which, depending on the type and location, will result in a voltage dip on one or multiple phases, and possible voltage spikes on some of the healthy phases. The duration of such disturbances will depend on the response time

of the protection scheme, often lasting only a few tenths of a second, but can also last up to several seconds leading to stability issues for some wind farms. Voltage dip and duration limits, often referred to as Fault Ride-Through (FRT) or Low-Voltage Ride-Through (LVRT) requirements, are therefore set by grid codes, specifying the voltage limits during which renewable generation needs to remain connected, and when it is allowed to disconnect (Papathanassiou and Tsili, 2009). These limits are usually represented on a graph, such as in Figure 2.1, illustrating the LVRT requirements for different countries.

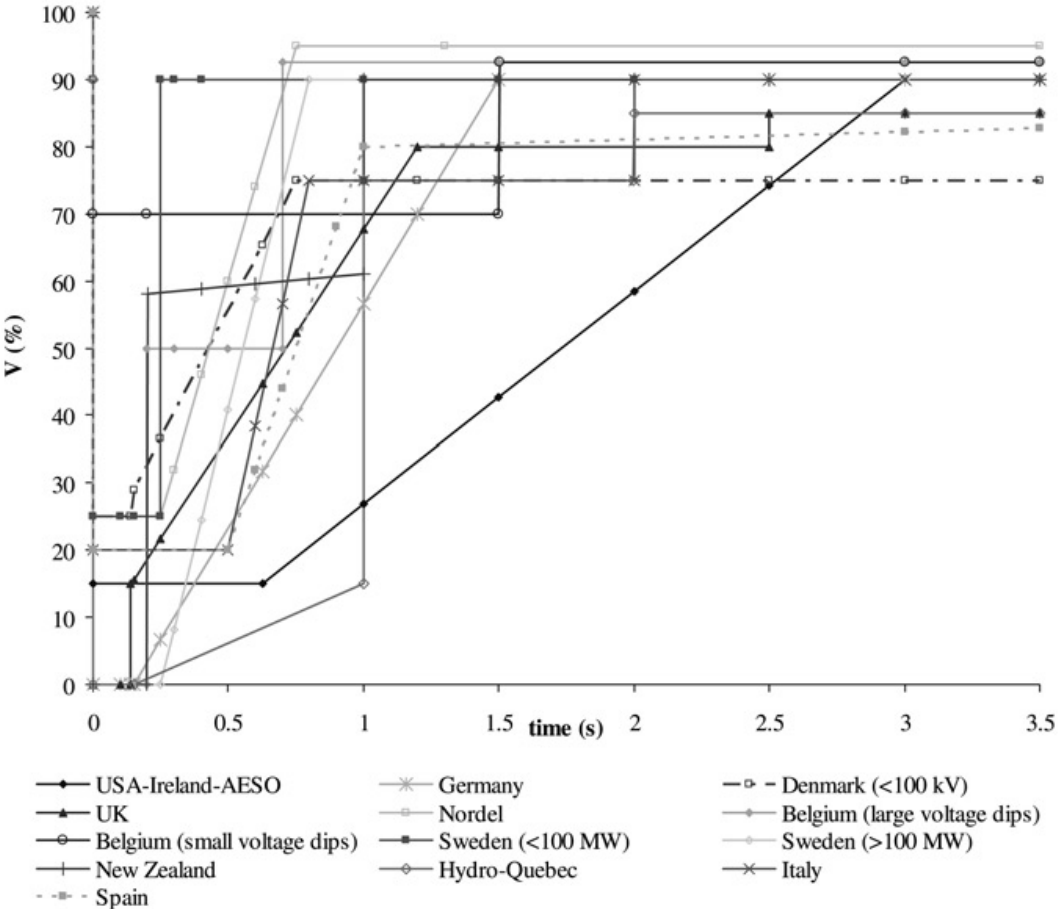


**Figure 0.1: LVRT requirements set by different grid codes of different countries (Papathanassiou and Tsili, 2009)**

The graph of Figure 2.1 furthermore shows that grid codes often require wind turbines to remain connected initially even when the nominal voltage drops to 0%. This value is commonly measured at the connection point to the grid and therefore, taking into consideration the impedance values of the transformer and lines, the voltage value at the wind-turbine terminals can be calculated to be roughly 15%, when the grid connection point reaches 0%. Renewable generation is therefore

required to remain connected for voltage levels above the line set by its relevant grid code, in the event of a grid disturbance and is only allowed to disconnect once venturing below the limit line (Papathanassiou and Tsili, 2009).

Another requirement imposed by grid codes is that of active power control according to frequency deviations, usually by one of three modes. In the first, active power generated is provided to the grid up to a predetermined maximum value which is not to be exceeded (Papathanassiou and Tsili, 2009). This mode of active power control is illustrated in Figure 2.2.

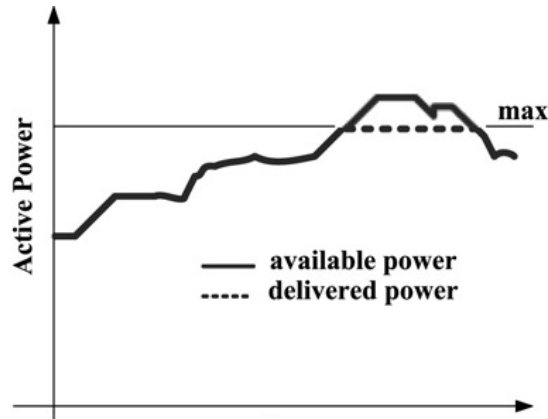


**Figure 0.2: Mode 1 of active power control**  
(Papathanassiou and Tsili, 2009)

In the second, a percentage of the available active power is delivered, so as always to maintain a reserve of available power. This mode of active power control is illustrated in Figure 2.3.

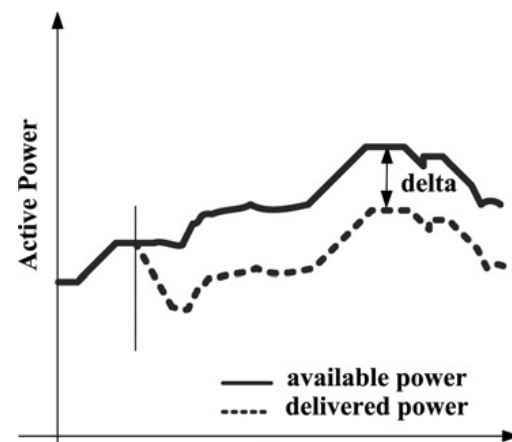


**Figure 0.3: Mode 2 of active power control**  
(Papathanassiou and Tsili, 2009)

The third mode of control limits the rate of change of the delivered active power, in relation to that generated. This mode of active power control is illustrated in Figure 2.4.

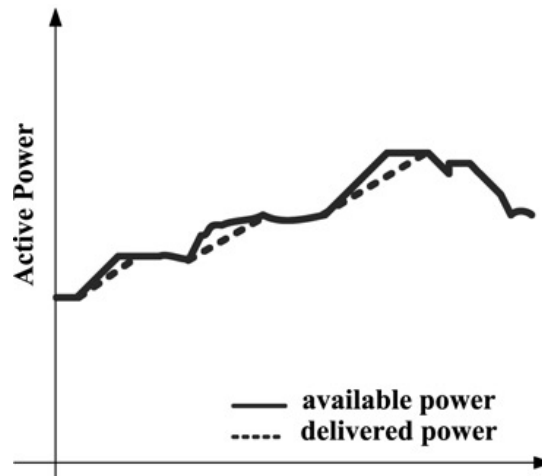
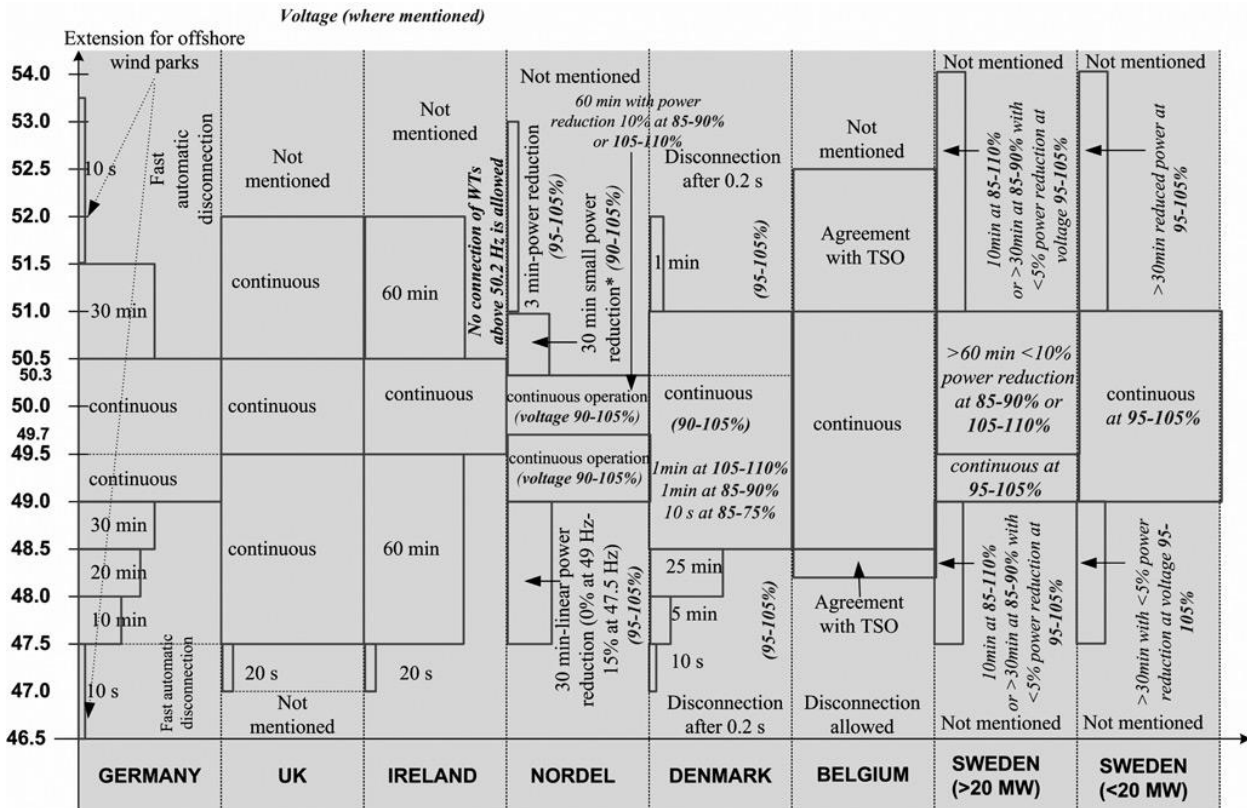


**Figure 0.4: Mode 3 of active power control  
(Papathanassiou and Tsili, 2009)**

An important reason for active power control is the ability of a wind turbine to provide ancillary services by allowing frequency control, which requires having a spinning reserve. Reducing the active-power output will allow for the correction of over-frequency problems, while using the active power reserve, as illustrated in Figure 2.3, to increase the active-power output during an under-frequency event, assisting the grid in recovering from under-frequency events. Although different grid codes specify different ramp rates and extents of active power control, most agree that active power control, especially with the use of wind turbines, is essential to assist in regulating system frequency. Economically, active power control has the disadvantage of reducing efficiency, yet this is a necessary compromise to provide the ancillary services required of wind farms and other renewable technologies to operate more like a conventional power plant (Papathanassiou and Tsili, 2009).

The rate and amount of active power required during under- or over-frequency events will subsequently be determined by the degree of deviation from normal operating frequency, and the control specifications set by the relevant grid codes. This can vary substantially, according to different grid codes applied in different countries, and the strength and stability of the local grid. It is therefore common to find that countries with an isolated and weak grid tend to have wider frequency limits, when compared to countries with stronger and more established grids (Papathanassiou and Tsili, 2009). This grid strength dependant variation in frequency requirements is supported considering the frequency limits of different countries, as illustrated in Figure 2.5.



\* the total duration of these operating conditions must not exceed 10 hours/year

**Figure 0.5: Operating frequency limits set by different grid codes (Papathanassiou and Tsili, 2009)**

In addition to active power control, reactive power control is another important requirement often demanded by grid codes. An example of such a code is 'E.ON', which requires wind turbines not only to supply reactive power during a fault, but also to consume reactive power in the event of a voltage dip. Furthermore, it demands reactive current control within one cycle following the recognition of an event, providing reactive current at a rate of 2% per percentage voltage drop, up to a maximum of 100% rated wind-turbine current. The maximum reactive power that can be supplied by a wind turbine is dependent on the parameters of the turbine used, and the characteristics of the network to which it is connected. These include the terminal voltage at the connection point, rated power, as well as the short-circuit capacity and impedance of the network to which it is connected. Grid-code specifications also often split reactive power requirements, specifying both the continuous and dynamic requirements from wind turbines. Regulating the amount of reactive power generated or consumed in response to abnormal power system voltage events is done by a controller assisting the grid, much like a conventional power plant would. The controller regulates reactive power by controlling the power factor of the supply to the grid and this

can be done in one of several ways depending on the type of wind turbine used. The most well-known of these would be to control the rotor power of a DFIG, using a converter. Not all wind-turbine technologies, however, have such a convenient ability of reactive power control, while they are also often located in remote areas resulting in major reactive power transmission losses. These factors present an ongoing challenge for wind turbines, with regard to the aim of ultimately being able to operate like a conventional power plant (Papathanassiou and Tsili, 2009).

Some grid codes, such as those of Eltra and Elkraft, require a simulation-type test to verify renewable-generation behaviour during abnormal voltage events, before being allowed to connect to the grid. This involves the simulation of a three-phase short circuit while operating at rated power, nominal rotor speed, and full compensation (Papathanassiou and Tsili, 2009). The system is modelled at 10 kV and represented by a Thevenin equivalent circuit of impedance  $0.1 + j 1.0$  ohm. During the simulation, the RMS value of the Thevenin circuit is varied according to the graph in Figure 2.6, after which the turbine is allowed no more than 10 seconds following the disturbance to reach its rated power output again. This test is followed by two three-phase short-circuit tests, two minutes apart. If a modelled wind turbine can ride through the simulated disturbances without disconnecting, it is seen as a pass (Papathanassiou and Tsili, 2009).

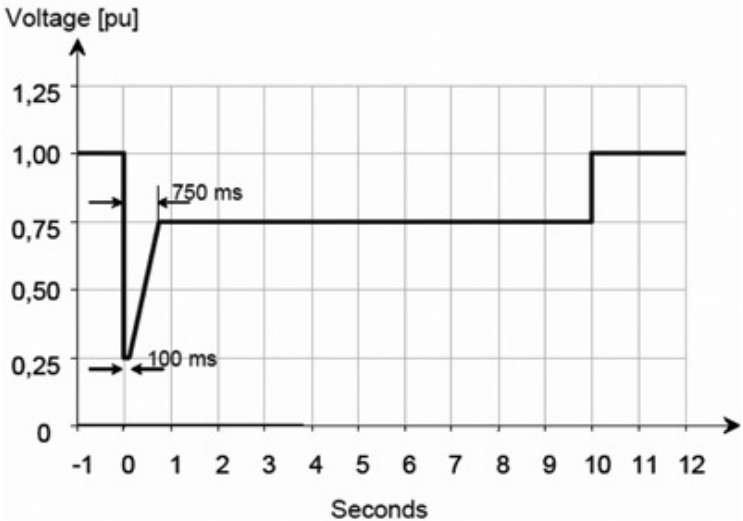


**Figure 0.6: RMS voltage variation for grid-code compliance test (Papathanassiou and Tsili, 2009)**

Danish grid codes specify a similar type of simulation for system voltages above 100 kV, requiring wind turbines to stay connected following asymmetrical faults on the grid. These include two-phase and single-phase transmission line faults, with unsuccessful reclosure. It is also required, as by most grid codes, that data exchange occurs between wind farms and system operators,

normally using supervisory control and data acquisition (SCADA) systems. Information exchanged includes that of voltage, current, active and reactive power output, setpoint values, wind speed, and operating status (Papathanassiou and Tsili, 2009).

## 2.6 South African grid-code requirements for renewable power plants

Like the grid codes of the other countries mentioned, South Africa has set its own standards and requirements for renewable power plants, before being allowed to connect to the South African grid. These requirements are specifically aimed at renewable generation methods including photovoltaic, concentrated solar power (CSP), small hydro, landfill gas, biomass, biogas, and wind. Generation methods are categorised based on output, as either one of the following: (NERSA, 2016).

- Category A: 0 to <1 kVA
- Category A1: 0 to 13.8 kVA
- Category A2: >13.8 kVA to <100 kVA
- Category A3: 100 kVA to <1 MVA
- Category B: 1 MVA to <20 MVA
- Category C: 20 MVA or greater.

RPPs in South Africa are required to withstand voltage and frequency deviations at the POC during both normal and abnormal operating conditions while providing grid support to maintain stability during abnormal events. That which is considered normal and abnormal differs depending on the category of RPP and must comply accordingly (NERSA, 2016).

### 2.6.1 Normal operating conditions

Normal operating conditions, during which an RPP should operate continuously without disconnecting, are defined for Category A as the voltage range from -15% to +10% of nominal voltage at the POC. For Categories B and C, normal deviation depends on the bus voltage at the POC, for which the respective ranges are provided in Table 2.1 (NERSA, 2016).

**Table 0.1: Normal operating range for category B and C RPPs in South Africa (NERSA, 2016)**

Nominal ( $U_n$ ) [kV]	$U_{min}$ [pu]	$U_{max}$ [pu]
132	0.90	1.0985
88	0.90	1.0985
66	0.90	1.0985
44	0.90	1.08



Nominal (Un) [kV]	Umin [pu]	Umax [pu]
33	0.90	1.08
22	0.90	1.08
11	0.90	1.08

The nominal frequency of the National Integrated Power System (NIPS) in South Africa is 50 Hz, for which the required continuous operating range is defined in grid codes. The two graphs of Figures 110 and 111 in Appendix A illustrate the minimum operating range required by the grid code for RPPs, during frequency deviations over the lifespan of the RPP, and system frequency disturbances respectively. Accordingly, RPPs are only allowed to disconnect under the following frequency disturbance conditions (NERSA, 2016):

- 1) If the frequency remains above 51.5 Hz for longer than four seconds.
- 2) If the frequency remains below 47.0 Hz for longer than 200ms.
- 3) If the frequency's rate of change exceeds 1.5 Hz per second.

Once disconnected, synchronisation to the NIPS is required before being allowed to reconnect. For Category A RPPs, the voltage should be in the range of -15% to +10% nominal voltage, and between 49 Hz and 50.2 Hz for a minimum of 60 seconds before being allowed to connect, or as otherwise agreed with the SO for special circumstances. For Categories B and C RPPs, TS connected RPPs should be within -5% to +5% nominal voltage range or should adhere to the requirements of Table 2.1 when DS is connected. The frequency should also be in the range of 49 Hz to 50.2 Hz, all for a minimum of three seconds before being allowed to connect, or as otherwise agreed with the SO during special circumstances (NERSA, 2016).

### **2.6.2 Abnormal operating conditions**

To support the grid in recovering from abnormal events, RPPs are required to withstand and ride through a variety of abnormal events without disconnecting or reducing their output. This includes phase jumps at the POC of up to 20°, after which normal operation should resume following a short settling period of no longer than five seconds. RPPs should also be able to tolerate sudden voltage drops or spikes, within the boundaries set by the grid code. Category A1 and A2 RPPs are required to adhere to the voltage conditions at the POC, as illustrated in Figure 112 of Appendix B. These are to be used in conjunction with the maximum disconnection-time table, available as Table 7.1 in Appendix B, establishing the boundary voltage conditions and times during which Categories A1 and A2 are required to remain connected.

Similar boundaries are set for the remaining Categories, A3, B, and C RPPs. These are illustrated by the bold lines representing the voltage limits for all phases during all types of faults in Figures 113 to 115 of Appendix B, apart from Area D on the graphs only applying to Category C RPPs. RPPs are therefore required to remain connected according to the boundaries set by the graphs while supplying or absorbing reactive current, as illustrated by Figure 116. RPPs should furthermore remain connected for a minimum time of 0.150 seconds, following a voltage drop to zero at the POC, except for Category B synchronous generators during symmetrical three-phase faults. Area D on the graphs requires Category C RPPs to withstand voltage spikes at the POC up to 120% for a minimum of two seconds, before being allowed to disconnect. If, during an abnormal voltage event, the voltage returns to Area A of the graph, subsequent drops will be considered as a new fault condition. Faults resulting in the voltage entering Area C allow for disconnection of the RPPs.

During symmetrical fault conditions in Areas B and D of Figures 113 to 115 in Appendix B, RPPs apart from synchronous generating units are required to contribute to reactive power control, as specified in Figure 116 of Appendix B. In Areas B and D, RPPs should remain connected, supplying or absorbing reactive current within their design capabilities to help stabilise voltage, with inverter-driven RPPs of Categories B and C required to be capable of disabling reactive-power support at any time if requested by the SO. When the voltage at the POC drops below 20%, RPPs are still required to supply reactive power within their design capabilities, only being allowed to disconnect once boundaries set in Figures 113 to 115 of Appendix B are breached. Reactive power control of RPPs is required to follow the characteristics set in Figure 116 of Appendix B with an accuracy of  $\pm 20\%$  after 60ms. When voltages enter Area B, the supply of reactive power takes a priority above that of active power, although the supply of active power is still required to be maintained during voltage drops. When voltage drops reach below 85%, a proportional reduction of active power is required regarding the design specifications of the RPP. Once a fault is cleared, it is required that the RPP restores active power production to at least 90% of the pre-fault value within one second.

Just like active power control assisting in stabilising grid voltages, power-frequency control is also required of RPPs to assist in stabilising grid frequency. This is done as per the graph Figure 117 of Appendix C, illustrating the mandatory active power reduction requirements set for all RPPs, which should meet an accuracy of  $\pm 10$  MHz or better. The limits set by the graph require RPPs to reduce their active power as a function of change in frequency once the NIPS frequency exceeds 50.5 Hz. If 51.5 Hz is exceeded for more than four seconds, RPPs are allowed to disconnect.

RPPs of Category C are required to provide power-frequency response per Figure 118 of Appendix C and, except for the mandatory frequency response discussed above 50.5 Hz, are not allowed to perform any frequency response before having reached an agreement with the SO over the values of  $f_1$  to  $f_6$ ,  $f_{min}$  and  $f_{max}$  on the graph. RPPs should therefore be able individually to set these values with an accuracy of 10m Hz or greater, to any value in the range of 47 Hz to 52 Hz. Points  $f_1$  to  $f_4$  on the graph are used to form a dead band, or control band, for the primary frequency response of RPPs, while points  $f_4$  to  $f_6$  are used to set the mandatory crucial power-frequency response, as discussed. The frequency droop settings of the graph are to be provided by the SO using the values of the various points and should be adjustable in the range of 0% to 10%. Should the active power be regulated down to a value below the design limit of an RPP, shutting down of the unit is allowed. RPPs should also be designed with the ability to provide  $P_{Delta}$ , which is the available active power reserve for frequency stabilisation, with a value of no less than 3%  $P_{available}$ . Depending on which yields the highest tolerance, accuracy of power-frequency control is required not to deviate more than  $\pm 2\%$  from the setpoint value, or  $\pm 5\%$  of rated power. Default values for  $f_1$  to  $f_6$ ,  $f_{min}$  and  $f_{max}$  are provided in Table 7.2 of Appendix C. However, as mentioned, values  $f_1$ ,  $f_2$  and  $f_3$  should first be agreed on with the SO before being applied (NERSA, 2016).

### 2.6.3 Reactive power requirements

Reactive power and power factor are always measured at the POC, unless specified otherwise. Categories A1 and A2 RPPs are required to operate at a unity power factor, unless otherwise agreed with the SO, while it is required of Category A3 RPPs to have the ability to operate at a power factor ranging from 0.95 lagging to 0.95 leading between 20% and 100% rated power. The default power factor is, however, unity, but the RPP should be able to operate according to a power factor characteristic curve, should it be required by the SO or National Strategic Plan (NSP).

It is required of Category B RPPs to be able to provide both voltage-power factor and reactive power control. Reactive-power support requirements measured at the POC are illustrated in Figure 119 of Appendix D when operating between 5% and 100% rated power. As  $Q_{min}$  and  $Q_{max}$  are voltage dependent, limits are defined in Figure 121 of Appendix D, according to voltage. Figure 120 of Appendix D is used to illustrate the reactive power requirements when operating at nominal POC voltage. No other reactive power requirements are specified when operating below 5% rated power; however, this should be in the range illustrated by points A to D on the graphs mentioned, which do not exceed  $\pm 5\%$  rated power.

Like Category B RPPs, it is required of Category C RPPs to be able to provide both power factor and reactive power control. Reactive-power support requirements measured at the POC are illustrated by Figure 122 of Appendix D when operating between 5% and 100% rated power, with

the  $Q_{\min}$  and  $Q_{\max}$  voltage dependent limits defined by Figure 123 of Appendix D. When operating at nominal voltage, reactive power requirements are defined by Figure 123 of Appendix D. No other reactive power requirements are specified when operating below 5% rated power; however, this should be in the range illustrated by points A to D on the graphs mentioned, which again do not exceed  $\pm 5\%$  rated power (NERSA, 2016).

#### **2.6.4 Reactive power and voltage control requirements**

RPPs of Categories B and C are required to have reactive power and voltage control at the POC, using setpoints and gradients determined by the NSP and SO. Although it is required of these RPPs to have voltage, power factor, and Q control, only one of the three is required to be achievable at a time.

Q control refers to the ability of an RPP, independent of active power and voltage, to be able to supply or absorb reactive power at the POC, according to the control function illustrated by Figure 124 of Appendix E. It is required that value changes made by the SO are executed within two seconds and that the RPP should be able to respond within 30 seconds following notification of the required setpoint changes. Setpoints are required to be implemented, depending on which yields the highest tolerance, with an accuracy of  $\pm 2\%$ , or  $\pm 0.5\%$  of the maximum reactive power, and a Q setpoint of at least 1 KVar. Power factor control refers to the control of reactive power at the POC, proportional to the active power output, as illustrated by the constant gradient of Figure 124 of Appendix E. It is required that changes made by the SO to these values are executed within two seconds and that the RPP should be able to respond within 30 seconds following receipt of the setpoint changes. Accuracy requirements state that the setpoint is not allowed to deviate more than  $\pm 0.02$  from the requested power factor value. Voltage control refers to the control of the voltage at the POC. It is required that changes requested by the SO to these values are executed within two seconds and that the RPP should be able to respond within 30 seconds following receipt of the setpoint changes. Voltage setpoint accuracy should be within  $\pm 0.5\%$  of the nominal voltage and should not deviate more than  $\pm 2\%$  from the absorbed or injected reactive power according to the droop characteristics, as defined by Figure 125 of Appendix E. The droop refers to the voltage change in pu, resulting from the change in reactive power. Upon reaching the design limit of the available range of an RPP, the RPP should wait for additional control measures, such as a tap changer to be implemented (NERSA, 2016).

#### **2.6.5 Power quality and protection requirements**

An extended set of power quality requirements are given in the South African grid-code document (NERSA, 2016), which includes the following main requirements. RPPs of Categories B and C are required, at minimum, to monitor and report on flicker, harmonics, and unbalanced voltages at the

POC using an IEC 61000-4-30 Class A monitoring device, as per the requirements and graphs discussed. It is furthermore the responsibility of the RPP to protect its facility, as well as the TS and DS, against damage that might arise from frequency deviations, supply and connection interruptions, voltage variations and dips, harmonics, flicker, voltage unbalance, and under- and over-voltages.

RPPs of all categories should also be capable of detecting islanded operation effectively, during which it is required of Category A RPPs to shut down generation within 0.2 seconds, or two seconds for Categories B and C RPPs. Although protection responsibilities mainly lie with the RPP, it is also required of the NSP to provide the RPP with all information required, such as the highest and lowest short-circuit current expected at the POC, to enable the RPP to establish the necessary protection for both its facility, and the TS and DS.

#### **2.6.6 Active power constraint requirements**

It is required that Categories A3, B, and C RPPs are able to curtail their active power output, mainly for system security reasons. This refers to the ability of an RPP to operate at a reduced active-power output level, helping to avoid imbalances in the NIPS, and overloading of the TS and DS during unstable conditions. This is like the three active power output operation modes discussed in the general grid-code requirement section and are defined by the South African grid code as follows:

The first constraint mode is known as the Absolute Production Constraint, which limits the active power output from the RPP at the POC to a predefined MW value. This mode is usually applied to provide protection for the TS and DS against overloading. Any changes in the predefined setpoint, apart from SHPPs, are required to commence within two seconds following receipt of the request and be completed within 30 seconds, with an accuracy of  $\pm 2\%$  of the setpoint value, or  $\pm 0.5\%$  of the rated power depending on which yields the highest tolerance. For SHPPs, the only difference is that changes should commence within five seconds following the request and should be completed in the minimum time with the highest accuracy achievable within its design limitations.

The second constraint mode is known as the Delta Production Constraint, which constrains the active power output of the RPP proportional to the achievable active power. This mode is usually applied to create a control reserve for frequency control purposes. Any changes in the predefined setpoint are required to commence within two seconds following receipt of the request, and to be completed within 30 seconds, with an accuracy of  $\pm 2\%$  of the setpoint value, or  $\pm 0.5\%$  of the rated power, depending on which yields the highest tolerance.

The third constraint mode is known as the Power Gradient Constraint, which limits the maximum rate of active power output change, considering the ability of available output power to support the gradients. This mode is usually applied to help limit the impact of changes in active power, which might affect the stability of the TS and DS. Any changes in the predefined setpoint are required to commence within two seconds following receipt of the request, and to be completed within 30 seconds, with an accuracy of  $\pm 2\%$  of the setpoint value, or  $\pm 0.5\%$  of the rated power depending on which yields the highest tolerance (NERSA, 2016).

The effect of implementing these three modes respectively can be seen illustrated in Figure 2.7, considering the different points, as indicated.

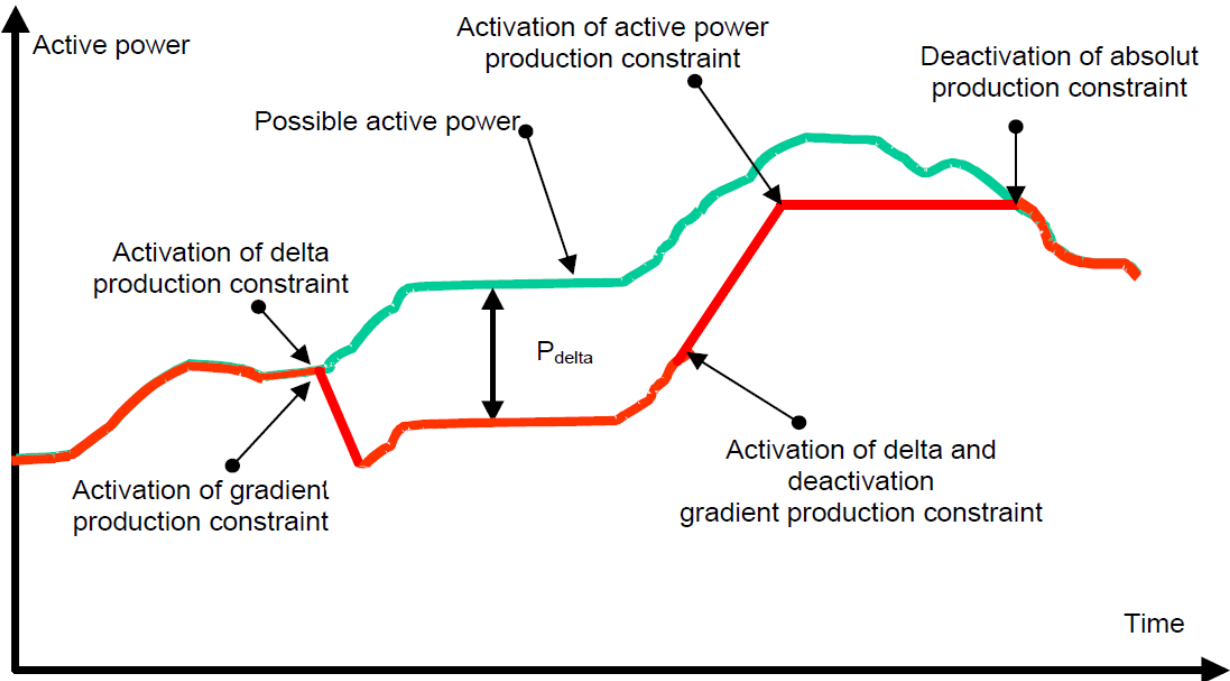


**Figure 0.7: Active power control functions (NERSA, 2016)**

**2.6.7 RPP control requirements**

It is required of RPPs to be able to control the ramp rate of their active power output, as set by the SO or NSP, during any range of operations including positive ramp rate during start-up and normal operation, as well as negative ramp rate during controlled shut-downs. Further control requirements set for the different category RPPs are listed in Table 2.2.

**Table 0.2: RPP control requirements****(NERSA, 2016)**

Control function	Category A3	Category B	Category C
Frequency control	-	-	X
Absolute production constraint	X	X	X
Delta production constraint	-	-	X
Power gradient constraint	X	X	X
Q control	-	X	X
Power factor control	-	X	X
Voltage control	-	X	X

**2.6.8 RPP data and control signal requirements**

A full list of signal requirements is available in the South African grid-code requirements for RPPs (NERSA, 2016), for which those most important are summarised here. It is first required that all digital signals be time-stamped with an accuracy of +/- 1 millisecond or greater and should be available within one second following any changes required to be reported. These include changes greater than or equal to the following:

- Frequency changes of 0.01 Hz or greater.
- Power factor changes of 0.01 or greater.
- Active power changes of 1% rated power or greater or, in the case of rated power being greater than 50 MW, value changes of 0.05 MW or greater.
- Ramp rate changes of 1 MW/min or greater.
- All other changes in full-scale or nominal values of 1% or greater.

**2.6.9 Signal and data requirements from RPPs to SO**

The following section on data requirements applies to Categories B and C RPPs, unless stated otherwise, and is required to be made available to the NSP/SO. The first set of data requirements surrounds the generating capacity of the RPP, as well as the forecasted output that is essential to the NSP and SO to maintain a stable and balanced system. These data requirements include the following, as specified in the South African RPP grid codes:

- Available MW power value, as well as the forecasted hourly available power for the day ahead, and week to come.
- Available MW and hourly forecast for the coming six hours, updated 10 to 20 minutes before each hour.

- Available forecasted MVar for the coming six hours, updated 10 to 20 minutes before each hour.

These are, however, only a fraction of the data and information required from RPPs. The rest are divided into logical groups based on functionality, forming several signal lists required to be made available for the POC via designated communication gateway equipment located at the RPP site. List #1 consists of the general signal requirements and requires the information below, as taken from the South African grid-code requirements for RPPs (NERSA, 2016):

- Actual sent out (MW) at the POC
- Actual ramp rate of the entire RPP
- Reactive power import/export (-/+Mvar) at the POC
- Current sent out
- Power factor
- Voltage output
- Frequency
- Breaker status
- Isolator status
- Supervisory switch status
- Plant islanded
- Plant shutdown
- Plant trip on loss of grid detection

List #2 consists of the RPP generator meteorological data and requires the following information to be made available, as taken from the South African grid-code requirements for RPPs (NERSA, 2016):

- Wind speed (within 75% of the hub height) – measured signal in meters/second (for *WPP only*)
- Wind direction (within 75% of the hub height) – measured signal in degrees from true North (0-359) (for *WPP only*)
- Air temperature-measured signal in degrees centigrade (-20 to 50)



- Air pressure-measured signal in millibar (800 to 1400)
- Air density (for WPP only)
- Diffuse solar radiation (for solar power plants only)
- Direct solar radiation (for solar power plants only)

It is furthermore required that data be provided utilising a dedicated meteorological mast, or equipment with similar or greater accuracy, positioned at the RPP site to provide optimised predictability. This is especially important for widely dispersed wind turbines, which would require meteorological data from several individual masts to achieve the desired accuracy. As a guideline, minimum requirements are set by grid codes as at least one meteorological data mast for every 10x10 km square area.

List #3 requires the frequency response system settings and consists of only one essential requirement to be made available, as taken from the South African grid-code requirements for RPPs (NERSA, 2016).

- Frequency response system mode status indication (ON/OFF) as a single bit point

List #4 consists of the active power constraints and requires the following information to be made available, as taken from the South African grid-code requirements for RPPs (NERSA, 2016):

- Curtailment mode status (ON/OFF) as a single bit point
- Curtailment in progress as a single bit point
- Curtailment setpoint feedback
- Curtailment mode state (Not ready/Ready) as a single bit point
- P-delta constraint mode (ON/OFF) as a single bit point
- P-delta setpoint feedback
- P-delta mode (Not ready/Ready) as a single bit point
- Power gradient constraint mode (ON/OFF) as a single bit point
- Up-ramp rate setpoint feedback
- Down-ramp rate setpoint feedback
- Power gradient constraint mode (Not ready/Ready) as a single bit point

List #5 consists of the reactive power and voltage control data, and requires the following information to be made available, as taken from the South African grid-code requirements for RPPs (NERSA, 2016):

- Reactive power control mode (ON/OFF) as a single bit point
- Reactive power control setpoint/raise or lower command
- Reactive power lower limit
- Reactive power upper limit
- Reactive power control mode (Not ready/Ready) as a single bit point
- Power factor control mode (ON/OFF) as a single bit point
- Power factor control setpoint/raise or lower command
- Power factor control setpoint feedback
- Power factor control mode (Not ready/Ready) as a single bit point
- Voltage control mode (ON/OFF) as a single bit point
- Voltage control setpoint/raise or lower command
- Voltage control mode setpoint feedback
- Voltage control mode (Not ready/Ready) as a single bit point

#### **2.6.10 Signal and data requirements from so to RPPs**

The following control signals are provided by the SO, which RPPs should be able to receive and act on accordingly. These are taken from the South African grid-code requirements for RPPs (NERSA, 2016), which requires the following:

- A connection point circuit breaker (CB) trip facility provided by the NSP to allow disconnection of the RPP at the high-voltage side of the POC. Trip signals should be able to be provided by both the SO and NSP
- Primary frequency control ON/OFF
- Primary frequency control ON/OFF
- Curtailment mode ON/OFF

- Curtailment setpoint command
- Stop command
- P-delta mode ON/OFF
- P-delta setpoint command
- Power gradient constraint ON/OFF
- Up ramp rate setpoint command
- Down ramp rate setpoint command
- Reactive power control mode ON/OFF
- Reactive power control setpoint command
- Power factor mode ON/OFF
- Power factor setpoint command
- Voltage control mode ON/OFF
- Voltage control setpoint

#### **2.6.11 Communication specifications and requirements**

It is required that the SCADA Master Station protocol compatible communication gateway be owned, operated, maintained, and located at the RPP control room. Communication requirements are further specified extensively in the South African grid-code document (NERSA, 2016). However, since it is not relevant to the scope of this study, it will not be reviewed in detail here.

#### **2.7 Faults and disturbances on South Africa's electrical network:**

The first to be considered is known as a low-frequency incident. This refers to occurrences where system frequency drops to below 49.5 Hz for more than one second, as specified in the grid codes discussed. Such an occurrence is usually caused by an imbalance between supply and demand, often owing to a lack of reserve capacity in the system. Considering the time from 2007 to 2012, during which a total 117 low-frequency incidents occurred, it can be noted that low-frequency events very rarely exceed 15 per year. In 2008, however, low-frequency events reached 69, which is concerningly high compared to other years. It is worth noting that this was during the time when South Africa experienced several load shedding events, as a result of a lack of generation capacity, which presents the evidence that low-frequency events can be curtailed by having adequate reserve capacity (NERSA, 2012; Ateba and Prinsloo, 2019).

Another common disturbance is line faults, caused either by environmental or design influences. Commonly, the majority of these are caused by environmental conditions, such as lightning, contamination, birds, or fires. Considering the same period as above, around 2.5 line faults occurred on average per 100 km in South Africa. During this time, most occurred in 2011, at which time 2.72 faults per 100 km were recorded. Increased line maintenance and additional fire-management teams can be implemented to reduce this number. However, on average, it tends to remain relatively constant, as it is often caused by uncontrollable natural circumstances (NERSA, 2012).

As an overall indicator of the electrical network's stability in South Africa, transmission-system interruption time can be considered. This refers to the duration and amount of time that supply is interrupted, expressed in minutes of peak national demand, not including planned load shedding. This is divided into two categories, of which the first refers to network incidents contributing less than one system minute. For such smaller, shorter-duration incidents, interruption time remained between 2.63 and 4.73 minutes per year, considering the same period as above. The second category considers larger events contributing one or more system minutes per event. These remained between 0 in 2011 and 9.87 in 2008, which again was the year when South Africa struggled to maintain supply, and had to implement planned load shedding (NERSA, 2012; Ateba and Prinsloo, 2019).

## **2.8 South Africa's grid infrastructure**

To develop an efficient and effective testbed for renewable-integration studies in South Africa, it is important to have a test grid resembling that of the South African grid, as each is unique. The existing infrastructure, generation, and distribution layout can therefore be assessed, contributing to the accuracy of the South African grid-representing model.

The power industry in South Africa is almost exclusively dominated by Eskom, South Africa's primary electricity supplier, with most private and independent power producers only entering the market since 2003, following the approval of private-sector participation in the electrical industry divided between Eskom (70%), and Independent Power Producers (IPPs) (30%). Regulation of the state-owned company Eskom falls on NERSA, who grants all licences to Eskom according to the relevant electricity acts of South Africa. Eskom still supplies approximately 90% of the electricity consumed in the country, and 40% of the electricity consumed in Africa, using a combination of coal, gas, hydro, nuclear, and pumped storage power stations. In 2018, Eskom owned 30 operational power stations contributing approximately 44 134 MW to the total installed capacity of 51 309 MW, as indicated by the 2018 energy sector review of the Ministry of Energy. Of Eskom's installed capacity, 36 441 MW are generated using coal, 2 724 MW using pumped

storage, 2 409 MW using gas-fired power plants, 1 860 MW using nuclear, 600 MW of hydropower, and 100 MW using the Sere wind farm. The remaining 10% of grid capacity comprises 3 162 MW or 6% in renewable power connected to the grid through the REIPPPP as of the start of 2018, while the remaining 4% comes from 22 small municipally owned power stations. Grid-integrated REIPPPP renewables are, however, increasing and, by the start of 2019, the programme already produced about 6 400 MW from its projects, of which 4 000 MW were grid connected at the time, compared to the 3 162 MW approximately a year earlier (Eskom, 2009; 2018, 2019b; Power Africa, 2018; RSA Department of Energy, 2018).

According to the Eskom website, their current fleet of power plants with their respective capacities can be categorised as per Table 2.3. Note in the status column that some are still under construction and not yet fully operational, since partially operational power plants under construction were also considered. Planned power plants were, however, not included, as there is no guarantee that they will enter the construction phase. For this study, the capacities from partially operational power plants will be considered once completed and fully operational shortly, as this provides a more accurate representation of the network for renewable-integration studies (Eskom generation division, 2019).

**Table 0.3: Eskom-owned and operated power plants**

#	Power station name:	Status:	Generation type:	Fuel type:	Location:	No. of units:	Total capacity (MW):
1	Arnot	Operational	Base load	Coal	Mpumalanga	6	2 352
2	Duvha	Operational	Base load	Coal	Mpumalanga	6	3 600
3	Hendrina	Operational	Base load	Coal	Mpumalanga	10	2 000
4	Kendal	Operational	Base load	Coal	Mpumalanga	6	4 116
5	Koeberg	Operational	Base load	Nuclear	Western Cape	2	1 940
6	Kriel	Operational	Base load	Coal	Mpumalanga	6	3 000
7	Lethabo	Operational	Base load	Coal	Mpumalanga	6	3 708
8	Majuba	Operational	Base load	Coal	Mpumalanga	6	4 110
9	Matimba	Operational	Base load	Coal	Limpopo	6	3 990
10	Matla	Operational	Base load	Coal	Mpumalanga	6	3 600
11	Tutuka	Operational	Base load	Coal	Mpumalanga	6	3 654
12	Camden	Operational	Base load	Coal	Mpumalanga	8	1 510
13	Grootvlei	Operational	Peak load	Coal	Mpumalanga	6	1 200
14	Komati	Operational	Base load	Coal	Mpumalanga	9	1 000
15	Gariiep	Operational	Peak load	Hydro	Border of Eastern Cape	4	360
16	Vanderkloof	Operational	Peak load	Hydro	Northern Cape	2	240
17	Drakensberg	Operational	Peak load	Pumped storage	KwaZulu-Natal	4	1 000

#	Power station name:	Status:	Generation type:	Fuel type:	Location:	No. of units:	Total capacity (MW):
18	Palmiet	Operational	Peak load	Pumped storage	Western Cape	2	400
19	Acacia	Operational	Peak load	Gas turbine	Western Cape	3	171
20	Port Rex	Operational	Peak load	Gas turbine	Easter Cape	3	171
21	Ankerlig	Operational	Peak load	Gas turbine	Western Cape	9	1 338
22	Gourikwa	Operational	Peak load	Gas turbine	Western Cape	5	746
23	Sere	Operational	Self-dispatching	Wind	Western Cape	46	100
24	Medupi	Partially operational	Base load	Coal	Limpopo	6	4 788
25	Kusile	Partially operational	Base load	Coal	Mpumalanga	6	4 800
26	Ingula	Partially operational	Peak load	Pumped storage	Free State and KwaZulu-Natal border	4	1 332
27	First Falls	Operational	Stabilise distribution network	Hydro	Eastern Cape	1	6
28	Second Falls	Operational	Stabilise distribution network	Hydro	Eastern Cape	1	11
29	Colley Wobbles	Operational	Stabilise distribution network	Hydro	Eastern Cape	1	42
30	Ncora	Operational	Stabilise distribution network	Hydro	Eastern Cape	1	2

**Total (MW): 55 287**

**Table 2.3 generated using: Newbery and Eberhard (2008), Sourcewatch (2011), Generation Communication (2011), NERSA (2012), Eskom (2016; 2017; 2018; 2019d; 2019c; 2019a), Gupta (2017a; 2017b; 2017c), Barradas (2019), Prinsloo and Burkhardt (2019), SABC News (2019), Eskom generation division (2019).**

It should be noted that the total installed capacity of 55 287 MW shown Table 2.3 differs from the 51 309 MW stated in the 2018 energy sector overview of the Ministry of Energy. This is because the study took the total capacity of Medupi and Kusile power station into account once finished, as they are already partially operational and set to be completed. The current status, as of mid-2019, is that Medupi has four units operating with two yet to be commissioned and grid synchronised, while Kusile has three operating with three yet to be commissioned and grid synchronised (Sourcewatch, 2011; Barradas, 2019; SABC News, 2019; TimesLive, 2019). Eskom, therefore, owns and operates 15 coal, 6 hydro, four gas turbine, three pumped storage, one nuclear, and one wind power plant. Considering that half of Eskom's power plants, and most of

the power generated, use coal, it once again confirms South Africa's major reliance on fossil fuels, and specifically coal to supply its electrical needs.

**Table 0.4: Share of renewables connected to the South African grid**

#	Technology:	Operational capacity (MW):	Commissioned grid-connected capacity (MW):	Determined capacity after completion of 7 <sup>th</sup> bid window (Bid window 2S2)
1	Onshore wind:	3 357	1 980	6 360
2	Solar photovoltaic (PV):	2 292	1 474	6 225
3	Concentrated solar power (CSP):	600	300	1 200
4	Other (biogas, biomass, landfill gas and small hydro):	173	22	940
<b>Total (MW):</b>		<b>6 422</b>	<b>3 776</b>	<b>14 725</b>

**Table 2.4 generated using: Department of Energy and Department of National Treasury (2018), RSA Department of Energy (2018).**

Table 2.4 illustrates the success achieved by the REIPPPP until March 2018, in producing energy from renewables in South Africa. As illustrated, 3 776 MW usable capacity from 62 projects is already connected to the South African grid, having produced 24 913 GWh of electricity since the first project was commissioned and grid connected in November 2013. The connected capacity of 3 776 MW represents 54% of the 2020 target and contributes 21% towards the 2030 target of the IRP. In total, 112 projects with a capacity of 6 422 MW are already operational, representing 44% of the targeted renewable capacity of 14 725 MW identified by four separate ministerial determinations between 2011 and 2016. Of the 112 operational projects, 68 are solar, which represents the largest number of IPP projects. These projects are mostly concentrated in the Northern Cape, while the Eastern and Western Cape are proving to be most ideal for wind projects, with 17 and 14 projects respectively (D'Sa, 2005; Department of Energy and Department of National Treasury, 2018).

In addition to the Eskom and REIPPPP power plants, municipalities and private companies also own several smaller power plants. These will, however, not be considered for this study, as they tend to have limited capacity and minimal impact on the larger grid network. These are also mostly operated in a manner where most to all electricity produced is consumed on-site, limiting external sales to the unconsumed electricity generated. In fact, in most cases these sites tend to consume more electricity from the grid than they feed in which, as mentioned, is why they are not worth considering (NERSA, 2012; Sewchurran and Davidson, 2016).

Another important consideration in developing a real-time testbed for renewable-integration studies is the layout of the South African grid. An accurate representation could help to identify possible problems such as bottlenecks in the system, especially with the addition of renewable generation, as they tend to be location sensitive, depending on the resource. Eskom owns the national transmission system in South Africa, comprising 32 220 km of 88 kV to 765 kV transmission lines, and a combined total of 147 415 MVA in substation capacity. These also extend cross-border for electricity trade with Namibia, Botswana, Zimbabwe, Mozambique, Swaziland, and Lesotho. Additionally, 48 805 km of distribution lines, 296 188 km of reticulation lines, and 7 499 km of underground cables with a primary voltage of between less than 1 kV to 132 kV are also owned by Eskom, making it the largest power-line network in Africa. Annually, as per 2017 figures, these lines distributed 229 342 GWh of electricity to municipalities and industrial, mining, commercial, agricultural, and residential customers across South Africa (NERSA, 2012; Eskom, 2018; 2019b; RSA Department of Energy, 2018; Statistics South Africa, 2018).

The layout of South Africa's power system can be seen represented on maps (Eskom holdings limited, 2008; Newbery and Eberhard, 2008; Eskom, 2009; 2016; 2019b; Global Energy Network Institute, 2016). The latest version of these appears in the Transmission Development Plan 2019–2028 as Figure 126 of Appendix F. This document also includes close-up maps of the network of the respective provinces in both its current state, and with the proposed future alterations and upgrades indicated (Eskom, 2019b). Considering these, it is notable that much of the transmission network comprises 400 kV lines, while the 533 kV and 765 kV lines form the backbone of the network. It is also clear that most of the network is concentrated in areas where most power stations are located, which is to be expected.

## **2.9 South Africa's energy future**

It has been well documented and determined, following South Africa's struggle with load shedding in the past that an urgent need exists for expansion and upgrades to the electrical network and generation infrastructure in the country. This is not only essential to keep up with the increasing electricity demand, but also to replace existing aging infrastructure and power plants. The need for load shedding in the past is furthermore an indication that South Africa needs to increase its generation reserve margin which, by 2014, was as low as 1% of the installed grid-connected capacity, of around 44 000 MW at the time. This was set to be increased to at least 19%, or 54 000 MW of operational grid-connected capacity by 2019, to provide security of supply sufficiently. Recalling figures from the previous section on the current installed capacity, it can be concluded that this target was most likely never reached, based on early 2019 figures. Nevertheless, it is still within reach and an important target to pursue. Making this target reachable, are Eskom's two



major power plant projects under construction, namely Medupi and Kusile, combined with ongoing REIPPPP projects, which have already contributed significantly to increasing South Africa's reserve generation margin to date (Department of Energy and Department of National Treasury, 2018; Ateba and Prinsloo, 2019).

A generation addition target of 17 800 MW is set by the 2030 IRP for South Africa, of which 5 000 MW are set to be operational by the end of 2019, and an additional 2 000 MW by the following year. New capacity determinations by the 2030 IRP of South Africa can be broken down further as follows. They include the addition of the aforementioned 14 725 MW of renewables, consisting of 6 225 MW solar PV, 6 360 MW wind, 1 200 MW CSP, 195 MW small hydro, 25 MW gas, 210 MW biomass, 110 MW biogas, and small-scale renewable energy projects to a combined total of 400 MW. They also include the addition of 6 250 MW of coal-fired power, of which 3 750 MW is set to be from cross-border projects, as well as 1 800 MW of co-generation, 3 729 MW of gas-fired power, and 2 609 MW of imported hydro. Of the 14 725 MW addition of renewables target, 44% has already been reached, as previously discussed, which comes as a result of the seven successfully completed REIPPPP bid windows, of which all projects in bid windows 1 and 2, and 10 projects from bid window 3 are already operational (D'Sa, 2005; Department of Energy and Department of National Treasury, 2018; RSA Department of Energy, 2018).

To support the additional generation capacity, future energy mix, and changing needs of customers, upgrades to the transmission and distribution network should be regarded as just as important as the addition of renewables to the future generation mix. This need has since led to planned future upgrades noted as dotted lines indicated on the map of South Africa's transmission network in Figure 126 of Appendix F, as well as in Eskom (2016; 2019b). These upgrades are essential, since failure to upgrade and adapt weaker parts of the bigger network will result in weak spots, threatening the ability to ensure continuity and security of supply. Based on this, the need for a real-time simulation tool can once again be argued, because future expansions will result in a changing energy mix, which will require simulation to identify any problems and weak spots leading to physical construction and integration (Department of Energy and Department of National Treasury, 2018; Eskom, 2019b).

## **2.10 Cost of renewables in South Africa**

The increased use of renewable-generation technology worldwide has caused the initially high prices of these technologies to plummet in recent years, while continuous development has produced renewable-generation equipment that is much more efficient than its predecessors. A point has therefore been reached where renewables are not only able to compete with conventional technologies in terms of R/kWh, but are even able to exceed their abilities in

providing electricity at attractive prices (Department of Energy and Department of National Treasury, 2018).

Considering South Africa, the price of electricity produced by renewables at the start of the REIPPPP in 2013 was, on average, R2.65/kWh. This has since come down to an average of R0.86/kWh by 2018, and is still on the decrease. Considering the individual technologies, solar PV has seen the most substantial drop of 75% in price during this timeframe, now producing electricity at around R0.96/kWh. This is followed by wind, which has seen a reduction of 50% in price, now producing electricity at about R0.79/kWh. CSP has, on average, seen a reduction of 6%, to R3.50/kWh between REIPPPP bid windows 1 and 2, and an additional reduction of 7% to R1.90/kWh between bid windows 3 and 3.5. Small-scale renewable projects, which can be expected to produce electricity at higher prices owing to the smaller generation scale, have also seen a reduction. During their original bid window, it was projected that electricity will be produced at around R1.47/kWh; however, by the second bid window small solar PV projects have already managed to produce electricity at an average of R1.06/kWh (Department of Energy and Department of National Treasury, 2018).

While new and ongoing renewable installations still managing to decrease the R/kWh of the electricity produced, the same cannot be said of fossil fuel projects and power plants. An example of this would have to be the partially operational and still under construction Medupi and Kusile power plants. Original 2012 estimates quoted electricity production for these power plants at R0.54/kWh and R0.73/kWh respectively, which is still below the price capabilities of local renewable projects. Since then, increases in financing costs as well as for operating costs, such as coal prices, have caused prices to go up to a more realistic R0.71/kWh and R0.96/kWh respectively, which is similar to that for renewables. Industry counter-estimates for Medupi, however, estimate current generation costs to be even higher at about R1.28/kWh, which then becomes more expensive than generating electricity using renewable power plants (Department of Energy and Department of National Treasury, 2018).

### **2.11 Maximum renewable penetration and simulation of fault conditions on the Indian grid**

Establishing the effectiveness of grid codes and new generation is considered a vital step before implementation, as it would be impractical and dangerous to test the behaviour of equipment during abnormal conditions following implementation and grid commissioning. Testing equipment behaviour by considering possible abnormal events is traditionally done by simulating a network using the appropriate software package. Additionally, real-time simulators are now also used to obtain a better and more accurate representation of the real-world outcome.

A study that set out to determine the maximum wind penetration levels achievable in India's Tamil Nadu state by simulating the local network, produced the following conclusions. Such results are considered important, since increasing the penetration of, for example, wind power inevitably displaces the percentage of power produced by conventional power plants. This means that less power is now being supplied by conventional synchronous machines, of which the behaviour and control following an abnormal event are well known and understood by operators, and replaced with lesser-known asynchronous machines (Sreedevi *et al.*, 2016). Although it is now required by most grid codes that renewable power plants operate like conventional power plants in terms of contributing to grid stability during disturbances, earlier installations were not held to these standards and were not required to contribute to voltage or frequency control. Instead, they were simply required to disconnect in the event of a grid disturbance, which is problematic at high penetration levels as this can quickly lead to instabilities, even during otherwise harmless disturbances. Nevertheless, even modern turbines are limited in their capabilities, influencing the transient stability of a system. This is mainly due to wind turbines being located at different, and often remote locations as compared to conventional power plants, and having a different power flow for which most power systems are not optimised. Wind turbines also almost always require big step-up transformers, as they generate electricity at lower voltage levels as compared to conventional synchronous generation power plants, while also making use of different generator technologies (Sreedevi *et al.*, 2016).

For the Indian study to determine the maximum penetration limit of wind power without compromising the stability of the TANGEDCO network simulated, several penetration levels were considered. As per the Indian grid code, it is required that the network at its maximum penetration level, to be determined by the study, will have to be able to ride through single- and multi-phase faults at transmission voltage level (Sreedevi *et al.*, 2016).

Simulations of the TANGEDCO network were conducted and modelled using SIMPOW software. When constructing the network, wind turbines forming part of a wind farm were modelled as individual generators, integrated at either 11 kV, 33 kV or 110 kV. Conventional power plants were modelled as synchronous machines with one damper winding in the d-axis, two damper windings in the q-axis, and an IEEE-Type I exciter. Wind turbines in the TANGEDCO network are of both synchronous and asynchronous generator types. Synchronous generators were modelled as conventional generators, while the asynchronous turbines were modelled as induction generators (Sreedevi *et al.*, 2016).

After modelling the network, load-flow studies were conducted for two scenarios. In the first, the total network capacity is 14 947 MW, which corresponds to the actual value of the TANGEDCO

network at the time. Of this, 10 942 MW makes up the power produced by conventional power plants, while wind generation contributes the remaining 4 001 MW, representing 58.66% of the total installed wind capacity at the time. To ensure bus voltages remained within the limits of grid codes, capacitor compensation to the extent of 268 MVAR was added at 110 kV level. Wind capacity penetration for scenario 1 was calculated by dividing the MW contribution of wind power by the total MW capacity of the network, producing a wind penetration level of 26.8%. For scenario 1, the load flow converged, with no grid-code limit violations noted by the study (Sreedevi *et al.*, 2016).

Scenario 2 kept the TANGEDCO network capacity of 14 947 MW constant while increasing the percentage of power contributed by wind energy. The threshold value was found to be 67.17% of the total installed wind capacity, after which the load-flow solution did not want to converge. At 67%, voltage limits at the 400 kV buses were within the limits of 0.95 to 1.05 pu set by grid codes, while some of the 220 kV bus voltages were below 0.9 pu. The most notable code violations were, however, on the 110 kV buses, where power compensation to the extent of an additional 620 MVAR was required to comply with the allowable range of 0.92 to 1.1 pu. Wind capacity penetration at this point can then again be calculated using the method of scenario 1, yielding a maximum penetration level of 29.3% for scenario 2 (Sreedevi *et al.*, 2016).

Using the actual configuration of the TANGEDCO network, like that of scenario 1, stability studies were also conducted, considering the loss of conventional and wind generation, LVRT capability, load throw-off by connecting a highly inductive load, and reserve margin measures required for high wind penetration levels. In the first scenario, 920 MW of conventional generation were removed from the network, while studying the rotor angle of the remaining machines. It was found that for scenario 1, the system remained stable, with the rotor angles settling following the loss of generation. Scenario 2 considered the loss of wind turbines, for which the effect and extent of the voltage dip would vary depending on the type of wind turbines disconnected. For the TANGEDCO network, removing 12.6%, and then 14.2% of the power generated by wind turbines did not affect the stability of the system. It was only when all wind-turbine-generated power amounting to 16.71% of the total generation was removed, that the system experienced instability. This corresponds to removing 2497.76 MW from the network. The same tests were also conducted using the system of the scenario 2 load-flow study, which found that, when removing more than 14.95% of the wind generation from that system, it started to experience instability (Sreedevi *et al.*, 2016).

Next, the study considered the LVRT capabilities of the network. It can be noted that constant speed turbines are not capable of LVRT unless additional equipment is implemented to assist

during such disturbances. Wind turbines making use of DFIG or PMSG, on the other hand, can deal with such disturbances. The performance of the network during low-voltage conditions was tested by inserting three-phase to ground faults at different buses for the duration of eight cycles. This type and duration of fault were chosen, since generators are expected to remain connected during such events, according to local Indian grid codes. Results from this simulation revealed that the network met the standards set by local grid codes, being able to ride through all faults simulated without disconnecting (Sreedevi *et al.*, 2016).

The next test involved connecting a highly inductive load of 100 MW + j 105 MVAR to the network for one second. This resulted in a voltage spike at the connected bus, yet the system managed to remain stable. The final consideration for the network was that of the reserve required to maintain system stability, as loads connected to the network change constantly. As required by local Indian grid codes, a reserve of 3.7% to 4.7% is required for 30% wind penetration in a network. Calculated, this amounts to a reserve of 553 MW for load-flow scenario 1, and 579 MW for load-flow scenario 2 (Sreedevi *et al.*, 2016).

The study concluded that, for the current wind generation penetration of 26.8%, the network is stable, and complies with local Indian grid codes. It was found that, for the network simulated, the wind penetration level can only increase to 29.3%, after which it will become unstable. This information is vital, providing a threshold to keep in mind during future integration of wind energy if stability is to be maintained (Sreedevi *et al.*, 2016).

## **2.12 Wind turbine background**

An essential part of developing a real-time testbed for renewable-integration studies involves selecting the appropriate type of renewable generation to use in the simulation, allowing accurate studies to be performed on the network, to contribute positively to further development and improvements. Being able to identify the different types of wind turbines and solar technology, and the criteria which set them apart from one another, aids in selecting the appropriate equipment and generation to simulate.

Starting with wind turbines, the first criterion to be considered is size. By today's standards, wind turbines with a power output of 300 kW or less are generally considered small- to medium-sized and find their application in residential and commercial markets, often used to supplement other supply methods. The capacity of large wind turbines has seen a significant increase since their early days, with 126 m wingspan wind turbines now reaching outputs of 7.5 MW, and ongoing development to increase this even further (Wu *et al.*, 2011). The motivation to build wind turbines as large as limiting factors of the physical components and materials would allow, stems from the

exponential increase in output, which is a function of the square of the rotor radius, compared to cost.

As a result of the large output ability of large wind turbines, they often operate as part of a grid-connected system. They can, however, also be implemented for stand-alone applications where grid connectivity is unavailable, such as in remote villages, farms, or on islands. For a stand-alone system to generate a reliable supply of power, other forms of supply are often also incorporated, because a wind turbine's ability to generate power is subject to the availability of wind. For this reason, only a small percentage of wind turbines in operation form part of a stand-alone system, with most feeding the power generated to a grid (Wu *et al.*, 2011).

Location is another important consideration, especially for larger and multiple wind turbines intended to form part of a wind farm. Although traditionally, wind farms have mostly been situated on land, recent years have seen the increased installation of offshore wind farms, largely in European countries. This is done since the steady higher wind speeds present offshore increase efficiency while reducing the environmental impact of audible noise generated by unsightly wind turbines. Offshore wind farms, however, do not come without added challenges, as the harsher conditions at sea significantly increase installation and maintenance costs. To minimise this, especially maintenance costs, offshore wind-turbine designs often utilise direct-drive low-speed permanent-magnet-synchronous generators, eliminating maintenance-intensive elements such as a gearbox and brushes (Wu *et al.*, 2011). The trade-off to this simpler rugged design is a reduction in efficiency; however, increased offshore wind speeds and stability help to mitigate this, making it a worthy trade-off compared to the increased maintenance costs. However, little can be done about the capital costs associated with offshore installations, since increased cable spans and the complexity of projects is significantly higher when compared to on-land installations (Wu *et al.*, 2011).

In addition to the horizontal-axis wind turbines commonly thought of when considering wind turbines, vertical-axis designs, although much less common, are also available. This type of turbine makes use of spin axes positioned perpendicular to the ground, often kept upright with the help of guide wires. The orientation of the spin axis to the ground means that heavy equipment such as the generator and gearbox are installed at ground level, reducing tower-design complexity while simplifying construction and maintenance, ultimately reducing costs compared to that of horizontal-axis designs. The nature of this design does, however, require the need for a long rotor shaft, which is prone to mechanical vibrations, while a considerable percentage of the blade surface area is situated close to the ground in weaker air streams, limiting its aerodynamic performance. In contrast to this, horizontal-axis wind turbines are more efficient at utilising the

available wind resources, since the blades designed with features such as pitch control are positioned high on a tower, enabling better energy capture for a wider variety of wind conditions. Although slightly more expensive to construct and maintain, the higher efficiency and controllability in a variety of conditions have ultimately resulted in the horizontal-axis wind turbine dominating the market today (Wu *et al.*, 2011).

Wind turbines can further be classified according to their operating flexibility, as either fixed- or variable-speed wind turbines. Fixed-speed turbines operate at an almost constant speed, varying no more than 1% from the rated speed governed by grid frequency, gearbox ratio, and the number of generator poles (Papathanassiou and Tsili, 2009; Wu *et al.*, 2011). These types of generators therefore only have a given wind speed at which their efficiency is at its peak, with efficiency quickly degrading when this is not reached or exceeded. Its inability to speed up during wind gusts, or during higher than optimal wind speeds, also requires this type of turbine to make use more sturdily designed equipment, capable of absorbing the additional stresses generated during suboptimal wind conditions. The generated output power is also often less than ideal in quality, fluctuating with wind conditions which can cause disturbances on the grid (Wu *et al.*, 2011).

The main components of a fixed-speed wind turbine usually include a gearbox, converting turbine speed to the optimal generator speed for delivering rated power at the available wind speed. A transformer is also used for converting generator voltage to match that of grid voltage. A three-phase capacitor bank is installed to compensate for reactive power drawn by a squirrel-cage induction generator, which is used exclusively in fixed-speed wind turbines (Papathanassiou and Tsili, 2009; Wu *et al.*, 2011; Sreedevi *et al.*, 2016). Lastly, a soft starter is also installed, limiting the inrush currents during start-up, after which they are bypassed. Control of fixed-speed wind turbines is achieved through stall, active stall, and pitch control. The simplicity of fixed-speed wind turbines makes this a reliable and cost-effective design option for turbines with power ratings up to a few megawatts, widely accepted in the industry despite its associated disadvantages (Wu *et al.*, 2011).

In contrast to fixed-speed wind turbines, variable-speed wind turbines can achieve higher efficiency over a wider range of wind speeds, because of their ability to adjust turbine rotational speed to wind speed. This allows for increased and improved power output, while limiting wear and tear and mechanical stresses on equipment such as the gearbox, bearings, and supporting structure. This, in turn, extends equipment life span, and reduces the need for costly maintenance, while also allowing wind turbines to increase in size. The added flexibility, controllability, and improved output of variable-speed turbines can largely be attributed to the use of power converters in the system. The addition of a power converter is, however, not without its drawbacks, requiring

a power-converter interface for control purposes, as well as the additional converter itself, adding to the capital cost of a wind turbine. The added equipment also introduces additional losses to the system, affecting efficiency. These drawbacks are, however, easily offset by the increased and improved power output, which is why variable-speed wind turbines dominate the market today (Wu *et al.*, 2011).

Power-converter configurations in variable-speed wind turbines can further be classified as either full-capacity- or reduced-capacity power converters. In full-capacity power converters, 100% of the generated power goes through the converter connected between the generator and the grid-side transformer. For this reason, the power rating of the converter is chosen to match that of the generator. Converting all the power generated, consequently enhances the overall performance of the system greatly, allowing squirrel-cage induction generators, wound-rotor synchronous generators, or permanent-magnet synchronous generators to deliver power throughout their full speed range. Common converter configurations for full-capacity converters include two-level voltage-source converters in a back-to-back configuration, a diode-bridge rectifier with a DC-DC boost stage, and two-level voltage-source converter, or three-level neutral-point clamped converters in a back-to-back configuration (Wu *et al.*, 2011). Other advantages of full-capacity converters include decoupling the generator from the grid, allowing for smooth grid connection at start-up, and the ability to control the reactive power consumed or generated if required. Efficiency can be improved further when making use of a low-speed synchronous generator having many poles, as this configuration eliminates the need for a gearbox, reducing losses. The elimination of the gearbox will help additionally to cut down on the initial investment required, and the maintenance costs thereafter. Low-speed synchronous generators are, however, known for having a large diameter to accommodate the increased number of poles which, in turn, will make them more expensive to purchase and install initially. Overall, the main drawback when making use of full-capacity power converters is the increased cost and complexity of the system, as compared to other configurations making use of reduced-capacity power converters (Papathanassiou and Tsili, 2009; Wu *et al.*, 2011; Sreedevi *et al.*, 2016).

Reduced-capacity power converters work by controlling only the rotor current of a generator, as compared to a full-capacity power converter, which processes the full power of the system. For this reason, the use of a reduced-capacity power converter is limited to wound-rotor induction generators, which are connected only to the rotor circuit of the generator, while the stator is directly connected to the grid without a converter. Output control can then be achieved through control of the rotor circuit in one of two ways. The first is by varying the resistance of the rotor circuit using the connected power converter. This will affect the torque/speed characteristics of the generator,



allowing an adjustment range of up to 10% above synchronous speed. Subsequently, the added rotor resistance will increase the energy losses in the rotor circuit, which are offset ultimately by the increased ability to capture energy at different wind speeds. The main reason for making use of this configuration is therefore not to increase efficiency, but rather to improve output power quality and to limit equipment stresses. Additionally, this type of configuration will require a soft starter to limit inrush currents and reactive-power compensation (Papathanassiou and Tsili, 2009; Wu *et al.*, 2011).

The second control method, referred to as a doubly fed induction generator, implements rotor control using a power converter. This method of control differs from the first in that a grid-connected power converter is connected to the rotor circuit in place of the adjustable resistance, while the stator is again connected directly to the grid. The use of a grid-connected power converter provides better control, while additionally eliminating the need for a soft starter and reactive-power compensation. For this configuration, the converter only needs to manage up to 30% rotor slip power, cutting down on the size and cost of the converter required. The rotor-connected converter also supports bidirectional rotor-power flow, allowing control of the system power factor, and therefore the amount of active and reactive power produced, improving the overall efficiency of the wind turbine by extending its operational speed range. This range typically extends from 30% below synchronous speed to 30% above synchronous speed, which is a significant improvement over the fixed-speed wind turbines discussed. The improved efficiency and extended operating speed range result in doubly fed induction generators being widely accepted and used in today's market (Papathanassiou and Tsili, 2009; Wu *et al.*, 2011).

### **2.13 Solar technology**

The two main solar technologies implemented in South Africa, also included in the country's future energy mix plans, are solar photovoltaic (PV) and concentrated solar power (CSP). These differ substantially from one another in terms of the method used to utilise the sun's rays for electricity production.

Solar PV directly utilises the sun's rays to convert photons into electrons, using semiconductor materials. The process works through the partial absorption of available sunlight by the semiconductors in the form of photons, knocking electrons loose from their atoms during the process. Loose electrons are then free to travel to an external circuit using conductors, thus producing a DC electrical current. A single cell produces only a very small amount of electrical power, which is why they are interconnected to form solar panels and modules capable of producing hundreds of watts combined. A PV system, as we know it, usually consists of several components, which include the solar PV modules or panels, a charge controller, storage

commonly in the form of batteries, and an inverter to which a load can be connected. The charge controller serves the purpose of regulating electricity flow to the battery as it is being produced by the panels, preventing overcharging and other unfavourable conditions in order to extend battery life. The addition of a battery to the system, although not essential, conveniently allows for continuous operation during cloudy periods of the day, or when there is no sunshine. Lastly, there is the important addition of an inverter to the system, which converts the DC produced or stored into AC power, most used by everyday appliances and loads. On average, the efficiency of a solar PV system utilising crystalline silicon solar cells is between 14% and 20%; however, this can decrease easily considering different inverter- and charge-controller efficiencies, as well as the condition and age of the panels in use. In the past, PV has always been thought of as an expensive option for power generation, but recent years have seen a dramatic and ongoing reduction in cost, making it a competitor in generating clean renewable energy at affordable prices (Faraz, 2012; El-Azab and Amin, 2015; Sharma and Sharma, 2018).

In contrast to solar PV, CSP plants do not convert photons directly from the sun into electrical energy, but rather convert the heat absorbed to drive a turbine, which generates power. They are classified according to four different types, depending on their method of Direct Normal Irradiation (DNI) collection, which refers to the energy collected on a tracked surface perpendicular to the sun's rays. The first of these types is known as a parabolic trough system, made up of rows of curved mirrors focusing the sun's rays onto a central absorber tube. The sun's rays heat the tube and synthetic oil it contains to around 400°C, from where it flows to a heat exchanger to boil water, in turn creating super-heated steam to drive a turbine, much like the process of a conventional power plant. The remaining steam is condensed back into water using a cooling tower, recycled, and pumped back with the cooled oil to continue generating power. A major advantage of CSP over PV is its ability to incorporate thermal storage of energy to be used after sunset or during cloudy conditions, for as long as 6 to 8 hours. This is achieved using molten salt, where excess heat absorbed during the day is transferred from the heated oil to the salt, using an oil/salt heat exchanger. During unfavourable conditions, the salt is then pumped to what is known as the cold tank, and exchanged back to the oil, allowing the system to continue generating power. This allows a CSP plant to operate as a baseload plant, since it can store enough energy during the day to continue generating all night, improving its capacity factor (Faraz, 2012; Sharma and Sharma, 2018).

The second type, known as linear Fresnel reflectors, is like that of the first but uses flat or only slightly curved mirrors to focus the sun's rays onto a downward-facing tube above the mirror array. Additionally it allows for direct steam generation (DSG), eliminating the need for costly heat

exchangers; thus, also reducing the land area required to generate the same amount of power compared to the first. Although the linear Fresnel reflector type is overall less efficient compared to the first, it is seen as a cheaper alternative, making use of off-shelf components while taking up a smaller land area (Faraz, 2012; Sharma and Sharma, 2018).

The third type is known as a power tower or central receiver system, making use of distributed mirrors with two-way tracking capabilities to focus the sun's rays onto a fixed receiver placed on a central tower. Sunlight concentrated 600 to 1 000 times heats water, air, or liquid salts to higher temperatures of between 800°C and 1 000°C, improving the thermodynamic cycle to reduce storage costs, and improve overall efficiency (Faraz, 2012; Sharma and Sharma, 2018).

The fourth and final type is known as a parabolic dish system, in which the receiver is placed in the centre of a parabolic dish, heating a fluid to drive a small gas or sterling turbine. The system tracks the sun in two axes, moving in tandem to achieve the highest efficiency of 31.25%, compared to the others. When a sterling engine is used in the system, it works by using heated fluid to move the pistons, creating mechanical power to drive an alternator, ultimately generating power. The downside to this type of system is that it is not ideal for incorporating storage, and is difficult to incorporate with fossil-fuel generation as a hybrid system, often not making it an ideal choice, depending on the application (Faraz, 2012; Sharma and Sharma, 2018).

Comparing CSP to PV, it should be noted that a PV plant will require more space compared to a CSP plant to generate the same amount of power. PV is also more limited in terms of storage options, which is an important consideration considering continuity and quality of supply, as it is reliant on expensive batteries requiring replacement from time to time. Considering a developing country, for which the study (Faraz, 2012) set out to determine the best option between the two, in their case, specifically Bangladesh, it was concluded that CSP is the better option. This conclusion is largely related to the storage capability of CSP technology, compared to that of PV, and will depend on a multitude of different factors tailored to a specific country's needs, including the availability of land and solar radiation levels close to load centres to minimise transmission losses. It does become clear why CSP technology is also part of South Africa's planned future energy mix, since its ability to store energy more cheaply is a major advantage over most other renewable options, providing flexibility in the power network (Faraz, 2012; El-Azab and Amin, 2015; Sharma and Sharma, 2018; Buraimoh and Davidson, 2020).

#### **2.14 OPAL-RT real-time simulator**

A simulation, commonly defined as a representation of the operation or features of a system through the use or operation of another, is an essential part of the development and integration of new distributed generation into a network (Bélanger, Venne and Member, 2010). Simulators have

proven to be an efficient and effective way of studying power systems in a fast, precise, reliable, and economical way, and have become widely available following advances made in processor technology, leading to decreasing prices. This has led to the development and availability of a wide range of simulators today, of which the latest developed generation is known as fully digital real-time simulators, replacing the physical simulators of the past. The use of real-time simulators has become more prevalent in recent years, following the increased grid connection of fast-switching power electronic equipment such as inverters and stat coms, demanding simulators using very small time-steps for system equation solving to obtain accurate results. Furthermore, they allow for design errors to be detected early, for design periods to be scaled down, and can be used for numerous different applications and types of projects, including power generation, automotive, all electric ships and trains, aerospace, and robotics applications. Real-time simulators differ mainly from pure digital simulation tools in that they can perform complex simulations while providing results in real time for power system network analysis, meaning that they produce results at the same rate of speed as the physical components they represent and simulate.

Timing and the computational capability to achieve this is therefore essential for real-time simulation, compared to pure digital or offline simulators where the rate at which the results become available is irrelevant. Unsuccessful computing of results within a time resembling that of the physical component leads to what is known as overruns, resulting in erroneous results. To achieve successful real-time simulation, four steps need to be achieved within each time-step. First, inputs need to be read, and outputs generated, followed by the solving of the model equations. Results are exchanged with other simulation nodes, after which the simulator will idle and wait for the start of the next time-step. The use of real-time simulators also allows for hardware-in-the-loop (HIL) applications, which refer to the connection of a physical component, such as a controller for testing, to the real-time simulator which will represent, for example, a virtual plant. This feature allows the testing of new equipment even when a physical test bench is not available, while also allowing testing of extreme events normally unachievable when using the actual hardware. In addition to HIL, software in the loop (SIL) capabilities are also available on more powerful real-time simulator modules. SIL refers to the simulation of multiple equipment items, for example, both controller and power plant, using the same real-time simulator. The advantage of such simulations is that, since both are simulated using the same simulator, timing between the virtual equipment items becomes irrelevant, making it ideal when accelerated simulations are required (Bélanger *et al.*, 2010; Singh *et al.*, 2015; Li *et al.*, 2016; Noreen, Roy and Bayne, 2018).

Among the different real-time simulators is OPAL-RT of Canada, which is renowned for its reliable operation and performance, as well as for its flexible applications for both academic and industrial purposes. OPAL-RT accommodates several hardware integrated software, including eMEGAsim, HYPERSIM, eFPGAsim, and ePHASORsim. Of these, eMEGAsim is a hybrid real-time simulator making use of parallel computing to solve differential and algebraic equations, considered to be the most user-friendly, flexible, and scalable digital analogue among the different types. eMEGAsim includes, among other software, RT-LAB, which is significant for this study, as it uses SimPowerSystems toolboxes of MATLAB/SIMULINK, as its front end to enable easy and familiar editing and display of graphical models; therefore, making it the chosen software to be used in the development of the real-time testbed developed by this study (Bian *et al.*, 2015; Singh *et al.*, 2015; Li *et al.*, 2016; Noureen *et al.*, 2018).

To develop and simulate a network in the OPAL-RT real-time environment, several steps had to be followed and completed. The first includes modelling the desired design accurately using MATLAB/Simulink, ensuring that it runs flawlessly in the Simulink environment. The model then needs to be grouped into subsystems, commonly named SM\_Master, SS\_Slave, and SC\_Console, grouping the computational elements of the model in SM-Master or SS\_Slave, while the user-interface blocks and outputs displayed for real-time behaviour monitoring are grouped in the SC\_Console subsystem. Subsystems are ultimately created to allow each section to run in its respective core the simulator and target computer. Next, RT-LAB software is used to convert the Simulink model to C-code and to assign the subsystems to their respective cores, before executing the model. As the model is running in real-time, analysis can commence using the user-interface window. These steps are also detailed in the flow diagram of Figure 2.8, providing a better understanding of the platform development steps involved (Singh *et al.*, 2015; Li *et al.*, 2016; Noureen *et al.*, 2018).

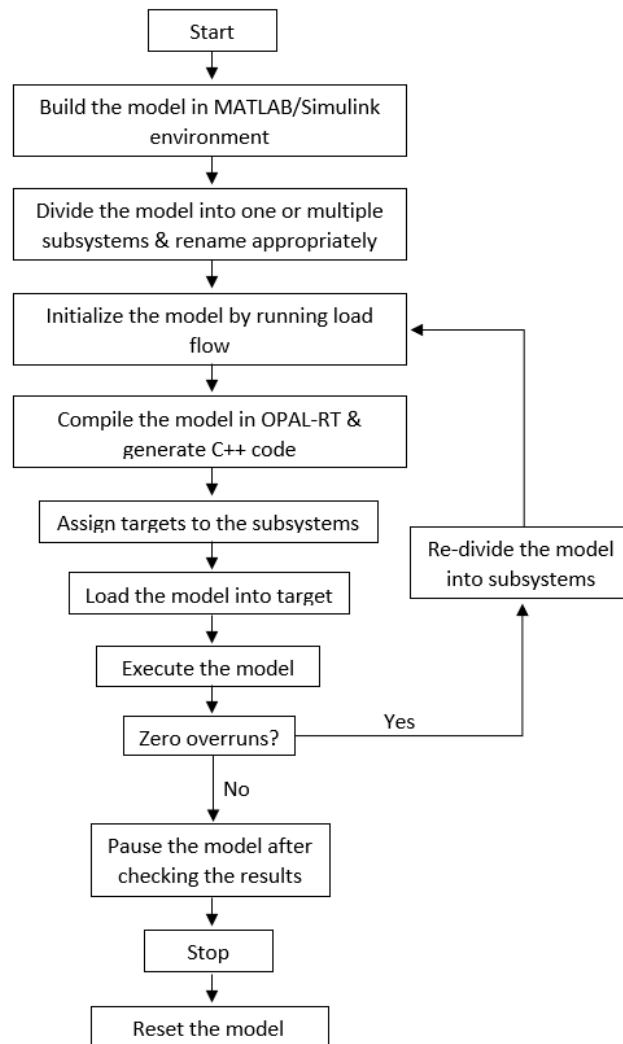


**Figure 0.8: Process of real-time modelling using OPAL-RT (Singh et al., 2015)**

A study recognising the need to develop tools for analysing the impact of adding distributed generation to an existing grid network, such as the real-time simulation platform developed for South Africa through this study, can be found in Paquin *et al.* (2007). Paquin *et al.* (2007) identify the growing demand for renewable energy, recognising that its integration will impact and change the characteristics of the network to which it is connected, thus requiring advanced and accurate simulations to be conducted before connection and grid commissioning. The alternative to simulation, testing network behaviour when adding distributed generation under different fault conditions using an actual network, will be costly, dangerous, and simply impractical, which is why having an accurate non-destructive testing method such as a real-time simulator platform is so important. The change in network characteristics comes largely from the power electronic nature

associated with adding distributed generation, creating new challenges when combining fast-switching power electronic devices with slow-responding existing synchronous generation. Naturally, the effects of connecting alternative distributed generation will remain negligible with minimal integration; however, a point has now been reached where technological advances, specifically in renewables, have enabled large-scale integration, creating an urgent need for tools and real-time simulation platforms to emulate their effects. This need for such tools is supported and once again becomes evident, considering the emphasis placed on making funding available for the development of such tools by countries such as Canada (Paquin *et al.*, 2007).

Paquin *et al.* (2007) further continue to develop and simulate a wind farm represented by eight DFIGs connected to a 24-bus network, using the Simulink-based eMEGAsim of OPAL-RT, to provide a platform for engineers to develop and test the effectiveness of wind-turbine controllers. Testing controllers is made possible by the hardware-in-the-loop (HIL) connection capability supported by eMEGAsim, enabling the direct connection of external equipment such as controllers to the real-time simulator. Detailed simulation models combined with HIL will therefore be able to provide accurate results very close to that of the real-world application. Ultimately, to test the platform developed by the study, a three-phase fault was simulated at one of the buses while a comparison between the real-time simulation results and offline results were made to validate its performance. This showed that the developed real-time platform yielded accurate results and could be useful for a wide range of HIL simulations (Paquin *et al.*, 2007).

Studies developing similar platforms using real-time simulators include that of Merabet *et al.* (2014), which developed a tool to be used for research, teaching and training purposes in the area of wind energy. This involved the development of a platform to emulate a wind-turbine-generator system, based on a permanent-magnet DC motor from Lab-Volt's electrical models. OPAL-RT was again used as the real-time simulator, while control algorithms were implemented using MATLAB/Simulink. RT-Lab software was also used, acting as the communication medium between the HIL application and the physical system. The model developed ultimately permits control system theories to be implemented, allowing the mathematical models from the simulation results to be extracted, and used for control design (Merabet *et al.*, 2014).

Singh *et al.* (2015) modelled the IEEE 9-bus and New England 39-bus systems respectively, using eMEGAsim of OPAL-RT, in combination with MATLAB/Simulink and RT-LAB software. The aim of their study was to develop a real-time test platform to simulate system behaviour, and the controller's ability to deal with a wide range of large and small network disturbances. Disturbances ultimately simulated for both networks included single line-to-ground faults, line outages, step-load change, and on-load tap changing. It is worth noting that the study experienced some limitations

when it came to the synchronous machine models of MATLAB/Simulink, noting numerical instability in discrete time-step when multi-machines were interconnected in the system. Additionally, it was mentioned that generators should not be connected directly to a bus without a transformer, as this creates simulation problems. Finally, the study validates the stability of the IEEE 9-bus, and New England 39-bus systems, while having developed the platforms for future stability testing on the respective networks (Singh *et al.*, 2015).

Li *et al.* (2016) aimed to go beyond the conventional pure digital and hardware-in-the-loop simulations by including power-in-the-loop to develop a hybrid digital analogue simulation platform for grid connecting new-generation studies. The idea was therefore that the platform developed would be suitable to study the effects of adding different types of new generation to a grid, whether a single unit or the addition of multiple units, with an accuracy beyond the capabilities of conventional simulation platforms. The setup of the developed platform includes the use of RT-LAB as the real-time simulation software of OPAL-RT, a power amplifier and flexible interface system, renewable power generation units, and an experimental area to emulate either a grid or the desired experimental environment. This experimental area was composed of, among other equipment, three programmable AC power supplies, a power-voltage sag device, and a three-phase RLC load. To test the feasibility of the platform, the effect on system inertia and the ability of a network to maintain stability was simulated by replacing increasing amounts of synchronous generation with renewables. To validate the developed platform, it was expected that system stability would decrease during disturbances as the power provided by renewables increases, owing to the very limited ability of renewable generation to provide inertia. Results produced from the developed platform ultimately confirmed this, proving its validity as a tool for, among other uses, system stability studies with regard to inertia (Li *et al.*, 2016).

Noureen *et al.* (2018) developed a test environment for PV module behaviour studies when connected to a grid, again making use of OPAL-RT real-time simulator and RT-LAB software. To validate the performance of the test environment created, a PV system was simulated in steady-state condition. Results proved the validity of the platform, which can be used for future PV system behaviour studies when integrated into a grid (Noureen *et al.*, 2018).

Luna, Manrique and Bocanegra (2018) used ETAP real-time and state estimators to study the effectiveness of SCADA systems in providing information to network operators to deal effectively and efficiently with the intermitted supply of renewable energy sources connected to a network. To validate the results obtained from the ETAP real-time simulation, OPAL-RT was used to emulate an equivalent model of the network. This ultimately resulted in a real-time simulation tool



that may help to identify shortcomings in a SCADA system, serving to increase the efficiency at which a power network operates by managing its generation effectively (Luna, *et al.*, 2018).

The more ambiguous Wang *et al.* (2019) discuss the China network modelled in HYPERSIM real-time simulator, developed following the limitations faced by the RTDS real-time simulator previously used by China's Southern Power Grid simulation laboratory, limited to a maximum of 60 simulation units. The new HYPERSIM simulation platform is an Electromagnetic Digital-analog Hybrid, similar to that developed in Li *et al.* (2016), but capable of simulating on a larger scale in real-time while incorporating more HVDC systems, essential in the case of China's network. Simulated on an SGI UV300 supercomputer, the new HYPERSIM real-time network model consists of 17 746 single-phase buses, and is capable of simulating AC-DC power systems accurately (Wang *et al.*, 2019).

Lastly, the study of Kemal *et al.* (2017) is also noteworthy, developing a test case for active power-management studies using the DiSC-OPAL library of OPAL-RT, in combination with MATLAB/Simulink. The test case aimed to validate the abilities of the OPAL-RT real-time simulator for use in energy balancing, loss minimisation, and the impact of communication constraints on supply management. The test network included both an MV and LV section, incorporating wind power plants, solar power plants, and energy storage devices for study purposes. Results obtained from the 16-hour Smart Energy System real-time HIL platform simulation revealed that, considering ideal communication conditions, an average error of 4.5% is noted, compared to the real-world non-ideal conditions simulated, yielding an error of 15.1%. The test case helps to validate the accuracy of the developed platform and can be used for future studies on the impact of communication technologies on active power management (Kemal *et al.*, 2017).

Having reviewed available literature and studies surrounding the current state of South Africa's electrical grid, and that which is planned, clarity begins to set in regarding the latter, yet not exclusive of challenges. Grid codes appear to offer a solution, addressing several renewable-integration concerns by having renewables operate and react in a certain way; however, RPP behavioural studies of grid-connected renewables are still needed to better understand the efficiency and effect of grid codes. Renewable-integration studies are presented in this chapter from other countries, which are considered important to provide insights into what lies ahead for South Africa, especially in terms of challenges faced, with the aim of providing foresight regarding the elimination of unnecessary integration obstacles. Finally, this chapter includes and expands on all relevant studies containing information required for the successful development of a tailored South African grid-code real-time testbed, laying the cornerstone for the development process to follow.

## **2.15 Summary**

This chapter was dedicated to the broad review of literature on the motivation and knowledge required for developing a real-time RPP grid-integration behavioural studies testbed. This included setting the scene for the significant change coming to South Africa's grid, where large-scale renewable integration is expected to transform its relatively passive network into an active multi-directional system, using wind and solar to lead the way. Along with this come new challenges and uncertainties, which have led engineers to note increased voltage levels and short-circuit currents, as well as deterioration in the reliability and quality of supply in countries further ahead with their renewable-integration endeavours. In response to these identified associated renewable challenges, Chapter Two considered grid codes in general, as well as those specific to RPPs in South Africa, revealing an array of RPP-support requirements that renewable generation needs to adhere to in mitigation of their somewhat unstable nature. Having identified wind and solar as the most prominent renewable technologies for South Africa, they were considered in more detail, which showed significant advances to have been made in terms of efficiency, to lower their associated costs. Finally, the process was reviewed of developing a real-time simulation testbed, revealing the steps later required when moving from a standard MATLAB model to an OPAL-RT-integrated real-time simulation testbed.

## CHAPTER THREE

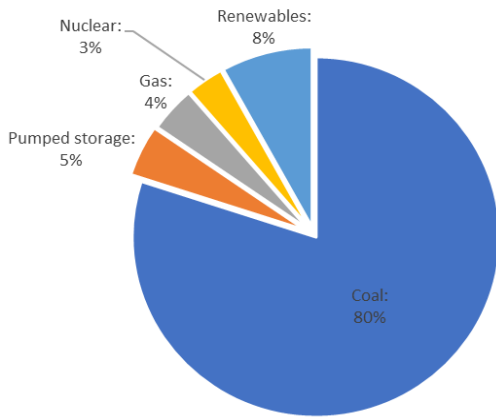
### LITERATURE ANALYSIS AND TESTBED DEVELOPMENT THEORY

#### 3.1 Introduction

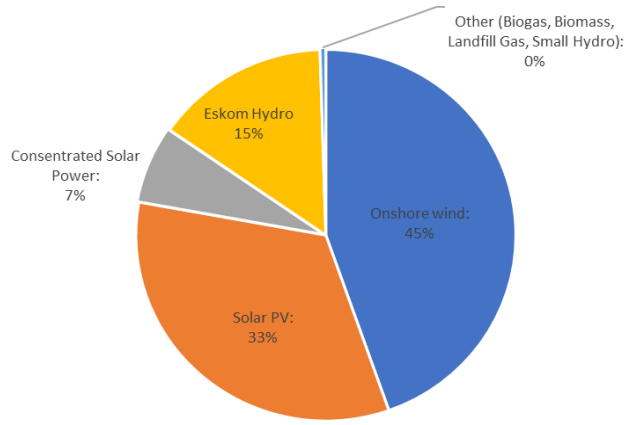
To better understand the effect of changing generation on the South African grid, it is important to consider both the current and future generation mix, revealing the degree of change that is set to occur. In this chapter, renewable addition targets of both the REIPPPP and 2030 IRP are reviewed, providing a point of reference representing the potential future energy mix, for comparison to the energy mix of today. As mitigation to these foreseen changes and associated effects, South Africa has developed RPP-specific grid codes, detailing the measures needed to maintain the stability of the South African grid as the percentage of renewables increase. This chapter, therefore, includes a detailed review of South Africa's RPP-specific grid codes, focusing on RPP-support, testing, and circuit requirements forming part of the forthcoming testbed's development. The potential effect of changing generation on the South African grid is considered through a further revision of the updated 2030 IRP, which allows the grid in 2019 to be compared to the one foreseen in 2030, while assessing the changes in terms of their effect on grid reliability, stability, and flexibility. Finally, the chapter considers wind-turbine options for the forthcoming case studies, as being among the most implemented and promising renewable technologies identified for South Africa.

#### 3.2 South Africa's current and future generation mix:

Tables 2.3 and 2.4 illustrate the significant imbalance which still exists in terms of infrastructure and the amount of electricity being supplied by Eskom, as compared to the renewable-focused IPPs. The tables, however, also contain important information with regard to South Africa's generation mix, and how it is set to change going forward. To better illustrate this, the data of Tables 3 and 4 were used to generate Figures 3.1 to 3.3. Figure 3.1 illustrates the contribution of the current grid-connected generation by type, accentuating the view of a coal-dominated South African generation mix, and the still minimal contribution made by renewables, representing a mere 8%, considering all types from all producers (Oyewo *et al.*, 2019).



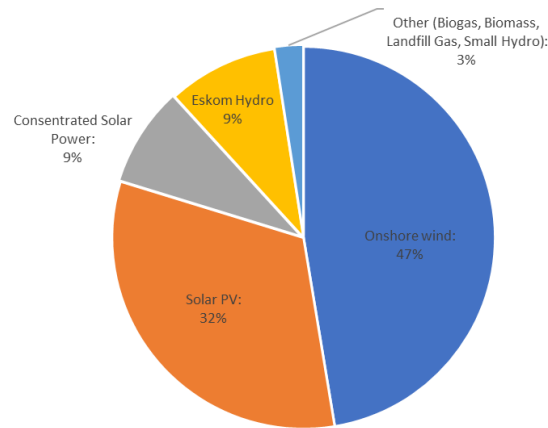
**Figure 0.1: SA's current generation mix**



**Figure 0.2: SA's grid-integrated renewable generation mix**

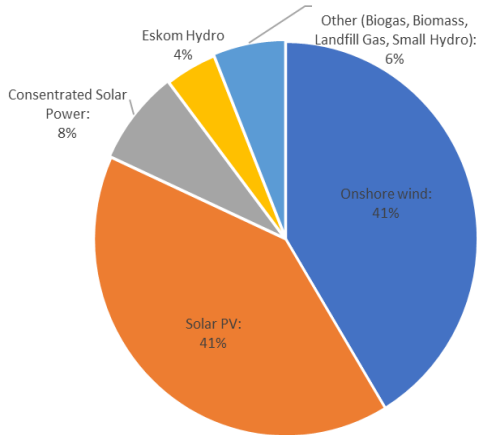
The 8% of renewables represented in Figure 3.1 can further be expanded to the graph in Figure 3.2, representing the composition of the 8% of renewables illustrated. It is worth noting in Figure 3.2 that onshore wind is still South Africa's most dominant form of renewable generation, closely followed by solar PV. Furthermore, even though Eskom almost exclusively owns and dominates all other forms of generation apart from renewables, it can be noted that it does contribute somewhat towards renewables, as it owns most of the peak-load hydro stations, supplying 15% of the renewable generation total, in addition to its 100 MW Sere wind farm, discussed in Chapter Two (Ayamolowo, Manditereza and Kusakana, 2022).

Figure 3.2, representing the grid-connected mix of renewable-generation can also be compared to Figure 3.3, perhaps being a better representation of the short-term future renewable-generation mix, considering both grid-connected renewables and those already operational and set to come online soon. The importance of gaining this knowledge lies in using it to ensure that the necessary preparations are performed and systems implemented, with the aim of successful integration and grid connection of this operational, yet still-to-be-integrated renewable generation.



**Figure 0.3: SA's operational renewable-generation mix**

Although it is known from the data in Table 2.4 of Chapter Two that all forms of renewable generation are set to see a future increase in capacity, it is seen, when comparing the graphs of Figures 10 and 11, that concentrated solar and onshore wind are expected to gain the most ground in terms of their contributions towards the overall short-term renewable-generation mix. Additionally, the commissioning and grid connection of several smaller projects is expected to start making a more notable contribution soon.



**Figure 0.4: REIPPPP renewable generation mix target**

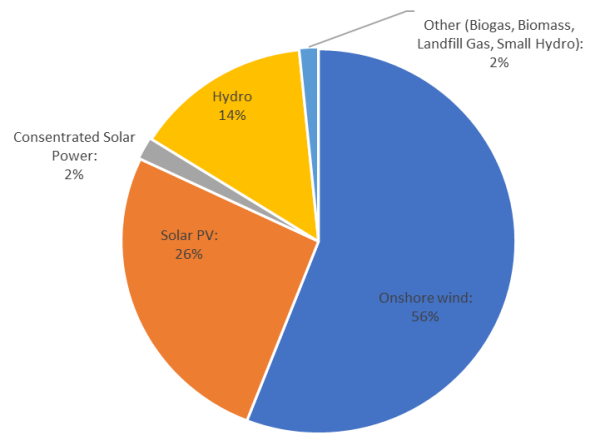


**Figure 0.5: 2030 IRP renewable generation mix target**

The data of Table 2.4 of Chapter Two furthermore includes the renewable addition targets per technology towards the 14 725 MW addition target established through four separate ministerial determinations between 2011 and 2016. This target is set to be reached by the end of the 7th bid window of the REIPPPP, for which the renewable contribution by generation type is represented in Figure 3.4 generated using Department of Energy and Department of National Treasury (2018).

Providing another insight into the possible future of South Africa’s renewable-generation mix is Figure 3.5, illustrating the updated renewable-generation targets per technology of 2030 IRP towards the 31 730 MW addition goal for 2030, generated using Cliffe Dekker Hofmeyr (2019) and Department of Mineral Resources and Energy (2019). In Figures 3.4 and 3.5 it is apparent that, depending on the origin and date of the targets set, different scenarios arise regarding what South Africa’s renewable energy future might look like. Nevertheless, onshore wind emerges as one of if not the largest anticipated producer of renewable generation going forward, closely followed by solar PV. For this reason, wind and solar PV technology will be the focus as this thesis evolves, since the integration of these technologies is expected to have the most significant effect on the South African grid in the future.

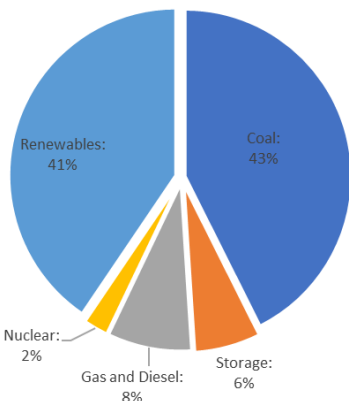


**Figure 0.7: SA’ s future generation mix as per the 2030 IRP**

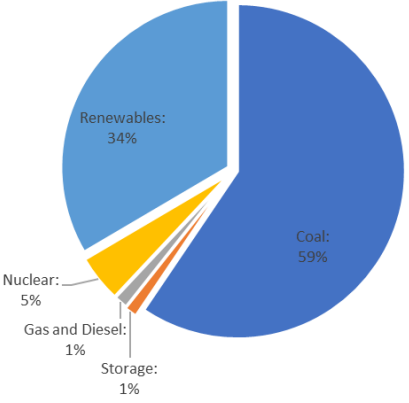


**Figure 0.6: 2030 forecasted % annual energy contribution by generation type**

Figure 3.6 illustrates the forecasted future generation mix of 2030 IRP considering all types of generation, which can also be compared to that of the current mix illustrated in Figure 3.1. It is seen that, in less than a decade, South Africa plans on changing its overall generation mix drastically, by installing renewables to a near-equal capacity as coal by 2030, making a 41% contribution towards South Africa’s total installed renewable capacity. Different generation types are, however, used for different purposes, such as for baseload or peak load, making it worth considering the annual energy contribution forecast of IRP 2030, illustrated in Figure 3.7. It is seen that, by 2030, coal is still expected to generate approximately 59% of South Africa’s energy demand, followed by renewables with a significant generation contribution of 34% (Cliffe Dekker Hofmeyr, 2019; Department of Mineral Resources and Energy, 2019; Ayamolowo *et al.*, 2022).

The reason for this being significant becomes apparent when again considering the renewable penetration study conducted in India, discussed in Chapter Two, during which instabilities and grid-code voltage violations were noted following a renewable penetration of 29.3% (Sreedevi *et al.*, 2016). It is also worth mentioning that no two grids are the same, yet consideration should be given to grid-code voltage violations that may occur at buses, such as in the case of the Indian study, in that South Africa plans to exceed the penetration level at which the study noted instabilities and violations. Additionally, it highlights the importance of renewable generation adhering to grid-code requirements, since failure to monitor this could result in renewables having the opposite effect to the increased reliability and stability that it hopes to bring to the South African grid.

### **3.3 South African renewable grid-code requirements summary**

For Section 3.3, all requirements, graphs, and graphics were obtained from the South African RPP grid-code requirements document (NERSA, 2019), unless referenced otherwise.

#### **3.3.1 Voltage requirements set for RPPs in South Africa**

Voltage requirements and control capabilities set for RPPs, as per their classification, refer to the degree of controllability required by South African grid codes of RPPs measured at the POC, and the operating boundaries they are required to adhere to. Measured values to confirm the adherence of an RPP to voltage ride-through requirements during different events are always taken and measured at the POC, unless stated otherwise. Requirements are further defined by category as follows.

##### **3.3.1.1 Category A RPPs**

Normal operating conditions, during which Categories A1 and A2 RPPs are required to operate continuously, allow for variations in voltage at the POC between -15% and +10%, indicated by the blue band of Figure 3.8. When operating in this band of continuous operation, as defined by the relevant South African grid codes, Categories A1 and A2 RPPs are not allowed to disconnect (Sewchurran and Davidson, 2017; NERSA, 2019).

Voltage ride-through requirements set for Categories A1 and A2 RPPs at the POC during abnormal events and grid disturbances are further defined considering the graph boundaries of Figure 3.8. Used in conjunction with the maximum disconnect times set for the specified RPPs defined in Table 3.1, boundaries are set specifying when Categories A1 and A2 RPPs are allowed to disconnect when operating under a fault condition.

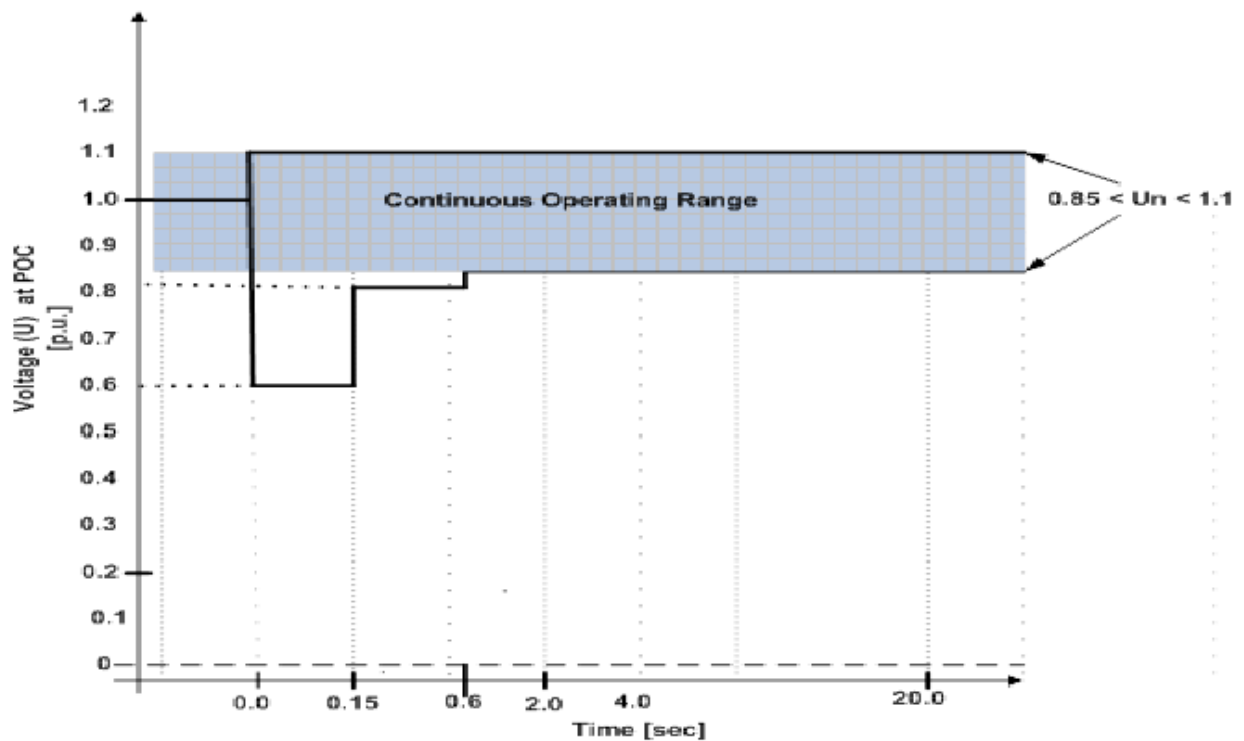


**Figure 0.8: Category A1 and A2 voltage ride-through requirements (NERSA, 2019)**

**Table 0.1: Category A1 and A2 RPP disconnect times (NERSA, 2019)**

PU voltage at POC:	Maximum trip time in seconds:
< 0.5	0.2 s
0.5 – < 0.85	2.0 s
0.85 – 1.1	Continuous operation.
> 1.1 - < 1.2	2.0 s
1.2	0.16 s

Normal operating conditions during which non-synchronous Category A3 RPPs are required to operate continuously, allow for variations in voltage at the POC between -10% and +10% of  $U_n$ , indicated by the blue area marked 'Area A' in Figure 3.9. When operating in this band of continuous operation, as defined by the relevant South African grid codes, Category A3 RPPs are not allowed to disconnect.

Voltage ride-through requirements set respectively for non-synchronous, and synchronous Category A3 RPPs at the POC during abnormal events and grid disturbances, are further defined considering the boundaries of the graphs in Figures 3.9 and 3.10. These include that the relevant RPPs should be able to withstand voltage drops to zero, for a minimum time of 0.15 seconds, with



the difference being the recovery times. Different voltage ride-through requirements, however, apply in the event of a 3-phase fault, when Category A3 RPPs are required to adhere to the graph in Figure 3.11. For Figures 3.9 to 3.11, it can then be said that, if voltage conditions remain in the areas marked 'Area A' or 'Area B', it is required of the RPP to operate and remain connected. Only when voltage conditions deviate outside these areas to that marked 'Area C', is it allowed to disconnect. For Category A3 RPPs, the area marked 'Area D' does not apply, and should be treated as part of Area C (Sewchurran and Davidson, 2017; NERSA, 2019).

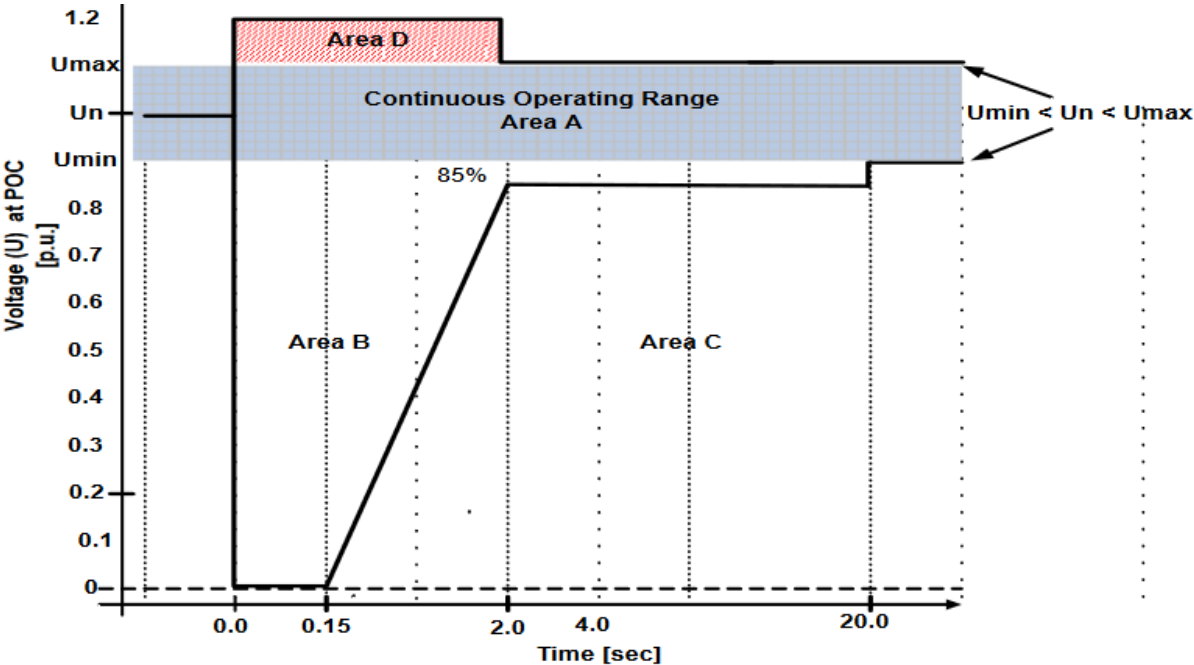


Figure 0.9: Non-synchronous Category A3, B and C voltage ride-through requirements (NERSA, 2019)

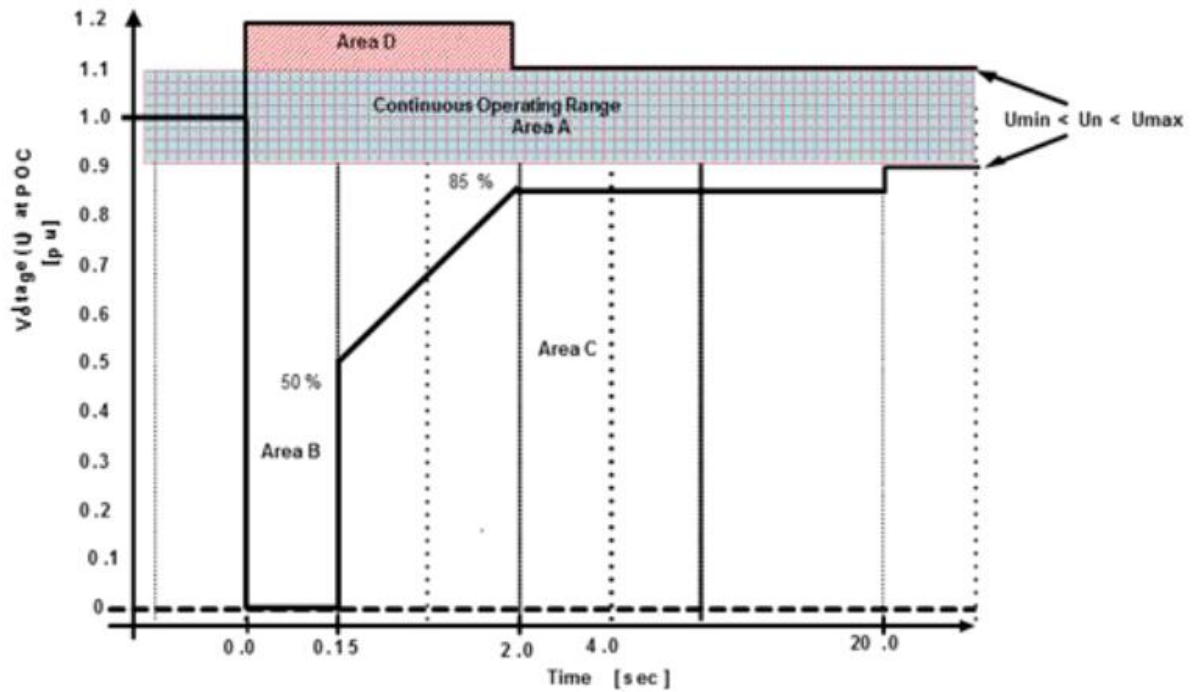


Figure 0.10: Synchronous Category A3, B and C voltage ride-through requirements (NERSA, 2019)

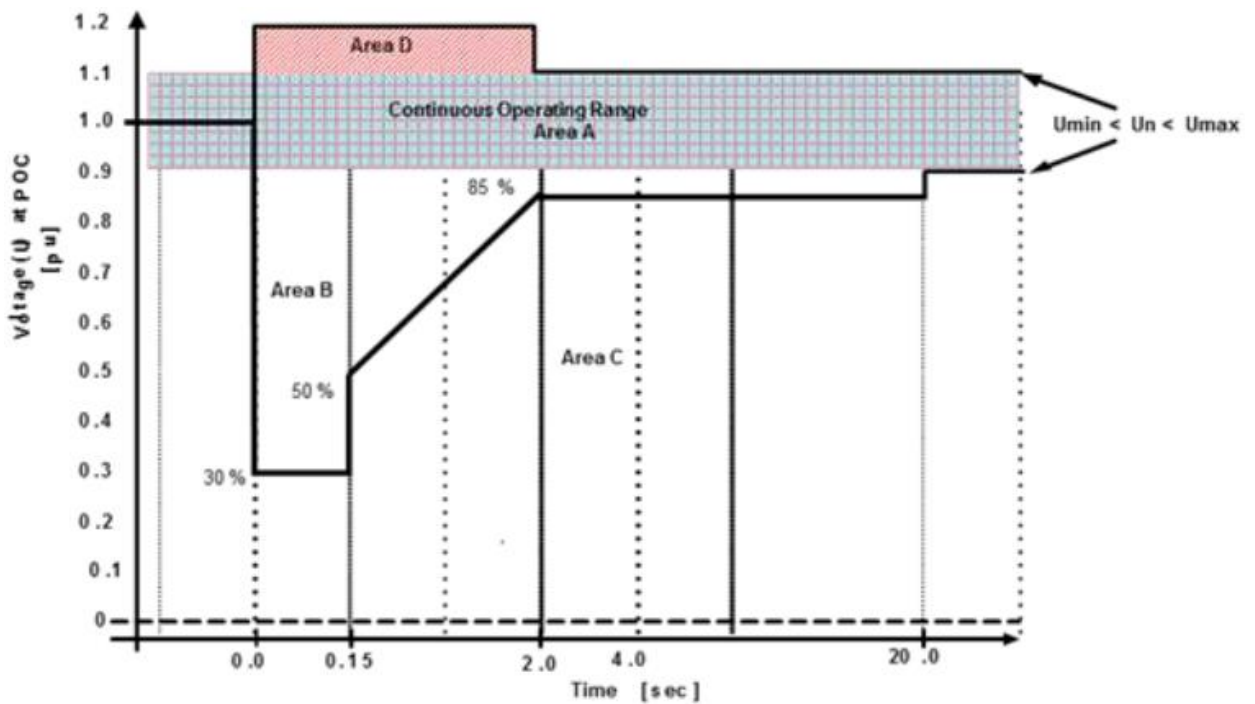


Figure 0.11: Synchronous Category A3 and B voltage ride-through requirements in the event of 3-ph faults (NERSA, 2019)

### 3.3.1.2 Category B RPPs

Normal operating conditions during which Category B RPPs of 11 kV, 22 kV, 33 kV, and 44 kV are required to operate continuously, allow for variations in the pu voltage at the POC between 0.90 pu and 1.08 pu. Category B RPPs of 66 kV, 88 kV, and 132 kV are required to operate continuously with variations in voltage at the POC between 0.90 pu and 1.0985 pu.

Voltage ride-through requirements set for non-synchronous Category B RPPs at the POC during abnormal events and grid disturbances are defined using the same graph as that of Category A3 RPPs in Figure 3.9. Similarly, boundary conditions set for Category B RPPs utilising synchronous machines are then also defined by Figure 3.10. Considering the two graphs, it can again be noted that in both cases it is required of RPPs to withstand voltage drops down to 0 V pu at the POC, for a minimum time of 0.15 seconds, with the difference being the minimum voltage-recovery requirements. Specific boundaries also exist for Category B RPPs in the event of a 3-phase fault when utilising synchronous machines, defined by the graph in Figure 3.11. These RPPs are required to withstand voltage drops down to 0.3 V pu at the POC, again for a minimum time of 0.15 seconds. The areas of the graphs as discussed for Category A3 RPPs again apply, with 'Area D' required to be treated as part of Area C considering Category B RPPs (Sewchurran and Davidson, 2017; NERSA., 2019).

### 3.3.1.3 Category C RPPs

Normal operating conditions during which Category C RPPs of 11 kV, 22 kV, 33 kV, and 44kV are required to operate continuously, allow for variations in the pu voltage at the POC between 0.90 pu and 1.08 pu. Category C RPPs of 66 kV, 88 kV, and 132 kV are required to operate continuously with variations in voltage at the POC between 0.90 pu and 1.0985 pu.

Voltage ride-through requirements set for non-synchronous Category C RPPs at the POC during abnormal events and grid disturbances are again defined considering the boundaries of the graph in Figure 3.9. Similarly, these include that Category C RPPs should be able to withstand voltage drops to 0 V pu, for a minimum time of 0.15 seconds. In addition, non-synchronous Category C RPPs are also required to withstand voltage spikes of up to 120% of the pu voltage at the POC, for a minimum time of 2 seconds, indicated by 'Area D' of the graph, which now applies for Category C RPPs. Boundary conditions set for Category C RPPs utilising synchronous machines are also defined in Figure 3.10. Considering the two graphs, it can be noted that, in both cases, it is required of RPPs to withstand voltage drops down to 0 V pu at the POC, for a minimum time of 0.15 seconds, with the difference being the minimum voltage-recovery requirements (Sewchurran and Davidson, 2017; NERSA., 2019).

### 3.4.1 Reactive power requirements set for RPPs in South Africa

Once operating conditions leave the area of normal operation, as defined for the respective RPP categories above, grid codes apply to specify reactive-power-support requirements set for RPPs, as per their respective category. These requirements, set in terms of reactive power support, are usually achieved using one of two control functions, known as reactive power (Q) control, or power factor (pf) control. Reactive power control refers to control of the amount of reactive power absorbed or supplied at the POC, independent from active power and voltage. In contrast to this, when using power factor control, the change in reactive power is proportional to the active power value at the POC. In South Africa, reactive-power support is required from Categories A3, B, and C RPPs, under specified conditions, while Categories A1 and A2 RPPs are required to operate at unity pf, unless otherwise specified by the NSP or SO. Reactive power support requirements apply in the event of symmetrical fault sequences, as per the graph in Figure 3.12, with the exception of those implementing synchronous machines (NERSA., 2019).

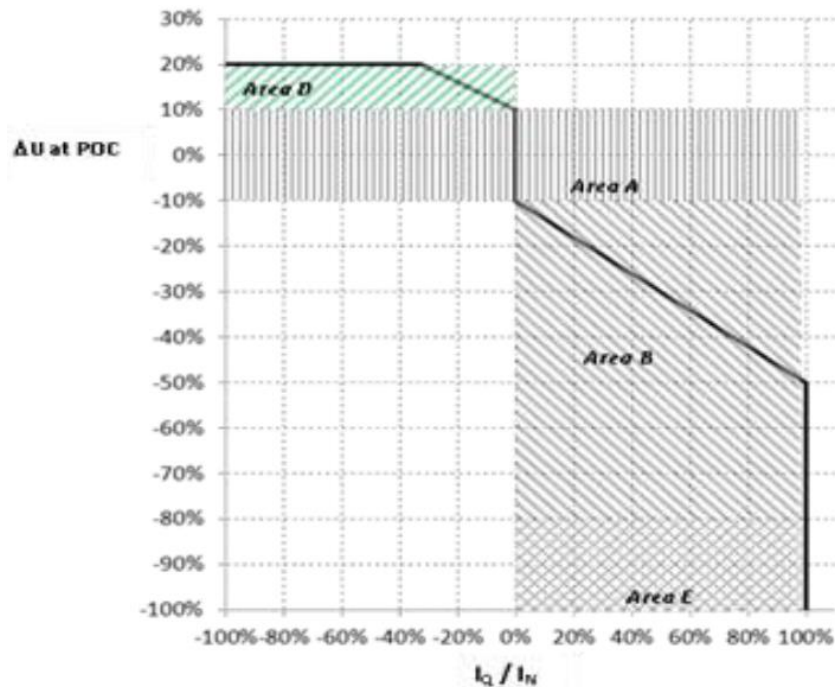


Figure 0.12: Reactive-power support requirements during voltage drops or spikes (NERSA, 2019)

Figure 3.12 considered, the respective areas and classes of RPPs to which they apply can be defined as follows:

**Area A:**

When operating in the region extending from 90% to 110% of the normal operating voltage 'U' at the POC, no reactive-power support is required from any RPPs.

**Area B:**

When operating in Area B, reactive-power support takes priority compared to active power, although it is still required of RPPs to maintain their active power supplied during voltage drops. A reduction in active power is, however, allowed for voltage drops exceeding 85%, in favour of reactive-power support to help stabilise the voltage. When operating in this region, Categories B and C RPPs are required to provide maximum voltage support by supplying a controlled amount of reactive current, assisting in the stabilisation of voltage. Inverter-driven Categories B and C RPPs are furthermore required to have the ability to disable reactive current support at any time during such an event if requested to do so by the network operator or SO. No reactive-power support is required of Category A RPPs when operating in Area B of the graph.

**Area D:**

When operating in Area D of the graph, Categories A3, B, and C RPPs are required to stay connected to the network, absorbing a controlled amount of reactive current, as per their abilities and design limits.

**Area E:**

When operating in Area E of the graph, RPPs of Categories A3, B and C are required to continue supplying reactive current within their design capabilities, only being allowed to disconnect once the voltage ride-through requirement boundaries of Figures 3.9 to 3.11 are breached.

Once an event is cleared, it is required of Categories A3, B, and C RPPs to restore normal active power production within 1 second, to a supply level of at least 90% of that before the disturbance or event. Category-specific reactive-power requirements are furthermore defined by South African grid codes, as follows:

**3.4.1.1 Category A RPPs**

As discussed, Categories A1 and A2 RPPs are only required to supply power at unity pf, unless otherwise agreed upon. Category A3 RPPs are expected to be designed to be able to supply rated power ( $P_n$ ) at a power factor ranging from 0.95 lagging to 0.95 leading at the POC, with a variable output of between 20% and 100%. The default pf is, however, always unity.

### 3.4.1.2 Category B RPPs

Category B RPPs are required to have the ability to operate in either voltage (V), power factor (Q), or reactive power (Mvar) control mode, with the operating mode, as well as the operating point to be specified by the NSP. Once specified, while operating between 5% and 100% rated power, RPPs of Category B are required to have the ability to vary reactive power (Mvar) support at the POC within the limits specified by Figure 3.13, of which the values of  $Q_{min}$  and  $Q_{max}$  are governed by the graph in Figure 3.14.

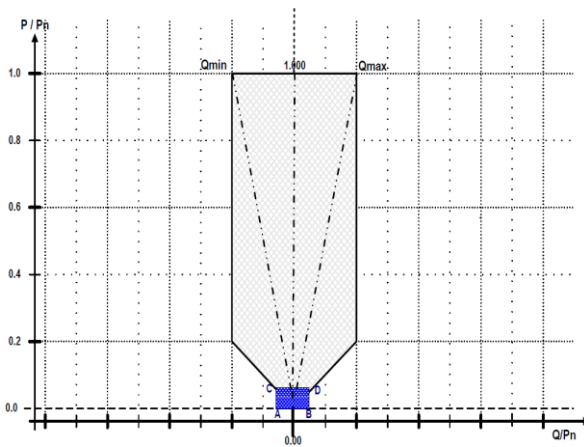


**Figure 0.14: Category B reactive power support requirements**

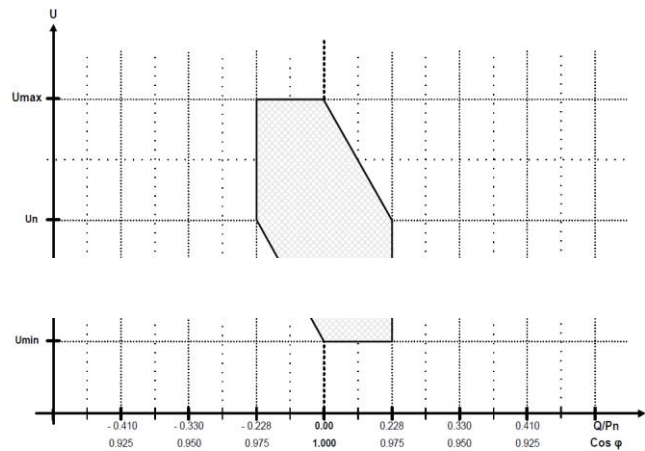


**Figure 0.13: Category B reactive power and voltage range requirements**

If the voltage at the POC remains within the normal range, as specified by Area A of Figure 3.12, reactive-power support requirements are defined by the graph in Figure 3.15. When operating below 5% rated power, no reactive support requirements apply; however, RPPs are required to continue operating within the blue highlighted boundary points A, B, C, D of the Figure 3.15 graph.

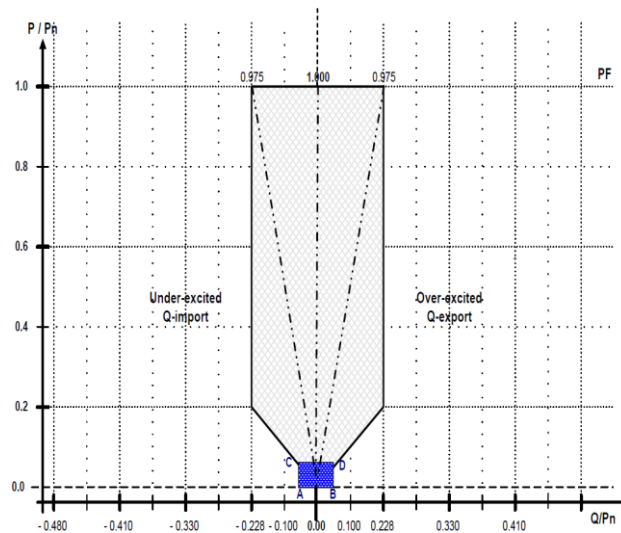


**Figure 0.15: Category B reactive power support requirements at normal POC voltage**

### 3.4.1.3 Category C RPPs

Like that of Category B, Category C RPPs are also required to have the ability to operate in either voltage (V), power factor (Q), or reactive power control (Mvar) control mode, with the operating mode as well as the operating point specified by the NSP. Once specified, while operating between 5% and 100% rated power, RPPs of Category C are required to have the ability to vary reactive power (Mvar) support at the POC within the limits specified in Figure 3.16, of which the values of  $Q_{min}$  and  $Q_{max}$  are governed by the graph of Figure 3.17.

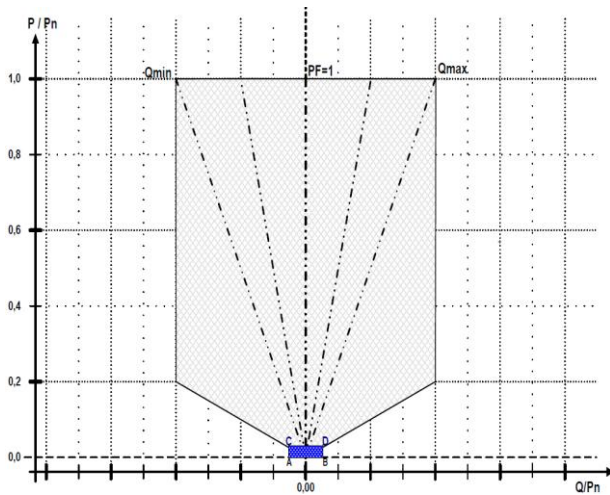


**Figure 0.17: Category C reactive power support requirements**

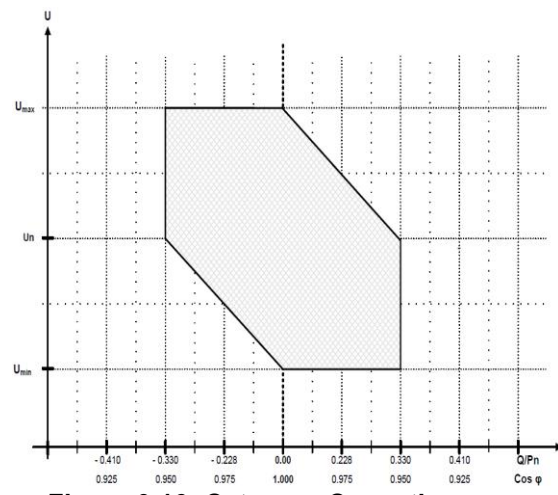


**Figure 0.16: Category C reactive power and voltage range requirements**

If the voltage at the POC remains within the normal range, as specified by Area A of Figure 3.12, the reactive-power support requirement is defined by the graph in Figure 3.18. When operating

below 5% rated power, no reactive support requirements apply; however, RPPs are required to continue operating within the blue highlighted boundary points A, B, C, D of the Figure 3.18 graph.

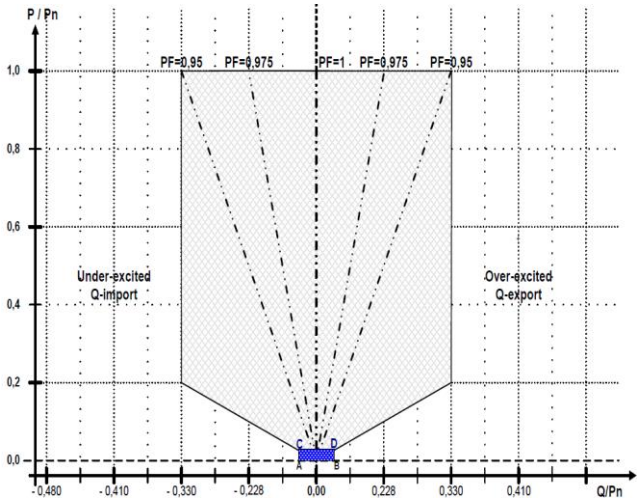


Figure 0.18: Category C reactive-power support requirements at normal POC voltage

**3.4.2 Frequency response requirements set for RPPs in South Africa**

During over-frequency events, categorised by South African grid codes as frequencies exceeding 50.5 Hz, all RPPs must assist in stabilising the grid through the reduction of the active power supplied at that given moment. This should be done as a function of change in frequency, defined by the graph in Figure 3.19. Once the frequency exceeds 51.5 Hz, for a period longer than 4 seconds, it is required of RPPs to trip to protect the NIPS.

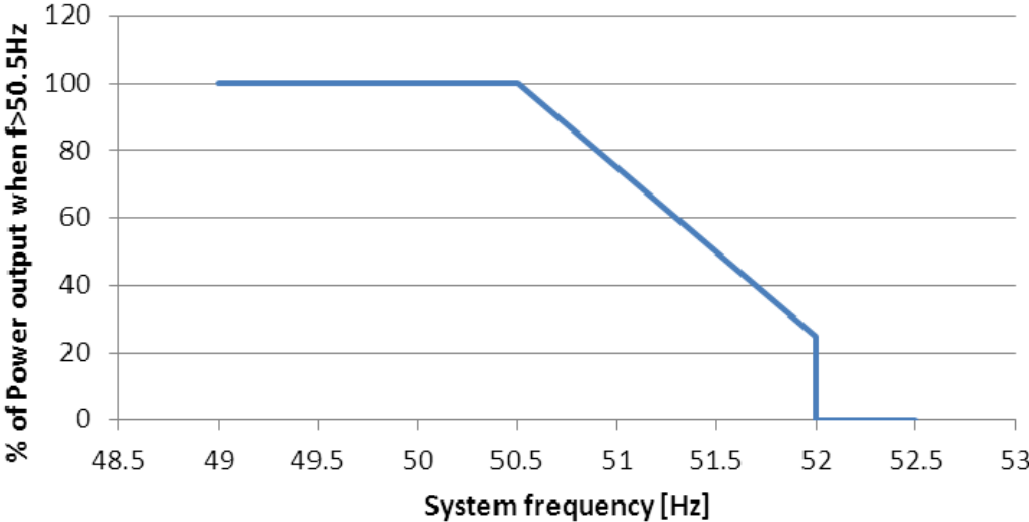


Figure 0.19: Power curtailment requirements during over-frequency events



In addition to the mandatory curtailment requirements set for all RPPs, it is also required for Category C RPPs to be equipped with frequency-droop-control capabilities, for which the settings are illustrated in Figure 3.20, allowing under-frequency support, as per the boundaries the graph of Figure 3.20. These droop settings are required to be adjustable between 0% and 10% while having the ability to regulate the active power supplied down to  $P_{min}$ , beyond which individual units of the RPP can be shut down. When operating between  $f_{min}$  and  $f_{max}$ , Category C RPPs should also be able to deactivate and reactivate these frequency control functions at any given moment, as requested.

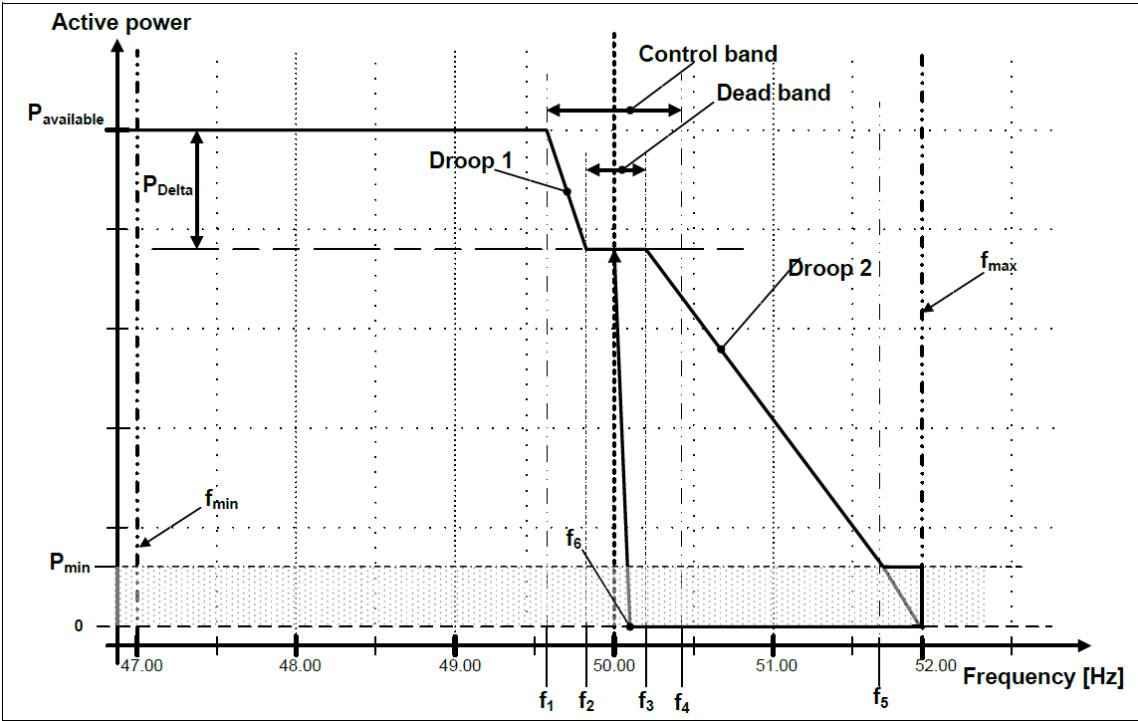


Figure 0.20: Category C frequency response requirements

Values for points  $f_{min}$ ,  $f_{max}$  and  $f_1$  to  $f_6$  are dependent on the design capabilities of the specific RPP, and are to be agreed upon between the RPP operator and SO. These should, however, be adjustable between 47 Hz and 52 Hz, with an accuracy of 10 MHz. Some default values are, however, also available, specified in the South African grid codes, as per Table 3.2.

Table 0.2: Default frequency values set for frequency support requirements

Parameter:	Magnitude (Hz):
Fmin	47
Fmax	52
f1	As agreed with SO
f2	As agreed with SO
f3	As agreed with SO

Parameter:	Magnitude (Hz):
f4	50.5
f5	51.5
f6	50.2

### 3.4.3 Grid-code compliance and testing procedures

The process of grid-code compliance verification requires revision of relevant documentation, including local grid codes, technical data, and models to establish the technical and generation asset requirements necessary to allow new generation to connect to the larger grid network. This requires a combination of practical and simulated tests and studies, to verify and ensure that the new generation will not affect the grid or grid infrastructure negatively during a variety of normal and abnormal conditions. The final step in proofing compliance requires actual measurements to be taken to validate model performance, after which connection to the grid is allowed. Obtaining approval and the necessary compliance certificates is therefore compulsory, making it a significant milestone in the development process of any new generation.

The responsibility of demonstrating grid-code compliance falls primarily to plant owners, after which it is expected of the relevant network operator to assess and confirm compliance results, as well as the procedures used to obtain them. Fulfilling compliance is also not a singular requirement and should be maintained and monitored throughout the lifespan of a facility, conducting periodical retests to validate technical capabilities and to verify the validity of simulation models previously used (Etxegarai *et al.*, 2017; NERSA, 2019).

These testing responsibilities are defined primarily by the grid-code documentation of a country, yet the same cannot always be said about the details of verification procedures. The study of Etxegarai *et al.* (2017) set out to review grid-code documents as well as studies on grid codes for several countries, focusing on those applicable to renewable wind power plants, in a quest to identify potentially insufficiently detailed areas of concern. Results from the study identified mainly a lack of details surrounding the requirements set with regard to grid-code compliance testing and the verification procedure requirements. Consequently, the study aimed to fill the research gap by suggesting testing- and compliance verification procedures for renewable generation, based on the review of international regulations and testing procedures, as well as on current use practices.

Grid-code compliance behavioural studies normally require a combination of physical tests, in addition to simulations, as previously mentioned, since both are limited in their abilities and in the extent to which they can validate grid-code compliance accurately. Currently, grid-code compliance behavioural studies are still carried out largely through physical testing, whether in a lab or on-site. Compliance validation can therefore take significant periods of time, and can easily

become a costly process, while damaging equipment during testing is also often a real concern. Physical testing is, however, still the preferred method of most network and system operators, achieving a higher degree of accuracy compared to conventional simulators. The OPAL-RT simulation model developed by the study consequently aims to challenge accuracy concerns using real-time simulation, capable of better simulation accuracy compared to conventional simulation models, without incurring the inherent costs, risks, and time constraints associated with physical testing.

When having to simulate an extensive power system, it is often recommended to apply simplification techniques such as model aggregation, reducing large sections of a network to a single equivalent section. An example of this would be representing an entire wind farm consisting of several generating units, as a singular wind turbine having the combined capacity of the wind farm (Etxegarai *et al.*, 2017). The effectiveness and consequences of model aggregation and simplification on the ultimate results produced are assessed by Asmine *et al.* (2011), who find the accuracy of such models indeed to be sufficient, leading to this technique being recognised by most network operators, and accepted as a valid practical solution to modelling extensive networks.

Recent years have also seen network operators often specifying compulsory, or preferred simulation software that should be used when creating such models. The software specified can be based on specific types of renewables in use on a network, since some software tools such as DigSILENT offer manufacturer-specific models, having the potential to yield a higher degree of accuracy. However, network and system operators generally prefer the use of standard models with the software of their choice. This allows models then to be adapted by adjusting parameters to represent equipment from a variety of manufacturers, while still having adequate accuracy and being simple enough to form part of a larger network simulation. Network operators also often allow for wind speed to be considered constant for up to 20 seconds when simulating wind turbines, helping to further simplify the simulations (Etxegarai *et al.*, 2017).

Constructing a new simulation model for use as part of grid-code validation behavioural studies, whether purely simulation based or implementing real-time simulation equipment like that developed by this study, requires mandatory accuracy validation before implementation or use, validating and proving its reliability and effectiveness. Validating a model's accuracy thus requires the collection of data, simulation of scenarios where the outcome is known and finally, comparison of the results produced with the known and expected outcome, after which the model's accuracy can either be accepted as being sufficient and correct, or rejected. Simulation models can furthermore be categorised according to their intended use. The three main categories consist of

load-flow- and short-circuit models used for basic design purposes, positive sequence- or RMS models used for system integration and stability studies, or detailed three-phase EMT models used to study the interfering effects of fast-switching electronic components. The model designed by this study is therefore of the second type, as its intended use is for performing renewable grid-integration behavioural studies (Etxegarai *et al.*, 2017).

#### **3.4.4 RPP testing specifications for South Africa**

Testing specifications set for all new power plants require a variety of physical lab- and on-site tests, as well as simulations to be performed validating that its integration will not affect the grid negatively in any way. Only once grid-code compliance has been validated, can commissioning occur. This refers to the point-to-point testing of signals to ensure proper configuration, followed by the final phase of grid integration. The importance of grid-code compliance testing thus comes to light, being among the mandatory first steps forming part of the testing process. Simulation-based testing can thus provide an acceptable and reasonable insight into grid-code compliance while being more economical and time efficient compared to the alternative of physical testing. The purpose of conducting simulations is also twofold, providing not only a means of validating grid-code compliance, but also of helping to identify areas of concern earlier in the testing process through RPP behavioural studies, after which alterations or mitigations can be applied to address them (NERSA, 2019).

The responsibility of conducting these tests is shared by both the NSP and plant operator, specified in the Grid connection code for renewable power plants connected to the electricity transmission system or distribution system in South Africa (NERSA, 2019). Compliance testing requirements vary greatly with power plant type and specifications, including whether it is renewable or conventional, and using synchronous or asynchronous turbines. For this study, the focus will fall on testing requirements set for renewable power plants, which are commonly of an asynchronous type (NERSA, 2019).

These types of power plants are characterised by their inverter-based connection to the grid, and include CSP, solar, and wind farms. The testing responsibilities of the Network Service Provider (NSP) in terms of new generation include load flow, short circuit, stability, and power quality studies to be conducted as part of the commissioning process. Testing responsibilities of the plant owner or operator can again be categorised based on the type of power plant. For asynchronous- and converter-based generation such as PV and wind farms, it is required that load-flow and short-circuit studies as well as quality of supply studies are conducted as part of the plant design process. Following this, grid-code compliance testing is required, which includes a power quality- and reactive-power capability assessment, as well as LVRT and HVRT studies to be conducted.

For synchronous generation such as biomass or hydro, testing requirements are very much the same, with the difference being in terms of the required grid-code compliance testing. Instead of having to verify the LVRT and HVRT capability and ability to comply with grid-code requirements, transient stability, and excitation system requirements, as per GCR3 of the current South African grid code, are required (NERSA, 2019).

Of the above-mentioned requirements specified in the South African grid codes, the developed real-time simulator will focus on the grid-code compliance testing of asynchronous generation, including compliance verification of LVRT, HVRT, LFRT, HFRT, and short-circuit requirements, through the simulation of different faults and short-circuit events. This area of testing is chosen based on the ability to verify compliance through simulation, compared to power quality or protection verification, which would additionally require physical on-site or lab testing. Verifying grid-code compliance is predominantly achieved by conducting fault ride-through simulations, establishing whether an RPP will remain connected while providing the necessary support, as required by grid-code documents. Grid codes additionally provide all the data required, assumptions allowed, and testing requirements when testing fault ride-through abilities, for results to be of an acceptable standard.

The first of these includes testing requirements set for short-circuit testing, which require the simulation to record specified parameters at increasing time intervals, up to  $t=500$  ms. At each time interval, active current, reactive current, and peak current are to be measured, for voltage drops representing 20%, 30%, 50%, and 80% of supply at the POC. Data obtained are required to be provided in the form of a table, such as that provided in the grid-code documents for a 20% voltage drop, represented in Figure 3.21. As data requirements for a 30%, 50%, and 80% voltage drop will be the same, the tables will also be similar, with the only difference being the percentage drop in voltage (NERSA, 2019).

dU=20%			
Time [ms]	I <sub>active</sub> [A]	I <sub>reactive</sub> [A]	I <sub>peak</sub> [A]
0			
5			
10			
20			
50			
100			
150			
200			
300			
500			

**Figure 0.21: Short-circuit testing table, 20% reduction in voltage (NERSA, 2019)**

Although routine compliance retests are not yet mandatory, all new RPPs, as well as RPPs having undergone major modifications or refurbishment are required first to pass grid-code compliance before being allowed to connect or reconnected to the grid. The basic requirements for these tests include proving that an RPP will stay connected within the limits set by grid codes, and using a dynamic simulator to simulate the behaviour of an RPP during fault conditions. Additionally, a report is also required by the SO, NSP, or network operator containing the compliance results, submitted no later than three months following commissioning of the RPP (NERSA, 2019).

The first step in developing the real-time test platform will therefore involve the construction of a test circuit, for which the grid-code documents specify certain design and construction requirements. The extensive requirements set are available in Appendix 12 of the grid-code requirement document for RPPs in South Africa, with the primary requirements surrounding the construction and modelling of a test circuit relevant to the development of a real-time platform summarised below (NERSA, 2019).

These include that a common voltage level should be attained at the POC, between the grid-representing- and renewable side of the test network. Loads connected to the surrounding network are to be lumped together and should have a maximum- and minimum load value based on actual metering data, where available. Similarly, additional generation connected to the surrounding network are also to be combined based on whether they are of a synchronous or asynchronous type and represented as an aggregated generic supply connected to the network. The generic supply models are furthermore required to be of a recognised type, such as IEC or IEEE standard models. Requirements set for additional loads and generation connected to the network at different voltage levels are very much the same, also having to be combined before network connection, at the POC network voltage. Feeders having a variety of generation and loads connected are also to be reduced to a singular generic generator, and singular combined load connected to the feeder (NERSA, 2019).

Example networks are provided in South African RPP grid-code documents, which can be seen in Figures 3.22 and 3.23.

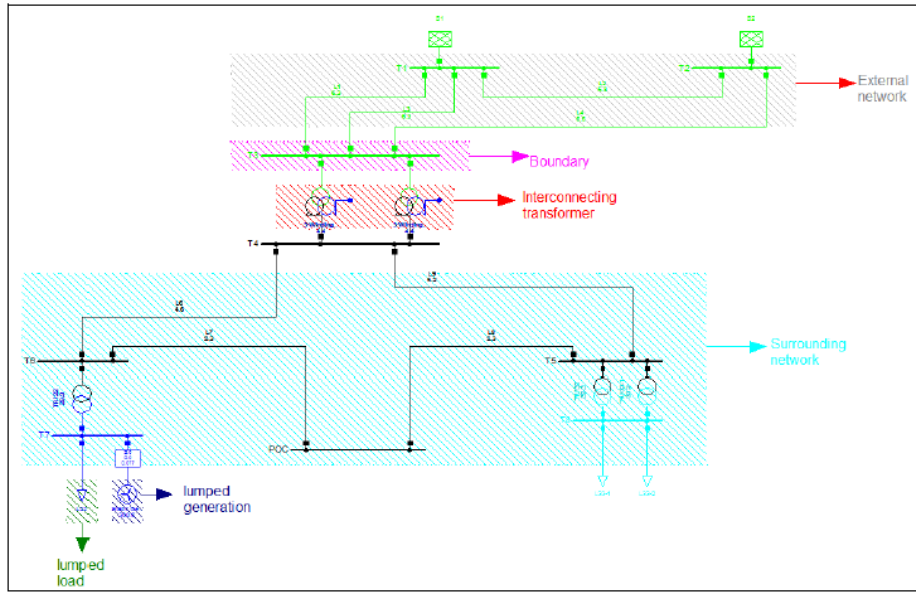


**Figure 0.22: Example test network  
(NERSA, 2019)**

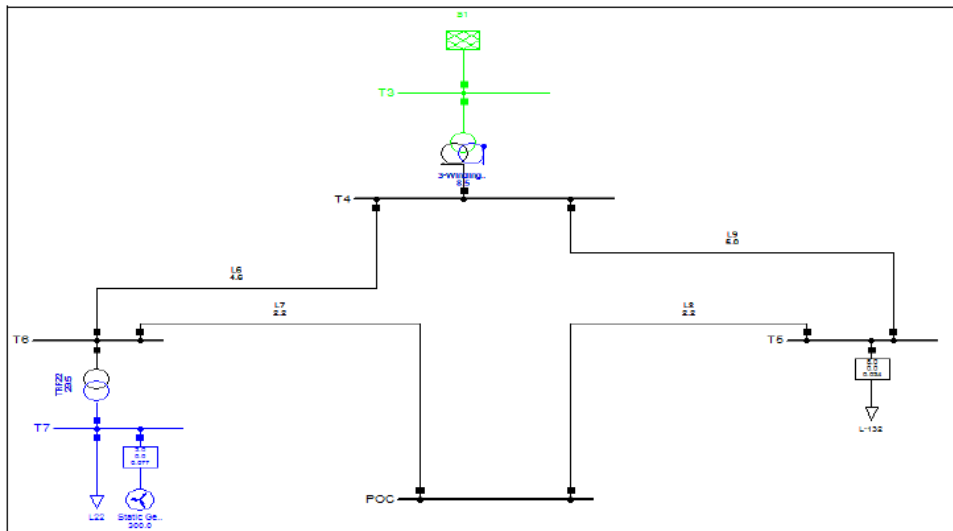


**Figure 0.23: Example test network combined and reduced  
(NERSA, 2019)**

Figure 3.22 represents an example network with its respective parts labelled. These include the external network or grid, a boundary in the form of a bus, interconnecting transformers to match the voltage at the POC, the surrounding network, and a feeder containing a lumped load and generation. Figure 3.23 represents the equivalent network of the circuit in Figure 3.22, after being reduced by applying the requirements set in grid codes. This includes representing the external network or grid as a singular unit, connected to the surrounding network using the same bus as a

boundary, and a singular interconnecting transformer. At T5, additional lumping of different loads also occurred, now to be represented as a singular equivalent load (NERSA, 2019).

The test circuit developed for the real-time testbed can thus draw its inspiration from the Figures 3.22 and 3.23 examples, with the RPP being tested represented like the lumped generation of T7.

### 3.5 Analysing the effects of the changing generation mix on the South African grid

The updated 2030 IRP (Department of Mineral Resources and Energy, 2019), being among the latest reliable information available, confirmed that South Africa plans to increase the amount of grid-connected renewables significantly leading up to 2030, which will affect the reliability, stability, and flexibility of the South African grid inadvertently. This should, however, not be associated instinctively with the deterioration of these parameters, because of the often unstable nature some renewables, in that different generation will affect the grid in different ways, often each with its own positive and negative attributes.

As a way of assessing the effect that changing generation has on the South African grid in terms of reliability, stability, and flexibility, Table 3.3 was created, making use of the updated 2030 IRP report data to consider the purpose and generation contributions by type in 2019, compared to that forecasted for 2030.

**Table 0.3: Grid assessment data**

Generation:	Generation purpose:	2019 Installed generation (MW):	% contribution:	2019/2030 MW Difference:	2030 Installed generation (MW):	% Contribution:
Coal	Base load	37 149	71,30	-3 785	33 364	42,59
Wind	Self dispatching	1 980	3,80	15 762	17 742	22,65
PV	Self dispatching	1 474	2,83	6 814	8 288	10,58
Gas and Diesel	Peak load	3 830	7,35	2 550	6 380	8,14
Pumped Storage	Peak load	2 912	5,59	2 088	5 000	6,38
Hydro	Peak load/ Grid stabilization	2 100	4,03	2 500	4 600	5,87
Nuclear	Base load	1 860	3,57	0	1 860	2,37
CSP	Self dispatching	300	0,58	300	600	0,77
Other (Distributed generatio, Co-generation, Biommass, Landfill, etc.)	(Various)	499	0,96	1	500	0,64
	<b>Total (MW):</b>	<b>52 104</b>	<b>100</b>	<b>26 230</b>	<b>78 334</b>	<b>100</b>
	<b>Total Base load (MW):</b>	<b>39 009</b>			<b>35 224</b>	
	<b>Total Peak load (MW):</b>	<b>8 842</b>			<b>15 980</b>	
	<b>Total Self dispatching load (MW):</b>	<b>3 754</b>			<b>26 630</b>	

**Table 3.3 generated using: Eskom (2009), Bello et al. (2013), Department of Energy and Department of National Treasury (2018), Department of Mineral Resources and Energy (2019), Eskom (2019b) Eskom generation division (2019), NERSA (2019).**

Using Table 3.3, the variety of available generation resources can first be assessed. Although the IRP does not mention any new forms of generation to be added to the South African grid between 2019 and 2030, amounts from existing generation produced by the respective technologies are expected to increase for almost all, apart from coal. It can further be noted that South Africa makes use of at least eight main types of generation, showing commitment to diversifying the South African energy mix. This will prove greatly beneficial in increasing the reliability and flexibility of



the South African grid, in that, if one type of generation were to experience supply difficulties, the effect will be mitigated by the several other unaffected technologies in use (Department of Mineral Resources and Energy, 2019).

The other important grid characteristic identified is that of stability, for which an indicator is the amount of synchronous generation connected to a grid, providing vital inertia combatting frequency changes brought about by load fluctuations. Considering the South African energy mix, most resources will contribute towards grid inertia, including coal, gas, diesel, pumped storage, hydro, and nuclear, all utilising synchronous generators. For the current generation mix, Table 3.3 can be used to calculate the inertia-providing generation for 2019 to be about 47 791 MW or 91.72% of the installed capacity. Compared to the forecasted 2030 inertia-providing generation of 51 204 MW, or 65.37% of the total 2030 generation, it is seen that, although the capacity of inertia-providing generation will increase by 2030, the significant increase in renewables connected to the grid leads to a reduction in the overall percentage of synchronous generation connected. The inertia of the South African grid therefore is expected to decrease inevitably, potentially limiting the number and size of grid disturbances that can be absorbed by the system, leading to decreased stability from an inertia point of view. This is, however, not the sole factor in determining grid stability and it is required that other generation also be considered, as well as the amounts of inertia provided by different types of synchronous generation, to allow a proper assessment of how much system inertia will be affected. Possibly counteracting the expected decrease in system inertia, is the fact that literature reviewed in Chapter Two demonstrated a combination of wind and solar to complement one another well for South African conditions, reducing the negative effects of their integration on system stability and reliability (Knorr *et al.*, 2016; Department of Mineral Resources and Energy, 2019).

Dispatchable or peak-load generation is another important consideration, as it is used to fill the generation gap during peak-load periods, or when renewables are unable to produce an optimal amount of generation owing to unfavourable conditions. The contribution of such generation can again be considered for 2019, calculated to be about 8 842 MW or 16.97% of the installed capacity, compared to the forecasted 2030 figure of about 15 980 MW, or 20.40%. An increase is noted in dispatchable or peak-load generation, which is to be expected considering the increase in renewables. This is significant since the nature of dispatchable, or peak-load generation allows it to be dispatched at short notice, which is vital to maintain stability and reliability when other forms of generation, such as renewables, experience a decrease in output following uncontrollable conditions like changes in weather. As another contingency to the uncontrollable nature of renewables, the 2019 updated version of the IRP also confirms future participation in cross-border

interconnections, strengthening the South African grid by securing a means of obtaining additional generation from surrounding countries if needed (Department of Mineral Resources and Energy, 2019).

Grid strength can further be assessed considering Figure 3.24, which illustrates the fault ride-through and voltage-recovery requirements of different countries, adapted to include those set for larger RPPs in South Africa by superimposing the respective South African voltage requirements onto Figure 2.1 of Chapter Two for comparison purposes, available at Papathanassiou and Tsili (2009). South African requirements are represented by both the added red and blue lines, representing the fault ride-through requirements of Categories A3, B, and C RPPs utilising non-synchronous and synchronous machines respectively. From the literature reviewed, it has been indicated that strict fault ride-through requirements set in grid codes could be an indicator of a weaker grid. Using Figure 3.24 to compare fault ride-through requirements set for South African RPPs to some of those set in other countries, it is noted that the South African requirements are largely on par with others. Considering the recovery slopes, especially those of non-synchronous machines in South Africa, it is noted that these RPPs, which will mostly include wind and solar PV generation, will be required to remain connected longer during faults, recovering slower compared to most others. Although not an unusual requirement, this could hint at a weaker grid system, therefore requiring as much generation to remain connected for as long as possible before disconnecting, in that way assisting in voltage recovery to maintain stability (Nhlapo and Awodele, 2020).

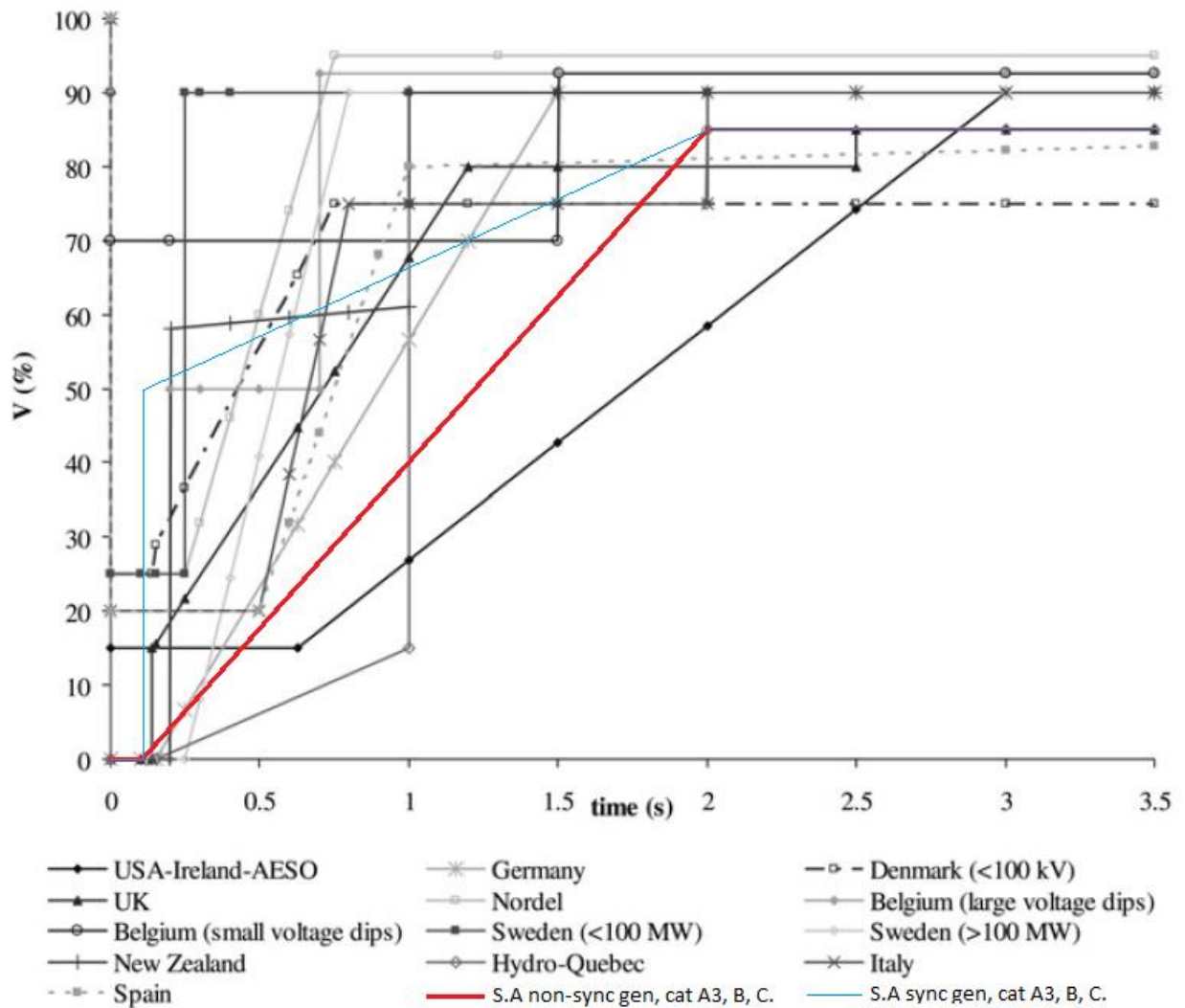


**Figure 0.24: Adapted voltage ride-through and recovery requirements by country**  
 Generated using; Papathanassiou and Tsili (2009), NERSA (2019)

### 3.6 Test wind turbine

As discussed, the MATLAB model exported and used in OPAL-RT has its origin in MATLAB's Simulink environment. The basic construction of the circuit consists of two sides, the first representing the renewable generation or RPP being tested, while the second consists of the grid-representing side to which the test RPP is connected. Consequently, any type of renewable generation can be connected to the circuit to study its behaviour, even though the focus falls on a wind farm modelled as an example for this study.

Using wind turbines as the technology of choice for conducting the case studies stems from the fact that, in South Africa, onshore wind dominates the renewable energy industry, accounting for the largest percentage of grid-connected renewables, the largest percentage of operational

renewables, and the largest percentage of planned renewables going forward (Department of Energy and Department of National Treasury, 2018; RSA Department of Energy, 2018). With this in mind, Eskom’s only grid-connected Sere wind farm is used as inspiration for the exemplary wind farm modelled in the case studies.

Eskom’s Sere wind farm, located in the Western Cape, South Africa, close to the town of Koekenaap, consists of 46 Siemens SWT-2.3-108 wind turbines of 2.3 MW each, which combine to have a total capacity of 100 MW (Eskom, 2015b, 2015a). Apart from Eskom’s Sere wind farm, this type of wind turbine can also be found implemented at several other locations in South Africa, including Jeffreys Bay wind farm, Kangnas wind farm, Khobab wind farm, Loeriesfontein wind farm, Noupoort wind farm, and Perdekraal East wind farm, making it among those implemented and most used in South Africa (Mainstream Renewable Power, 2016; 2017a; 2017b; 2018a; 2018b; GLOBELEQ, 2020). Siemens has established itself firmly as a reliable and trustworthy supplier of renewable energy equipment, such as wind turbines since the technology’s infancy. They are well known for producing efficient industry-leading equipment widely used not only in South Africa but worldwide (Siemens, 2011). Construction of the Sere wind farm took approximately one year, with the first 169-meter high turbines being erected on 2 December 2013, and the last string of six turbines being energised on 30 December 2014 (Eskom, 2015; 2015b). Key specifications of the Siemens SWT-2.3-108 turbines used at Sere are summarised in Table 3.4 (Siemens, 2011; Windpower Engineering & Development, 2020). A component and equipment layout also follows in Figure 3.25, as well as the power performance curve compared to wind speed in Figure 3.26 (Siemens, 2011).

**Table 0.4: Siemens SWT-2.3-108 key specifications**  
(Siemens, 2011; Windpower Engineering & Development, 2020)

<b>Siemens SWT-2.3-108 key specifications:</b>	
<b>Rotor:</b>	
Type:	3-bladed, horizontal axis
Diameter:	108 m
Speed range:	6-16 rpm
Power regulation:	Pitch regulation with variable speed
<b>Transmission system:</b>	
Gearbox type:	3-stage planetary/helical
Gearbox ratio:	1:91
<b>Generator:</b>	
Type:	Single-fed asynchronous
Nominal power:	2 300 kW
<b>LV grid terminals:</b>	
Nominal power:	2 300 kW

Siemens SWT-2.3-108 key specifications:	
Voltage:	690 V
Frequency:	50 Hz of 60 Hz
Operational data:	
Cut-in wind speed:	3-4 m/s
Rated power at:	11-12 m/s
Cut-out wind speed:	25 m/s
Maximum 3s wind gust:	59.5 m/s (IEC version)

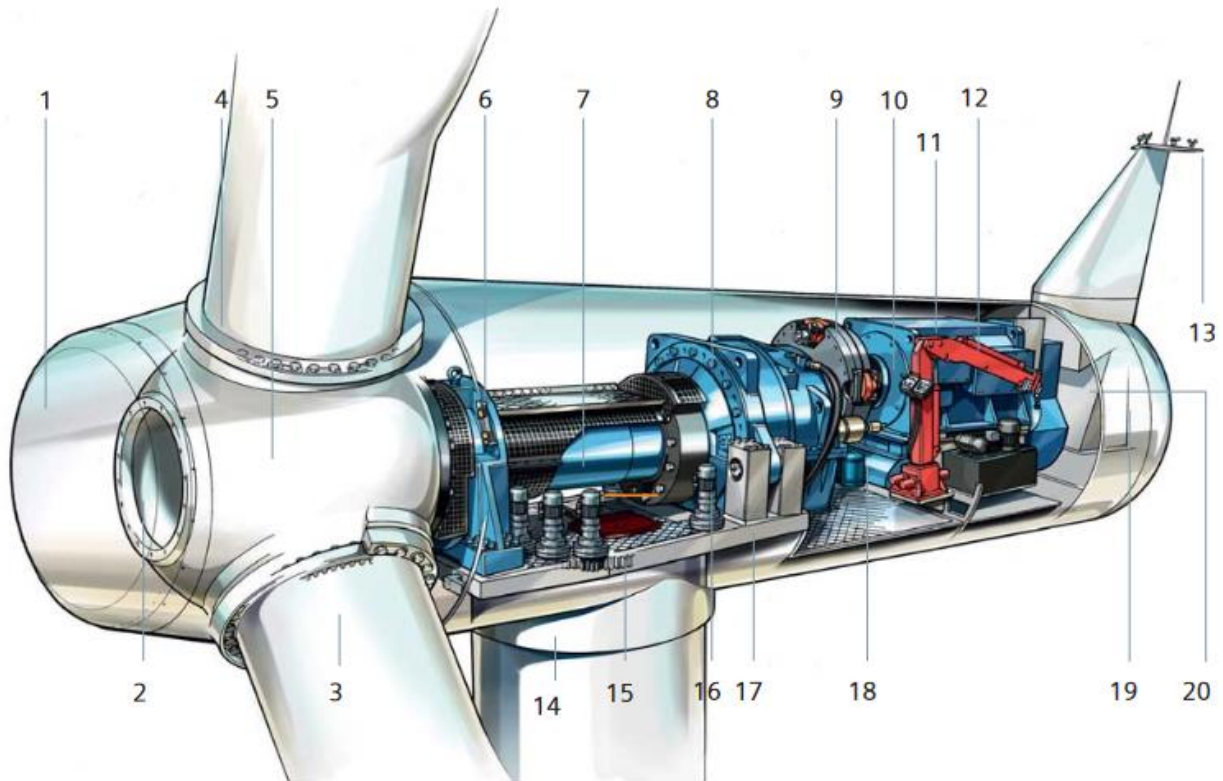


**Figure 0.25: Siemens SWT-2.3-108 turbine component layout  
(Siemens, 2011)**

The numbers, as marked in Figure 3.25, correspond to the following components (Siemens, 2011).

1. Spinner
2. Spinner bracket
3. Blade
4. Pitch bearing
5. Rotor hub
6. Main bearing

7. Main shaft
8. Gearbox
9. Brake disc
10. Coupling
11. Generator
12. Service crane
13. Meteorological sensors
14. Tower
15. Yaw ring
16. Yaw gear
17. Nacelle bedplate
18. Oil filter
19. Canopy
20. Generator fan

Power performance specifications of the Siemens SWT-2.3-108 relative to wind speed are represented by the graph of Figure 3.26 (Siemens, 2011).

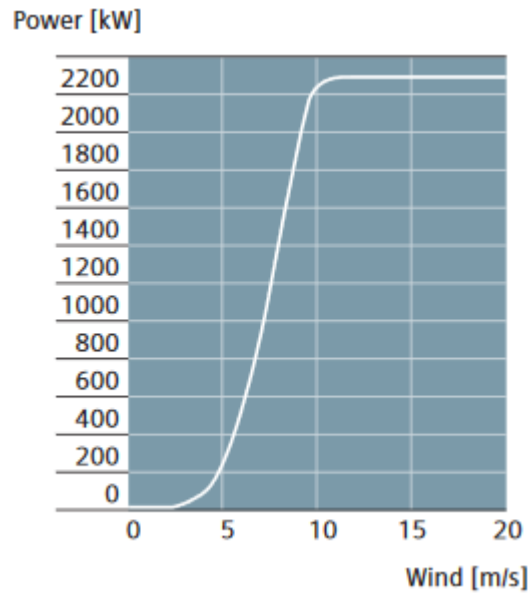


**Figure 0.26: Siemens SWT-2.3-108 power vs wind speed characteristic curve (Siemens, 2011)**

### 3.7 Summary:

In this chapter, a clearer overview was presented of the direction towards which South Africa aims to move in terms of the country's future generation mix and the possible associated resulting

challenges. In summary, a 33% increase in renewable-generation capacity is expected, as indicated by the 2030 IRP, utilising mainly onshore wind, and solar PV. The potential effect was analysed of these changes on grid reliability, stability, and flexibility, revealing that the contribution from synchronous inertia-providing generation towards the total generation mix is likely to decrease 26.35%. However, the overall generation capacity is set to increase by 33.48%, including a 3.43% increase in dispatchable generation, thus counteracting the unfavourable loss of grid inertia. Further analysis of grid codes reveals RPP testing requirements to include LVRT, HVRT, LFRT, HFRT, and short-circuit testing, aimed at assessing the ability of an RPP to provide grid support much as conventional generation would. South Africa's RPP voltage ride-through requirements were then compared to those of other countries and, although noted to be similar, they require RPPs to remain connected slightly longer than most, which may hint at stability concerns during the development of the requirements. Finally, 2.3 MW Siemens wind turbines were selected as the test RPP for the forthcoming case studies, in that onshore wind emerged as one of the fundamental technologies forming part of South Africa's renewable energy future. The specific wind turbine selected is also already used at seven wind farm locations in the country, including the Eskom-owned Sere wind farm, making it a likely candidate for future wind farm projects.

## **CHAPTER FOUR**

### **RESEARCH RESULTS/DELIVERABLES**

#### **4.1 Introduction**

The purpose of Chapter Four is to discuss the development process of the study's tailored South African real-time grid-integration behavioural studies testbed, implementing the RPP grid-code requirements and specifications reviewed in Chapter Three. Consequently, the chapter starts by discussing the testbed integration of grid-code requirements using a MATLAB live script, as a means of selecting the appropriate grid-code requirements for a given simulation, in a user-friendly manner. Next, the real-time simulation setup requirements of the MATLAB Simulink model are discussed, required later for RT-LAB integration, to allow OPAL-RT real-time simulation finally. The chapter continues to expand on the testbed's Simulink model development, considering its inputs, components, and outputs. This involves modelling the necessary components mathematically and discussing the functions of the testbed's subsystems, thus giving insight into the model's flow and the testbed's workings. Having covered the testbed's design details, Chapter Four swiftly reviews the host computer, and the OPAL-RT OP4510 real-time simulator's connection, and lab setup. The chapter concludes by developing a testing strategy for the developed testbed, aiming to illustrate its accuracy and effectiveness as an RPP grid-integration behavioural studies tool during the forthcoming case studies chapter.

#### **4.2 Development of the MATLAB live script**

The purpose of developing a MATLAB live script alongside the testbed's Simulink circuit, was to increase its versatility by allowing the testbed to accommodate any type and size of RPP, in a user-friendly manner. The MATLAB live script, therefore, aims to bridge the gap between the multiple manual parameter adaptations, which would be required when alternating between RPPs, allowing the operator instead only to input key parameters, after which the live script selects the appropriate grid-code specifications, automatically exporting it to the Simulink environment. Having studied South African RPP grid-code requirements (NERSA, 2019), these key parameters were identified as being the POC voltage, and RPP class, in that limits set for RPP frequency requirements remain constant irrespective of RPP type and size. The MATLAB live script, therefore, had to be developed to output the normal upper 'Vnu' and lower 'Vnl' voltage boundaries, as well as adjusting the High-and Low-Voltage Ride-Through (HVRT/LVRT) boundaries. The process used for generating the outputs required, given the POC voltage and RPP class as inputs, is then given by the diagrams in Figures 4.1 and 4.2 respectively.



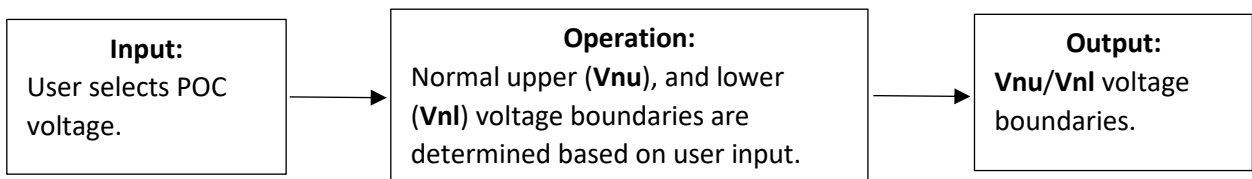


**Figure 0.1: Process of selecting Vnu and Vnl voltage boundaries based on user input**

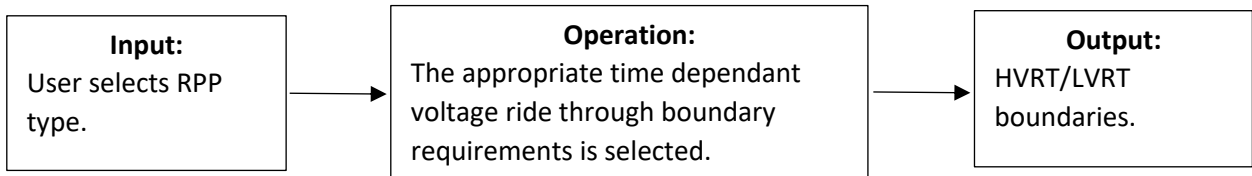


**Figure 0.2: Process of selecting HVRT, and LVRT boundaries based on user input**

As part of MATLAB live editor functions, drop-down menus were implemented allowing the user easily to select specific parameters from a larger field of equipment-specific requirements, as in the case of grid codes. Hence, the MATLAB live editor was set up to contain all the normal upper ‘Vnu’ and lower ‘Vnl’ voltage limits specified for RPPs of different POC voltages, as well as the voltage ride-through boundary conditions relative to time, based on the RPP type selected.

Combining the drop-down menus with ‘if’ functions allowed the live script only to require ‘RPP type’, and ‘POC voltage’ selection using the drop-down menus illustrated in Figure 4.3, after which the relevant grid-code requirements are generated automatically. The automatically selected Vnu, Vnl, HVRT, and LVRT details are then ready to be exported to the MATLAB Simulink environment, where they are used to test the simulated RPP in line with its applicable grid-code requirements.

```
POC_voltage = "11/22/33/44kV"; RPP_type = "Cat_C_non-sync";
```

**Figure 0.3: MATLAB live script user inputs**

To accommodate the full range of RPP types and sizes, the drop-down menu options include the following: To determine Vnu/Vnl values, the POC\_voltage menu of Figure 4.3 requires selection between the following options:

- ‘<11kV’ - RPPs with a POC voltage below 11 kV.
- ‘11/22/33/44kV’ – RPPs with an 11 kV, 22 kV, 33 kV, or 44 kV POC voltage.
- ‘66/88/132kV’ – RPPs with a 66 kV, 88 kV, or 132 kV POC voltage.

Similarly, to determine HVRT/LVRT boundaries, the RPP\_type menu of Figure 4.3 requires selection between the following options.

- ‘**Cat\_A1,A2**’ – RPPs <100 kVA.
- ‘**Cat\_A3,B\_non-sync**’ – Non-synchronous RPPs from 100 kVA to <20 MVA.
- ‘**Cat\_C\_non-sync**’ – Non-synchronous RPPs 20 MVA and greater.
- ‘**Cat\_A3,B\_sync**’ – Synchronous RPPs from 100 kVA to <20 MVA.
- ‘**Cat\_C\_sync**’ – Synchronous RPPs 20 MVA and greater.
- ‘**Cat\_A3,B\_sync\_3-ph\_fault**’ – Synchronous RPPs from 100 kVA to <20 MVA when simulating 3-phase faults.
- ‘**Cat\_C\_sync\_3-ph\_fault**’ – Synchronous RPPs 20 MVA and greater when simulating 3-phase faults.

Following user selection, the developed code of Appendix G will run automatically, selecting the appropriate RPP information in the manner discussed.

As a means of visualising the **Vnu**, **Vnl**, **HVRT**, and **LVRT** of the RPP boundaries prior to performing simulations. The developed code additionally plots and displays the selected data, as given in the example of Figure 4.4. The significance of these boundary values going forward relates to the limits governing conditions during which RPPs are required to remain connected and to support the grid, having been identified previously in Chapter Three as an essential RPP ability to maintain grid stability as the percentage of grid-connected renewables increase.

Vn1 = 0.9000  
Vnu = 1.0800

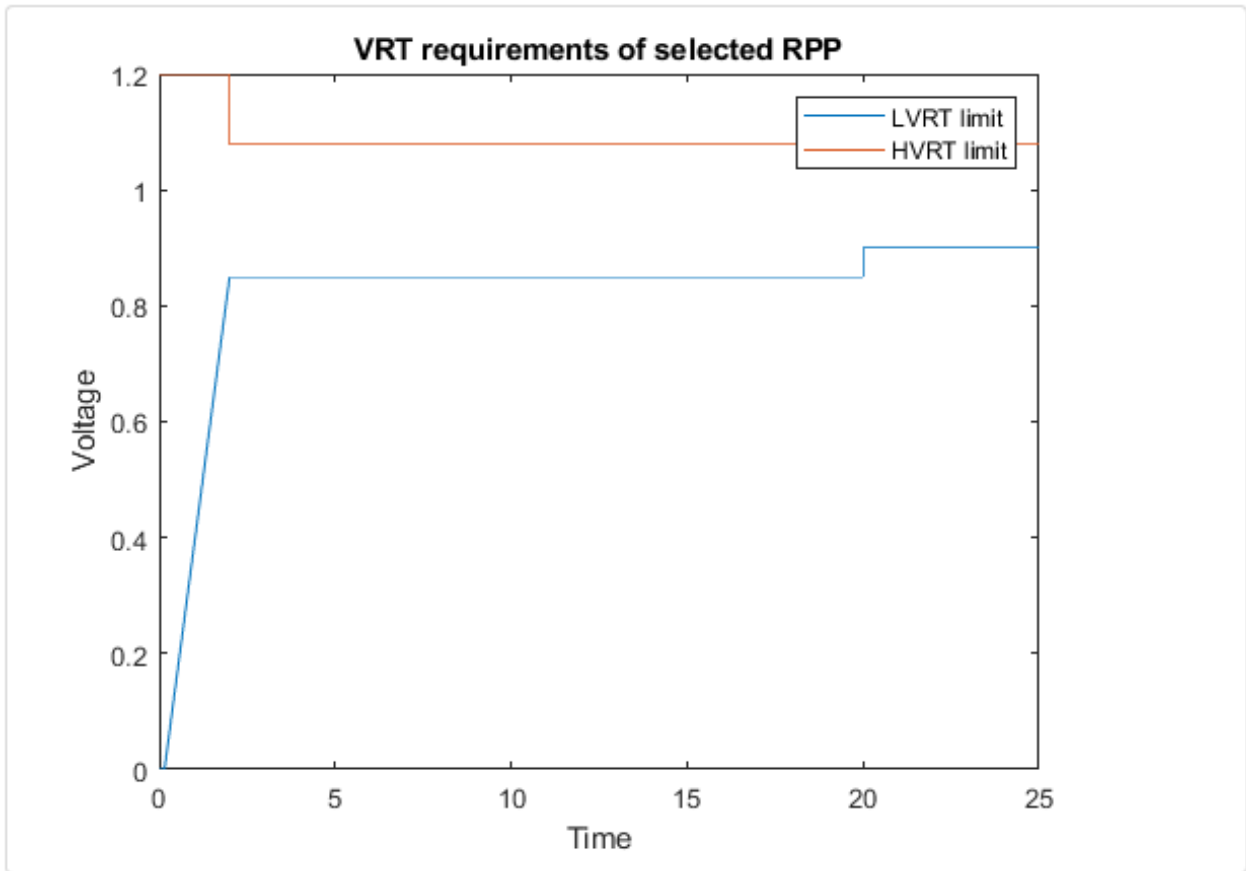
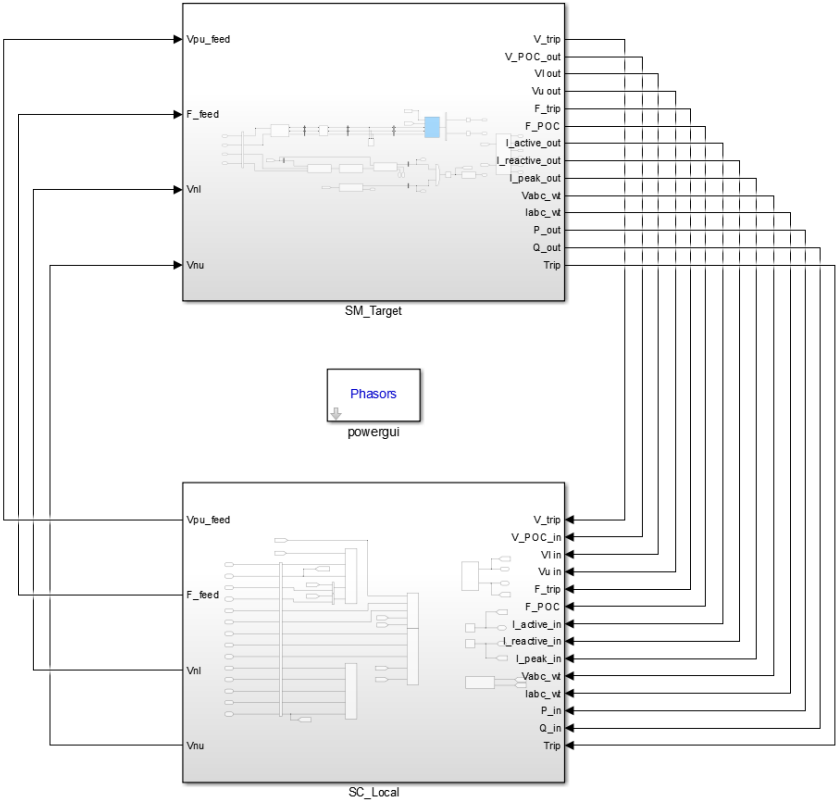


Figure 0.4: Normal and fault ride-through boundaries output based on user input

### 4.3 MATLAB circuit setup for real-time simulation

As the study aims ultimately to deliver a real-time testbed, the MATLAB circuit as part of its development had to consider the necessary RT-LAB requirements, which would allow it later to be executed using OPAL-RT's OP4510 real-time simulator. This involves grouping the developed MATLAB circuit into an SC (Console Subsystem), SM (Master Subsystem) and, if needed, SS (Slave Subsystems), thus directing the model sections to the desired cores of the respective real-time simulator and target computer during model execution (OPAL-RT Technologies, n.d.). The SM subsystem executed using the OP4510 real-time simulator also needs to house all circuit sections requiring calculations to be performed, which includes the main testbed circuit, grid-code validation subsystems, and measurement blocks. In addition to the SM subsystem, an SS subsystem can also be included in the event that overruns occur during the compilation and execution of the RT-LAB model. However, unless overruns occur, this subsystem will be excluded for simplification. The SC subsystem executed using the host computer will, on the other hand, house all data imports, and measurement output components. Real-time simulation furthermore

requires a fixed-step solver to be used as part of the design of the MATLAB Simulink model, and the placement of OpComm blocks at all inputs to the main subsystems, thus allowing communication to occur between the physically separated host computer and real-time simulator (OPAL-RT Technologies, n.d.; MathWorks, 2021a, 2021b). Figure 4.5 illustrates the grouped real-time testbed model, for which the ‘SM\_Target’ and ‘SC\_Local’ subsystems are shown.



**Figure 0.5: Grouped MATLAB testbed design**

**4.4 SM\_Target subsystem**

The section focuses on the SM\_Target subsystem housing the model developed as real-time testbed, and will elaborate on the inputs, sections of the main circuit, and subcircuits responsible for validating South African RPP grid codes in terms of voltage and frequency. The main circuit drew inspiration from the example circuits of Chapter Three while using the grid-code test-circuit specifications discussed as a guide in its design. The developed testbed circuit design is seen in Figure 4.6, followed by a discussion of its respective inputs, components, and outputs. It can further be mentioned that the MATLAB model was set up using an ‘ode4’ fixed-step solver, with a step size of 0.001 seconds, simulating in Phasor mode at 50 Hz (OPAL-RT Technologies, n.d.; MathWorks, 2021a; 2021b).

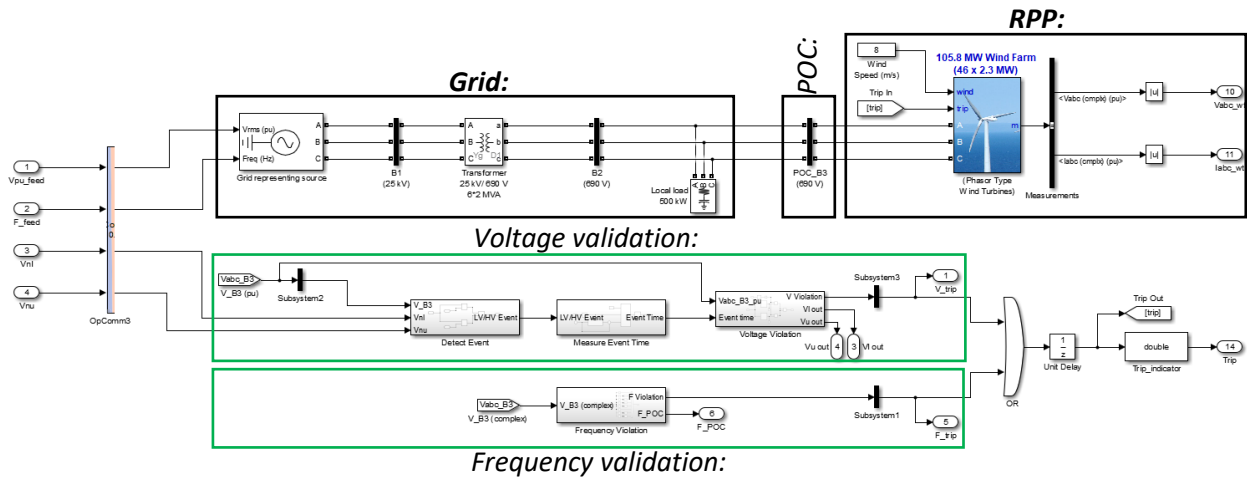


Figure 0.6: SM\_Target subsystem, testbed model circuit design

#### 4.4.1 Data imports

Part of developing the circuit was to make it adaptable, allowing any type and size of RPP to be inserted and simulated. As different category RPPs need to adhere to different requirements, variable inputs had to be obtained based on the simulated RPP, which include the normal upper and lower operating voltage boundaries  $V_{nu}$ , and  $V_{nl}$ . For increased versatility, the circuit uses a single source with inputs '**Vpu spreadsheet**' and '**f spreadsheet**' to represent the larger grid network, allowing the testbed to replay previously recorded grid conditions and events accurately and easily compared to an elaborate static-grid-representing circuit. All inputs additionally pass through an OpComm block, seen in Figure 4.6, allowing the input data from the SC\_Local subsystem executed on the host computer to be imported to the simulation environment simulated on the SM\_Target subsystem of the physically separated real-time simulator. The subsections, inputs, and outputs can then further be defined as follows:

##### 4.4.1.1 $V_{nu}$ and $V_{nl}$

The 'normal upper' ( $V_{nu}$ ) and 'normal lower' ( $V_{nl}$ ) voltage boundary inputs represent the continuous operating voltage range, specified according to an RPP class and POC voltage. These values, therefore, represent the upper and lower limits of the 'Continuous operating range' indicated on the grid-code voltage ride-through specification graphs discussed in Chapter Two. For the developed testbed, these limits are generated by the MATLAB live script discussed, from where they are imported to the MATLAB Simulink environment as ' $V_{nu}$ ' and ' $V_{nl}$ '. For the Eskom Sere-representing wind farm modelled in the study, these values are taken as  $V_{nu}=1.1$  pu and  $V_{un}=0.85$  pu.

#### 4.4.1.2 Vpu spreadsheet and f spreadsheet

'**Vpu spreadsheet**' and '**f spreadsheet**' respectively represent the pu voltage and frequency in Hz inputted to the grid-representing source as a value concerning time. This data is housed and imported from an Excel document, making it easy to repeat previously measured grid data and events, or to input custom data for testing purposes. As the study aims to demonstrate both the accuracy and abilities of the developed testbed, a combination of custom-, and real-world data are implemented to recreate the desired conditions during the forthcoming case studies.

### 4.4.2 Circuit components

#### 4.4.2.1 Grid-representing source

The 'grid-representing source' is seen as the first significant component forming part of the grid section labelled in Figure 4.6, using the imported '**Vpu spreadsheet**' and '**f spreadsheet**' data to generate a usable three-phase output to the circuit. To achieve this, a base voltage and nominal frequency of 25 kV at 50 Hz are selected for this source block, which then generates the three-phase output, according to (4.1).

$$V_{pu} = \frac{V_{out}}{V_{base1}} \quad (4.1)$$

Consequently, when applied to the grid-representing source,  $V_{pu} = \mathbf{Vpu\ spreadsheet}$ ,  $V_{base1} =$  the transformer's primary side voltage, and  $V_{out} =$  grid-representing source output voltage.

Therefore,

$$V_{out} = V_{pu\ spreadsheet} \times V_{base1} \quad (4.2)$$

However, since the per-unit voltage is of interest at the POC, being the primary input to the grid-code validation subsystems, it can be stated that the grid-representing source output is simply given by (4.3).

$$V_{out}(pu) = V_{pu\ spreadsheet} \quad (4.3)$$

#### 4.4.2.2 Transformer

Connected to the source through Bus 1 is a 25 kV/690 V step-down wye-delta transformer, of which the secondary voltage was chosen to match the output of the RPP simulated in the case

studies. In terms of per-unit values, the transformer's circuit impedance ( $Z_{T_{new}}$ ) can be represented by (4.4);

$$Z_{T_{new}} = Z_{old} \left( \frac{S_{B_{new}}}{S_{B_{old}}} \right) \left( \frac{V_{B_{old}}}{V_{B_{new}}} \right)^2 \quad (4.4)$$

where  $S_{B_{new}}$  and  $V_{B_{new}}$  represent chosen base circuit values, while  $S_{B_{old}}$ ,  $V_{B_{old}}$ , and  $Z_{old}$  respectively represent the transformer voltage, power, and impedance rating.

#### 4.4.2.3 Load

Connected to the transformer through Bus 2 is a 100 MW series RLC load, with a  $Q_C$  of 300 KVar, and a  $Q_L$  of 0. This can be modelled concerning per-unit values using (4.5);

$$Z_{load_{pu}} = \frac{Load}{Z_{B2}} \quad (4.5)$$

where  $Z_{B2}$  is given by (4.6);

$$Z_{B2} = \frac{V_{B2}}{S_B} \quad (4.6)$$

where  $V_{B2}$  = the secondary transformer voltage chosen as base, and  $S_B$  = the base power rating chosen for the circuit.

#### 4.4.2.4 Renewable power plant

Given that the RPP modelled in Figure 4.6 is based on Eskom's Sere wind farm, it consists of 46 x 2.3 MW asynchronous wind turbines with an output voltage of 690V. To maintain consistency in validating the respective model and validation subsystems going forward, wind speed is kept constant at 8 m/s for the case studies. Like the grid-representing source, the RPP's voltage ( $V_{pu(RPP)}$ ) can be represented in terms of the per-unit system by (4.7);

$$V_{pu(RPP)} = \frac{V_{out(RPP)}}{V_{base2}} \quad (4.7)$$

where  $V_{out(RPP)}$  = generated RPP terminal voltage, and  $V_{base2}$  = the secondary voltage of the transformer chosen as base.

#### 4.4.2.5 Point of connection

The POC labelled in Figure 4.6 represents the connection point of the simulated RPP to the rest of the network and is of particular significance in that all measurements are to be obtained from this bus, unless specified otherwise. This includes the complex per-unit voltage and current measurements used by the voltage- and frequency-validation subsystems. Consequently, considering Figure 4.6, power flows through the POC feeding the load- and/or grid-representing source, depending on simulated conditions. POC per-unit current ( $I_{pu(POC)}$ ) and voltage ( $V_{pu(POC)}$ ) can therefore be given by (4.8) and (4.9);

$$I_{pu(POC)} = I_{pu(Load)} - I_{pu(Grid)} \quad (4.8)$$

$$V_{pu(POC)} = I_{pu(POC)} \times Z_{circuit} \quad (4.9)$$

where  $I_{pu(Load)}$  is the current flowing to the load,  $I_{pu(Grid)}$  is the current flowing from, or to the grid-representing source, and  $Z_{circuit}$  is the impedance of the circuit with respect to the POC.

#### 4.4.3 Grid-code validation subsystems

The grid-code voltage- and frequency-validation subsystems of Figure 4.6 were developed to monitor POC conditions actively, thus allowing the simulated RPP to be operated in line with grid-code voltage and frequency requirements, as would be required of it once grid connected. This allows supply demands, and the RPP response to strains imposed by grid-code requirements to be studied under simulated fault conditions, allowing RPP grid-integration behavioural studies to be performed using the developed testbed. The respective voltage- and frequency-validation subsystem designs follow, broken down into their respective sub-circuitry and components.



#### 4.4.3.1 Voltage-validation subsystem

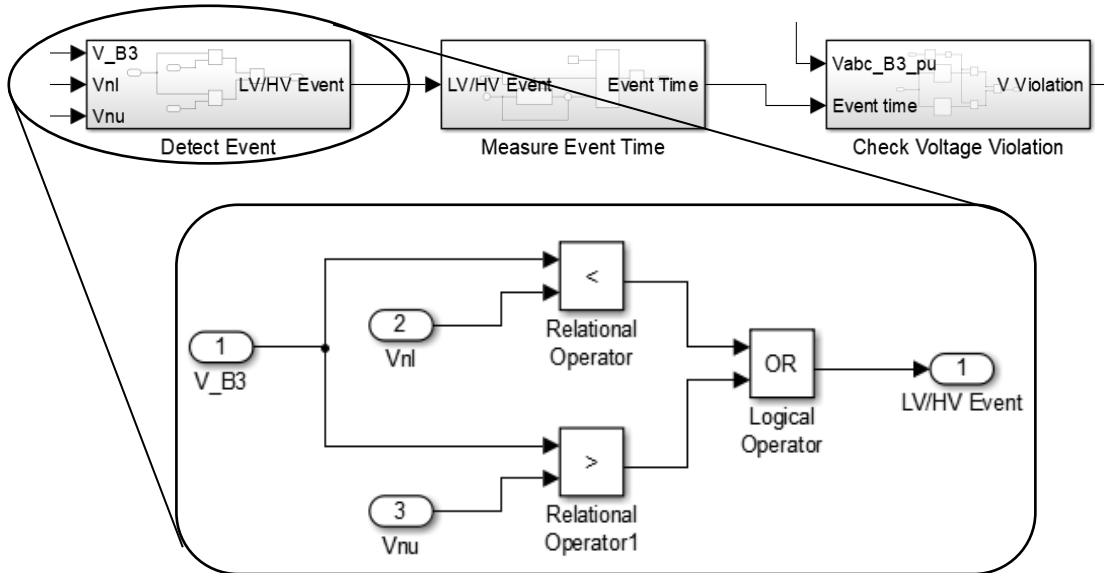


**Figure 0.7: Logic operation and circuit of the 'Detect Event' subsystem**

The voltage-validation subsystem labelled in Figure 4.6 consists of three respective parts, namely 'Detect Event', 'Measure Event Time', and Voltage Violation'. The first of these, 'Detect Event' for which the circuitry is seen in Figure 4.7, uses ' $V_{nu}$ ', ' $V_{nl}$ ', and the measured POC bus voltage ' $V_{POC}$ ' ( $V_{B3}$ ) as inputs to detect when POC conditions deviate outside normal ' $V_{nu}$ '/' $V_{nl}$ ' operating boundaries. This process works as follows:

If  $V_{POC} < V_{nl}$ , then  $LV/HV Event = 1$

Or

If  $V_{POC} > V_{nu}$ , then  $LV/HV Event = 1$

Otherwise

$LV/HV Event = 0$

Consequently, when a voltage event is present, a '1' is generated at the 'LV/HV Event' output and passed on to the adjacent 'Measure Event Time' section of Figure 4.8.

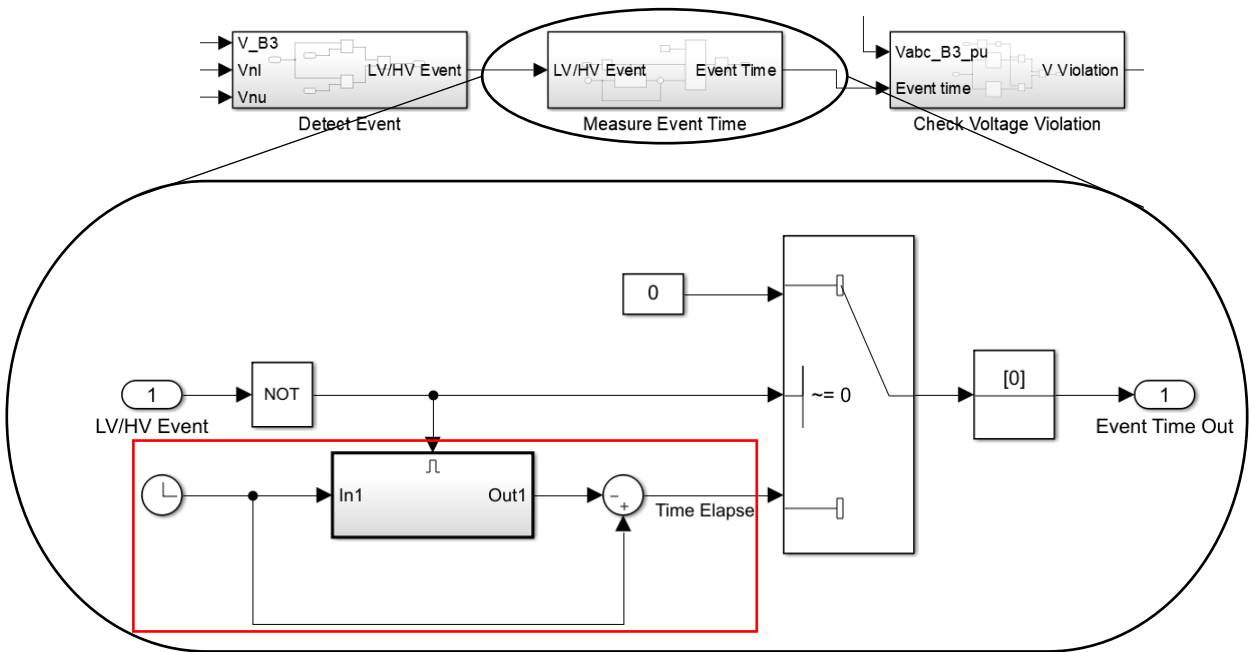


**Figure 0.8: Logic operation and circuit of the 'Measure Event Time' subsystem**

Under normal operating conditions when no event is present, the '0' entering the circuit will be converted to a '1' using the NOT logical operator block. This is recognised by the switch as not being = 0, in which case the '0' input is passed, indicating no event. When a positive indication or '1' enters the subsystem block, it is inverted to an '0', allowing the switch to pass the event time, as calculated by the red section of Figure 4.8, which works by subtracting the time until the start of the event, from the total simulation time. The value passed by the switch will therefore represent the '**Event Time**' in seconds. This process is also represented as follows:

If **LV/HV Event** = 1, Simulation time – Event detection time = **Event Time**

And

If **LV/HV Event** = 1, output **Event Time**

Or

If **LV/HV Event** = 0, output 0

Using the 'Event Time' obtained from the 'Measure Event Time' circuit section, the presence of a voltage violation is then determined by the 'Check Voltage Violation' section in Figure 4.9.

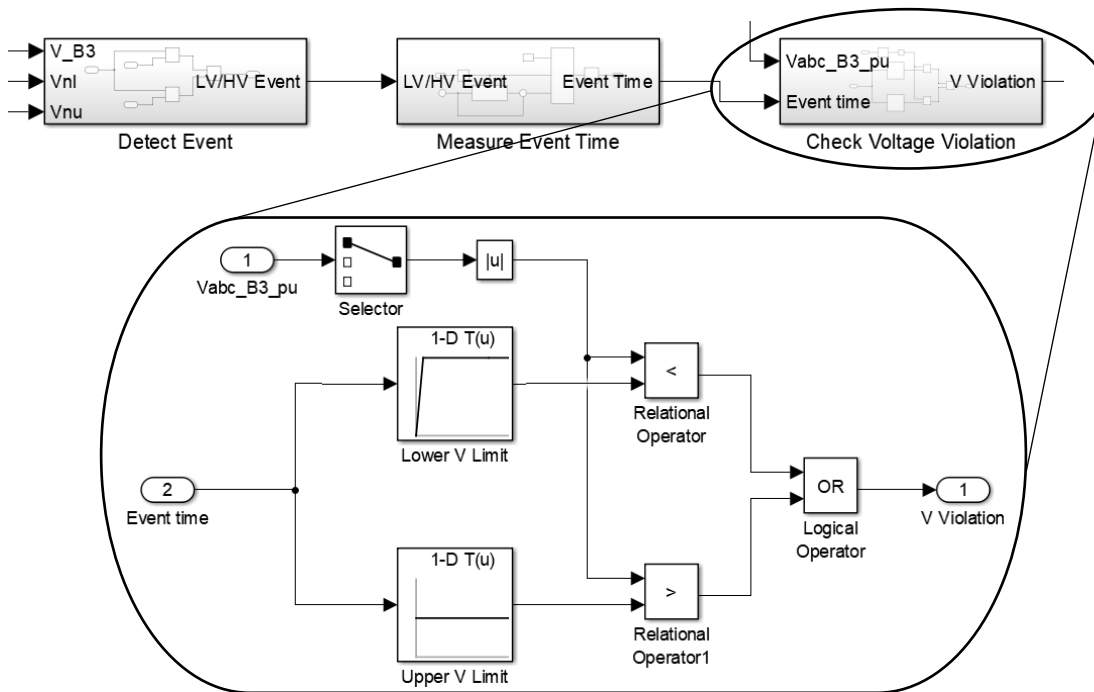


**Figure 0.9: Logic operation and circuit of 'Check Voltage Violation' subsystem**

The 'Check Voltage Violation' section of Figure 4.9 works by comparing continually an event's duration, to the grid-code voltage ride-through boundaries imported from the MATLAB live script, using lookup tables, allowing the maximum (**Vu out**) and minimum (**VI out**) instantaneous POC voltage boundaries to be generated as outputs. Comparing '**Vu out**' and '**VI out**' to the POC voltage '**V\_POC**' (Vabc\_B3\_pu) then allows grid-code voltage violations to be identified, at which time a '1' is generated at the '**V Violation**' output of the section. This works as follows:

If  $V\_POC < \text{'Lower V limit'}$ ,  $Trip = 1$

Or

If  $V\_POC > \text{'Upper V limit'}$ ,  $Trip = 1$

Otherwise

$Trip = 0$

The '**V Violation**' trip, generated by the 'Check Voltage Violation' section, is then passed on to the RPP, disconnecting it from the circuit. This process of detecting voltage violations is also indicated by the flow diagram of Figure 4.10, as a summary of the voltage-validation procedure discussed above.

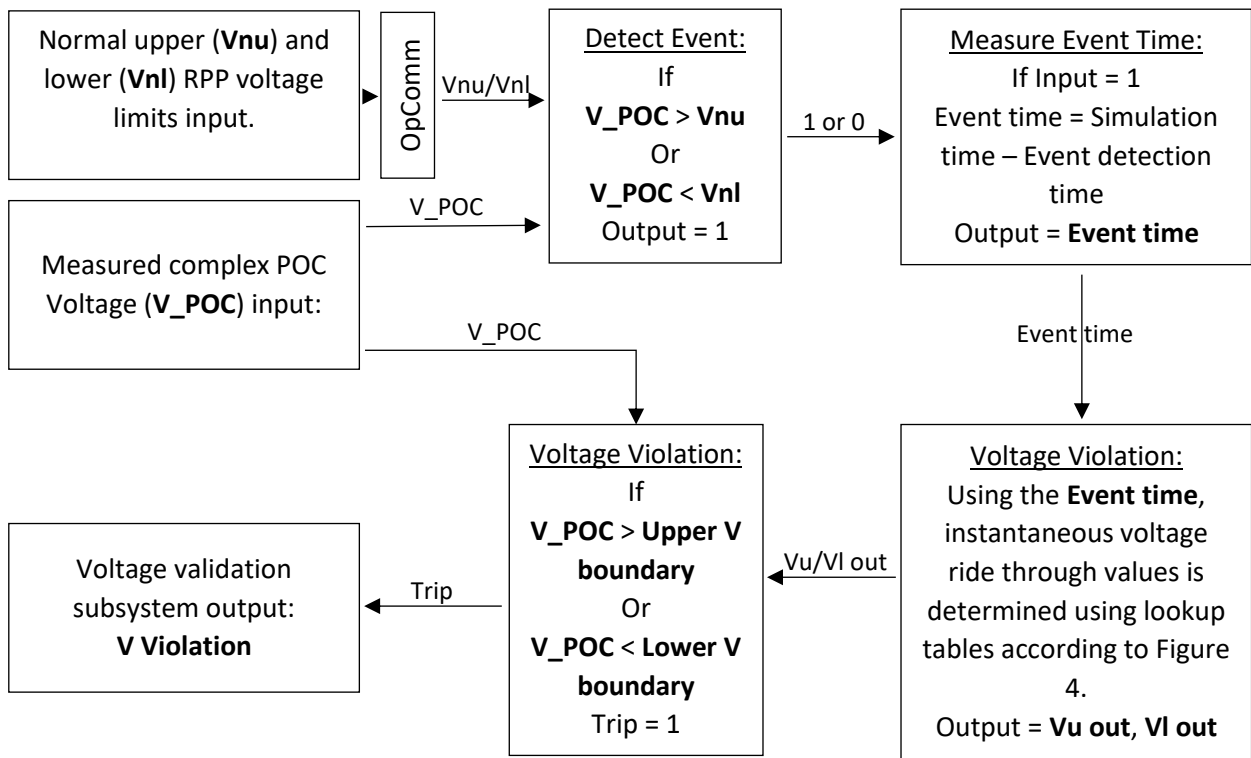


**Figure 0.10: Voltage-validation subsystem flow diagram**

#### 4.4.3.2 Frequency-validation subsystem

The purpose of the frequency-validation subsystem labelled in Figure 4.6 is to validate compliance set for RPPs by South African grid codes concerning frequency. Since frequency requirements remain constant irrespective of RPP class and POC voltage, the frequency-validation subsystem does not require external parameters to be imported to the model. Frequency can, however, not be measured directly at the POC, given the type of simulation, and therefore has to be obtained using the complex POC voltage 'V\_POC', also used as input to the voltage-validation subsystem. Considering the tools available in the MATLAB library, POC frequency could be determined using the 'frequency (Phasor)' block, if the phase angle in radians 'phase(rad)' is known. Using V\_POC, this was then determined. First, the complex POC voltage measured at the POC in the format given by (4.10) had to be converted to a more appropriate magnitude (|u|) angle (θ) format, respectively using (4.11) and (4.12).

$$V_{poc} = a + bi \quad (4.10)$$

$$|u| = \left| \sqrt{a^2 + b^2} \right| \quad (4.11)$$

$$\theta = \arctan \frac{b}{a} \tag{4.12}$$

The angle ( $\theta$ ) in degrees could then be converted to radians using (4.13), and used as input to the 'frequency(Phasor)' MATLAB library block, with output **F\_POC** representing the POC frequency.

$$rad = \frac{\pi}{180} \tag{4.13}$$

Grid-code frequency requirements were then considered to create the circuit of Figure 4.11, implementing formulae (4.10) to (4.13) in the red section, calculating the input to the 'Calculate frequency' block. This block is an adapted version of the standard 'phasor frequency' block later introduced in MATLAB (2018a); however, as the study was limited to the use of MATLAB (2015b), the 'Calculate frequency' block had to be self-fabricated, for which the circuitry is given by Figure 4.12. This circuit then works by calculating the derivative of the phase angle of the input voltages, concerning a phasor rotating at 50 Hz, thus determining the POC frequency '**F\_POC**' required (MathWorks, 2017).

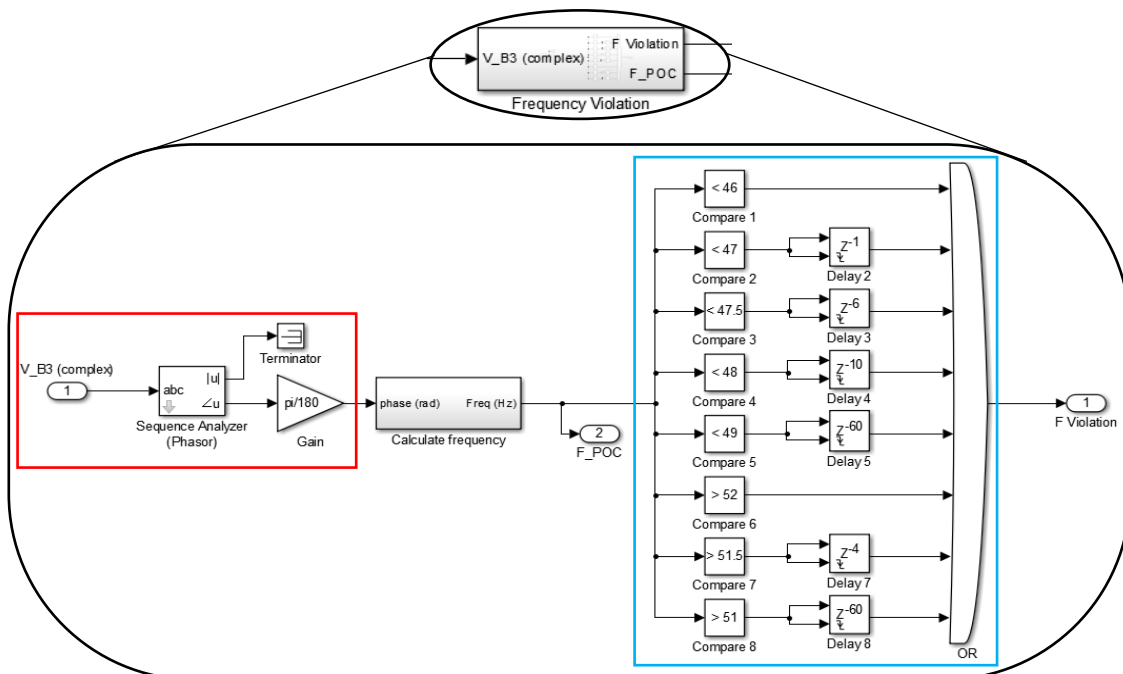
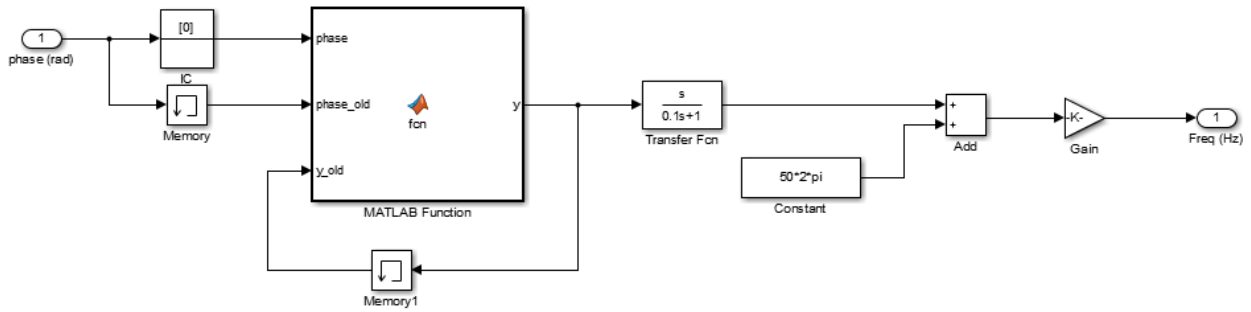


Figure 0.11: Logic operation and circuit of 'Frequency Violation' subsystem



**Figure 0.12: Adapted 'Calculate frequency' MATLAB block**

The blue highlighted section of Figure 4.11 represents the fixed grid-code frequency ride-through requirements for RPPs previously discussed and uses the calculated POC frequency ' $F_{POC}$ ' to determine the presence of a grid-code frequency violation '**F Violation**'. This works as follows:

If  $F_{POC}$ , < 49 Hz, **output** = 1, delayed 60 seconds

If  $F_{POC}$ , < 48 Hz, **output** = 1, delayed 10 seconds

If  $F_{POC}$ , < 47.5 Hz, **output** = 1, delayed 6 seconds

If  $F_{POC}$ , < 47 Hz, **output** = 1, delayed 10 seconds

If  $F_{POC}$ , < 46 Hz, **output** = 1

Or

If  $F_{POC}$ , > 51 Hz, **output** = 1, delayed 60 seconds

If  $F_{POC}$ , > 51.5 Hz, **output** = 1, delayed 4 seconds

If  $F_{POC}$ , > 52 Hz, **output** = 1

Otherwise,

**Output** = 0

Consequently, the comparators will output a '1' when their respective frequency boundary is violated which, after having been delayed according to frequency ride-through requirements, is passed to the '**F Violation**' output of the frequency-validation subsystem and the RPP, disconnecting it from the circuit. This process of detecting frequency violations is also given by the flow diagram of Figure 4.13, as a summary of the frequency-validation procedure discussed above.

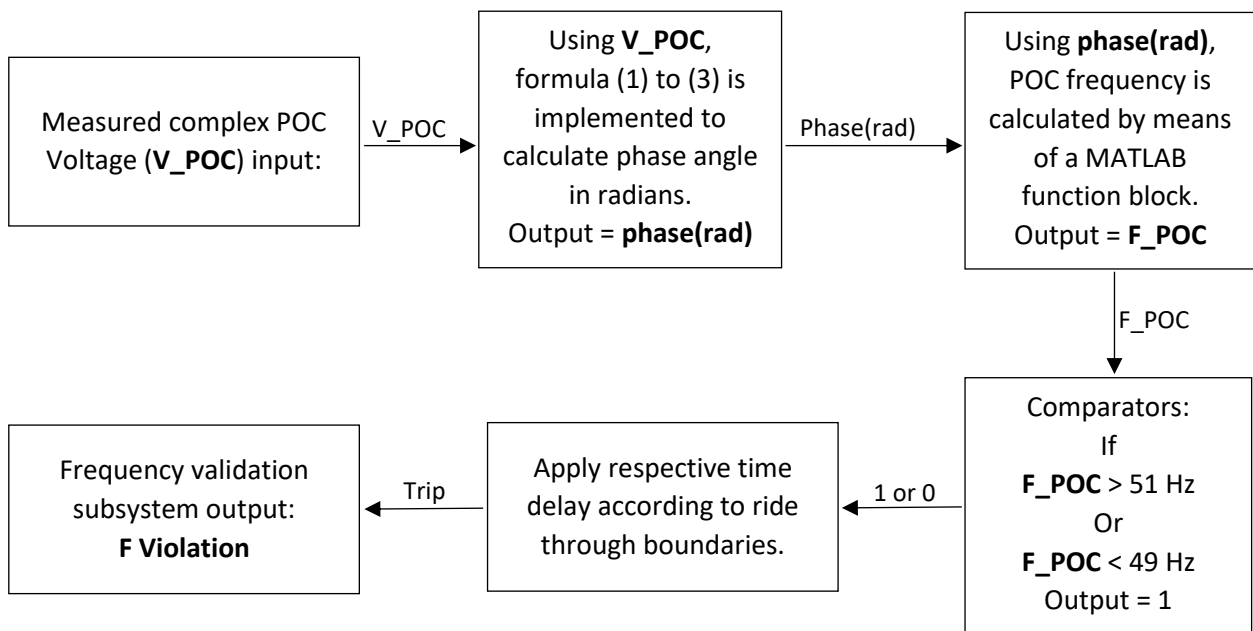


**Figure 0.13: Frequency-validation subsystem flow diagram**

#### 4.4.4 Wind turbine data acquisition subsystem

The final of the SM\_Target circuitry not displayed in Figure 4.6, is the 'Wind turbine data acquisition' subsystem shown in Figure 4.14. This subsystem was created in response to grid-code short-circuit testing specifications, which require RPP active '**I\_active**', reactive '**I\_reactive**', and peak '**I\_peak**' current measurements taken at set intervals during testing. The subsystem additionally outputs RPP active '**P\_out**' and reactive '**Q\_out**' power, included to provide further insight into the behaviour and response of the RPP, given simulated conditions.

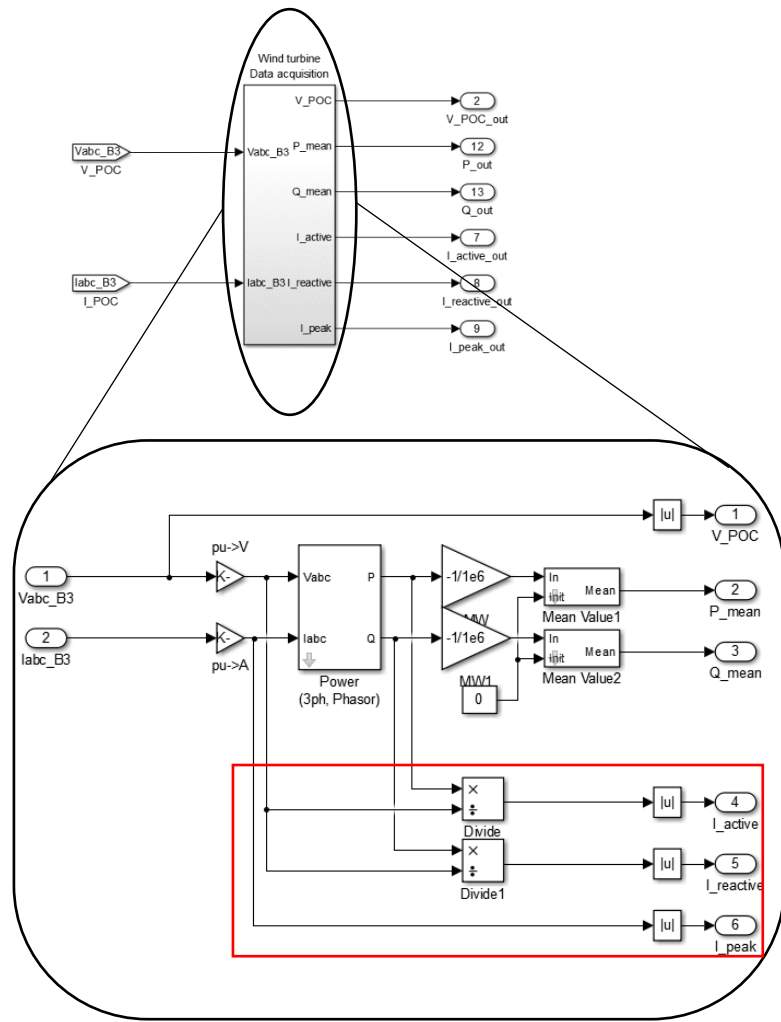


**Figure 0.14: Wind turbine data acquisition subsystem**

As the required parameters cannot be measured directly at the POC or RPP, they had to be obtained using the POC voltage '**V\_POC**' and current '**I\_POC**'. The circuitry of Figure 4.14 used to obtain these outputs can then be represented below.

First, '**P\_out**' and '**Q\_out**' generated by the 'Power (3ph, Phasor)' MATLAB block, can be represented by (4.14).

$$S = I_{complex} \times V_{complex} \tag{4.14}$$

And then, using 'S' to give (4.15):

$$S = P + jQ \tag{4.15}$$

Using '**P\_out**' and '**Q\_out**', active '**I\_active**', reactive '**I\_reactive**', and peak '**I\_peak**' current could then be determined using (4.16) to (4.18).



$$I_{\text{active}} = \left| \frac{P}{V} \right| \quad (4.16)$$

And

$$I_{\text{reactive}} = \left| \frac{Q}{V} \right| \quad (4.17)$$

And finally

$$I_{\text{peak}} = |I_{poc}| \quad (4.18)$$

## 4.5 SC\_Local subsystem

### 4.5.1 Measurements and outputs

The section focuses on the measurement scopes housed in the SC\_Local subsystem, included to display and log the real-time simulation result data. As the simulation result data are imported from the SM\_Target subsystem, it can be noted that they connect through an OpComm block for communication purposes. Based on grid-code RPP testing requirements, testbed-validation testing needs, and the testbed's purpose of being able to assist with RPP grid-integration behavioural studies, it was decided to include the combination of measurement scopes displayed in Figure 4.15, for which the purpose of each is discussed.

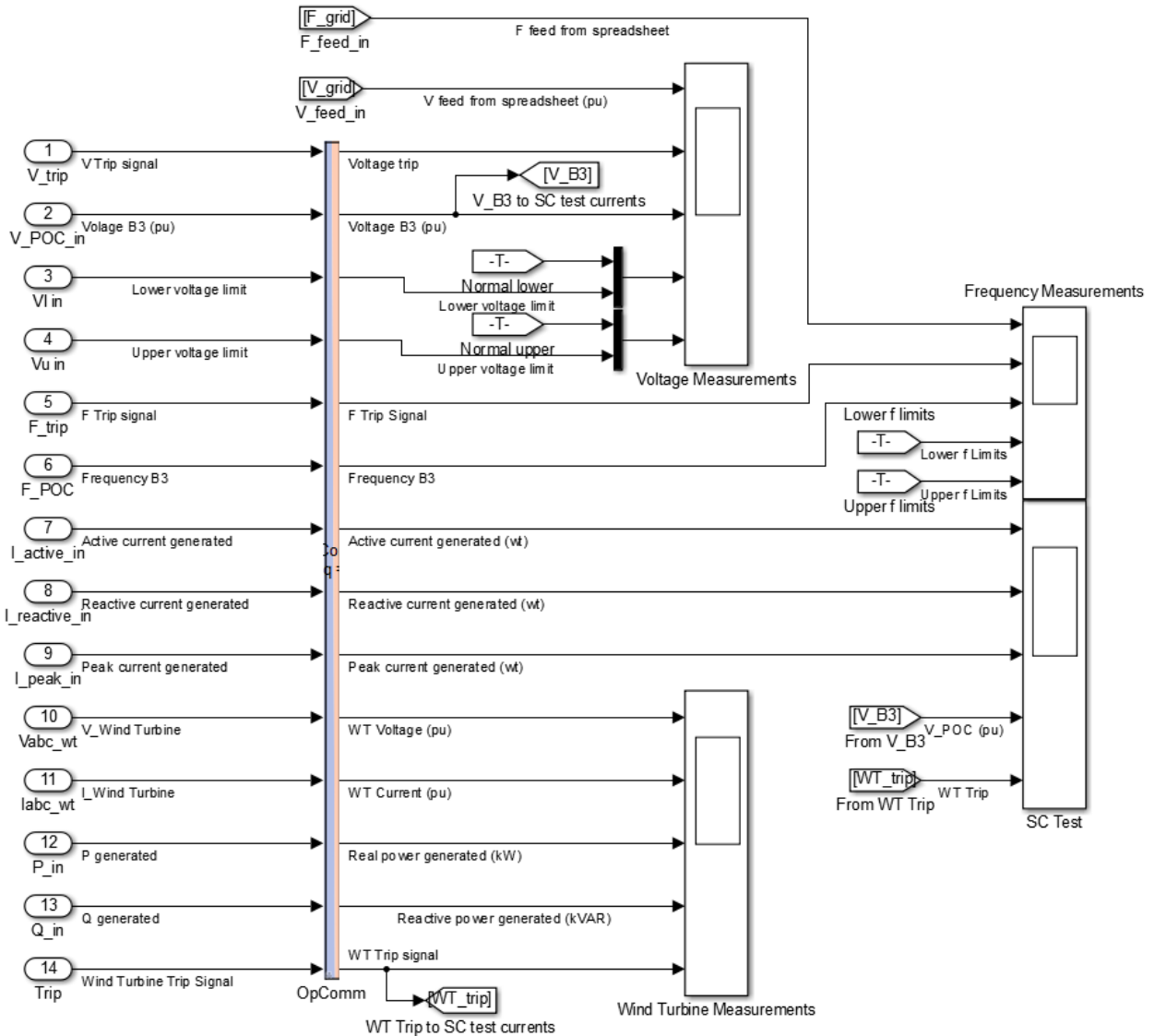


**Figure 0.15: Simulator measurements scopes**

#### 4.5.1.1 Voltage measurements scope

The Voltage Measurements scope of Figure 4.15 is used to output three graphs: the first displays the imported per-unit spreadsheet voltage '**Vpu spreadsheet**'; the second shows the voltage-validation subsystem output '**V Violation**', while the third gives the per-unit POC voltage '**V\_POC**' alongside the respective voltage boundary limits of the simulated RPPs, '**Vnu**', '**Vnl**', '**Vu out**', and '**VI out**'. This scope is aimed at monitoring voltage conditions when performing voltage-related simulations, such as Low-Voltage Ride-Through (LVRT), High-Voltage Ride-Through (HVRT), or short-circuit testing.

#### 4.5.1.2 Frequency measurements scope

The Frequency Measurements scope of Figure 4.15 again outputs three graphs: the first displays the imported spreadsheet frequency '**f spreadsheet**' in Hz; the second shows the frequency-validation trip signal '**F Violation**', while the third gives the POC frequency '**F\_POC**' alongside the constant normal, and frequency ride-through boundary limits, 'Fnu', 'Fnl', 'Lower f limits', and 'Upper f limits'. This scope is aimed at monitoring frequency conditions when performing frequency-related simulations, such as Low-Frequency Ride-Through (LFRT), and High-Frequency Ride-Through (HFRT) testing.

#### 4.5.1.3 SC test scope

The SC Test scope of Figure 4.15 is used to output four graphs, namely the active (**I\_active**), reactive (**I\_reactive**), and peak (**I\_peak**) currents determined by the RPP data acquisition subsystem, in addition to the final graph used for the POC voltage (**V\_POC**), and RPP trip input (**Trip in**). This scope is included to monitor RPP current, which grid-code documentation requires to be logged when performing mandatory RPP short-circuit testing. Nevertheless, the scope also provides valuable insight into the performance and behaviour of a simulated RPP, needed when performing RPP grid-integration behavioural studies in general.

#### 4.5.1.4 Wind turbine measurements scope

The final Wind Turbine Measurements scope of Figure 4.15 is used to display four graphs, indicating the per-unit wind-turbine voltage (**Vabc\_wt**), current (**Iabc\_wt**), active power generated in MW (**P\_out**), reactive power generated in MVAR (**Q\_out**), and the trip-input signal (**Trip in**). These signals are all obtained using direct wind-turbine measurement outputs, aimed at illustrating the load demands imposed on RPPs by grid-code requirements during testing. The scope also provides valuable insight into the performance and behaviour of a simulated RPP, needed when performing RPP grid-integration behavioural studies.

### 4.6 Experimental setup

The section is aimed at detailing the experimental lab setup used for testing the developed testbed during the forthcoming case studies. Having discussed the development of the MATLAB model sections, and preparations needed for RT-LAB, the next step involved setting up the equipment as per Figure 4.16, which involves the host computer, and OPAL-RT OP4510 real-time simulator, respectively shown in Figures 4.17 and 4.18.

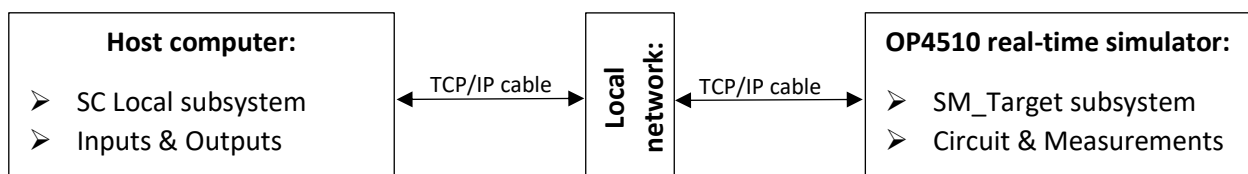
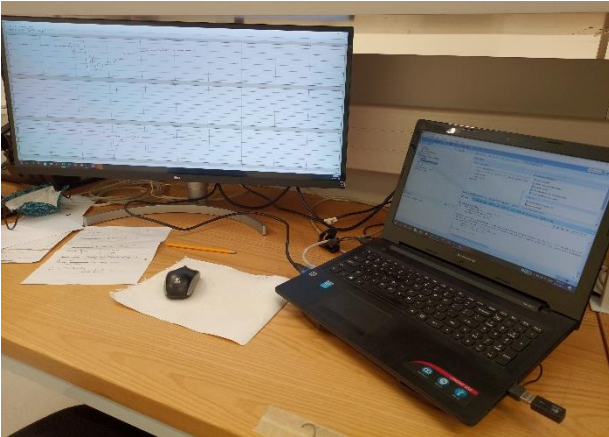


Figure 0.16: Lab equipment setup diagram



**Figure 0.17: Host computer**



**Figure 0.18: OPAL-RT OP4510 real-time simulator**

As seen from the diagram in Figure 4.16, a TCP/IP cable is used to establish a physically wired connection using the local network between the equipment, while communication is set up and configured using the host computer and RT-LAB software (Buraimoh and Davidson, 2022). The connection was then confirmed using the Windows command prompt to ping the real-time simulator from the host computer, after which the MATLAB model could be loaded, compiled, and executed in real-time.

#### **4.7 Testing strategy**

Developing a testing strategy again required consideration of grid-code RPP testing requirements, testbed-validation testing needs, and the testbed's purpose of being able to assist with RPP grid-integration behavioural studies. The selected case studies, therefore, had to produce meaningful results, showing the developed testbed's abilities and accuracy to fulfil its purpose. Therefore, in addition to validating the testbed's operation, the case studies also had to showcase its ability to provide RPP simulation data, needed to achieve its goal of being an effective RPP grid-integration behavioural studies tool. To recreate POC conditions, the 'V&F Grid import data' block discussed earlier was utilised. Using this, fed circuit data can be generated using a spreadsheet and introduced via the 'V&F Grid import data' block, creating the desired POC conditions. Details of the developed case study testing strategy are as follows.

##### **4.7.1 High-and low-voltage ride-through tests**

The first case studies are aimed at testing the testbed, and the HVRT and LVRT behaviour and response of RPP, to react in line with grid-code requirements when presented with a temporary

POC voltage spike or dip. Consequently, for both the HVRT and LVRT tests, three conditions will be recreated, as described.

- 1) The first will involve a slight voltage spike and dip, not violating the normal upper 'Vnu' and lower 'Vnl' voltage limits of the selected RPP. This will test the RPP response to normal voltage variations, during which it is expected of the RPP to remain connected indefinitely.
- 2) Second, a more substantial voltage spike and dip will be introduced, violating normal 'Vnu'/'Vnl' limits, entering the HVRT/LVRT operating region without violating its boundaries. Monitoring the RPPs response, it is expected of the RPP to remain connected and to support POC conditions while within the HVRT/LVRT boundaries, not generating a trip.
- 3) Lastly, a persistent substantial voltage spike and dip violating HVRT/LVRT boundaries will be introduced. Monitoring the RPP response, it is expected of the RPP to support POC conditions while within HVRT/LVRT boundaries, only generating a trip once these are violated.

#### **4.7.2 High-and low-frequency ride-through tests**

The second set of case studies is aimed at testing the testbed, and the HFRT and LFRT behaviour and response RPP, to react in line with grid-code requirements when presented with POC frequency spikes or dips. Consequently, for both the HFRT and LFRT tests, three conditions will similarly be recreated, as described.

- 1) The first will involve a slight frequency spike and dip, not violating normal upper **Fnu**= 51 Hz, and lower **Fnl**= 49 Hz frequency boundaries. This will test the RPP response to normal frequency variations, during which it is expected of the RPP to remain connected indefinitely.
- 2) The second will involve more substantial events, exceeding '**Fnu**'/'**Fnl**' limits, entering the HFRT/LFRT operating region without violating its boundaries. Monitoring the RPPs response, it is expected of the RPP to remain connected and to support POC conditions while within the HFRT/LFRT boundaries, not generating a trip.
- 3) Lastly, persistent substantial frequency events violating HFRT/LFRT boundaries will be introduced. Monitoring the RPP response, it is expected of the RPP to support POC conditions while within HFRT/LFRT boundaries, only generating a trip once these are violated.

#### **4.7.3 Short-circuit tests**

The short-circuit case studies are aimed at testing the RPP POC support response through monitoring the generated current of an RPP, when measured at grid-code specified voltage drops and intervals. South African grid-code requirements mandate short-circuit testing for all of Categories A3, B, and C RPPs, specifically to assess the ability of an RPP to provide reactive

power and current support. Data collection sheets are provided for these tests, of which the 20% POC voltage drop simulation test sheet is given in Table 4.1 as an example.

**Table 0.1: 20% POC voltage short-circuit example sheet**  
(NERSA, 2019)

dU=20%			
Time [ms]	$I_{\text{active}}$ [A]	$I_{\text{reactive}}$ [A]	$I_{\text{peak}}$ [A]
0			
5			
10			
20			
50			
100			
150			
200			
300			
500			

Similarly, these sheets also need to be completed for the 30%, 50%, and 80% POC voltage drops, which will not only allow the RPP support capabilities to be measured but will also provide insight into the RPP support demands for an increasing POC voltage drop. Such information can then be used and applied to select an appropriate type and size of RPP for a specific application or to study whether an RPP can provide the desired support during disturbances.

#### 4.7.4 Real-world data tests

Having validated the testbed’s abilities and response, the final case studies will make use of measured real-world grid data of previously recorded events. This aims to incorporate the testbed in its entirety, illustrating its worth as an RPP grid-integration behavioural studies tool.

#### 4.8 Summary

This chapter followed the development of the tailored South African real-time grid-integration behavioural studies testbed of the thesis. This saw the implementation of a MATLAB live script, utilising drop-down menus which require the user to select key RPP parameters, after which the RPP grid-code requirements are determined using ‘if’ functions and exported to the Simulink model. The split SM/SC subsystem design of the Simulink model was discussed, allowing the appropriate testbed sections to be simulated, respectively using the host computer, and OPAL-RT OP4510 real-time simulator. The testbed’s model was considered in greater detail starting with

the inputs, using a data-import block which provides a means of replaying recorded grid data, aiming to produce simulation results of greater accuracy and significance. Model components were discussed, which include the grid-code voltage- and frequency-validation subsystems, designed to provide active RPP POC voltage and frequency grid-code validation during simulations. The model's outputs then saw the implementation of four measurement scopes, jointly aiming to log the necessary POC and RPP data for effective testbed testing, and grid-integration behaviour studies. The lab setup then showed how utilising the local network, the physically separated host computer, and OP4510 real-time simulator are set up and connected, providing perspective on the use of OpComm blocks during the Simulink circuit's design. Finally, testing requirements were considered of both the testbed and RPP, leading to the development of a case study testing strategy to assess not only the testbed's abilities and success, but also to showcase its worth as a real-time RPP grid-integration behavioural studies testbed.

## **CHAPTER FIVE**

### **CASE STUDIES**

#### **5.1 Introduction**

Having discussed the development of the real-time testbed and testing procedures required to validate its effectiveness and abilities leading up to Chapter Five, the objective is now to evaluate the developed testbed's success through testing of the respective circuit sections, while assessing RPP behaviour and response in the process. To achieve this, the case studies of Chapter Five are divided into three sections, the first two of which are aimed at assessing the efficacy of the testbed's respective voltage and frequency-validation subsystems, to react and control the simulated RPP in line with the requirements given by grid codes. This entails their ability to recognise, analyse, and track POC conditions, which would require them to maintain RPP operation, or disconnect the RPP. The third section is then more RPP orientated, aiming to illustrate the developed testbed's value in studying RPP behaviour, given the demands placed on RPPs by grid-code requirements during the short-circuit- and real-world data case studies performed. Based on the simulation data generated, a preliminary analysis and assessment of results are made considering the testbed and RPP response to the conditions of each case study, which will then be expanded on and considered in greater detail during the Chapter Six analysis.

#### **5.2 Voltage subsystem validation studies**

The first case studies aim to illustrate the abilities and accuracy of the voltage-validation subsystem, highlighted red in Figure 5.1. To do this, Case studies 1 to 3 focus on recreating conditions that require the RPP to operate within the respective continuous, fault ride-through, and trip region of operation. This is achieved by altering the voltage imported through the 'V & F Grid import data' block, highlighted blue in Figures 5.1 and 5.2, representing the larger grid network. The 'Voltage' scope of Figure 5.2 will then log POC voltage and trip data, allowing the ability of the developed testbed to react appropriately in line with grid-code requirements to be assessed. In addition to the 'Voltage' scope data for assessing testbed response, the 'Wind turbine' scope will also log RPP voltage, current, and power data as a representation of the effect that each disturbance has on the RPP itself, allowing the RPP grid-integrated behaviour and fault response to be assessed.



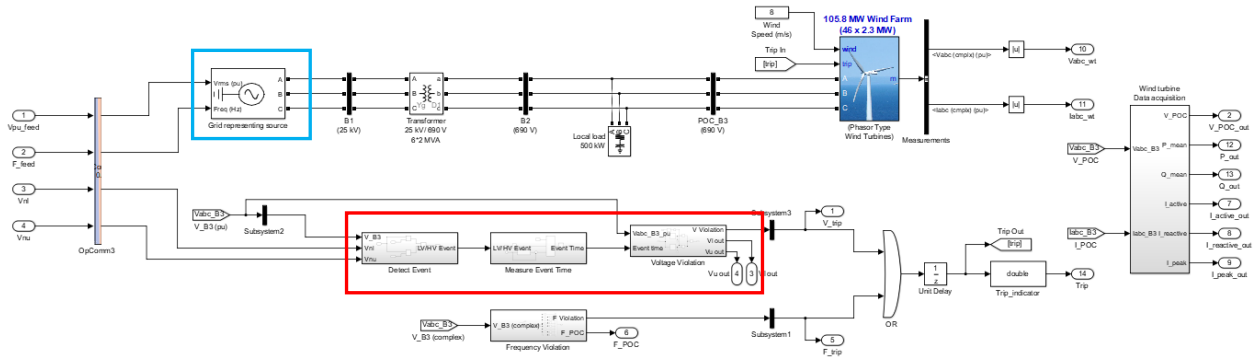


Figure 0.1: Real-time simulation testbed circuit, SM\_Target subsystem

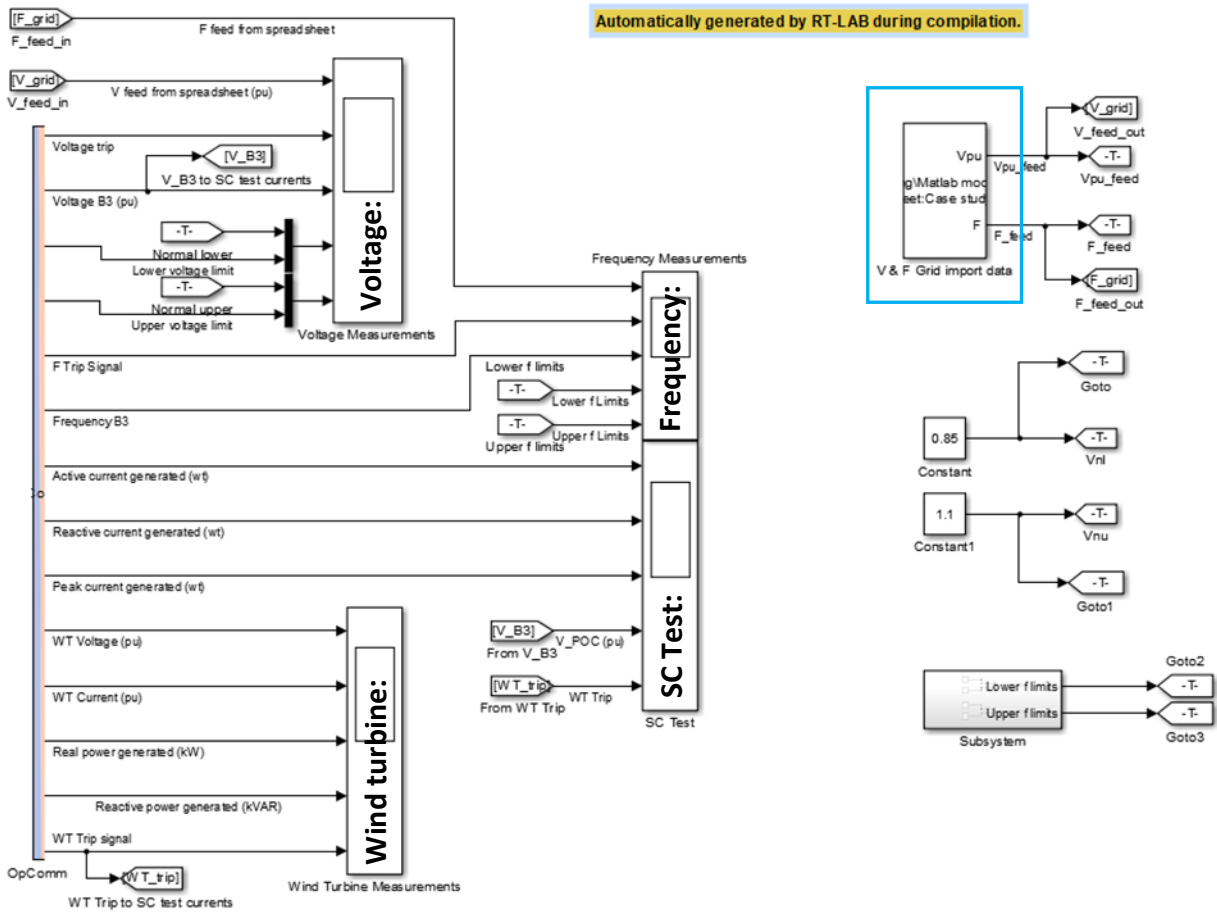
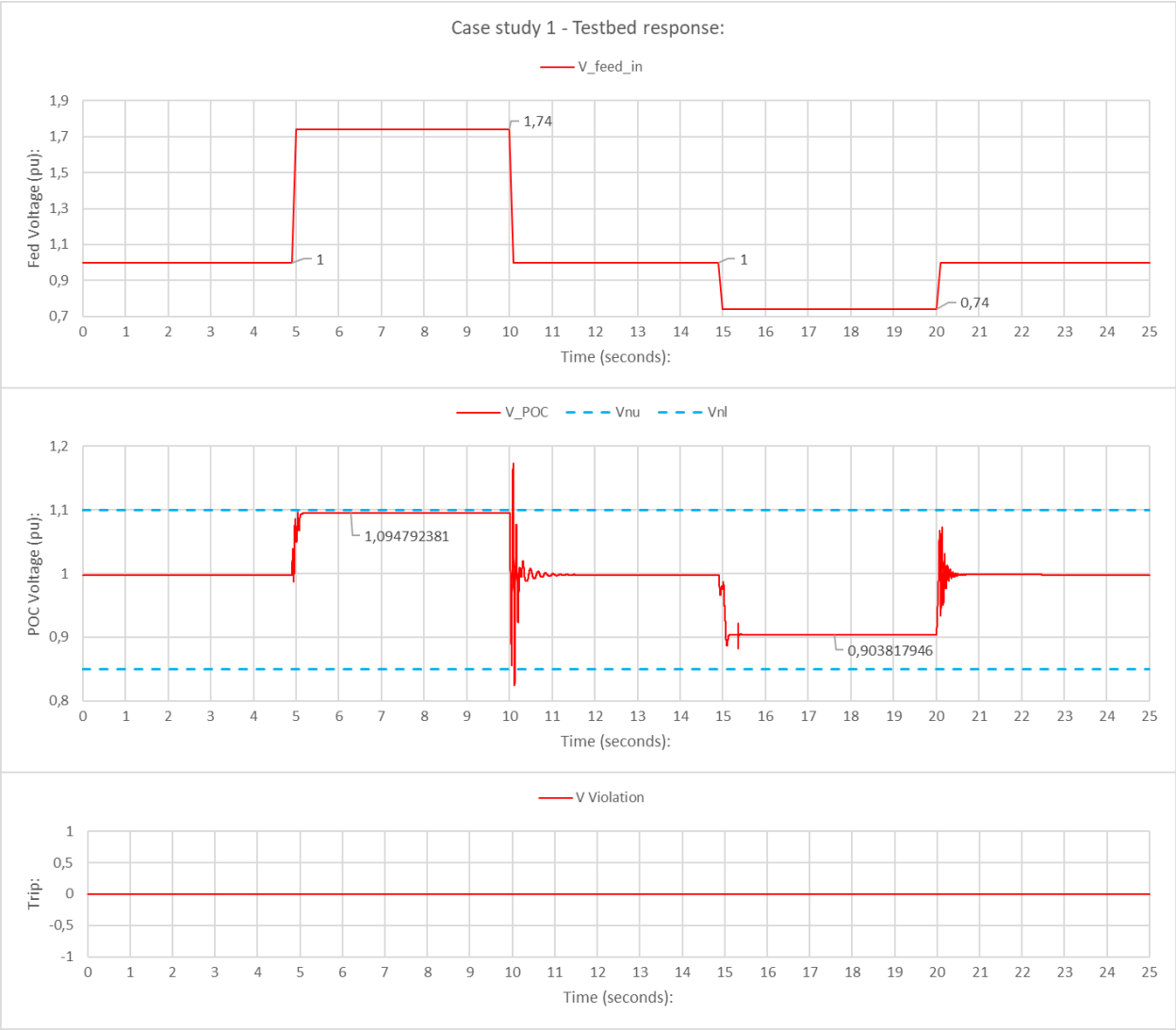


Figure 0.2: Real-time simulation inputs and outputs/measurements, SC\_Local subsystem

### 5.2.1 Case study 1

Case study 1 is aimed at evaluating the developed model, and simulated RPP response concerning RPP grid-code requirements during normal voltage fluctuations within the continuous  $V_{nu}/V_{nl}$  band of RPP operation. These conditions represent everyday minor voltage fluctuations,

and it is therefore expected that the RPP will remain connected indefinitely. To analyse effectively the appropriateness of the response of the voltage validation subsystem, the ability of the frequency-validation subsystem to trip the RPP is disabled temporarily for Case study 1. Furthermore, the frequency 'F\_feed\_in' fed via the 'V & F Grid import data' block is kept constant at 50 Hz, while the imported voltage 'V\_feed\_in' is altered to generate the necessary voltage fluctuations at the POC 'V\_POC'. Having isolated the circuit's response to that of the voltage-validation subsystem, the simulation was performed using the OPAL-RT OP4510 real-time simulator, for which the results obtained are presented in Figures 5.3 and 5.4.



**Figure 0.3: Case study 1: testbed voltage event response**

The three graphs of Figure 5.3 respectively illustrate the adapted imported per-unit test voltage 'V\_feed\_in', measured POC voltage 'V\_POC', and trip input 'V Violation' obtained from the output of the voltage-validation subsystem for the 25-second simulation of Case study 1. The POC

voltage graph of Figure 5.3 additionally includes the continuous operating band given by the '**V<sub>nu</sub>/V<sub>nl</sub>**' limits of the simulated RPP and is seen dotted in blue.

Considering the simulation results of Case study 1 in Figure 5.3, the first noteworthy event starts at t=5 seconds with the introduction of a voltage spike, up to which point baseline values of V=1pu at 50 Hz were fed to the circuit. From t=5 to t=10 seconds, a raised per-unit voltage '**V<sub>feed\_in</sub>**' of 1.74 Vpu is fed, causing a rise in POC voltage '**V<sub>POC</sub>**' to just below the blue dotted upper continuous operating boundary '**V<sub>nu</sub>**'. Base values are then restored between t=10 and t=15 seconds, after which a voltage '**V<sub>feed\_in</sub>**' dip of 0.74 Vpu is introduced via the imported grid voltage. This causes the POC voltage to dip between t=15 and t=20 seconds, without violating the RPP lower continuous voltage operating boundary '**V<sub>nl</sub>**'. Finally, baseline values are restored until the simulation is terminated at t=25 seconds.

Apart from a voltage surge caused by resetting conditions to baseline values around t=10 seconds, it is observed that the POC voltage '**V<sub>POC</sub>**' remained within the continuous operating band of the simulated RPP for Case study 1. Consequently, the voltage-validation subsystem never generates a trip, in line with what is required by RPP grid-code requirements. Based on initial observations, the response of the voltage-validation subsystem can be considered appropriate for the simulated conditions of Case study 1. Figure 5.4 can then be considered, illustrating the effect that these disturbances had on the RPP simulated, showing its response respectively in terms of voltage '**V<sub>WT</sub>**', active '**P<sub>WT</sub>**', and reactive '**Q<sub>WT</sub>**' power generated.

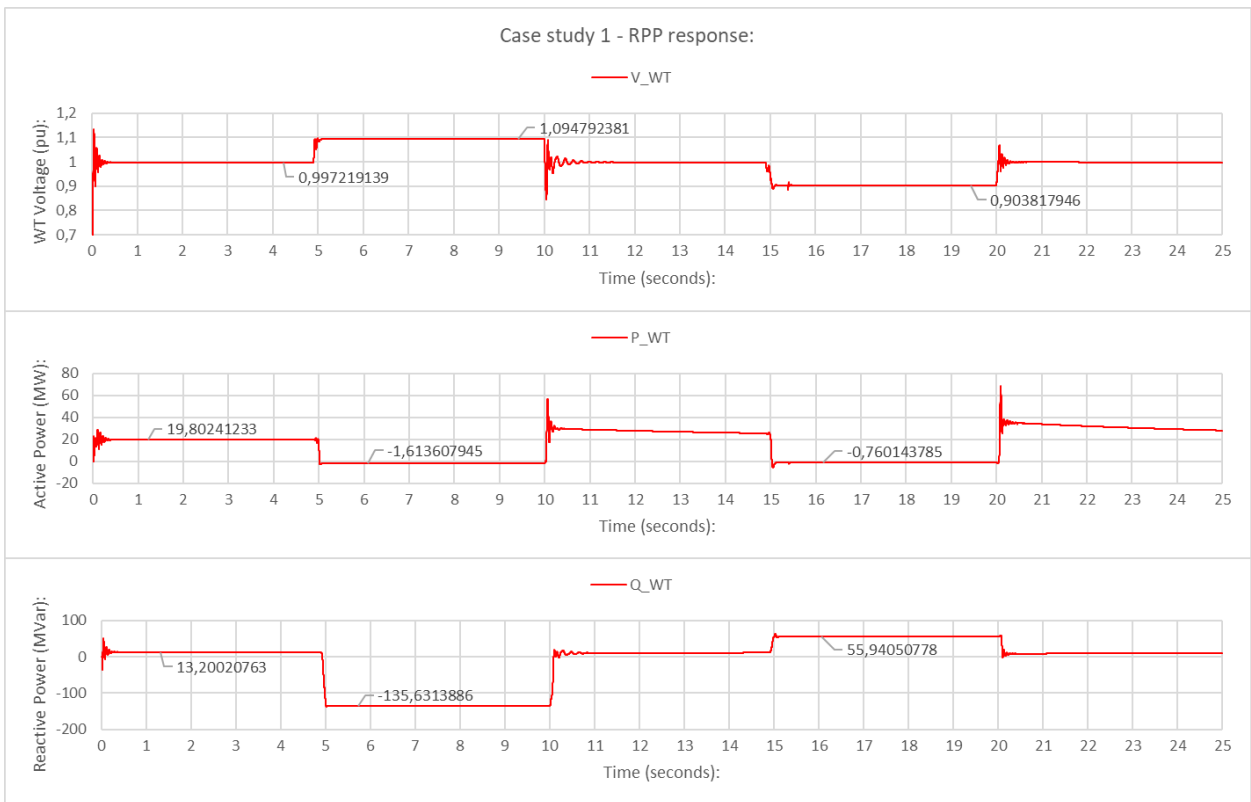


**Figure 0.4: Case study 1: RPP voltage event response**

Figure 5.4 is a graphical representation of the wind turbine scope outputs, representing the RPP response to the simulated conditions of Case study 1. This is important, since grid codes require some RPPs, including the Category C test RPP, to support the grid during disturbances. The RPP response can therefore be considered regarding generated active '**P\_WT**' and reactive '**Q\_WT**' power, during the respective voltage spike and dip at  $t=5$  to  $10$  seconds, and  $t=15$  to  $20$  seconds.

Starting with the  $t=5$ - to  $10$ -second voltage spike, it is observed that, when initiated, active '**P\_WT**' and reactive '**Q\_WT**' power is curtailed to the point where the RPP starts to absorb access power, thus attempting to lower POC voltage '**V\_POC**'. During the voltage dip at  $t=15$ - $20$  seconds, it is observed that active '**P\_WT**' power is curtailed in favour of increasing the generated reactive '**Q\_WT**' power, which will assist in raising POC voltage conditions. Therefore, based on preliminary observations of the RPP response, it can be said that the RPP responded in line with what is required by grid codes, since it supported POC conditions through power adjustments to stabilise POC conditions.

### 5.2.2 Case study 2

Case study 2 is aimed at evaluating the model and simulated RPP response regarding RPP grid-code requirements during short-lived substantial voltage events violating **V<sub>nu</sub>/V<sub>nl</sub>** boundaries,

entering the HVRT/LVRT operating region. These conditions represent short-lived grid disturbances substantial enough to qualify as a fault, but with a duration brief enough to necessitate a fault ride-through response rather than a trip. To isolate and assess effectively the ability of the voltage-validation subsystem to react in line with grid-code requirements during such events, the ability of the frequency-validation subsystem to trip the RPP will again be disabled, while keeping the fed frequency 'F\_feed\_in' constant at 50 Hz. Using the fed voltage 'V\_feed\_in' to alter POC voltage 'V\_POC' conditions, the simulation was performed using the OPAL-RT OP4510 real-time simulator, for which the results are presented in Figures 5.5 and 5.6.

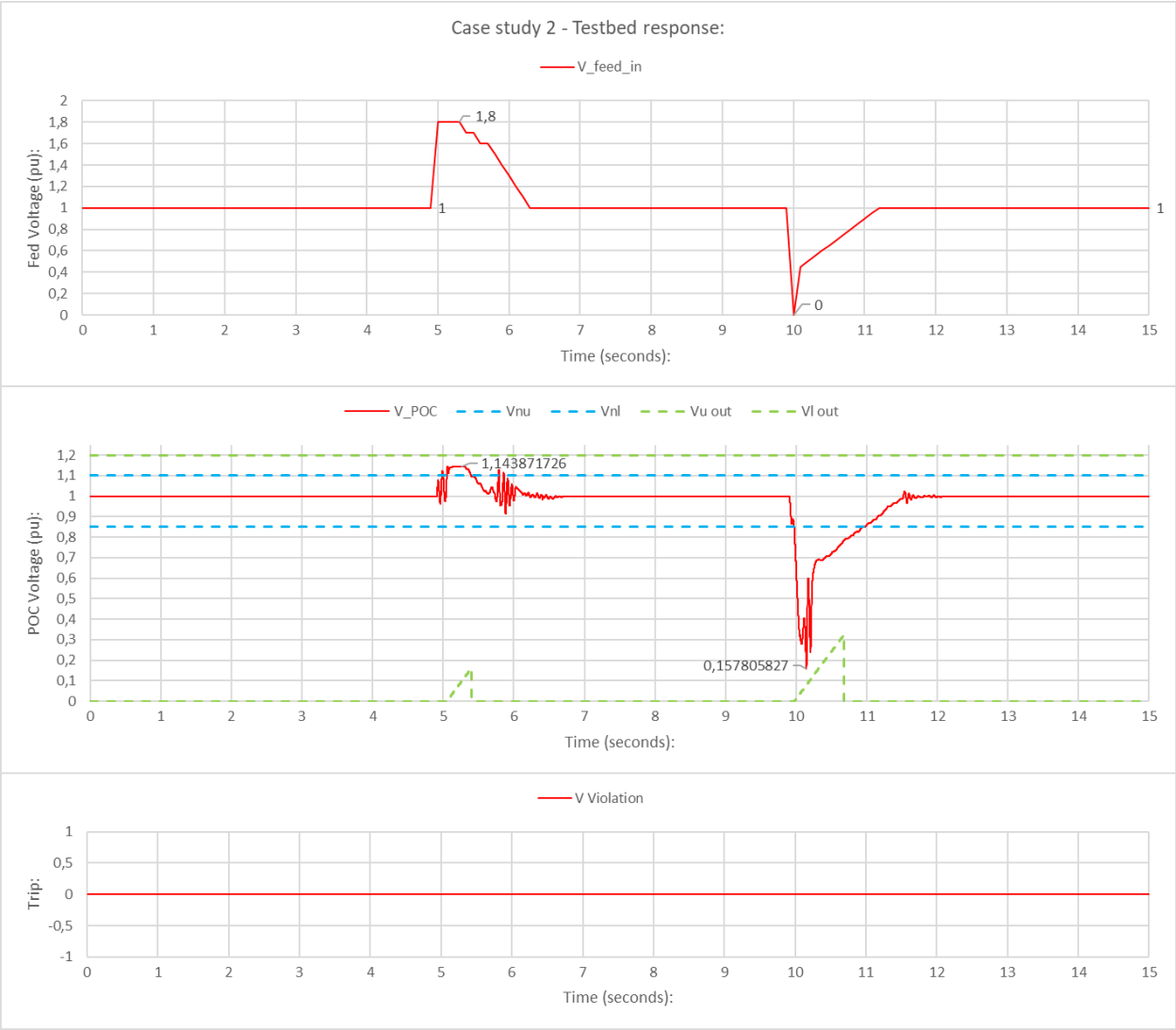


**Figure 0.5: Case study 2: testbed voltage event response**

The three graphs of Figure 5.5 respectively illustrate the adapted per-unit test voltage 'V\_feed\_in' imported, measured POC voltage 'V\_POC', and trip input 'V Violation' obtained from the output of the voltage-validation subsystem for the 15-second simulation of Case study 2. The POC

voltage graph of Figure 5.5 additionally includes the continuous operating band given by the '**V<sub>nu</sub>**'/'**V<sub>nl</sub>**' limits of the simulated RPP in blue, and the adjusting time-dependent HVRT/LVRT boundaries in green.

Considering the simulation results of Case study 2 in Figure 5.5, two events can again be noted. The first of these, introduced at t=5 seconds, is a short-lived '**V<sub>feed\_in</sub>**' voltage spike of 1.8 Vpu, causing POC voltage '**V<sub>POC</sub>**' conditions to violate blue '**V<sub>nu</sub>**' boundary limits, and to venture into the fault ride-through region of operation, after which the fault swiftly clears. The second introduced at t=10 seconds, is a short-lived '**V<sub>feed\_in</sub>**' voltage short of 0 Vpu, causing the POC voltage '**V<sub>POC</sub>**' to violate blue '**V<sub>nl</sub>**' boundary limits, and to venture well into the fault ride-through region before the fault is swiftly cleared.

For both events, it is observed that conditions enter fault ride-through regions of operation, to which the voltage-validation subsystem responds by adjusting HVRT/LVRT boundaries according to grid-code specifications, regarding the duration of the event. A trip is, however, never generated, as green dotted HVRT/LVRT boundaries are not violated. Case study 2 thus shows the ability of the testbed to recognise voltage events, ride through such events while within the ride-through region of operation, and then reset when the event is cleared without generating a trip. Based on these observations, the response of the voltage-validation subsystem can be considered appropriate and effective for the simulated conditions of Case study 2. Figure 5.6 follows, illustrating the effect that these disturbances had on the RPP simulated, showing its response respectively in terms of voltage '**V<sub>WT</sub>**', active '**P<sub>WT</sub>**', and reactive '**Q<sub>WT</sub>**' power generated.

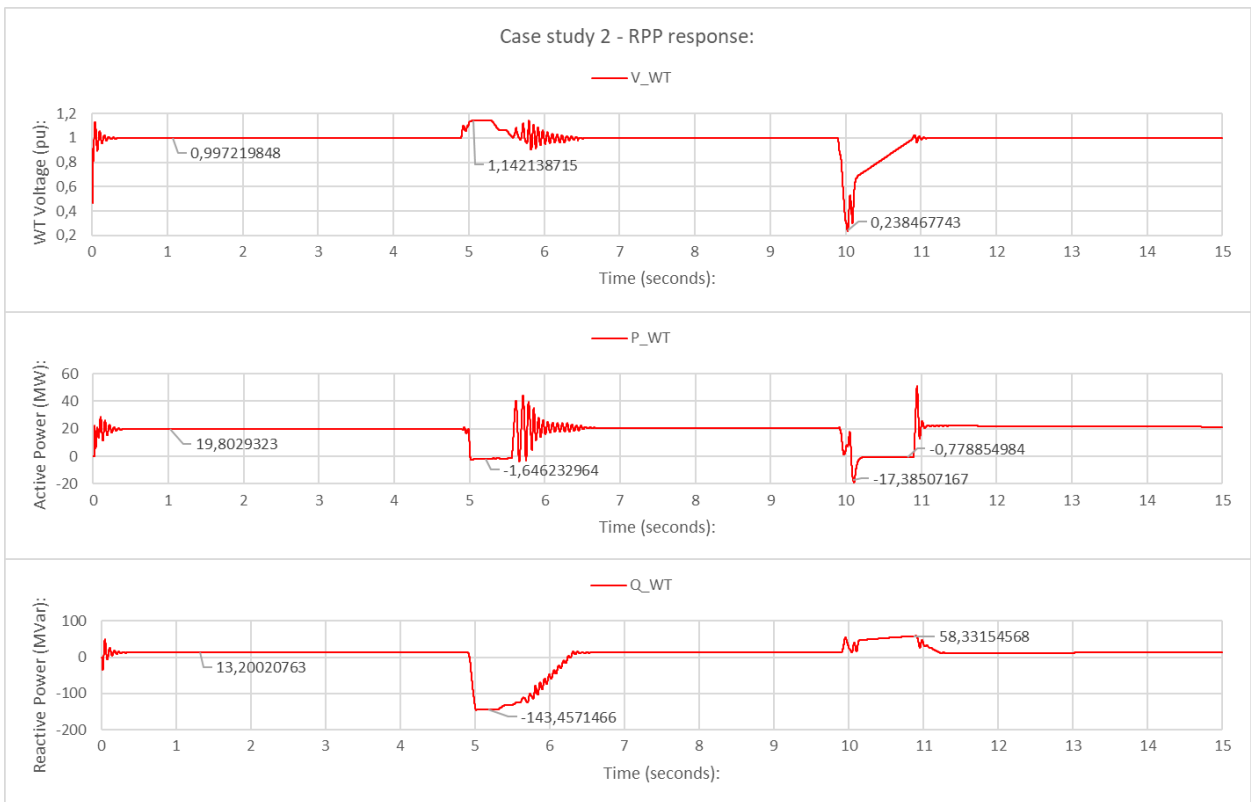


**Figure 0.6: Case study 2: RPP voltage event response**

Figure 5.6 is a graphical representation of the wind turbine scope outputs, representing the RPP response to the respective events at  $t=5$ , and  $t=10$  seconds for Case study 2. Like Case study 1, the voltage spike at  $t=5$  seconds causes the RPP to go from generating active '**P\_WT**' and reactive '**Q\_WT**' power, to absorbing the excess power, thus attempting to lower and stabilise voltage conditions. Although for Case study 2 the RPP absorbs slightly more power compared to the less intense spike of Case study 1, it is noted to be very much similar. This is also true for the voltage dip at  $t=10$  seconds, during which the generation of active '**P\_WT**' power is again curtailed in favour of an increased reactive '**Q\_WT**' power generation, thus attempting to raise voltage conditions. Based on these observations of the RPP response during Case study 2, it can be said that the RPP responded in line with what is required by grid codes, as it supported POC conditions through power adjustments to stabilise POC conditions.

### 5.2.3 Case study 3

Case study 3 is aimed at evaluating the model and simulated RPP response concerning RPP grid-code requirements during persistent and significant voltage events, leading to a violation of HVRT/LVRT boundaries. These conditions represent severe grid disturbances substantial enough to necessitate a trip, whether because of their intensity, or their inability to clear. To isolate and

assess effectively the ability of the voltage-validation subsystem to react in line with grid-code requirements during such events, the ability of the frequency-validation subsystem to trip the RPP will again be disabled, while keeping the fed frequency 'F\_feed\_in' constant at 50 Hz. Using the fed voltage 'V\_feed\_in' to alter POC voltage 'V\_POC' conditions, the simulation was performed using the OPAL-RT OP4510 real-time simulator, for which the results are presented in Figures 5.7 to 5.10.

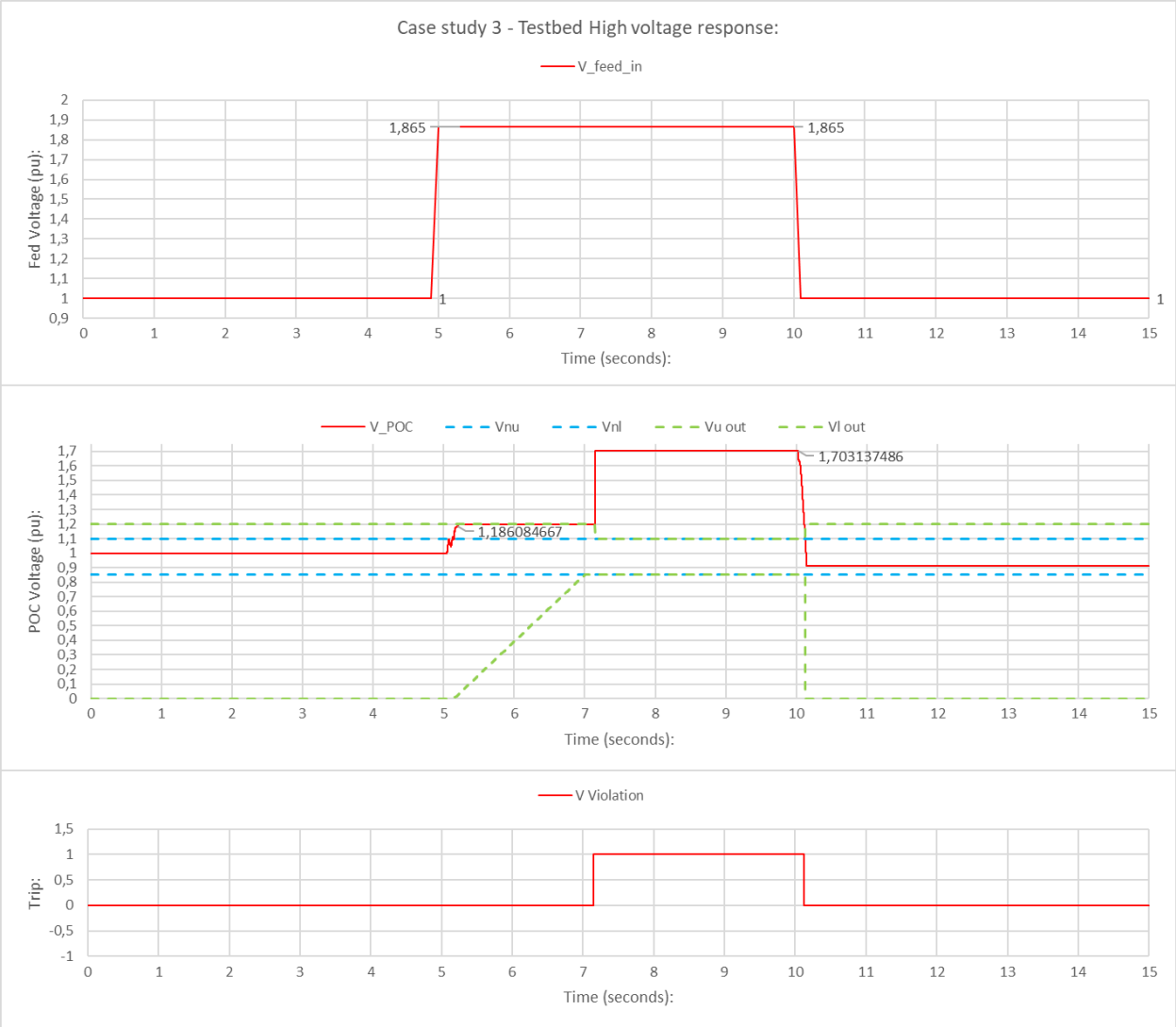
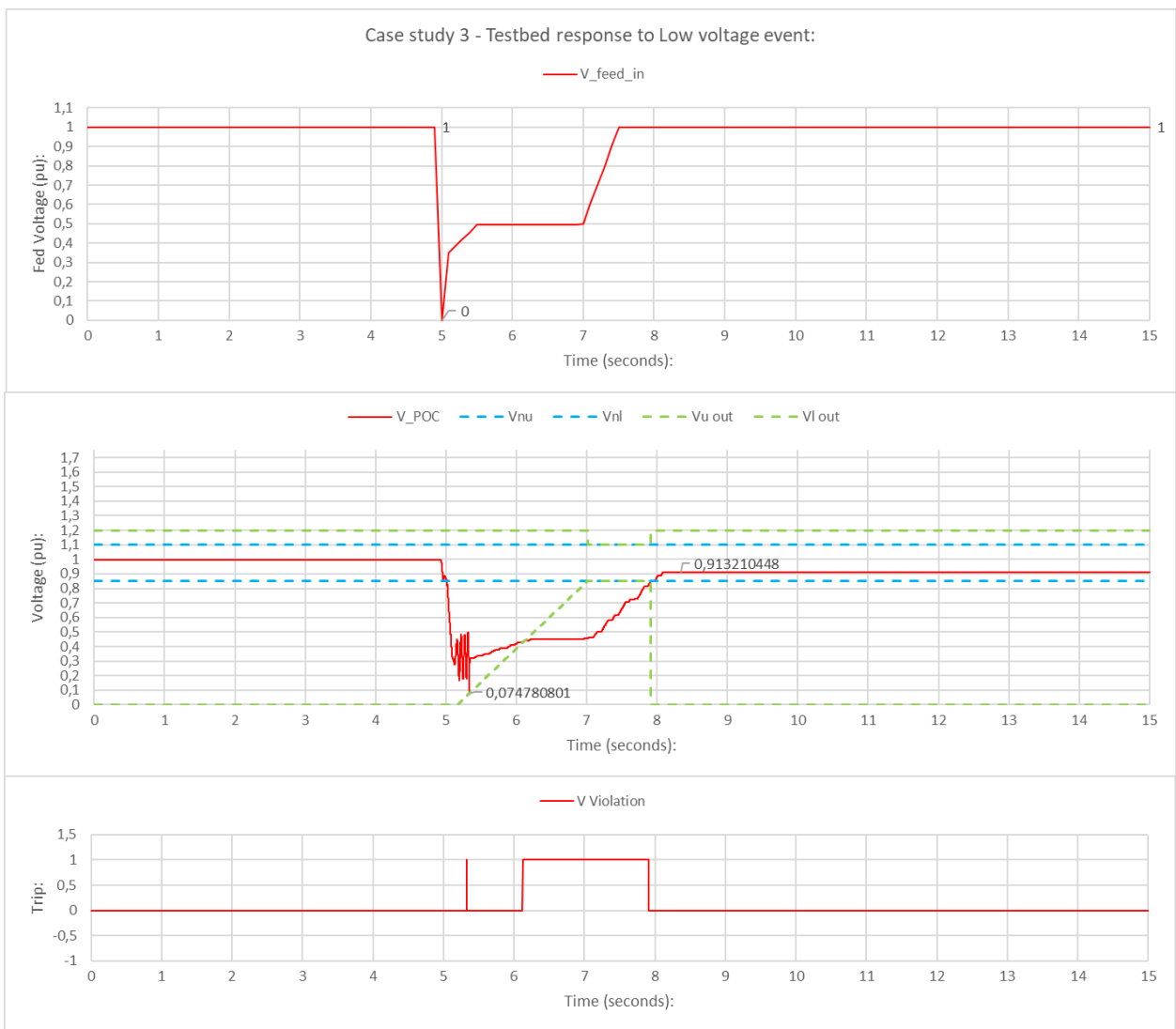


Figure 0.7: Case study 3: testbed high-voltage event response





**Figure 0.8: Case study 3: testbed low-voltage event response**

The three graphs of Figures 5.7 and 5.8 respectively illustrate the adapted per-unit test voltage ' $V_{feed\_in}$ ' imported, measured POC voltage ' $V_{POC}$ ', and trip input ' $V\ Violation$ ' obtained from the output of the voltage-validation subsystem for the 15-second high- and low-voltage disturbance simulations of Case study 3. The POC voltage graph of Figures 5.7 and 5.8 includes the continuous operating band given by the ' $V_{nu}$ '/' $V_{nl}$ ' limits of the simulated RPP in blue, and the adjusting time-dependent HVRT/LVRT boundaries in green.

Considering the first simulation results of Case study 3 in Figure 5.7, the introduction of a 1.865 Vpu spike is seen introduced at  $t=5$  seconds via the imported ' $V_{feed\_in}$ ' voltage. This causes the POC voltage ' $V_{POC}$ ' initially to enter the HVRT region of operation, without violating its boundary. Unlike that of the previous case, the high-voltage event then persists and, as the green

HVRT limit continues to adjust with time, according to the RPP voltage ride-through grid-code requirements, it is finally violated soon after  $t=7$  seconds, at which point a trip is observed from the '**V Violation**' graph. Similarly, a low-voltage event down to 0 Vpu is observed from the '**V\_feed\_in**' the graph of Figure 5.8. This causes the POC voltage '**V\_POC**' to venture well into the LVRT region of operation, initially without violating its green dotted limit. The fault persists, however, leading to a violation of the adjusting LVRT limit soon after  $t=5$  seconds, at which time a corresponding trip signal is noted from the '**V Violation**' graph.

For both events, it is observed that conditions enter fault ride-through regions of operation, initially without generating a trip as the RPP rides through the disturbances. However, the persistent nature of the disturbances, combined with the adjusting time-dependent HVRT/LVRT limits, causes these boundaries to be violated soon after, leading to a corresponding trip. Case study 3 thus shows the ability of the testbed to recognise voltage events, ride through such events while within ride-through boundaries, and then disconnect the RPP in line with voltage grid-code requirements, when RPP voltage ride-through boundaries are violated. Based on these observations, the response of the voltage-validation subsystem can be considered appropriate and effective for the simulated conditions of Case study 3. Figures 5.9 and 5.10 follow, illustrating the effect that these high- and low-voltage disturbances had on the RPP simulated, showing its response respectively in terms of voltage '**V\_WT**', active '**P\_WT**', and reactive '**Q\_WT**' power generated.

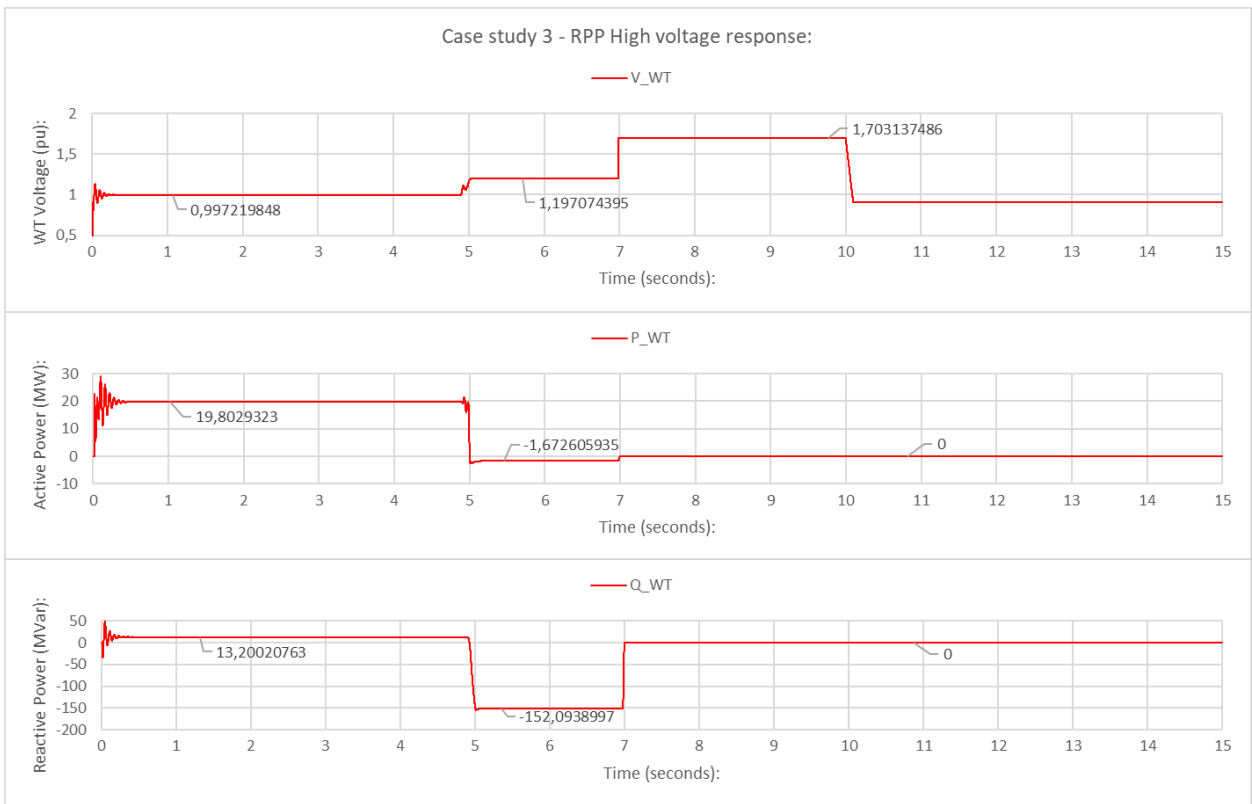


**Figure 0.9: Case study 3: RPP high-voltage event response**

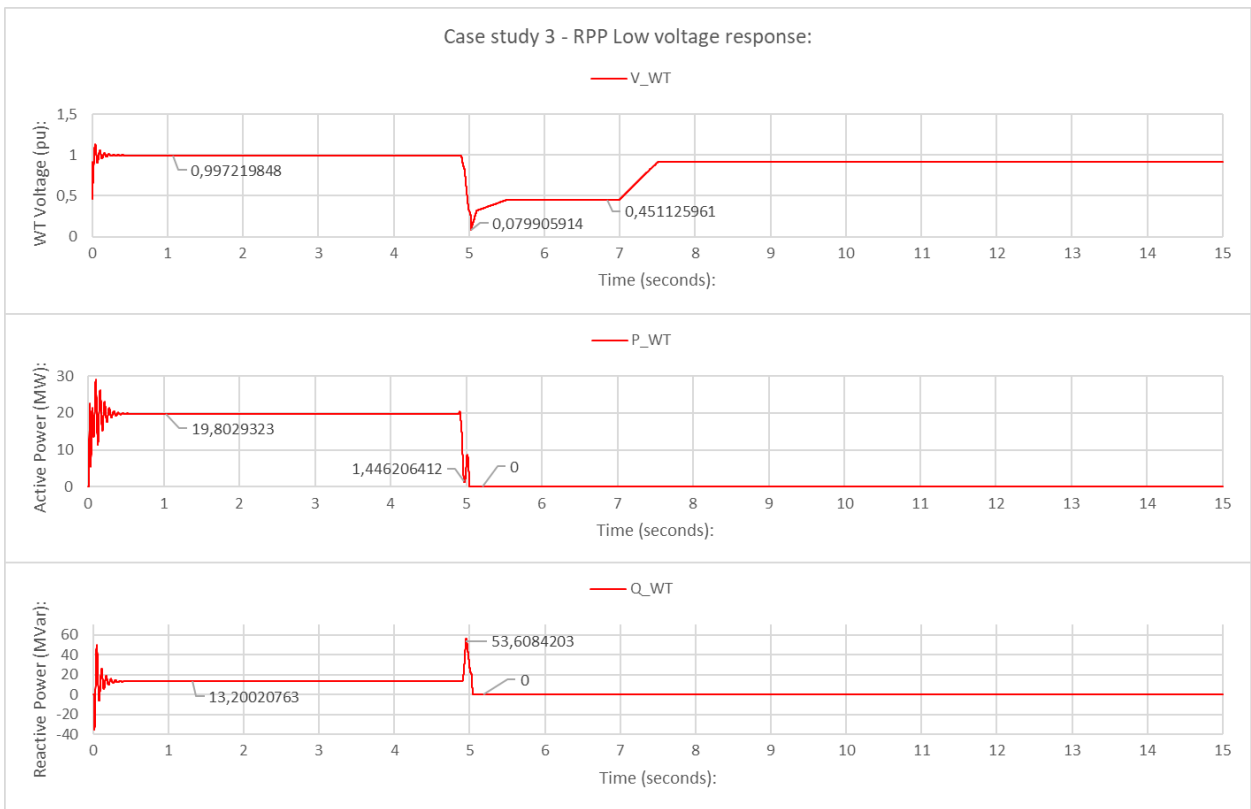


**Figure 0.10: Case study 3: RPP low-voltage event response**

Figures 5.9 and 5.10 are graphical representations of the wind turbine scope outputs, representing the RPP response to the respective high- and low-voltage events of Case study 3. Like Case studies 1 and 2, support from the RPP can be observed during the high-voltage event of Figure 5.9, when the RPP shifts from generating active '**P\_WT**' and reactive '**Q\_WT**' power, to absorbing excess power following initiation of the high-voltage event at  $t=5$  seconds. It is observed that the generated power drops off to 0 soon after, corresponding to the time that the trip was generated. This is to be expected, as the RPP stops generating power when the '**V Violation**' trip is generated, thus confirming that the RPP was disconnected successfully from the network. Figure 5.10 portrays the RPP response during the low-voltage event of Case study 3, where it is noted that active '**P\_WT**' power is again curtailed in favour of an increase in reactive '**Q\_WT**' power flow at  $t=5$  seconds, to raise the POC voltage following initiation of the low-voltage event. The generated power, however, then falls to 0, corresponding to the '**V Violation**' trip, confirming its successful disconnection. Based on these observations of the RPP response during Case study 3, it can be said that the RPP responded in line with what is required by grid codes, supporting POC conditions through power adjustments while within the ride-through region of operation, seizing generation when a '**V Violation**' trip was generated.

### 5.3 Frequency subsystem validation studies

The second of the case study categories in Chapter Five is aimed at illustrating the abilities and accuracy of the frequency-validation subsystem highlighted red in Figure 5.11. To do this, Case studies 4 to 6 focus on recreating conditions allowing the RPP to operate within the respective continuous, fault ride-through, and trip region of frequency operation. This is achieved by altering the frequency 'F\_feed\_in' imported through the 'V & F Grid import data' block highlighted blue in Figure 5.11, representing the larger grid network. To assess the performance and ability of the testbed to respond in line with grid-code frequency requirements, the 'Frequency' scope of Figure 5.2 is employed to log POC data for the frequency-validation subsystem case studies. Using the 'Wind turbine' scope of Figure 5.2, RPP voltage and power data will again be logged, allowing the RPP grid-integrated behaviour and fault response to be assessed.

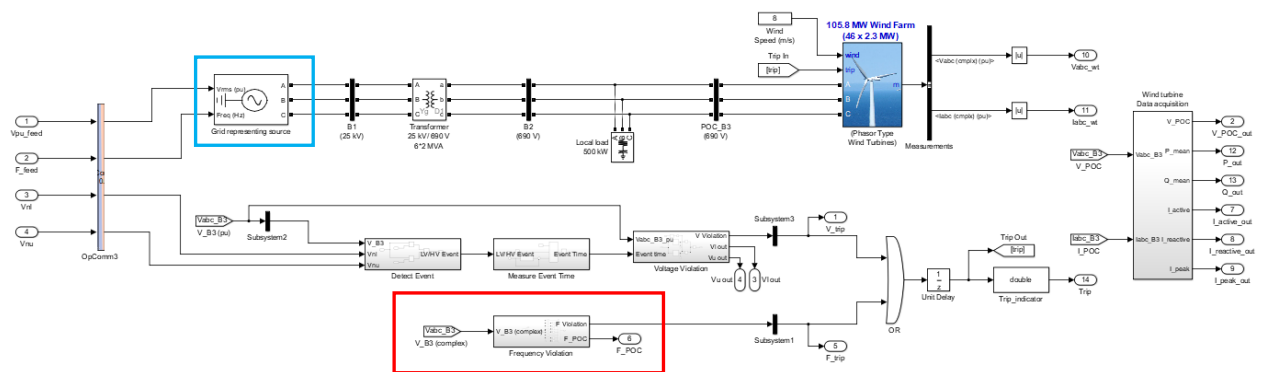
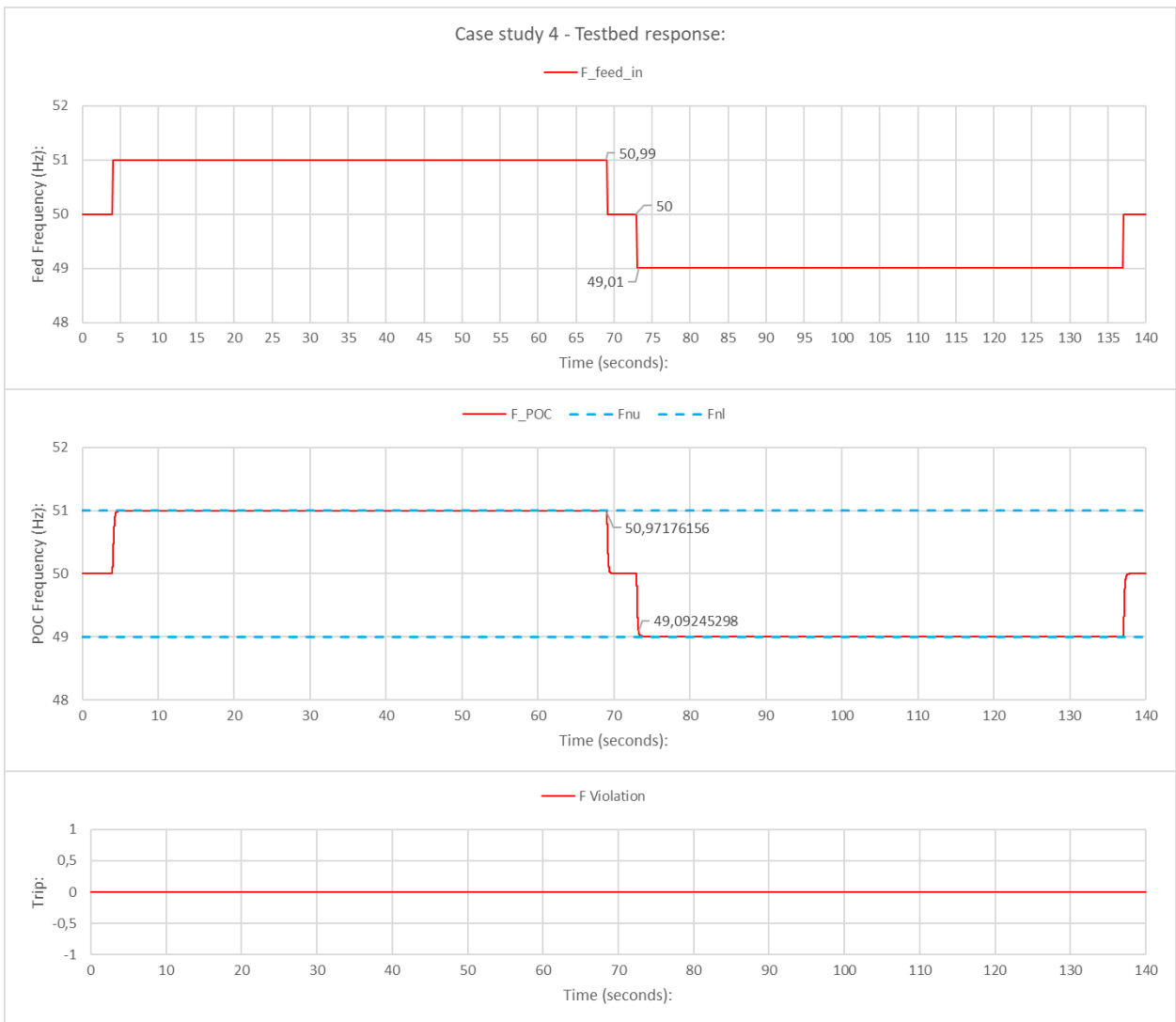


Figure 0.11: Real-time simulation test circuit: frequency validation

#### 5.3.1 Case study 4

Case study 4 is aimed at evaluating the model and simulated RPP response regarding RPP grid-code requirements during normal frequency fluctuations within the continuous 'Fnu'/'Fnl' band of RPP operation. These conditions represent everyday minor frequency fluctuations, therefore requiring RPPs to remain connected indefinitely. To analyse effectively the appropriateness of the response of the frequency-validation subsystem, the ability of the voltage-validation subsystem to trip the RPP will be disabled temporarily for Case study 4. Furthermore, the 'V & F Grid import data'-fed voltage 'V\_feed\_in' is kept constant at 1 pu, while the imported frequency 'F\_feed\_in' is altered to generate the necessary frequency fluctuations at the POC 'F\_POC'. Having isolated the response of the circuit to that of the frequency-validation subsystem, the simulation was performed using the OPAL-RT OP4510 real-time simulator, for which the results obtained are presented in Figures 5.12 and 5.13.



**Figure 0.12: Case study 4: testbed frequency event response**

The three graphs of Figure 5.12 respectively illustrate the adapted per-unit test frequency ' $F_{feed\_in}$ ' imported, measured POC frequency ' $F_{POC}$ ', and trip input ' $F_{Violation}$ ' obtained from the output of the frequency-validation subsystem for the 140-second simulation of Case study 4. The POC frequency ' $F_{POC}$ ' graph of Figure 5.12 additionally includes the continuous operating band given by the ' $F_{nu}$ '/' $F_{nl}$ ' limits of the simulated RPP and is seen dotted in blue.

Considering the simulation results of Case study 4, displayed in Figure 5.12, an extensive ' $F_{feed\_in}$ ' frequency rise is observed to 50.99 Hz, starting at  $t=4$  seconds, causing the POC frequency ' $F_{POC}$ ' to increase to 50.97176156 Hz, just slightly below the RPP ' $F_{nu}$ ' boundary of 51 Hz. After recovering to baseline conditions for a moment, this is then followed by an extensive ' $F_{feed\_in}$ ' frequency dip to 49.01 Hz at  $t=73$  seconds, causing the POC frequency ' $F_{POC}$ ' to decrease to 49.09245298 Hz, just slightly above the RPP ' $F_{nl}$ ' boundary of 49 Hz.

From the simulation results, it is observed that, although extensive frequency fluctuations were introduced, the POC frequency remained within the 'Fnu'/'Fnl' boundaries of the RPP for Case study 4. Consequently, the frequency-validation subsystem never generated a trip, in line with what is required by RPP grid-code requirements. Based on these initial observations, the response of the frequency-validation subsystem is considered appropriate for the simulated conditions of Case study 4. Figure 5.13 can then be considered, illustrating the effect that these disturbances had on the RPP simulated, showing its response respectively in terms of voltage 'V\_WT', active 'P\_WT', and reactive 'Q\_WT' power generated.

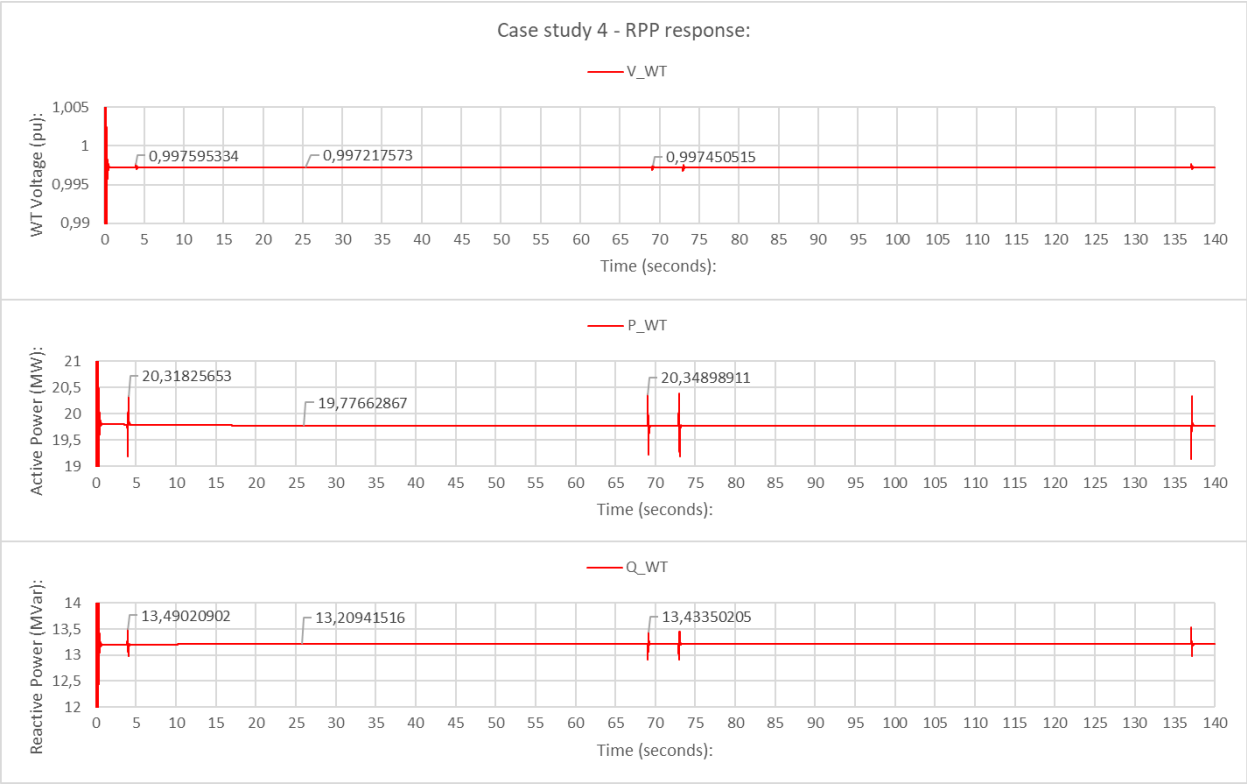


**Figure 0.13: Case study 4: RPP frequency event response**

Figure 5.13 is a graphical representation of the wind turbine scope outputs, representing the RPP response to the simulated conditions of Case study 4. Unlike the voltage simulations, it is observed that the simulated frequency fluctuations, other than a surge at its initiation and recovery, had minimal effect on the generated power. This minimal effect is observed since the fed voltage 'V\_feed\_in' is kept constant, showing POC voltage 'V\_POC' to be the dominant determining factor governing power response, as compared to frequency. Based on these observations, the RPP negligible response is considered normal, and in line with grid-code RPP-support requirements for Case study 4.

### 5.3.2 Case study 5

Case study 5 is aimed at evaluating the model and simulated RPP response concerning RPP grid-code requirements during short-lived frequency events violating 'Fnu'/'Fnl' boundaries, entering the HFRT/LFRT operating region. These conditions represent short-lived grid disturbances substantial enough to qualify as a fault, but with a duration brief enough to necessitate a fault ride-through response rather than a trip. To isolate and assess effectively the ability of the frequency validation subsystem to react in line with grid-code requirements during such events, the ability of the voltage-validation subsystem to trip the RPP will remain disabled, while keeping the fed voltage 'V\_feed\_in' constant at 1 pu. Using the fed frequency 'F\_feed\_in' to alter POC frequency 'F\_POC' conditions, the simulation was performed using the OPAL-RT OP4510 real-time simulator, for which the results are presented in Figures 5.14 and 5.15.

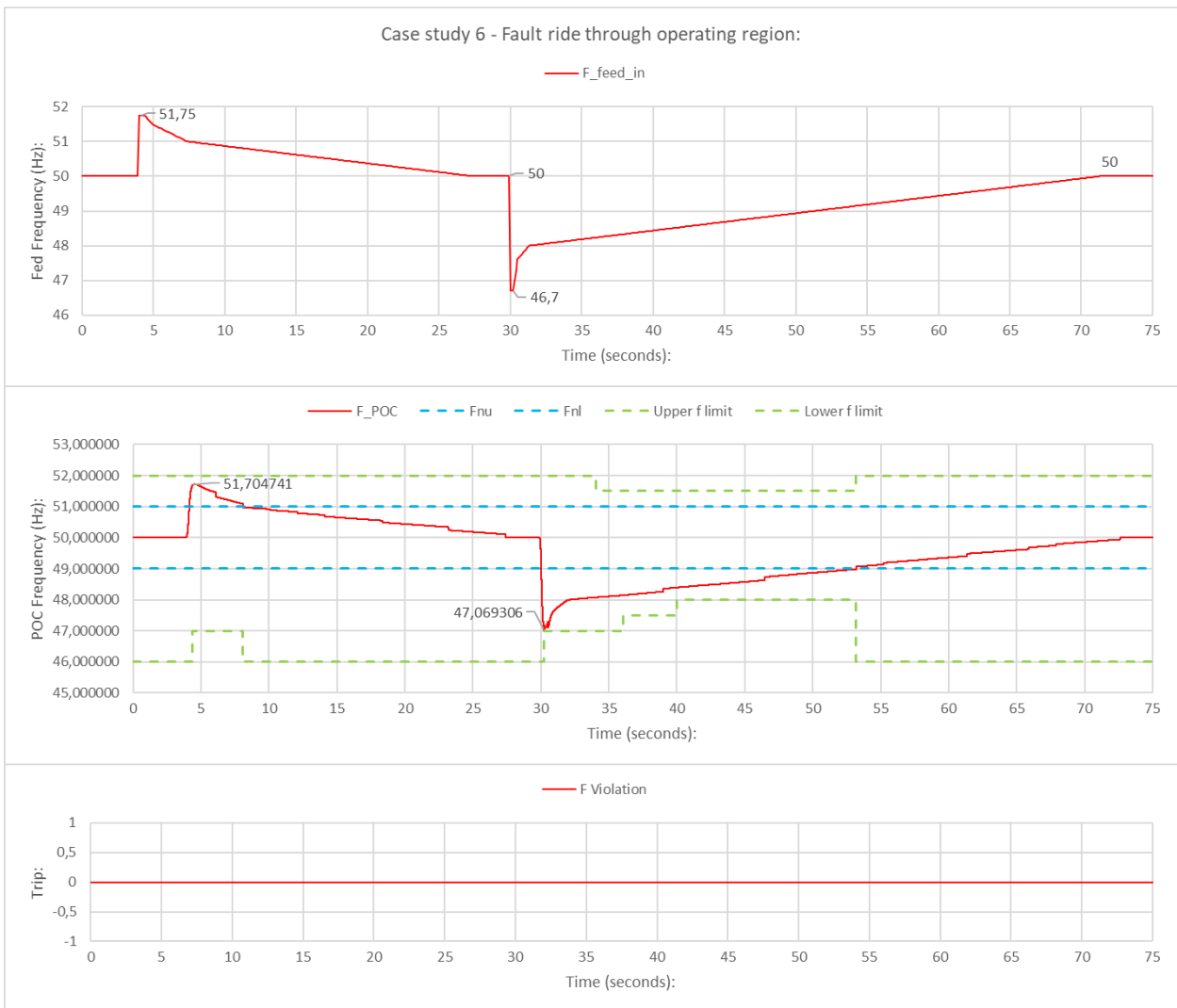


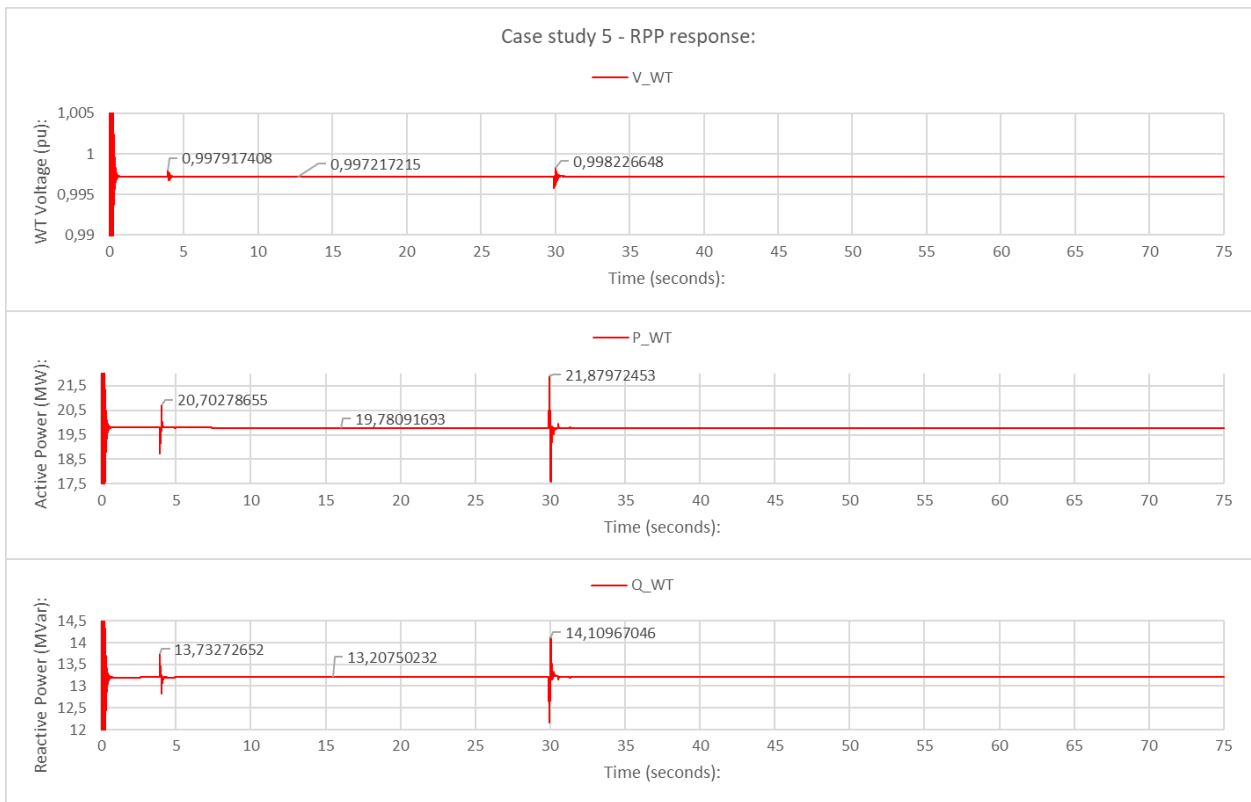
Figure 0.14: Case study 5: testbed frequency event response



The three graphs of Figure 5.14 respectively illustrate the adapted imported frequency '**F\_feed\_in**', measured POC frequency '**F\_POC**', and trip input '**F Violation**' obtained from the output of the frequency-validation subsystem for the 75-second simulation of Case study 5. The POC frequency '**F\_POC**' graph of Figure 5.14 additionally includes the continuous operating band given by the '**Fnu**'/'**Fnl**' limits of the simulated RPP in blue, and the adjusting time-dependent HFRT/LFRT boundaries in green.

Considering the simulation results of Case study 5 in Figure 5.14, two events can be observed. The first of these, introduced at  $t=4$  seconds, is a short-lived '**F\_feed\_in**' frequency spike of 51.75 Hz, resulting in a POC frequency '**F\_POC**' rise violating blue '**Fnu**' boundary limits, venturing into the fault ride-through region of operation, after which the fault is cleared. The second, introduced at  $t=30$  seconds, is a short-lived '**F\_feed\_in**' frequency dip to 46.7 Hz, causing the POC frequency '**F\_POC**' to violate blue '**Fnl**' boundary limits, and to venture into the fault ride-through region before the fault again clears.

For both events, it is observed that conditions enter fault ride-through regions of operation, represented by the adjusting time-dependent HFRT/LFRT boundaries governed by grid codes. A trip is, however, not generated, since green dotted HFRT/LFRT boundaries are not violated, although having come close during the frequency-dip event. Case study 5 thus shows the ability of the testbed to recognise frequency events, ride through such events while within ride-through boundaries, and then reset when the event is cleared without generating a trip. Based on these observations, the response of the frequency-validation subsystem is considered appropriate and effective for the simulated conditions of Case study 5. Figure 5.15 follows, illustrating the effect that these disturbances had on the RPP simulated, showing its response respectively in terms of voltage '**V\_WT**', active '**P\_WT**', and reactive '**Q\_WT**' power generated.



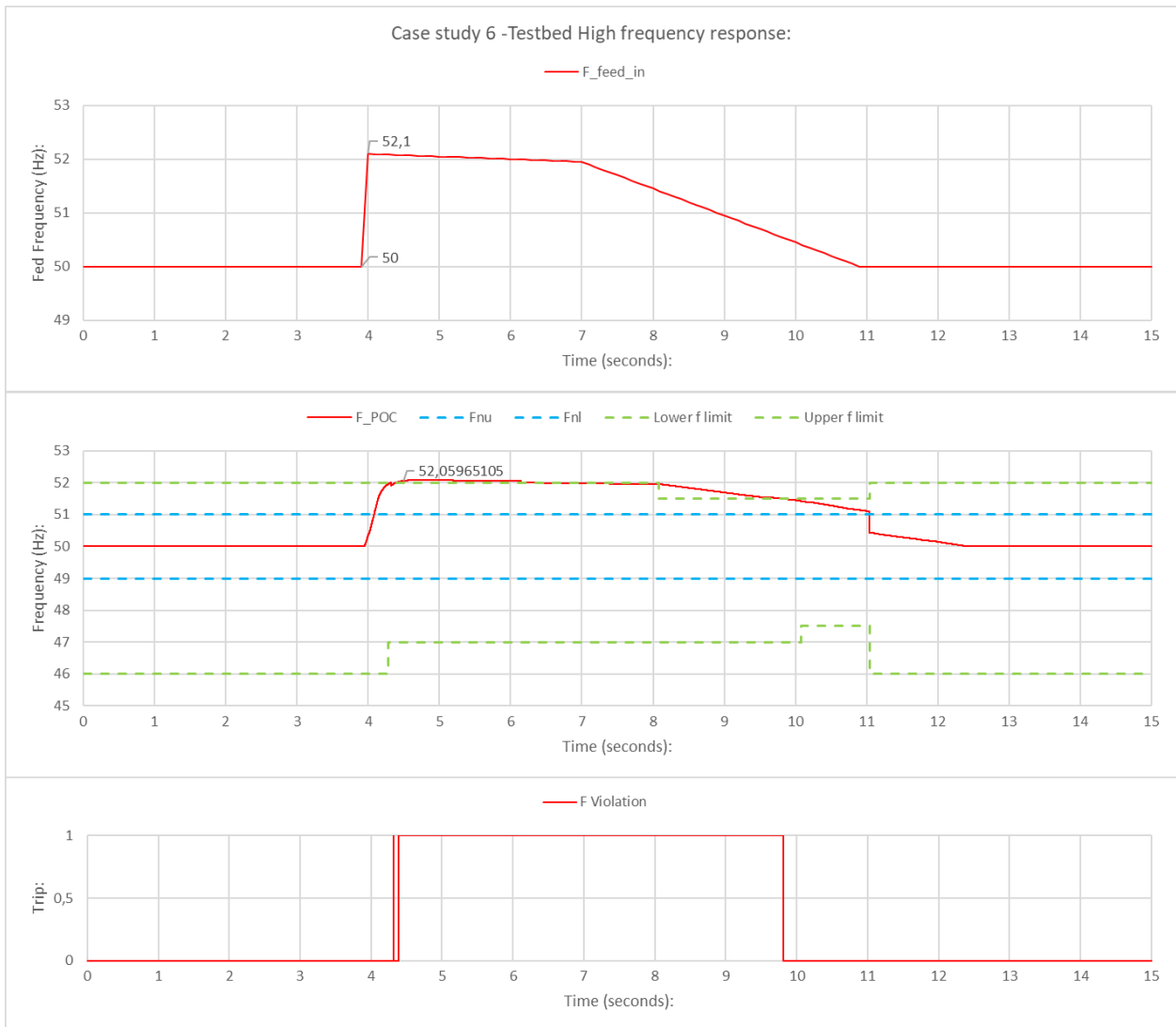
**Figure 0.15: Case study 5: RPP frequency event response**

Figure 5.15 is a graphical representation of the wind turbine scope outputs, representing the RPP response to the simulated conditions of Case study 5. As with Case study 4, a minimal effect is observed with regard to generated power during the simulated frequency events, other than a surge at the time of initiation. This minimal effect can again be attributed to the fed voltage 'V\_feed\_in' being kept constant, confirming the POC voltage 'V\_POC' to be the determining factor governing power response, compared to frequency. Based on these preliminary observations, the negligible response of the RPP is considered normal, and in line with grid-code RPP-support requirements.

### 5.3.3 Case study 6

Case study 6 is aimed at evaluating the model and simulated RPP response regarding RPP grid-code requirements during significant frequency events, leading to a violation of HFRT/LFRT boundaries. These conditions represent severe grid disturbances substantial enough to necessitate a trip, whether because of their intensity, or their inability to clear. To isolate and assess effectively the ability of the frequency-validation subsystem to react in line with grid-code requirements during such events, the ability of the voltage-validation subsystem to trip the RPP will remain disabled, while keeping the fed voltage 'V\_feed\_in' constant at 1 pu. Using the fed

frequency 'F\_feed\_in' to alter POC frequency 'F\_POC' conditions, the simulation was performed using the OPAL-RT OP4510 real-time simulator, for which the results are presented in Figures 5.16 to 5.19.



**Figure 0.16: Case study 6: testbed high-frequency event response**

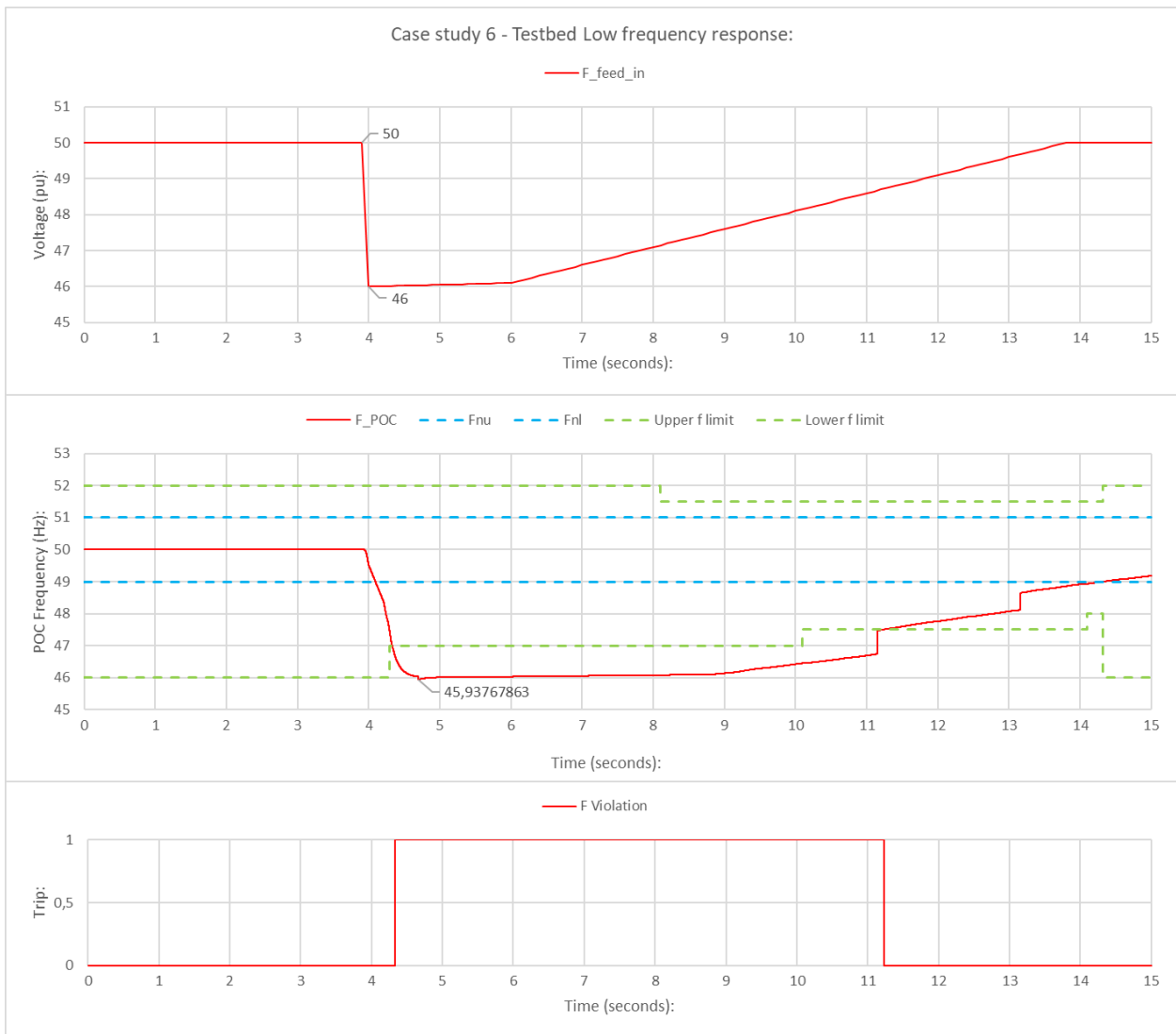


**Figure 0.17: Case study 6: testbed low-frequency event response**

The three graphs of Figures 5.16 and 5.17 respectively illustrate the adapted per-unit test frequency '**F\_feed\_in**' imported, measured POC frequency '**F\_POC**', and trip input '**F Violation**' obtained from the output of the frequency-validation subsystem for the respective 15-second high- and low-frequency disturbance simulation of Case study 6. The POC frequency graph of Figures 5.16 and 5.17 additionally displays the continuous operating band given by the '**Fnu**'/'**Fnl**' limits of the simulated RPP in blue, and the adjusting time-dependent HFRT/LFRT boundaries in green.

Considering the first of the simulation results of Case study 6 in Figure 5.16, the introduction of a 52.1 Hz spike is seen, introduced at t=4 seconds, via the imported '**F\_feed\_in**' frequency. This causes the POC frequency '**F\_POC**' to enter and violate the green dotted HFRT boundary soon after, leading to a corresponding '**F Violation**' trip at that time. Similarly, a low-frequency event of

46 Hz can be observed from the 'F\_feed\_in' graph of Figure 5.17. This causes the POC frequency 'F\_POC' to enter and violate the LFRT boundary soon after, confirmed by the corresponding 'F Violation' trip signal generated.

It is observed during both events that conditions enter fault ride-through regions of operation without an immediate trip, since the RPP rides through each disturbance briefly. Conditions then deteriorate swiftly beyond HFRT/LFRT boundaries, at which point a trip is generated. Case study 6 thus shows the ability of the testbed to recognise frequency events, ride through such events while within ride-through boundaries, and then disconnect the RPP in line with frequency grid-code requirements when RPP frequency ride-through boundaries are violated. Based on these observations, the response of the frequency-validation subsystem can be considered appropriate and effective for the simulated conditions of Case study 6. Figures 5.18 and 5.19 follow, illustrating the effect that these high- and low-frequency disturbances had on the RPP simulated, showing its response respectively in terms of voltage 'V\_WT', active 'P\_WT', and reactive 'Q\_WT' power generated.

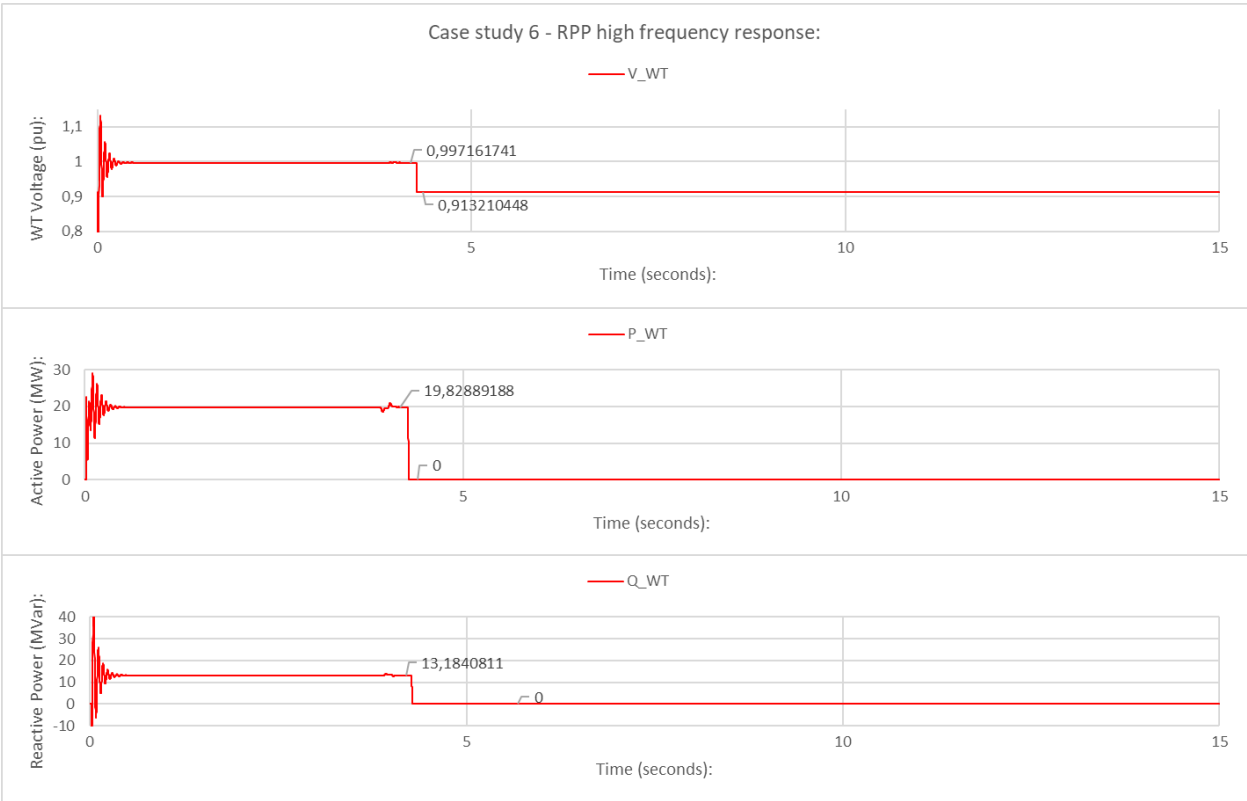
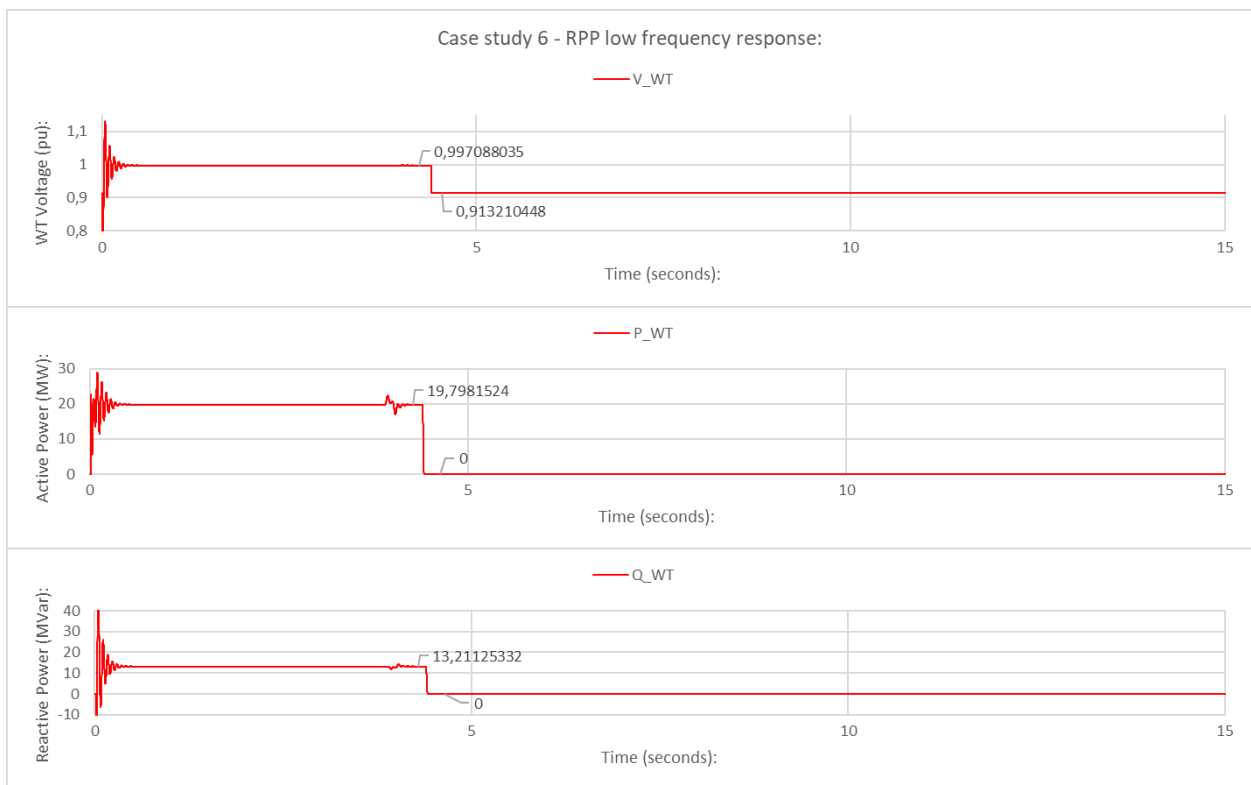


Figure 0.18: Case study 6: RPP high-frequency event response



**Figure 0.19: Case study 6: RPP low-frequency event response**

Figures 5.18 and 5.19 is a graphical representation of the wind turbine scope outputs, representing the RPP response to the simulated conditions of Case study 6. As with Case studies 4 and 5, a minimal effect is observed on generated power during the simulated frequency events, since the fed voltage '**V\_feed\_in**' were again kept constant. For Case study 6 it can, however, additionally be noted that generating active '**P\_WT**' and reactive '**Q\_WT**' power drops off to 0 following the '**F Violation**' trip, confirming the successful disconnection of the RPP. Based on the initial observations of a lacking RPP response, followed by the RPP operation being terminated at the time the trip was generated, its response is considered appropriate and in line with grid-code RPP-support requirements.

#### 5.4 Short-circuit studies

Having Case studies 1 to 6 exhibiting the abilities of the developed real-time testbed, and its respective voltage and frequency-validation subsystems to react and control simulated RPPs in line with what is required by South African grid codes, the focus of the final section now shifts to the testbed's purpose of performing RPP behavioural studies. Case study 7 follows, carried out in response to RPP testing requirements set by South African grid codes, aimed at evaluating an RPP response and POC support during short-circuit events. Testing procedures mandate voltage drops of 20%, 30%, 50%, and 80% at the POC, monitoring the active, reactive, and peak-current

response of the RPP in 0.5-second intervals using the grid-codes document-provided tables, and the logged 'SC Test' scope data of Figure 5.2. For Case study 7, the '**V\_feed\_in**' voltage is adapted to recreate the desired voltage drops at the POC, while the fed frequency '**F\_feed\_in**' is kept constant at 50 Hz. Four simulations were performed for the respective POC voltage drops, implementing the OPAL-RT OP4510 real-time simulator for which the results and completed data tables are presented in Figures 5.20 to 5.23, and Tables 5.1 to 5.4.

## 5.4.1 Case study 7

### 5.4.1.1 20% Voltage drop test

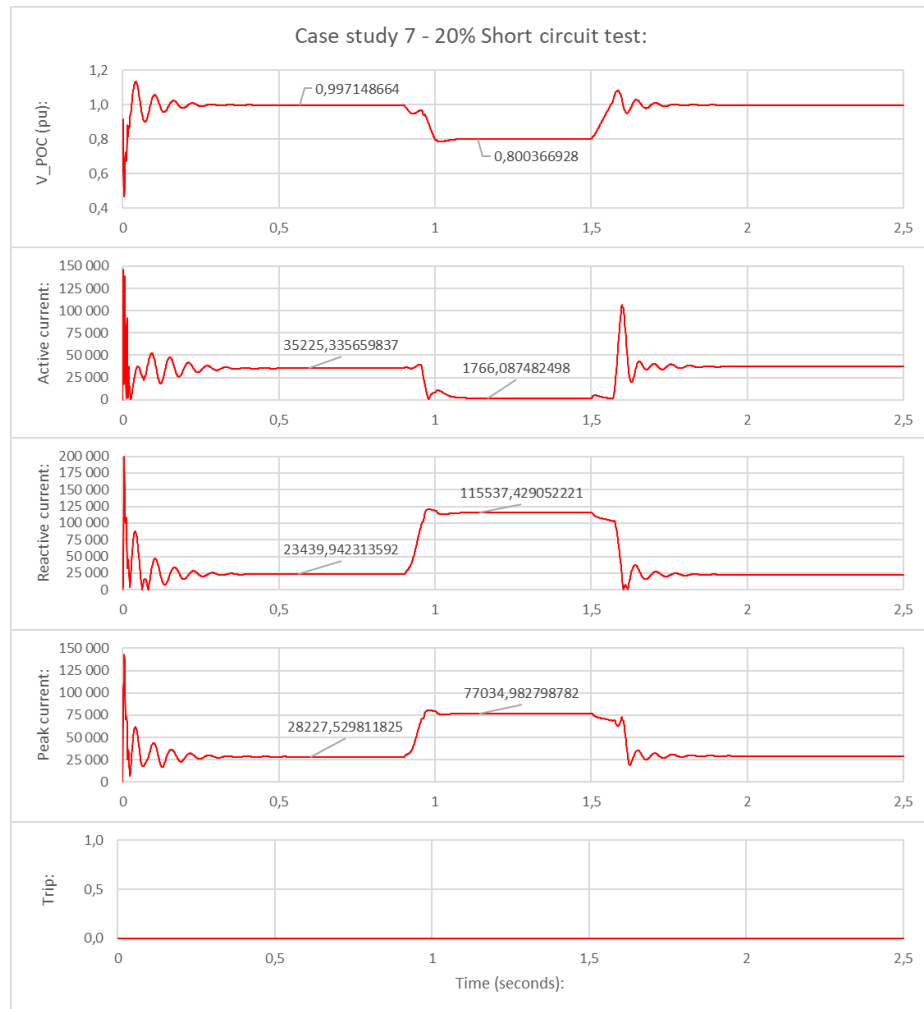


Figure 0.20: Case study 7: RPP 20% short circuit at POC response

Table 0.1: Case study 7: 20% short-circuit test data

20% Voltage drop at POC			
Time (ms)	I <sub>active</sub> (A)	I <sub>reactive</sub> (A)	I <sub>peak</sub> (A)
0	8 015	118 823	79 395
5	9 913	117 327	78 496
10	10 555	114 642	76 751
20	9 167	113 132	75 669
50	3 893	114 330	76 264
100	1 971	115 449	76 977
150	1 780	115 541	77 037
200	1 755	115 548	77 041
300	1 752	115 548	77 040



20% Voltage drop at POC			
Time (ms)	I <sub>active</sub> (A)	I <sub>reactive</sub> (A)	I <sub>peak</sub> (A)
500	1 752	115 548	77 040

#### 5.4.1.2 30% Voltage drop test

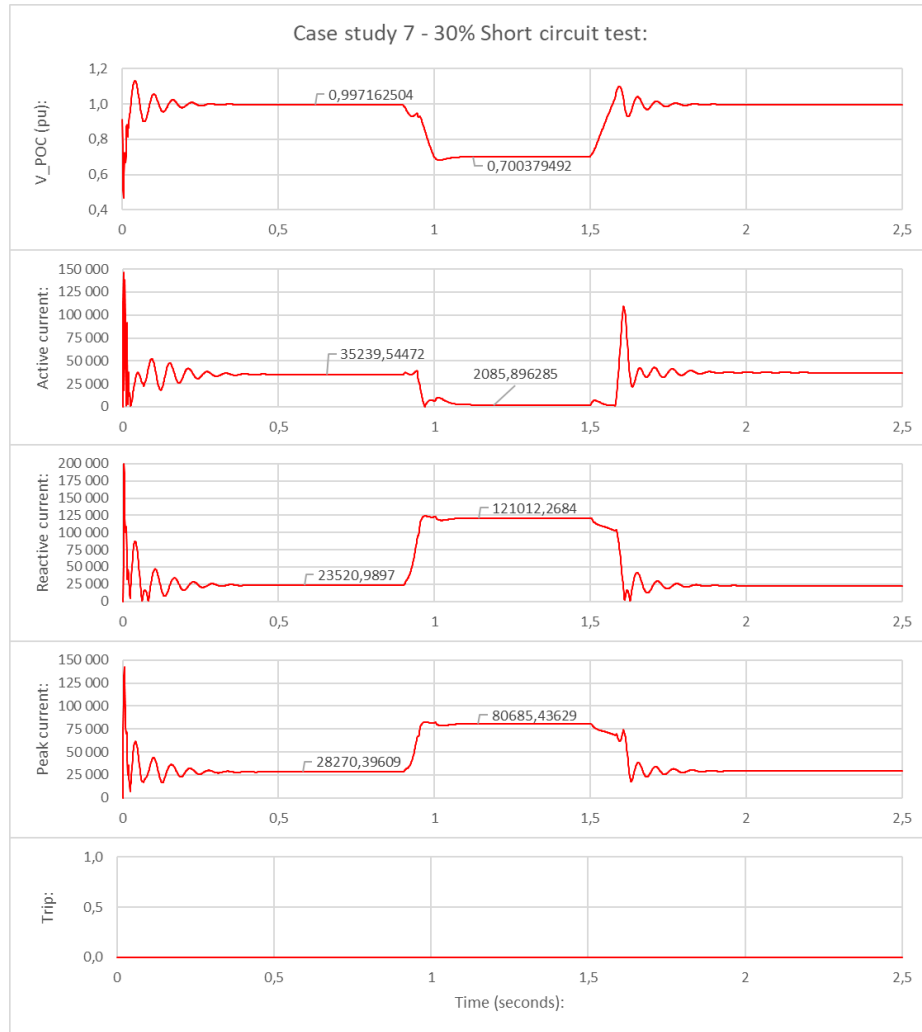


Figure 0.21: Case study 7: RPP 30% short circuit at POC response

Table 0.2: Case study 7: 30% short-circuit test data

30% Voltage drop at POC			
Time (ms)	I <sub>active</sub> (A)	I <sub>reactive</sub> (A)	I <sub>peak</sub> (A)
0	6 257	122 785	81 963
5	8 530	121 804	81 401
10	9 811	118 950	79 570
20	9 171	117 642	78 666
50	4 363	119 306	79 591

30% Voltage drop at POC			
Time (ms)	I <sub>active</sub> (A)	I <sub>reactive</sub> (A)	I <sub>peak</sub> (A)
100	2 284	120 852	80 582
150	2 107	121 021	80 693
200	2 084	121 040	80 705
300	2 080	121 043	80 707
500	2 080	121 043	80 707

#### 5.4.1.3 50% Voltage drop test

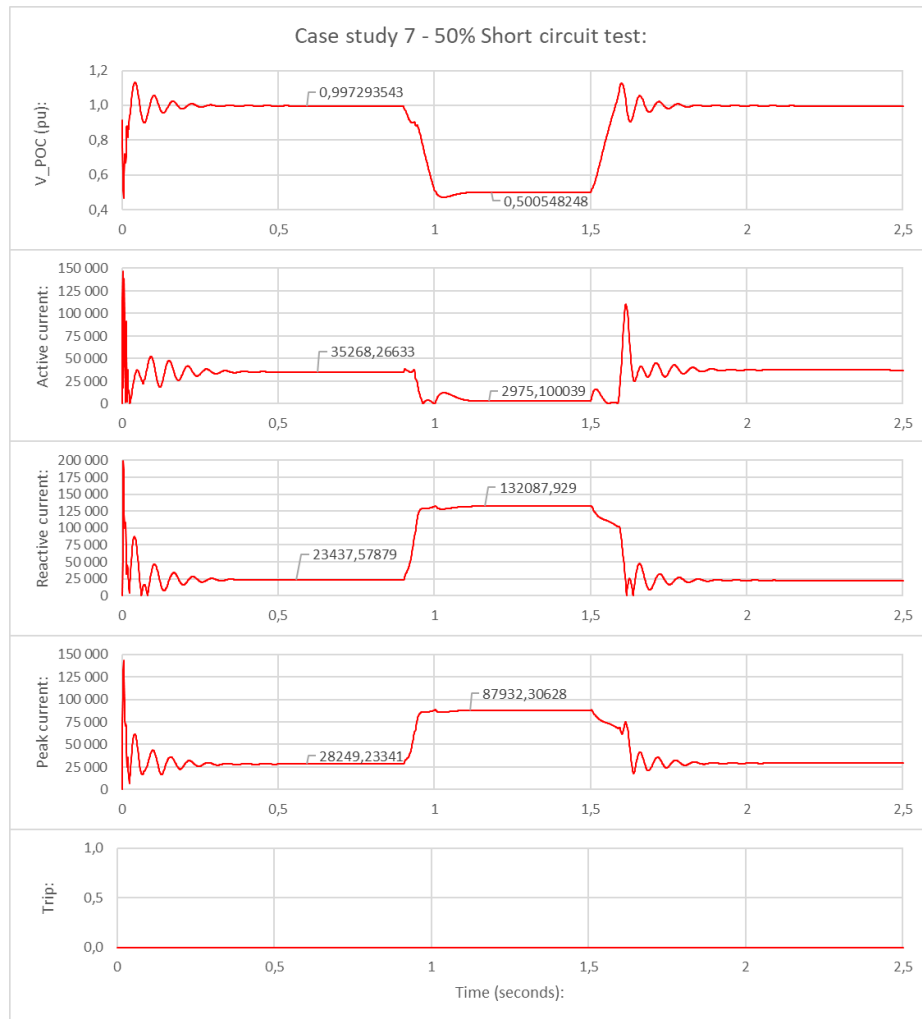
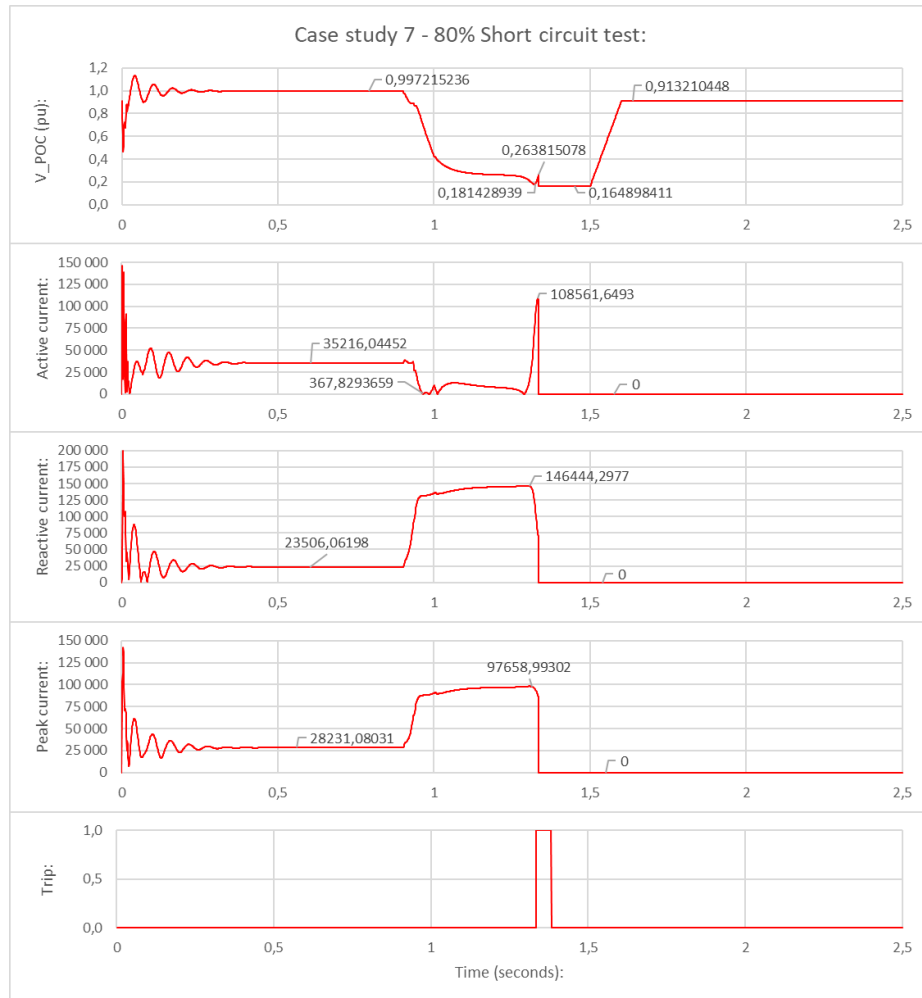


Figure 0.22: Case study 7: RPP 50% short circuit at POC response

**Table 0.3: Case study 7: 50% short-circuit test data**

50% Voltage drop at POC			
Time (ms)	I <sub>active</sub> (A)	I <sub>reactive</sub> (A)	I <sub>peak</sub> (A)
0	862	131 998	88 000
5	3 335	132 185	88 151
10	7 559	129 177	86 266
20	11 259	128 080	85 716
50	10 272	129 273	86 454
100	4 057	131 630	87 795
150	2 898	132 078	88 073
200	3 082	132 078	88 076
300	3 151	132 067	88 070
500	3 146	132 068	88 070

**5.4.1.4 80% Voltage drop test**



**Figure 0.23: Case study 7: RPP 80% short circuit at POC response**

**Table 0.4: Case study 7: 80% short-circuit test data**

80% Voltage drop at POC			
Time (ms)	$I_{\text{active}}$ (A)	$I_{\text{reactive}}$ (A)	$I_{\text{peak}}$ (A)
0	9 945	135 043	90 273
5	5 667	136 357	90 983
10	490	134 197	89 465
20	5 456	134 724	89 890
50	12 269	138 104	92 432
100	11 460	142 119	95 054
150	9 130	144 026	96 210
200	7 689	144 842	96 697
300	7 829	146 815	98 015
500	0	0	0

Considering the 20%, 30%, 50%, and 80% short-circuit test results of Case study 7 in Figures 5.20 to 76, it can first be observed from the '**V\_POC**' graphs that the simulated short circuits causing the respective POC voltage drops, were for each case introduced between  $t=1$  and  $t=1.5$  seconds. Considering the corresponding RPP current response graphs, curtailment of active current in favour of reactive current is observed for each case, much like that of the earlier power response of the RPP during the voltage-dip tests. This response occurs as the RPP attempts to raise and restore POC voltage conditions by increasing its reactive output component, and is the response expected considering the simulated conditions of Case study 7. In terms of the total, or peak-current generated, it is also observed to increase significantly compared to its baseline value leading up to each event at  $t=1$  second. These observations are confirmed by the summarised logged data of Tables 5.1 to 5.4, better exhibiting the current response relative to short-circuit intensity, which is also observed to be nonlinear because of the simulated generation limitations of the RPP. These generation limitations are additionally thought to be the cause of the trip in Figure 5.23 during the 80% short-circuit test as the RPP fails to provide sufficient POC support to recover, causing the generated currents to drop off to 0 by 500 milliseconds. Based on these preliminary observations, it is seen that the RPP supported the grid within its generation limitations during the simulated short-circuit events, in line with the RPP-support requirements. The trip generated during the 80% short-circuit test then also again confirms the testbed's ability to disconnect the RPP from the circuit, in the event that voltage or frequency conditions are violated.

## **5.5 Real-world event data studies**

Case studies 8 and 9 is aimed at illustrating the testbed, and RPP operation and response using real-world data. The fabricated test data of previous case studies fed using the 'V & F Grid import data' block is consequently replaced with measured PMU grid data recorded during previous grid disturbances, allowing the RPP performance to be assessed during recorded grid events. Accordingly, the simulations of Case studies 8 and 9 will incorporate the testbed and its subsystems in their entirety, allowing results to be obtained using the logged data from the 'Voltage', 'Frequency', and Wind turbine' scopes of Figure 5.2. Although it is known that the simulated real-world data originated from actual grid measurements, the recorded location was not disclosed, since such data are often regarded as sensitive information. Nevertheless, for Case studies 8 and 9, the type of data is more important than its origin and is considered an accurate representation of the conditions which could be encountered by RPPs connected to an actual grid (MathWorks, 2020).

### **5.5.1 Case study 8**

Case study 8 involves the real-time simulation of a 100-second dataset known to have been recorded during a grid disturbance, for which the details were initially unknown. The dataset was fed, and the simulation was allowed to run using the developed real-time testbed, and OPAL-RT OP4510 real-time simulator, for which the results are presented in Figures 5.24 to 5.26.

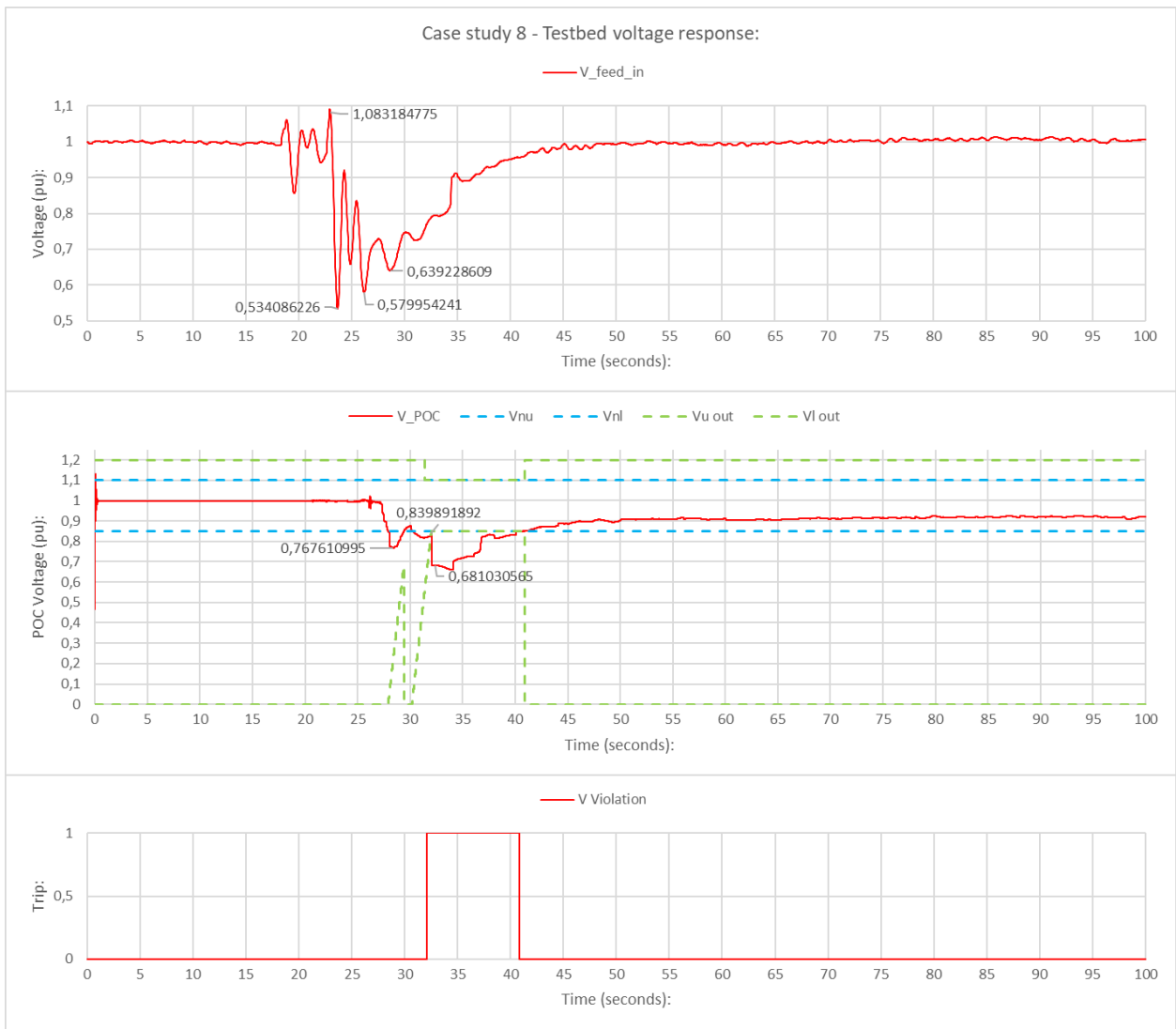


**Figure 0.24: Case study 8: testbed voltage response**

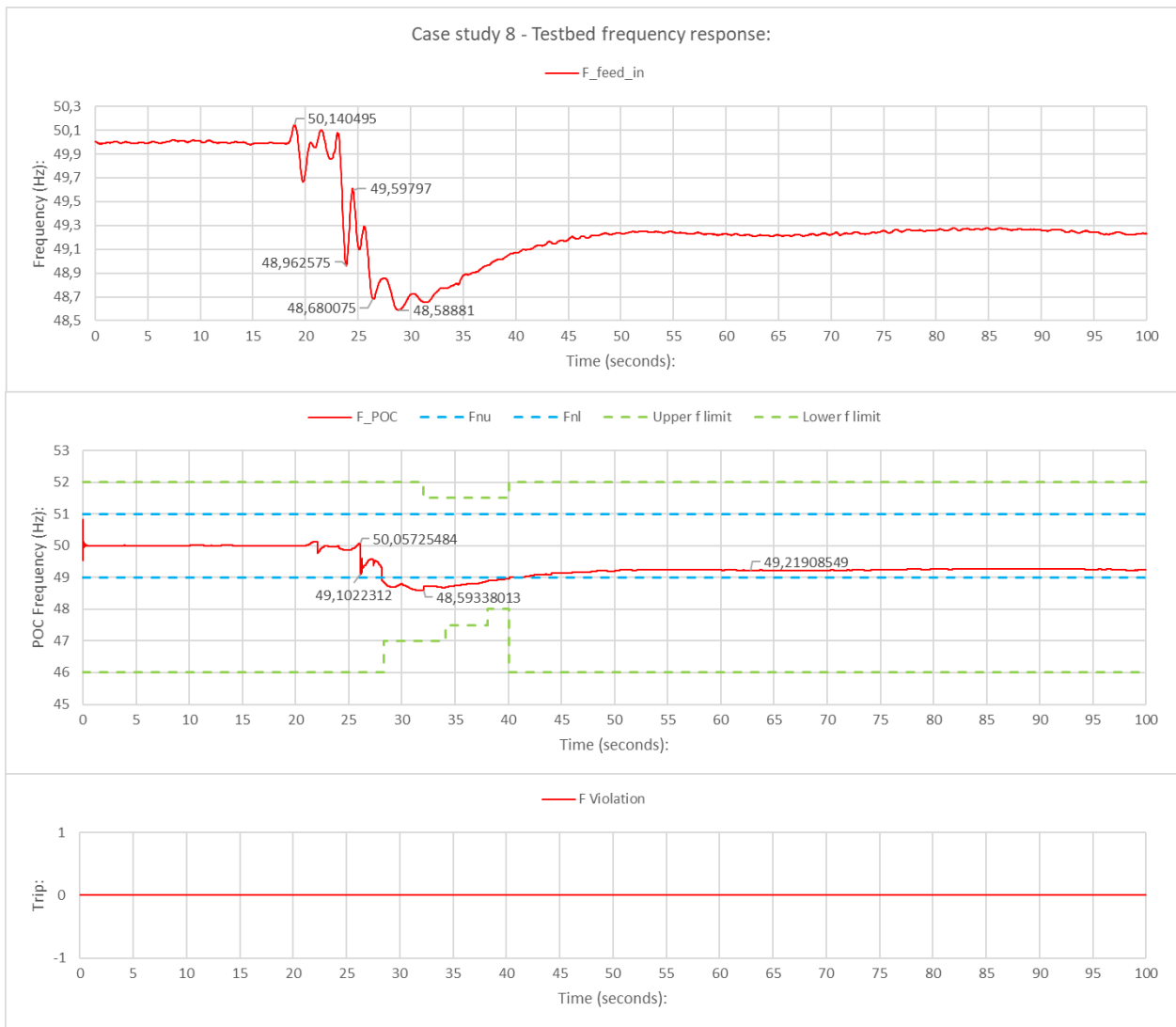


**Figure 0.25: Case study 8: testbed frequency response**

The three graphs of Figure 5.24 respectively illustrate the imported measured voltage data 'V\_feed\_in', POC voltage 'V\_POC', and trip input 'V Violation' obtained from the voltage-validation subsystem. Similarly, the three graphs of Figure 5.25 respectively illustrate the imported measured frequency 'F\_feed\_in', POC frequency 'F\_POC', and trip input 'F Violation' obtained from the frequency-validation subsystem. The POC voltage and frequency graphs of Figures 5.24 and 5.25 additionally include the continuous operating bands dotted blue and the adjusting time-dependent ride-through boundaries in green.

Simulation results considered, it is observed that both POC voltage 'V\_POC' and frequency 'F\_POC' conditions violate their respective blue dotted 'Vnl'/'Fnl' boundary limits, entering the LVRT/LFRT band of operation following a disturbance that commenced around t=18 seconds. The disturbance is acknowledged given the adjusting green ride-through limits, which see conditions

enter and exit the fault ride-through region before ultimately leading to a trip, as POC voltage 'V\_POC' conditions failed to recover in time. This brings to light the undesirable effect that disconnecting generation has on system stability, as POC voltage is then seen to deteriorate quickly afterward. Figure 5.26 follows, illustrating the effect that the events of Case study 8 had on the RPP simulated, showing its response respectively in terms of voltage 'V\_WT', active 'P\_WT', and reactive 'Q\_WT' power generated.

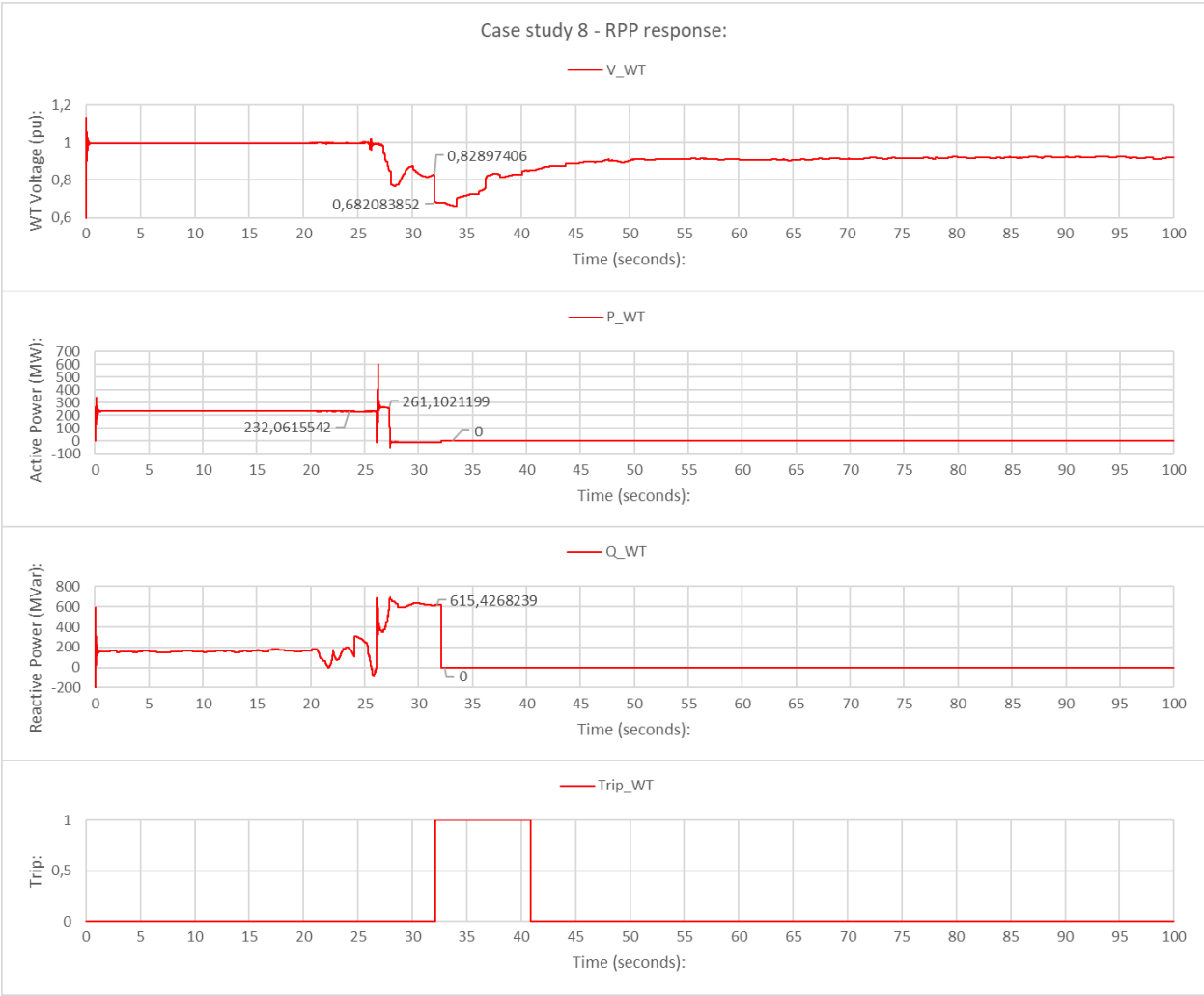


**Figure 0.26: Case study 8: RPP response**

Obtained directly for the simulated RPP, the results of Figure 5.26, in line with those of the previous case studies, show the RPP to support POC conditions while the disturbance is active. This is evident from the increase in active 'P\_WT' and reactive 'Q\_WT' power generated, as additional support is provided to raise the dwindling POC voltage 'V\_POC', to avoid a trip. POC voltage conditions, however, did not recover in time, leading to the trip, at which point it is seen that the generated power drops to 0, confirming the RPP disconnecting. Based on these observations, the



testbed and RPP response, given the fed real-world simulation data of Case study 8, is in line with what would be expected, as the RPP supported and disconnected from the grid as is required by South African grid codes.

### 5.5.2 Case study 9

Case study 9 involves the real-time simulation of a 134-second dataset known to have been recorded during a grid disturbance, for which the details were initially unknown. The simulation dataset was again imported, fed, and simulated using the developed real-time testbed, and OPAL-RT OP4510 real-time simulator, for which the results are presented in Figures 5.27 to 5.29.



Figure 0.27: Case study 9: testbed voltage response

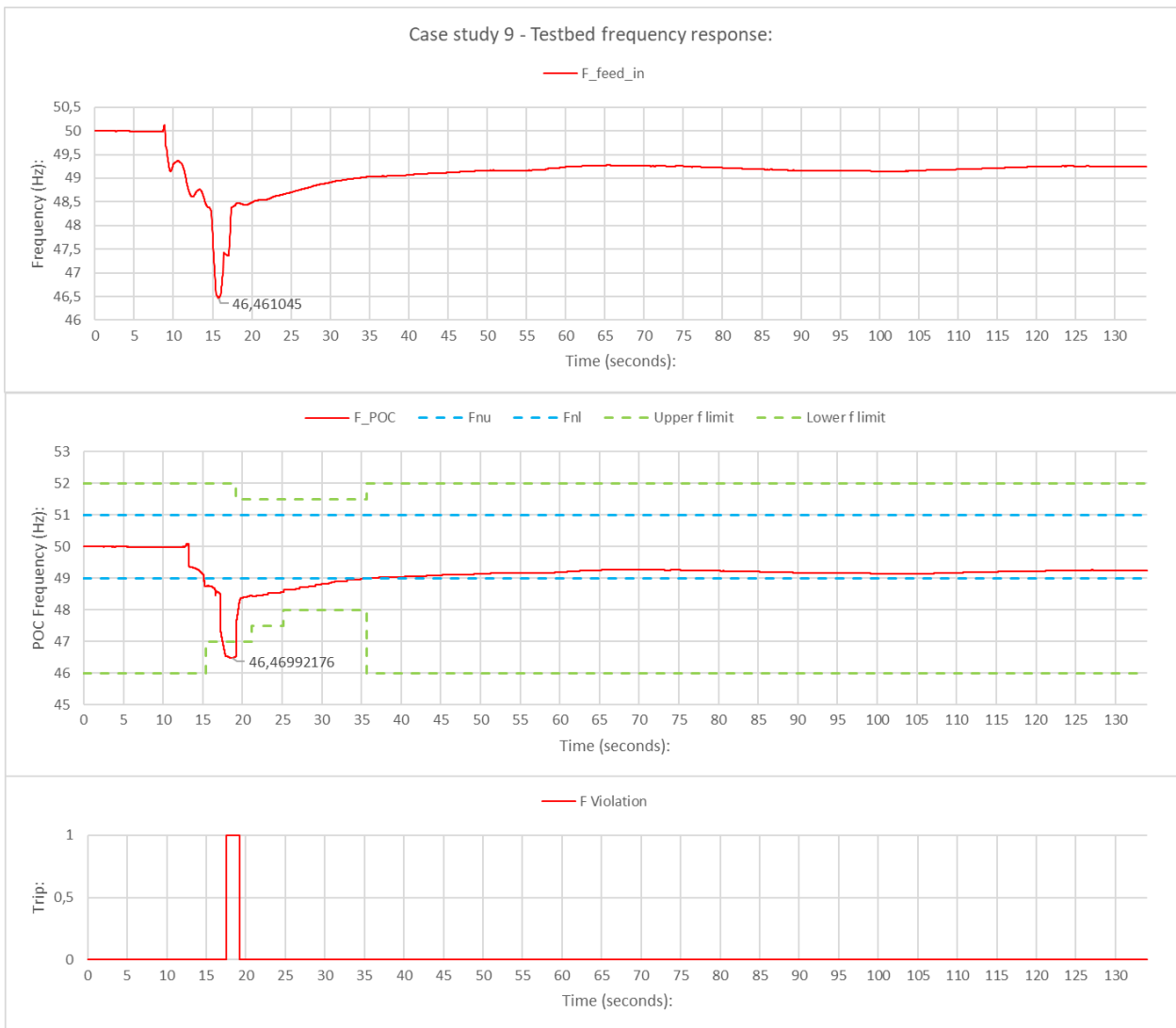


**Figure 0.28: Case study 9: testbed frequency response**

The three graphs of Figure 5.27 again respectively illustrate the imported measured voltage data ' $V_{feed\_in}$ ', POC voltage ' $V_{POC}$ ', and trip input ' $V_{Violation}$ ' obtained from the voltage-validation subsystem. Similarly, the three graphs of Figure 5.28 respectively illustrate the imported measured frequency data ' $F_{feed\_in}$ ', POC frequency ' $F_{POC}$ ', and trip input ' $F_{Violation}$ ' obtained from the frequency-validation subsystem. The POC voltage and frequency graphs of Figures 5.27 and 5.28 additionally include the continuous operating bands dotted blue and adjusting time-dependent ride-through boundaries in green.

Simulation results considered, it is observed that both the POC voltage ' $V_{POC}$ ' and frequency ' $F_{POC}$ ' quickly violate their respective blue dotted ' $V_{nl}$ '/' $F_{nl}$ ' boundary limits, entering the LVRT/LFRT band of operation, following a disturbance that commenced around  $t=10$  seconds. The acknowledgment by the testbed of this is observed through the adjusting green ride-through

limits, then violated soon afterward, leading to a trip. It is observed that the initial trip came because of an LFRT violation, seen to have the same accelerated deteriorating effect on POC conditions as with Case study 8. A second LVRT violation trip occurs soon after, coming as a direct result of the lost RPP support. Figure 5.29 follows, illustrating the effect that the events of Case study 9 had on the RPP simulated, showing its response respectively in terms of voltage 'V\_POC', active 'P\_WT', and reactive 'Q\_WT' power generated.

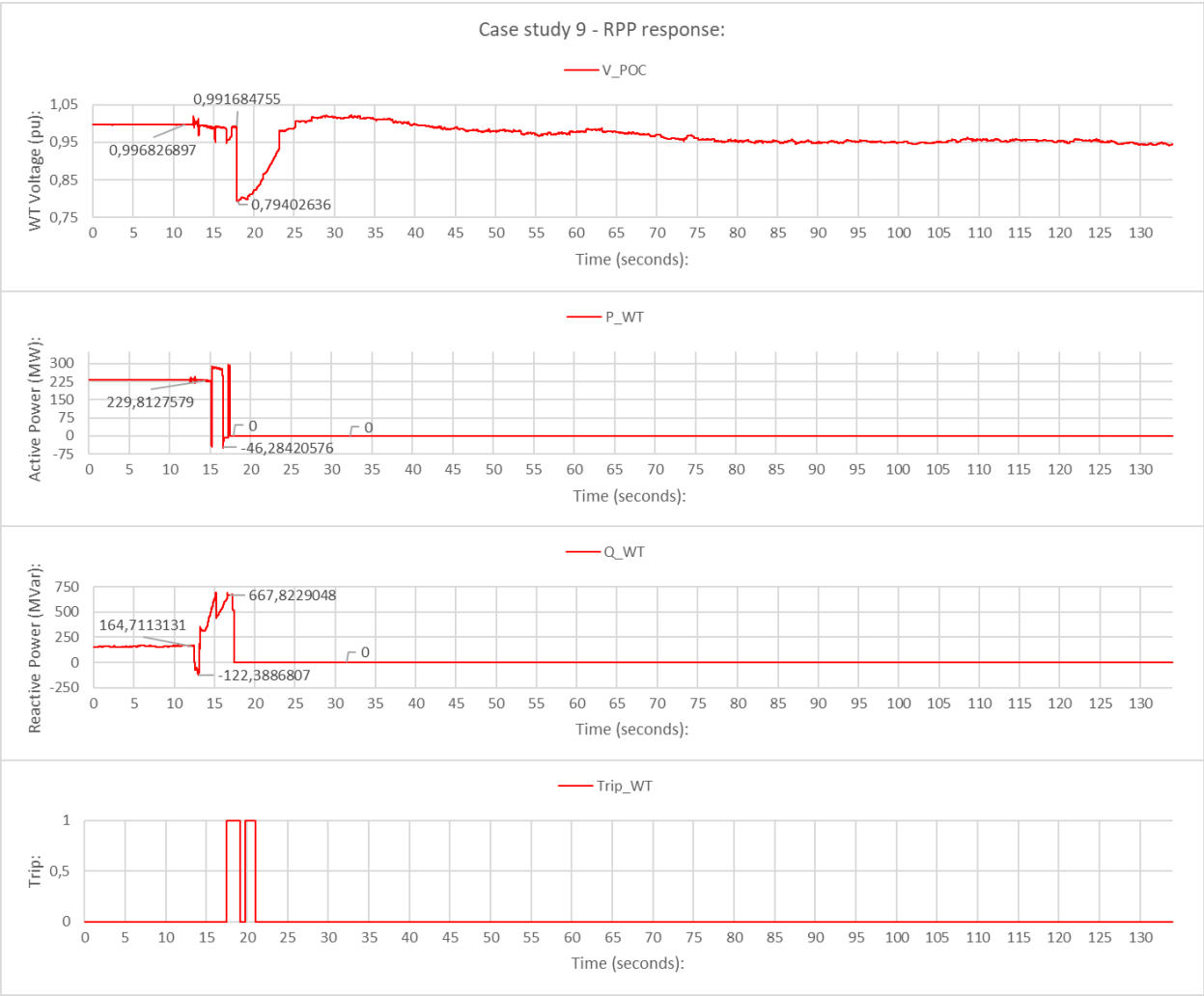


**Figure 0.29: Case study 9: RPP response**

Obtained directly for the simulated RPP, the results of Figure 5.29, in line with those of the previous case studies, show the RPP to support POC conditions while the disturbance is active. For Case study 9, this includes the swift absorption of excess power during an initial voltage spike, followed by an increase in active 'P\_WT' and reactive 'Q\_WT' power generated when POC voltage falls, as the RPP aims to avoid a trip. However, the disturbance of Case study 9 is severe and, although POC voltage conditions improve leading up to the trip, the support capabilities of the RPP were

insufficient to avoid it. At that time, it is seen that the generated power again falls to 0, confirming that the RPP has disconnected because of an LFRT violation. Based on these observations, the testbed and RPP response, given the fed real-world simulation data of Case study 9, is in line with what would be expected, as the RPP supported and disconnected from the grid as is required by South African grid codes.

## **5.6 Summary**

This chapter was aimed at evaluating the effectiveness of the real-time testbed, and its ability to assist with South African RPP grid-integration behavioural studies. To do this, the case studies of Chapter Five first recreated POC conditions operating the simulated RPP in its respective continuous, fault ride-through, and trip region of operation, thus allowing the operation of the voltage- and frequency-validation subsystems to be assessed. These results showed the testbed to evaluate and react effectively to POC conditions, a crucial component of the accuracy and validity of RPP grid-integration behavioural study results going forward. Having shown that the testbed will react and operate in line with grid-code requirements, the succeeding case studies focused on RPP response during short-circuit and real-world events. These showed the RPP to support POC conditions within support capabilities throughout the simulations performed, as is required by South African grid-code requirements for the simulated RPP. The case studies also show the ability of the testbed to disconnect RPPs when POC conditions deteriorate beyond that for which the RPP can compensate, to limit potential damage. Ultimately, based on preliminary observations, Chapter Five shows the testbed to react and operate accurately to RPPs in line with grid-code voltage- and frequency requirements. This allows the loads placed on RPPs, and the consequent response of RPPs to simulated disturbances to be studied, both vital abilities when developing an effective RPP grid-integration behavioural studies testbed.

## **CHAPTER SIX**

### **ANALYSIS AND SUMMARY OF RESULTS**

#### **6.1 Introduction**

This chapter is aimed at summarising and analysing both the theoretical and simulative aspects forming part of the testbed's development and testing. Accordingly, the chapter provides a swift review of South Africa's intent to increase grid-connected renewable generation significantly going forward, corroborating the need for accurate and efficient grid-integration RPP behavioural study tools, such as those developed. The influence of grid-code specifications on the final testbed design is considered, contrasting elements of an example circuit with the final testbed design. The chapter's primary objective, however, is to analyse the simulation results of Chapter Five thoroughly, using the logged real-time simulation data recorded. A case study analysis consequently examines the events noted in the Chapter Five graphs, analysing the corresponding logged real-time simulation data as accurate means of assessing testbed-, and RPP behaviour and response. The chapter furthermore hopes to feature the testbed's worth, being able both to monitor and assess actively POC voltage and frequency conditions, while providing additional means of passive RPP assessment through the power and current measurement outputs, and RPP behavioural observations. This allows a verdict to be reached on the success of the developed real-time simulation testbed, given the appropriate behaviour of both testbed and RPP, in line with South African RPP-specific grid-code requirements.

#### **6.2 Research findings summary**

Research forming part of developing the real-time simulation testbed tailored to South African conditions and grid-code requirements, started by considering the current state of South Africa's electrical industry, and the direction in which it is most likely to be headed in the future. This revealed South Africa's electrical industry to be divided between government-owned Eskom, having an approximate market share of 70%, and independent power producers contributing towards the remaining 30%. As Eskom's generation fleet consists predominantly of coal-generation plants, most of the country's energy needs are still being met by coal, which is comprehensible given that South Africa has the 5th largest retrievable coal reserves in the world. The exact contribution of coal, however, is elusive, considering that generation capacity differs in terms of the contribution of technology towards a country's electrical needs. Of these, the latter is expected to be the more significant amount for coal, since coal is classified as baseload generation, therefore generating continuously compared to renewables, for example. Nevertheless, coal's generation contribution, considering all literature reviewed, appears to be between 71% and 80% of the country's energy needs, with the 2030 IRP giving the generation contribution of coal as 71.30% (Department of Mineral Resources and Energy, 2019).

Through reviewing officially released papers and policies from as early as 1998, it became clear that South Africa has long been planning to diversify its energy mix, hoping to break away from its significant dependence on coal by substituting it with renewable alternatives. Of the papers and policies reviewed, the 2030 IRP emerged as the most relevant and promising, after having seen updates in October 2019 (Department of Mineral Resources and Energy, 2019). Summarising the objectives of the latest 2030 IRP, Figure 6.1 illustrates the 2030 IRP forecast for renewable generation leading up to 2030. The trends noted in Figure 6.1, in essence, also represent the overall renewable-generation addition trends observed through the study’s research, where plans to increase the amount of grid-connected renewables significantly are supported and endorsed by similar projects such as the REIPPPP. These plans include gradual decommissioning of older coal-generation plants in the years to come, while increasing grid-connected renewables substantially, with a specific focus on onshore wind and solar PV. As noted earlier in this study, the planned rate of renewable integration is set to outweigh decommissioning of coal-generation plants, in that renewables are intended in South Africa not solely as a replacement for fossil-fuel generation, but more so as a way of increasing generation capacity to attend to the country’s ongoing energy crises (Oyewo *et al.*, 2019).

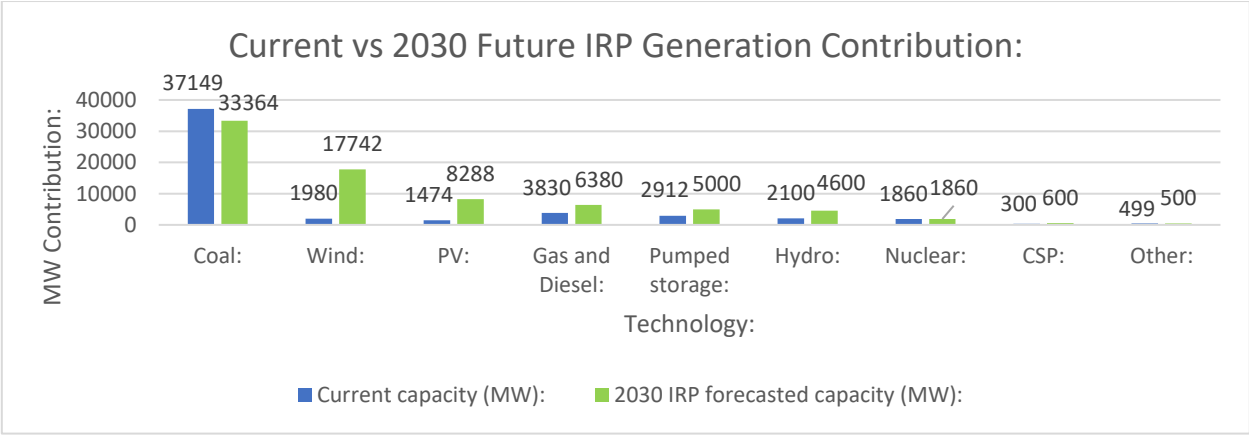


**Figure 0.1: Current vs 2030 IRP predicted generation contribution**

Research has established the intention of South Africa to continue its ongoing integration of renewable generation, with the focus falling on wind and solar as dominant future technologies. This study, therefore, wanted to explore the feasibility of these plans, reviewing research papers on renewable technologies best suited for South Africa. This revealed onshore wind and solar PV as an ideal combination for South African conditions, with South Africa receiving an abundance of sun and wind in most provinces, leading to these being among the most viable technologies. The most compelling advantage of this combination in the South African context is the fact that, when wind performance reaches a minimum at noon, solar reaches its peak, thereby aiding one another

potentially to provide continuous generation throughout the day (Knorr *et al.*, 2016; Mulaudzi and Bull, 2016; Jain and Jain, 2017; Naicker and Thopil, 2019).

Ultimately, the undeniable fact emerges that significant amounts of renewable generation are set to be grid-connected and integrated leading up to the IRP 2030 target, goals also shared by other papers, plans, and projects that were reviewed. As depicted by the graph in Figure 6.1, South Africa's future generation mix is set to change, bringing with it new challenges associated with renewable generation. This then supports a need for tailored South African simulation tools and testbeds, developed to simplify and to study renewable-generation integration effects reliably.

Governing RPP performance requirements set for all RPPs in South Africa are the South African RPP-specific grid codes, to which all RPPs must conform to be allowed grid connection. Grid-code documentation, in addition to performance specifications, specifies how compliance should be validated, which involves testing, and test-circuit requirements. These specifications have had a profound impact on the ultimate design of this study's testbed, as illustrated by Figure 6.2, presenting a comparison between the example test circuit available from the South African grid-codes document (NERSA, 2019), and the developed real-time testbed.

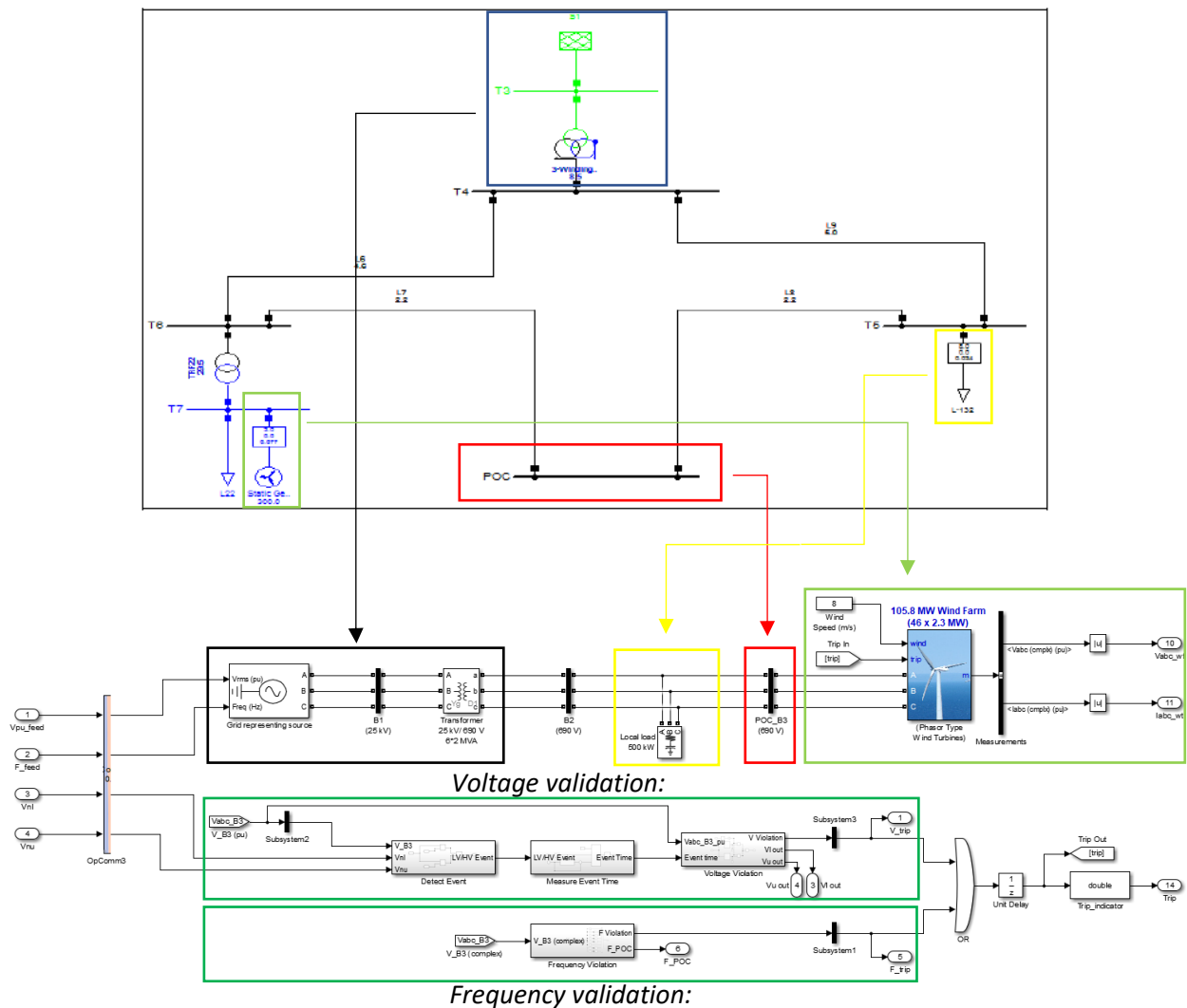


**Figure 0.2: Grid-code-specified test circuit vs developed test circuit**

It can be observed from Figure 6.2 that the elements illustrated as part of the grid-code example circuit, have also been incorporated into the developed real-time testbed, thus adhering to the circuit requirements set by South African grid codes. The testbed of Figure 6.2 additionally includes the labelled voltage and frequency-validation subsystems, responsible for tracking POC conditions, and operating the RPP accordingly. Voltage and frequency monitoring were chosen as primary RPP grid-code adherence criteria, being essential parameters with set grid-code requirements, based on POC voltage, and RPP class. A wider range of grid-code requirements also exist; however, these often demand additional location-specific inputs, following discussions with the NSP and SO surrounding abilities and limitations of a planned RPP (NERSA, 2019). The testbed was therefore developed to include additional outputs for parameters such as power and current, providing the necessary means to assess such parameters effectively, following the necessary grid-code specified discussions. Active RPP grid-code compliance monitoring at the



POC is therefore in terms of voltage and frequency, while additional requirements can be assessed passively using simulation results.

### 6.3 How this study compares to existing work

To evaluate the novelty of this study's research, other comparable work in the field can be considered. Table 6.1 presents a summary of this study, and the elements of comparable studies for comparison.

**Table 0.1: Summary of comparable studies**

<b>Aim/Function:</b>	<b>Software:</b>	<b>Real-time Simulator:</b>	<b>Findings:</b>	<b>Study Reference:</b>
Development of a real-time testbed tailored for South African renewable-integration studies.	MATLAB / RT-LAB	OPAL-RT OP4510	The testbed proved itself to be an effective grid-integration studies tool, in line with local grid-code requirements.	This study
Offline, and real-time performance analysis of a wind farm.	MATLAB Simulink / eMEGAsim	eMEGAsim	eMEGAsim produced accurate results for the simulated three-phase bus fault, while allowing additional parameters of the model also to be studied.	(Paquin <i>et al.</i> , 2007)
Development of a wind turbine-emulating platform, used for research, teaching, and training.	MATLAB Simulink / RT-LAB	OPAL-RT OP5600	The developed model allows control system theories to be implemented successfully, while allowing mathematical models to be extracted from simulation results.	(Merabet <i>et al.</i> , 2014)
Performance evaluation of commonly used dynamic models, simulating common system disturbances.	MATLAB Simulink / RT-LAB	OPAL-RT eMEGAsim	Single line-to-ground faults, line outages, step-load changes, and on-load tap changes were simulated successfully for the IEEE 9-bus and New England 39-bus systems, noting several software limitations and challenges which arose.	(Singh <i>et al.</i> , 2015)
Development of a power-in-the-loop simulation platform for new-generation grid connection studies.	RT-LAB	OPAL-RT	The model was shown to have strong experimental abilities, while being capable of simulating grid	(Li <i>et al.</i> , 2016)

<b>Aim/Function:</b>	<b>Software:</b>	<b>Real-time Simulator:</b>	<b>Findings:</b>	<b>Study Reference:</b>
			connection characteristics of multiple new-generation units.	
Development of a test environment for studying grid-connected PV module behaviour.	MATLAB Simulink / RT-LAB	OPAL-RT	The simulated test PV system proves real-time simulators to be a valuable tool for designing and analysing power electronic, and power systems.	(Noureen <i>et al.</i> , 2018)
A study of the effectiveness of SCADA systems using real-time simulation.	ETAP	OPAL-RT	Real-time simulations were proven to help identify SCADA shortcomings, which is essential for increasing overall power network efficiency.	(Luna <i>et al.</i> , 2018)

Just like that used by this study, it is observed from Table 6.1 that MATLAB-integrated OPAL-RT models for real-time simulation, is among the favourite for its interface familiarity and ability to produce accurate results. In addition to MATLAB’s Simulink environment, this study additionally implements a MATLAB live script, thus improving on the versatility of most standard Simulink developed models by allowing tailored simulation parameters to be selected from a wide field of specifications. This study additionally differs from most with respect to making use of a single data-import source block to represent the grid, compared to implementing elaborate static networks. This was done for the purpose of better representing the characteristics of a specific grid section for which measured grid data can now be fed, compared to a static network which would require extensive and complex adjustments to calibrate characteristics to a specified grid section. Comparable studies also rarely incorporate grid-code requirements as part of the control of simulated generation, which this study focused on as a means of tailoring the testbed to South African RPP requirements. This study is then also more orientated towards RPP and POC behaviour and parameters, in that that it is intended as a RPP grid-integration behaviour studies tool, compared to similar studies which often focus on parameters surrounding a specific network point, for example, the point where a fault is initiated.

Though the foundation of this study has elements in common with comparable work, it also varies from most in significant ways. These variations are to accommodate the specific purpose of the developed testbed, to serve as a novel tailored RPP grid-integration behaviour studies tool for South Africa. As with most of these studies, this study also notes the value of real-time simulators implemented for studying generation and grid behaviour, owing to their versatility, and accuracy.

**6.4 Simulation results analysis and findings**

To evaluate the successful development of the real-time testbed, each case study was selected with the specific purpose of validating a distinct section or function, while assessing RPP behaviour. Preliminary testbed- and RPP response have already been considered, based on the simulation result graphs obtained for the case studies in Chapter Five. Although giving valuable insight into the testbed and RPP response, the graphs alone are not considered detailed enough to evaluate the testbed and RPP response thoroughly. For this reason, Chapter Six considers the logged data of the Chapter Five graphs, allowing the outcome of each case study and recorded events to be assessed.

**6.5 Voltage case studies**

The primary objective of case studies 1 to 3, was to isolate and assess the accuracy and efficiency of the grid-code voltage-validation subsystem, thus corroborating its design. This was achieved by reproducing the three potential operating conditions which might occur at the POC, namely the normal, fault ride-through, and trip region of operation. Governing the boundaries of these regions is the graph in Figure 6.3, selected based on the simulated RPP class, and POC voltage. The respective continuous, fault ride-through, and trip regions of operation can be defined for the simulated RPP as follows:

- Normal pu POC voltage range =      Figure 6.3, Area A = 0.85 – 1.1 pu.
- POC voltage ride through =      As defined by Figure 6.3, Areas B and D.
- RPP trip =      As defined by Figure 6.3, Area C.

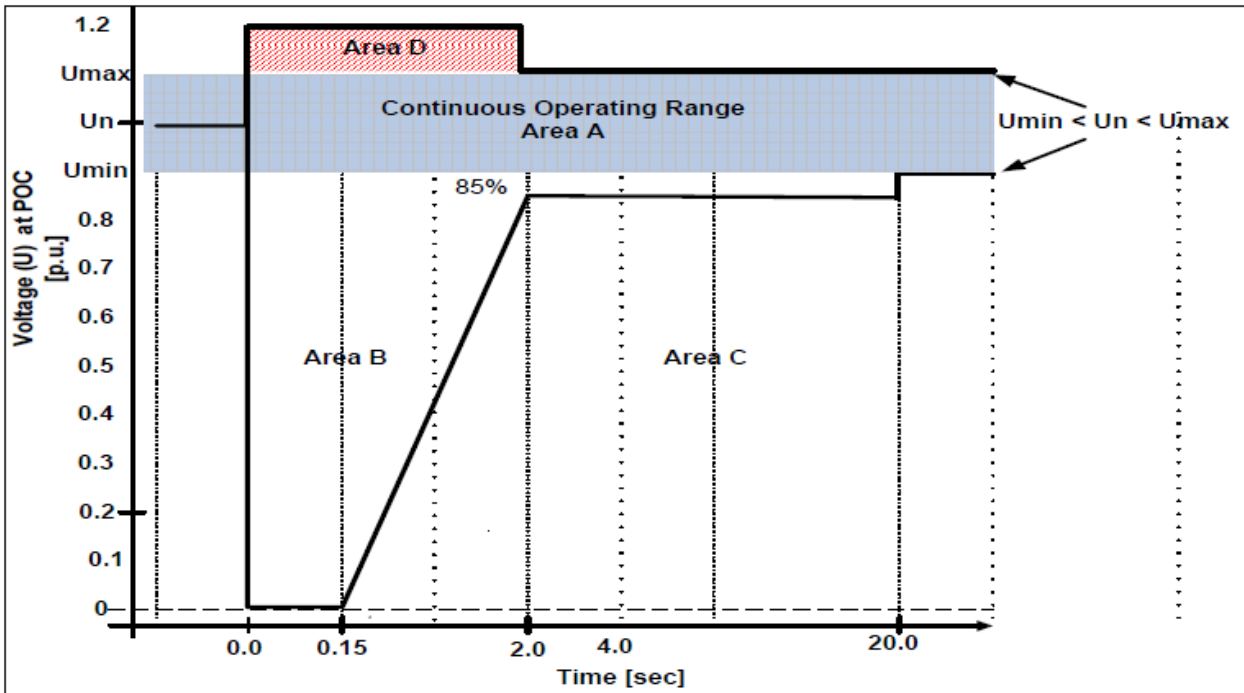


Figure 0.3: Voltage ride-through requirements set for test RPP as per SA grid codes

Case study 1 was aimed at recreating POC voltage variations within the continuous operating range of Figure 6.3 which, for the test RPP, were selected as ' $V_{nu}$ '=1.1 pu to ' $V_{nl}$ '=0.85 pu. A summary of the logged Case study 1 data can be considered in Table 6.2, representing key data points for the Case study 1 graphs discussed in Chapter Five.

Table 0.2: Case study 1: simulation data summary

	POC Voltage (pu):	Time (s):
Max V_POC:	1,173577322	5,11
Min V_POC:	0,823907701	10,121
Vspike avg:	1,094381711	5 > t < 10
Vdrop avg:	0,904444408	15 > t < 20

Given the summarised data of Table 6.2, it is first noted considering the recorded maximum (Max Vpoc) and minimum (Min Vpoc) POC voltage, that the ' $V_{POC}$ ' did exceed normal operating voltage boundaries, which should mean entering a fault ride-through condition indicated by Areas C and D of Figure 6.3. However, having previously noted in Case study 1 of Chapter Five, that a voltage surge occurred at initiation and termination of the events, these values cannot solely be considered as a representation of the recreated POC voltage conditions. Instead, these values

should be viewed as logged part of a voltage surge, which becomes evident when considering their respective times, having been recorded within milliseconds following the initiation of the voltage events at 5 and 10 seconds respectively. Since the recreated disturbances were constant, the average POC voltage can be considered instead which, when keeping in mind the POC voltage graphs discussed in Chapter Five, shows that for both the voltage spike and drop events, the POC voltage, for the most part, operated within the normal operating range. For the conditions simulated in Case study 1, the summarised logged data of Table 6.2 then confirm the appropriate response of the testbed to continue operating normally throughout because conditions, apart from an initial spike, remained within continuous operating boundaries.

Case study 2 was aimed at recreating POC voltage variations entering and exiting the HVRT/LVRT regions of operation given by Areas B and D of Figure 6.3, without requiring a trip. The purpose was to illustrate the ability of the developed voltage-validation subsystem not only to identify a voltage event but also to track POC conditions continually, which would allow it to reset for disturbances, recovering in time. A summary of the logged Case study 2 data follows in Table 6.3, representing key data points for the Case study 2 graphs discussed in Chapter Five.

**Table 0.3: Case study 2, simulation data summary**

	<b>POC Voltage (pu):</b>	<b>Time (s):</b>
<b>Max V_POC:</b>	1,145885596	5,062
<b>Min V_POC:</b>	0,157805827	10,144

Given the summarised data of Table 6.3, it is seen that ‘V\_POC’ violates normal ‘Vnu’=1.1 pu and ‘Vnl’=0.85 pu boundaries, therefore entering a fault ride-through state. This confirms the initial observation of adjusting HVRT/LVRT boundaries in Chapter Five, which would indicate the presence of a disturbance. A trip was, however, not generated for the conditions of Case study 2, since the disturbances cleared within the respectively allowed ride-through times. This proves the ability of the voltage-validation subsystem to track POC voltage conditions continually, allowing it to reset when conditions re-enter ‘Vnu’/‘Vnl’ boundaries. The logged Table 6.3 data, therefore, supports initial observations that the testbed responded in line with what is required by grid codes, allowing the RPP to support POC conditions while within the HVRT/LVRT regions, and then resetting when conditions recover to within normal limits.

Case study 3 was aimed at recreating POC voltage conditions violating HVRT/LVRT boundaries, entering Area C of Figure 6.3, therefore necessitating a trip. The purpose was to illustrate the ability of the voltage-validation subsystem to recognise and disconnect simulated RPPs when HVRT/LVRT limits are breached. A summary of the logged high-voltage disturbance data for Case

study 3 is given in Table 6.4, followed by the logged low-voltage disturbance data in Table 6.5, both of which represent key data points for the graphs discussed in Chapter Five.

**Table 0.4: Case study 3, high-voltage event simulation data summary**

	<b>Time (seconds):</b>	<b>V_POC (pu):</b>	<b>HVRT limit (pu):</b>	<b>Trip:</b>
	5,125	1,099626805	1.2	0
	5,126	1,101810613	1.2	0
	5,127	1,103811965	1.2	0
	7,146	1,197074395	1.2	0
	7,147	1,197074395	1.1	1
	7,148	1,703137486	1.1	1
<b>Trip Time:</b>	2,021			

Given the high-voltage event data summarised in Table 6.4, the first noteworthy event can be considered to be when the 'Vnu' boundary of 1.1 pu is breached at t=5,126 seconds, highlighted green. This is followed by the yellow highlighted event at t=7,147 seconds, representing the moment HVRT limits are breached, causing a trip to be generated. The reason is given by Area D of Figure 5.22, showing that if 'V\_POC' violates 'Vu'=1.1 pu, and remains within the region marked Area D, it is expected that the RPP would trip after 2 seconds, since HVRT boundaries then adjust from 1.2 pu to 1.1 pu. Using the logged data of Table 6.4, the measured RPP trip response was calculated by subtracting the green highlighted time at which HVRT conditions are entered, from the trip time highlighted yellow. This equates to a testbed trip time of 2.021 seconds, compared to the expected time of 2 seconds given by Area D of Figure 5.22, for which the slight variation can be attributed to rounding off numbers, or slight delays which may have occurred during the simulation. The data of Table 6.4, therefore, confirm the appropriate behaviour and response of the testbed during the high-voltage event of Case study 3, as the RPP is required to first ride through the disturbance, after which it is tripped following an HVRT violation.

**Table 0.5: Case study 3, low-voltage event simulation data summary**

	<b>Time (seconds):</b>	<b>V_POC (pu):</b>	<b>LVRT limit (pu):</b>	<b>Trip:</b>
	5,012	0,852205773	0	0
	5,013	0,844411273	0	0
	5,014	0,838311031	0	0
	5,332	0,147405164	0,078108108	0
	5,333	0,074780801	0,078567568	1
	5,334	0,284465055	0,079027027	0
	6,122	0,441263289	0,441081081	0
	6,123	0,441263289	0,441540541	1
	6,124	0,441263289	0,442000000	1
<b>Trip Time:</b>	0,32			

Given the low-voltage event data summarised in Table 6.5, the first noteworthy event is when the 'Vnl' boundary of 0.85 pu is breached at t=5,013 seconds, highlighted green. This is followed by the red highlighted event at t=5.333 seconds, when a single voltage-dip data point violates LVRT limits, causing a trip to be generated. Even though the POC voltage at this stage immediately re-enters the LVRT region, it has caused the RPP to disconnect, which is the initial swift-trip signal noted in the Chapter Five graph. The second trip generated at t=6.123 seconds, highlighted yellow, represents when POC voltage conditions re-enter the trip region, although having had no effect on the already-disconnected RPP, and representing the second lengthy trip signal noted in the Chapter Five graphs. Using the logged data of Table 6.5, the measured RPP trip response was calculated to be 0.32 seconds by subtracting the green highlighted time at which LVRT conditions are entered, from the initial trip time highlighted red. To confirm if this is correct, the expected trip time can be calculated using the measured 'V\_POC' at the time that the trip occurs, alongside the Figure 6.3 graph. This was done as follows:

First, the Area B recovery slope ( $S_B$ ) of Figure 6.3 can be calculated using known slope coordinates, (0.15:0) and (2:0.85), and formula (6.1).

$$S_B = \frac{Y_2 - Y_1}{X_2 - X_1} \quad (6.1)$$

$$\begin{aligned} S_B &= \frac{0.85 - 0}{2 - 0.15} \\ &= \frac{0.85}{1.85} \\ &= 0.4594594595 \end{aligned}$$

With  $S_B$  known, the trip time of the measured voltage can be calculated, represented as  $X_2$  in formula (6.1), while 'V\_POC' from Table 6.5 can be used as 0.074780801 Vpu for  $Y_2$ . Then, using (0.15:0) to represent ( $X_1:Y_1$ ), the expected trip time ( $X_2$ ), can be calculated using (6.1).

$$S_B = \frac{Y_2 - Y_1}{X_2 - X_1}$$

$$0.4594594595 = \frac{0.074780801 - 0}{X_2 - 0.15}$$

$$X_2 - 0.15 = \frac{0.074780801}{0.4594594595}$$

$$X_2 = 0.162758214 + 0.15$$

$$X_2 = 0.31275821 \text{ seconds}$$

$$X_2 = 0.31 \text{ seconds}$$

Comparing the calculated trip time of 0.31 seconds, to the real-time simulation trip time of 0.32 seconds, it can be said that they are essentially the same, since the 0.01-second difference can be attributed to rounding off numbers, or to slight delays which may have occurred during the simulation. The logged data summarised in Table 6.5 consequently corroborate initial Chapter Five observations, confirming the appropriate testbed behaviour, given the conditions simulated for Case study 3.

**6.5.1 Frequency case studies**

Like the voltage focussed case studies, the primary objective of Case Studies 4 to 6 was to corroborate the design of the frequency-validation subsystem by isolating and assessing its accuracy and efficiency. This was achieved by reproducing normal, fault ride-through, and trip conditions at the POC, monitoring both the testbed- and RPP responses. Grid-code parameters governing frequency requirements remain the same for all classes of RPPs in South Africa and are given by the frequency ride-through requirements graph of Figure 6.4, for which the respective operating regions are further defined.

Normal POC frequency range = Figure 6.4, Area A, 49 Hz to 51 Hz.

POC frequency ride-through = Within the Area B boundaries given by Figure 6.4.

RPP trip = Area C, given by Figure 6.4.

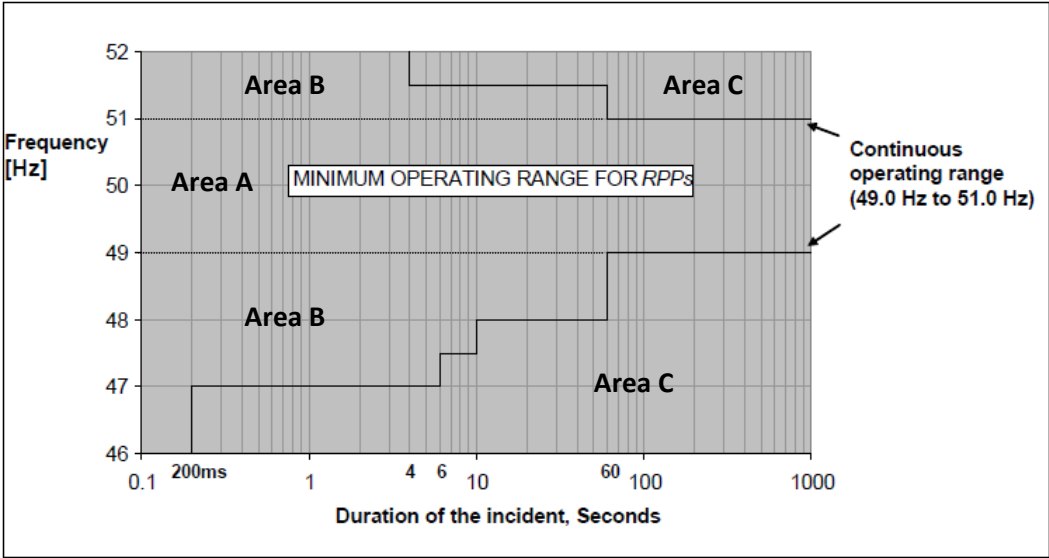


**Figure 0.4: Frequency ride-through requirements set for all RPPs during a disturbance**

Case study 4 was aimed at recreating POC frequency variations within the continuous operating range of Figure 6.4 which, for RPPs in South Africa, are governed by 'Fnu'=51 Hz to 'FnI'=49 Hz.



A summary of the logged simulation data during Case study 4 can be considered in Table 6.6, representing key data points for the Case study 4 graphs discussed in Chapter Five.

**Table 0.6: Case study 4: simulation data summary**

	<b>POC Frequency (Hz):</b>	<b>Time (s):</b>
<b>Max F_POC:</b>	50,99000002	52,483
<b>Min F_POC:</b>	49,01000002	90,878

Given the summarised data of Table 6.6, it is noted considering the recorded maximum (Max **F\_POC**) and minimum (Min **F\_POC**) POC frequency, that conditions for Case study 4 remained within '**Fnu**'/'**Fnl**' limits. This confirms the appropriate lack of fault ride-through and trip noted in Chapter Five, since no response would be expected while within '**Fnu**'/'**Fnl**' boundaries. The RPP thus correctly continued operation unaffected by the frequency variations introduced, in line with those required by grid codes.

Case study 5 was aimed at recreating POC frequency variations within the fault ride-through region given by Area B of Figure 6.4, which would recover in time not to necessitate a trip. The purpose was to illustrate the ability of the developed frequency-validation subsystem not only to identify frequency events but also to track POC conditions continually, allowing it to reset for short-lived disturbance. A summary of the logged Case study 5 simulation data follows in Table 6.7, representing key data points for the Case study 5 graphs discussed in Chapter Five.

**Table 0.7: Case study 5: simulation data summary**

	<b>POC Frequency (Hz):</b>	<b>Time (s):</b>
<b>Max F_POC:</b>	51,72352022	4,522
<b>Min F_POC:</b>	47,00257431	30,329

Given the summarised data in Table 6.7, it is seen that '**F\_POC**' violates normal '**Fnu**'=51 Hz and '**Fnl**'=49 Hz boundaries, therefore entering a fault ride-through state. This validates the initial observation of adjusting HFRT/LFRT boundaries in Chapter Five, which would indicate the presence of a disturbance. A trip was, however, not generated for the conditions of Case study 5, as the disturbances cleared within the respectively allowed ride-through times. This proves the ability of the frequency-validation subsystem to track POC frequency conditions continually, allowing it to reset when conditions re-enter '**Fnu**'/'**Fnl**' boundaries. The logged Table 6.7 data thus supports initial observations that the testbed responded in line with what is required by grid codes, allowing the RPP to support POC conditions within the HFRT/LFRT regions while being able to recognise and reset when conditions recover to within normal limits.

Case study 6 was aimed at recreating POC frequency conditions violating HFRT/LFRT boundaries, entering Area C of Figure 6.4, necessitating a trip. The purpose was to illustrate the ability of the frequency-validation subsystem to recognise and disconnect simulated RPPs when HFRT/LFRT limits are breached. A summary of the logged high-frequency disturbance data for Case study 6 is given in Table 6.8, followed by the logged low-frequency disturbance data in Table 6.9, both of which represent key data points for the graphs discussed in Chapter Five.

**Table 0.8: Case study 6, high-frequency event simulation data summary**

Time (Seconds):	F_POC (Hz):	HFRT Limit (Hz):	Trip:
4,081	50,99206356	52	0
4,082	51,00081133	52	0
4,083	51,00955909	52	0
4,319	51,99994748	52	0
4,320	52,00089110	52	1
4,321	51,90856898	52	0
4,389	51,99993030	52	0
4.390	52,00085884	52	1
4.391	52,00177765	52	1
<b>Trip Time:</b>	0,238		

Given the high-voltage event data summarised in Table 6.8, the first noteworthy event can be considered to be when the ‘Fnu’ boundary of 51 Hz is breached at t=4,082 seconds, highlighted green. This is followed by the red highlighted event at t=4,320 seconds, representing the moment a single high-frequency data point breaches HFRT limits, causing the RPP to trip. At this stage, the POC frequency re-enters the LFRT region, which was why an initial swift-trip signal tripping the RPP was noted in Chapter Five. The second lengthy trip observed in Chapter Five is generated at t=4,390 seconds, highlighted yellow, which is when POC frequency conditions re-enter the trip region, although not affecting the already-disconnected RPP. Compared to the voltage violation trips of Case study 3 following insufficient recovery times, it is noted from Table 6.8 data that the Case study 6 frequency trip occurred because of fault intensity, breaching the instantaneous frequency trip limit of 52 Hz. The trip time of 0.238 seconds observed from Table 6.9 can therefore not be compared to an expected trip time, since it is verified by the Table 6.8 data itself, showing at t=4,32 seconds that, when the instantaneous trip limit of 52 Hz is violated, a trip is immediately generated. The logged data of Table 6.8, therefore, confirm the appropriate behaviour and response of the testbed for the high-frequency event of Case study 6, as the RPP first rides through the disturbance, and trips when the instantaneous trip limit of 52 Hz is breached.

**Table 0.9: Case study 6, low-frequency event simulation data summary**

	<b>Time (Seconds):</b>	<b>F_POC (Hz):</b>	<b>LFRT Limit (Hz):</b>	<b>Trip:</b>
	4,095	49,00042077	46	0
	4,096	48,99496019	46	0
	4,097	48,98949960	46	0
	4,330	47,00344181	47	0
	4,331	46,99429920	47	1
	4,332	46,98533426	47	1
<b>Trip Time:</b>	0,235			

Given the low-voltage event data summarised in Table 6.9, the first noteworthy event can be considered to be when the 'Vnl' boundary of 49 Hz is breached at t=4,096 seconds, highlighted green. This is followed by the yellow highlighted event at t=4,331 seconds, representing the moment LFRT limits are breached, causing a trip to be generated. Trip validation comes in considering the frequency ride-through Area B of Figure 6.4, showing that, after 200 milliseconds of entering the fault ride-through region, the LFRT boundary adjusts from 46 Hz to 47 Hz, which is also observed in Table 6.9. Considering the fault duration of 235 milliseconds given in Table 6.9, it is seen that the LFRT limit at this point has already adjusted to 47 Hz, which is then breached at t=4.331 seconds, initiating the trip. Table 6.9 data, therefore, assist in confirming the appropriate behaviour and response of the testbed for the low-frequency event of Case study 6, as the RPP first rides through the disturbance, after which a trip is generated following the LFRT violation logged.

### **6.5.2 Short-circuit case study**

The primary objective of Case study 7 was to introduce grid-code specified short circuits, while measuring the RPP response in terms of current, evaluating the RPP POC grid support abilities. This was achieved by reproducing a 20%, 30%, 50%, and 80% POC voltage 'V\_POC' drop, implementing the developed testbed in its entirety. Figures 6.5 to 6.8 follow, representing the summarised logged result data given by Tables 5.1 to 5.4 of Chapter Five for the respective short-circuit simulations of Case study 7.

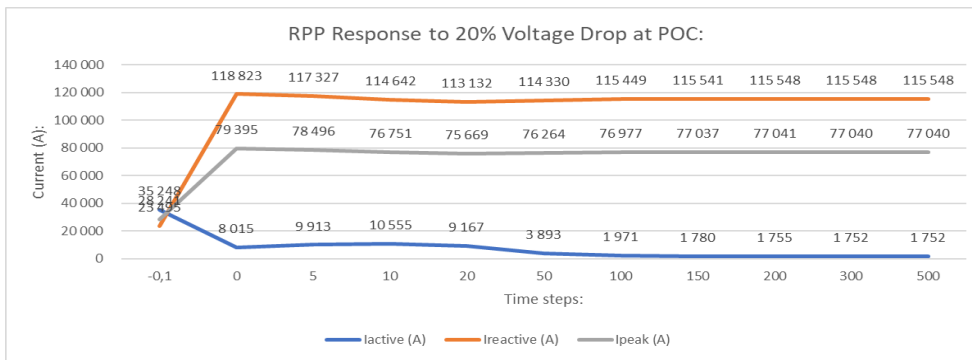


**Figure 0.5: Case study 7 RPP response to 20% POC voltage drop**

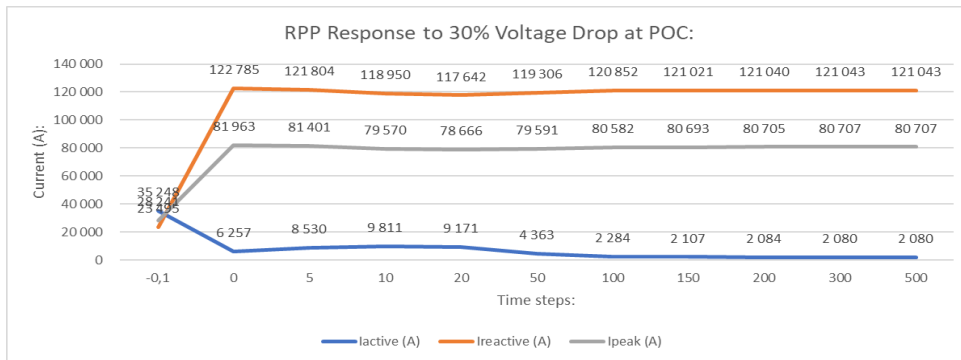


**Figure 0.6: Case study 7 RPP response to 30% POC voltage drop**

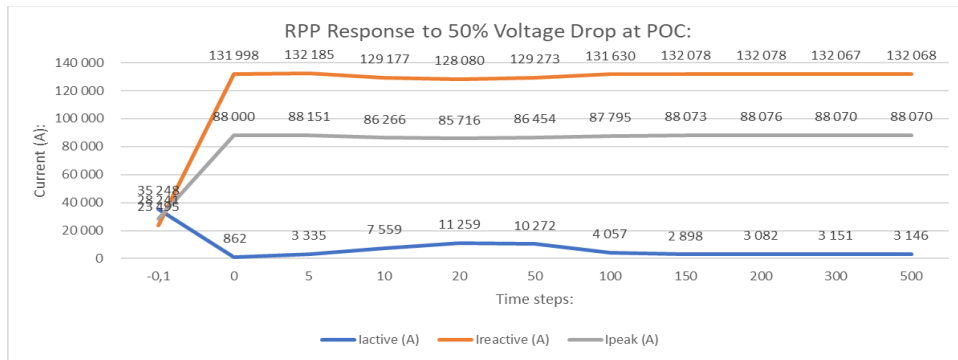


**Figure 0.7: Case study 7 RPP response to 50% voltage drop**

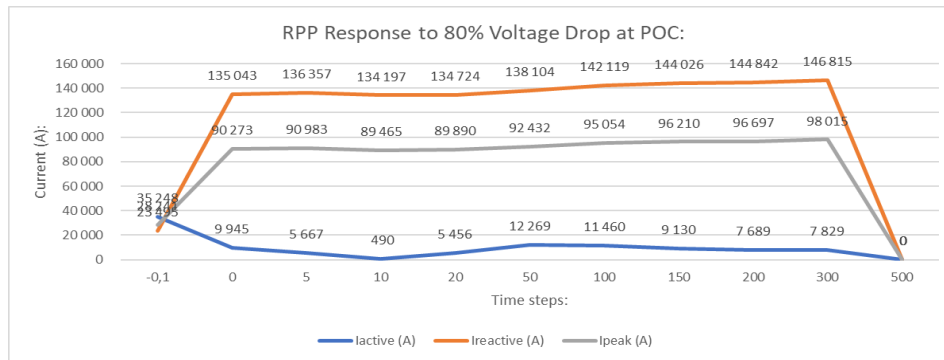


**Figure 0.8: Case study 7 RPP response to 80% POC voltage drop**

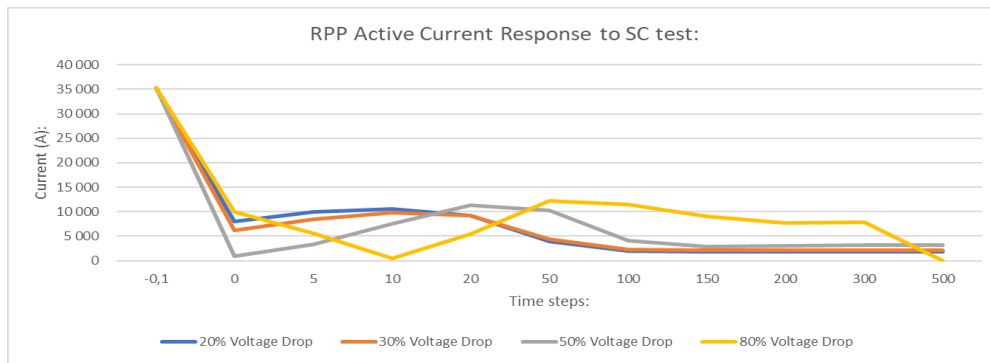
Given the summarised data represented in Figures 6.5 to 6.8, it becomes apparent that, for the most part, the RPP response to the different voltage drops is similar, curtailing the active current produced in favour of increasing the reactive significantly; hence, peak-current flow, in support of POC voltage. Additionally, compared to the 20%, 30%, and 50% '**V\_POC**' drops, a trip occurs near the end of the 80% '**V\_POC**' drop, represented by Figure 6.8. To identify the cause of this trip, Table 6.10 can be considered, representing the summarised logged data for the 80% '**V\_POC**' short-circuit simulation.

**Table 0.10: Case study 4, 80% voltage drop at POC data summary**

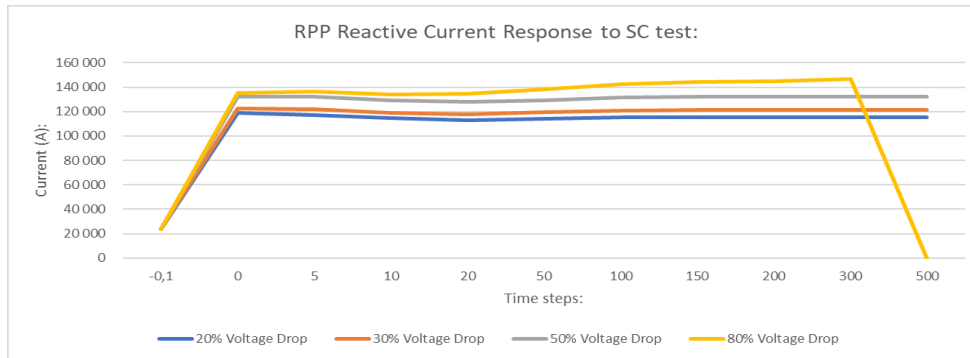
Time (seconds):	V_POC (pu):	V Trip:	F_POC (Hz):	F Trip:	Active current (A):	Reactive current (A):	Peak current (A):
1,333	0,2516	0	46,1026	0	108452,8112	72639,94369	87021,25841
1,334	0,2638	0	45,9829	1	107867,5826	70914,13844	86060,00595
1,335	0,1649	0	43,5628	1	0	0	0
1,454	0,1649	0	48,0417	0	0	0	0
1,455	0,1649	1	48,0612	0	0	0	0
1,456	0,1649	1	48,0804	0	0	0	0

Table 6.10 considered, it is observed in the highlighted red section, that the trip generated for the 80% POC voltage '**V\_POC**' short circuit, resulted from the POC frequency '**F\_POC**' venturing below the instantaneous frequency trip boundary of 46 Hz. Since the disturbance was introduced at t=1 second, it can be calculated using the Table 6.10 data that the trip occurred 334 milliseconds following the introduction of the 80% POC voltage '**V\_POC**' short circuit, causing the RPP to trip and remain disconnected for the remainder of the simulation. At this point, the RPP is no longer providing POC support to the ongoing short circuit, causing the POC voltage '**V\_POC**' to deteriorate and to violate voltage ride-through boundaries at t=1,455 seconds, highlighted green. This results in an additional trip, although not affecting the already-disconnected RPP.

To better compare RPP support, given the various degrees of short circuits, Figures 6.9 to 6.11 can be considered. The graphs respectively compare active-, reactive-, and peak-current support provided given that the various short circuits introduced are made to include a single t=-1 time-step before initiation of the faults, representing the baseline pre-fault currents.



**Figure 0.9: Case study 7 active current generated during respective POC voltage drops**



**Figure 0.10: Case study 7 reactive power generated during respective POC voltage drops**

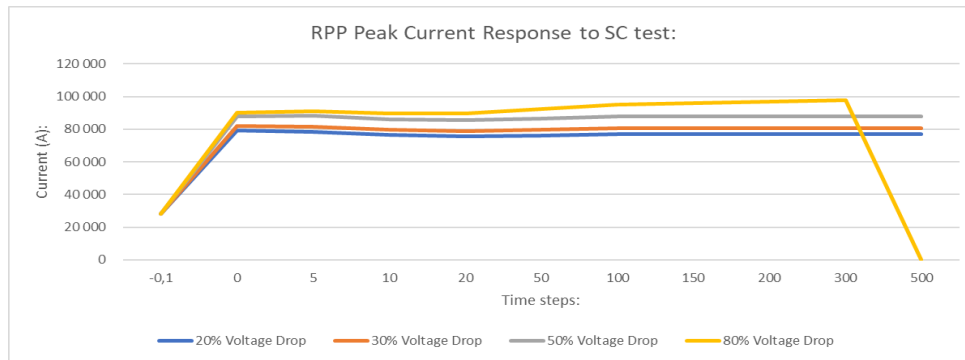


**Figure 0.11: Case study 7 peak-current generated during respective POC voltage drops**

Given the comparative result graphs of Figures 6.9 to 6.11, the extent to which the RPP reacts in support of POC conditions now becomes apparent, concerning the pre-fault data point at  $t=-1$  second. For active current generated in Figure 6.9, it is observed, as in Chapter Five, that the RPP-curtailed active current, in favour of the reactive current support in Figure 6.10, with increasing intensity as the severity of the short circuits increased. This occurs as reactive current and power assists in raising voltage, recognised by the RPP to be low at the POC. Similarly, the total current flow given in Figure 6.11 also sees a significant increase within the RPP-support capabilities, concerning the intensity of the short circuits. The nonlinear RPP-support response to

short-circuit intensity is attributed to the support limitations of the simulated RPP, supported by the fact that a trip is generated during the 80% short-circuit test, since the RPP has by this time reached the limit of its support capabilities. For Case study 7, it can be said that the RPP responded in line with what is required by grid codes, providing support to the POC and grid within its support capabilities, disconnecting once its support limitations cause grid-code POC requirements to be breached. Such information can prove useful additionally in assessing the appropriateness of a specific RPP before implementation, as part of essential grid integration and RPP behavioural studies required.

### 6.5.3 Real-world data case studies

The objective of Case studies 8 and 9 was to illustrate the testbed's operation in its entirety, monitoring RPP behaviour and response to real-world event data obtained from previously recorded events. A summary of the logged event data for the respective case studies follows in Tables 6.11 and 6.12, which are then analysed to allow assessment of the testbed, and simulated RPP behaviour.

**Table 0.11: Case study 8: noteworthy events summary**

Event:	Time (s):	V_POC (pu):	V Trip	F_POC (Hz):	F trip:	Real power produced (MW):	Reactive power produced (Mvar):
1	27,912	0,85009494	0	49,39808	0	-7,13568	633,80183
	27,913	0,84984449	0	49,39759	0	-7,15944	633,66545
	27,914	0,84960783	0	49,39707	0	-7,18908	633,51748
2	28,071	0,8366075	0	49,32597	0	-7,10134	625,71502
	28,072	0,77745042	0	48,93926	0	-8,32816	597,41495
	28,073	0,77744653	0	48,93884	0	-8,25982	597,41930
3	29,394	0,84987718	0	48,71024	0	-9,73955	627,22028
	29,395	0,8500601	0	48,71047	0	-9,74511	627,30218
	29,396	0,85022487	0	48,71070	0	-9,74988	627,38438
4	30,172	0,85004187	0	48,75215	0	-7,96652	628,92145
	30,173	0,84997021	0	48,75182	0	-7,99200	628,86811
	30,174	0,84989155	0	48,75153	0	-8,02689	628,80699
5	32,071	0,82887131	0	48,59336	0	-9,11429	618,49526
	32,072	0,68208385	1	48,72063	0	0,00000	0,00000
	32,073	0,68210552	1	48,72065	0	0,00000	0,00000

Given the summarised Case study 8 data of Table 6.11, the first noteworthy event, highlighted blue, can be observed at t=27.913 seconds, when the POC voltage 'V\_POC' violates the 'Vnl'

boundary of 0.85 pu, entering an LVRT state. As with similar recreated conditions during the previous test case studies, the RPP then continues operation, riding through the fault while generating additional reactive power in support of the dwindling POC voltage. By t=28.072 seconds, marked event 2 and highlighted grey, it is seen that POC conditions enter an LFRT state when 'F\_POC' conditions fall below the 'Fnl' boundary limit of 49 Hz, yet the RPP remained connected and continued to support POC conditions. By t=29.395 seconds, marked Event 3 and highlighted green, it is seen that the POC voltage 'V\_POC' recovers enough to re-enter the normal region of operation, resetting the event timer of the voltage-validation subsystem. At t=30.173 seconds, marked Event 4 and highlighted yellow, it is again observed that the POC voltage 'V\_POC' descends to below 'Vnl' boundaries, re-entering the LVRT region for a second time. This time, the POC voltage is, however, unable to recover in time, and an LVRT violation is generated at t=32.072 seconds, given by Event 5 highlighted red in Table 6.11. At the time the trip is generated, it is seen from the power-production columns in Table 6.11 that the RPP still attempts to improve POC voltage conditions, given by the negative active-power reading, and production of additional reactive power leading up to the trip. Unfortunately, this is to no avail, since a trip follows, after which the RPP power generation drops to 0. It is again worth mentioning that this would be an undesirable outcome, supported by the initial observation from the simulation result graphs in Chapter Five, confirming a further swift deterioration in POC conditions that followed the loss of RPP POC support. Nevertheless, having considered each noteworthy event logged for Case study 8, it is concluded that the testbed and RPP, during each event, reacted as required by grid codes, providing support while within the ride-through regions, only disconnecting once reaching support limitations causing POC conditions to deteriorate below acceptable limits.

Table 6.12 and its analysis follow, summarising the noteworthy events logged during the final Case study 9 real-time simulation performed in Chapter Five.

**Table 0.12: Case study 9: noteworthy events summary**

Event:	Time (s):	V_POC (pu):	V Trip	F_POC (Hz):	F trip:	Real power produced (MW):	Reactive power produced (Mvar):
1	15,153	0,97469	0	49,00510	0	179,88844	652,96546
	15,154	0,97199	0	48,99531	0	173,96138	653,62548
	15,155	0,97057	0	48,98801	0	167,42766	654,16579
2	17,502	0,99048	0	47,00065	0	286,51344	503,81835
	17,503	0,99052	0	46,99974	1	0	0
	17,504	0,99055	0	46,99884	1	0	0
3	17,902	0,99162	0	46,57349	1	0	0
	17,903	0,79316	0	46,52272	1	0	0



Event:	Time (s):	V_POC (pu):	V Trip	F_POC (Hz):	F trip:	Real power produced (MW):	Reactive power produced (Mvar):
	17.904	0,79316	0	46,52283	1	0	0
4	19,193	0,79795	0	46,53536	1	0	0
	19,194	0,80369	0	47,60546	0	0	0
	19,195	0,80375	0	47,60685	0	0	0
	19,779	0,81219	0	48,35595	0	0	0
5	19,780	0,81224	1	48,35624	0	0	0
	19,781	0,81229	1	48,35653	0	0	0

Given the summarised Case study 9 data of Table 6.12, the first noteworthy event, highlighted blue, is observed at t=15,154 seconds, when POC frequency 'F\_POC' violates the 'Fnl' boundary of 49 Hz, entering an LFRT state. At this stage, both 'V\_POC' and 'F\_POC' are on the decline, causing the RPP real power generated gradually to decline in favour of an increase in reactive power which, in turn, should assist in improving POC conditions. By t=17.503 seconds, marked Event 2 and highlighted grey, it is seen that POC frequency 'F\_POC' conditions deteriorate to below the LFRT limit of 47 Hz, causing a frequency trip to be generated, and generated power to drop to 0. As confirmation of the 47 Hz LFRT limit at that time, Figure 6.4, discussed earlier, can be considered, illustrating an LFRT limit adjustment from 46 Hz to 47 Hz 200 milliseconds after initiation of a frequency event. By t=17,903 seconds, marked Event 3 and highlighted green, the POC voltage 'V\_POC' is seen to have deteriorated to below the 'Vnl' limit of 0.85 pu, causing it to enter an LVRT state. By t=19,194 seconds, marked Event 4 and highlighted yellow, it is observed that POC frequency 'F\_POC' recovers enough to re-enter the LFRT region, causing the active trip signal to fall away, although this would not affect the already-disconnected RPP. By t=19.780 seconds, marked Event 5 and highlighted red, POC voltage 'V\_POC' is seen to violate the LVRT boundary at that time, generating the final LVRT violation trip, although again not affecting the already-disconnected RPP. Considering Case study 9 simulation graphs of Chapter Five along with the logged event data of Table 6.12, it can again be noted how the initial trip causes further deterioration of POC conditions, most likely being the cause of the second voltage trip generated. All events considered, it can be said that the testbed and RPP responded in line with what is required by grid codes, confirming for a final time its effective operation, and its ability to assist with RPP grid-integration behavioural studies.

## 6.6 Simulation summary

Case studies 1 to 9 were selected aimed at testing and illustrating the operation and abilities of the developed real-time simulation testbed, and its contained subsystems. Additionally, these case studies through the simulation data provided, and the testbed's ability to evaluate and operate RPPs in line with South African grid codes, aimed to illustrate the worth of the developed testbed as grid-integration- and RPP behavioural studies tool. This involved Case studies 1 to 6, testing the response of the subsystems to normal, fault ride-through, and trip regions of operation, showing their ability to assess, track, and react to POC conditions. Case studies 7 to 9 then focused on illustrating RPP response, through monitoring of key voltage, current, and power parameters. A case study summary follows in Table 6.13, summarising the purpose of each, and subsequent real-time simulation outcome.

**Table 0.13: Voltage and Frequency-validation subsystem case study test results**

<b>Case study:</b>	<b>Purpose:</b>	<b>Result/Outcome:</b>
<b>Voltage Case Studies</b>	<b>1</b> To show the testbed's ability to operate unaffected by voltage variations within the normal ' <b>Vnu</b> '/' <b>Vnl</b> ' operating range.	As anticipated, no testbed or RPP response was observed while operating within the normal range of voltage variations.
	<b>2</b> To show the testbed's ability to track POC voltage conditions continually, allowing it to recognise, ride through HVRT/LVRT conditions, and reset once a fault clears.	The testbed efficiently recognised the presence of both the HVRT and LVRT event, riding through the disturbance, providing POC support. The testbed also recognised the fault being cleared, automatically resetting the subsystem to avoid a trip.
	<b>3</b> To show the testbed's ability to recognise fault conditions violating HVRT/LVRT boundaries, requiring the RPP to be disconnected.	The testbed efficiently recognised and rode through both HVRT and LVRT event. A trip was then also generated when HVRT/LVRT limits were violated, at which time the RPP was disconnected successfully.
<b>Frequency Case Studies</b>	<b>4</b> To show the testbed's ability to operate unaffected by frequency variations within the normal ' <b>Fnu</b> '/' <b>Fnl</b> ' operating range.	As anticipated, no testbed or RPP response was observed while operating within the normal range of frequency variations.
	<b>5</b> To show the testbed's ability to track POC frequency conditions continually, allowing it to recognise, ride through HFRT/LFRT conditions, and reset once a fault clears.	The testbed efficiently recognised the presence of both the HFRT and LFRT event, riding through the disturbance, providing POC support. The testbed also recognised the fault being cleared,

Case study:		Purpose:	Result/Outcome:
			automatically resetting the subsystem to avoid a trip.
	6	To show the testbed's ability to recognise fault conditions violating HFRT/LFRT boundaries, requiring the RPP to be disconnected.	The testbed efficiently recognised and rode through both HFRT and LFRT event. A trip was then also generated when HFRT/LFRT limits were violated, at which time the RPP was disconnected successfully.
Short-circuit Case Studies	7	To show and study the RPP-support abilities, when presented with a 20%, 30%, 50%, and 80% voltage drop at the POC.	When presented with POC voltage drops or short circuits, the RPP responded by curtailing generated active current, in favour of an increased reactive current. This is an appropriate POC support response, since reactive current/power assists in raising POC voltage. The support response was furthermore noted to escalate with short-circuit intensity, though not linearly because of the RPP-support limitations.
Grid Data Case Studies	8	To show the testbed, and RPP response to real-world grid recorded events, implementing the testbed in its entirety.	Simulation results confirm all previous response observations, since the testbed efficiently recognised POC conditions entering both LVRT, and LFRT boundaries. In response, the RPP generated additional power, particularly reactive power, recognising the need to raise and restore POC conditions. Conditions ultimately deteriorate to violate LVRT boundaries, at which point a trip is generated and the RPP is disconnected.
	9	To show the testbed, and RPP response to real-world grid recorded events, implementing the testbed in its entirety.	The testbed again managed to efficiently recognise POC conditions entering LFRT, and then LVRT conditions. The RPP responds by providing additional support within its capabilities, favouring reactive power generation to improve and restore POC conditions. Frequency conditions, however, deteriorate to the point where LFRT boundaries are violated, at which point a trip is generated, and the RPP is disconnected.

The summary of Table 6.13 along with the simulation results of Chapter Five, and the analyses thereof in Chapter Six, consequently shows the developed testbed to be capable of tracking POC voltage and frequency conditions accurately, allowing it to control simulated RPPs in line with what is required by South African RPP-specific grid codes. This, in turn, allows the demands imposed on RPPs by grid-code voltage- and frequency requirements to be studied, forming part of the RPP behavioural grid-integration studies required to support the successful integration of South Africa's long-term renewable-integration goals. The developed platform hopes to assist in streamlining the integration process, by helping to identify potential obstacles early on, allowing the necessary adjustments to be made accordingly. Furthermore, the testbed hopes to assist with RPP selection, since it allows for RPP behaviour to be studied at a specific point feeding previously recorded data representing potential conditions anticipated for a proposed RPP.

### **6.7 Summary**

This chapter, through goals set by initiatives such as the updated 2030 IRP, again showed South Africa to be planning an ambitious renewable energy integrated future, bringing with it new unfamiliar challenges. In response, the study developed a real-time testbed to aid in studying RPP grid-integration behaviour which, in Chapter Six, showed the circuit design to conform to grid-code test-circuit requirements. The main objective of the chapter was, however, to investigate the effectiveness and accuracy of the testbed and simulated RPP behaviour, considering the logged real-time simulation data recorded during the case studies in Chapter Five. Results showed the testbed to be capable of distinguishing accurately between continuous, fault ride-through, and trip regions of operation, operating the simulated RPP accordingly. This includes the testbed's ability to monitor and track POC parameters actively, allowing it throughout a simulation to hold a trip when operating outside ride-through boundaries, and to reset when conditions re-enter the normal range of operation. Results furthermore showed the simulated RPP to support POC conditions throughout the simulations performed, being able to recognise and respond to POC conditions. Chapter Six then summarises the purpose and outcome of each case study performed, to show jointly how the developed testbed and its accompanying subcircuits were tested in their entirety, and in line with what is required by grid-code documentation. Based on the findings made examining the logged testbed and RPP response data, given the case studies performed, it can be concluded through the Chapter Six findings that the South African real-time testbed was indeed developed successfully.

## **CHAPTER SEVEN**

### **CONCLUSION**

#### **1.1 Introduction**

This chapter concludes the study by summarising the research findings and the undertaking of developing a tailored South African real-time renewable energy integration testbed, in response to the original problem statement and aim. The contribution, intended application, and value of the developed testbed is reviewed, followed by the limitations of the study, and recommendations for future work. Finally, the chapter and study are concluded through the closing summary.

#### **7.2 Study summary**

The major aim of the study was to develop a real-time renewable generation testbed that is tailored to the unique grid-code requirements for RPPs in South Africa, to assist with essential RPP grid-integration behavioural studies in a simplified and efficient manner. The need for such a tool stemmed from South Africa's aggressive renewable integration goals, given by initiatives such as the 2030 IRP, to include renewable generation additions to a capacity almost equal to that of coal by 2030. This brings about new challenges associated with the large-scale integration of renewable generation, in that the overwhelmingly passive generation synonymous with inertia-providing spinning masses, definitely will be displaced by renewables that have an active multi-directional electronic power nature. Potentially, this will increase the instability of a network, which is foreseen to have an undesirable effect considering South Africa's already ongoing struggle to supply the country's energy needs reliably. South Africa was, however, identified as being unique, in that its renewable integration plans are less directed at replacing existing fossil fuel generation, and more towards adding much-needed capacity to the grid, making the success of renewable energy integration plans crucial. As mitigation to the foreseen challenges associated with significant renewable integration, South Africa developed and implemented RPP-specific grid-code requirements. These are largely aimed at having renewable generation react much like conventional generation during disturbances, requiring RPPs to provide grid support, unlike early specifications which would have allowed RPPs simply to disconnect.

This study set out to develop a real-time simulation testbed capable of governing RPP POC voltage and frequency conditions accurately and efficiently in line with grid-code requirements, allowing effective RPP grid-integration behavioural studies to be performed for RPPs connected to the South African grid. Development started with the design of a MATLAB live script, allowing the user to customise multiple RPP grid-code requirement parameters using only two key RPP inputs, improving the testbed's versatility to accommodate any size and type of RPP in a user-friendly manner. Acting as a guide, South African RPP grid-code requirements were used

alongside MATLAB's Simulink environment to develop the testbed circuit, making sure to adhere strictly to both applicable circuit- and RPP requirements. The circuit was furthermore designed to incorporate a data-import source block on its grid side, compared to an elaborate static grid-representing circuit, giving it the ability to replay measured grid events accurately during RPP behavioural studies, while increasing testbed versatility, widening its application. Voltage- and frequency grid-code requirements were identified as essential POC monitoring parameters, leading to the development of the voltage- and frequency validation subsystems. These are responsible for active RPP POC grid-code validation, operating the RPP in line with voltage- and frequency grid-code requirements, thus allowing the strain imposed on RPPs by these requirements to be studied. To achieve this, measurements in addition to voltage and frequency also extended to those of power and current, giving insight into the RPP response, and ability to adhere to mandatory RPP support requirements during simulated disturbances.

A developed testbed testing strategy followed, aimed at isolating and testing the respective circuit sections and subsystems while illustrating the testbed's abilities and worth as a real-time RPP grid-integration behavioural studies tool. This required the consideration of both testbed- and grid-code testing requirements, after which case studies were chosen to include HVRT, LVRT, HFRT, LFRT, short-circuit, and real-world data simulations, of varying intensities. This occurred in the order of nine case studies assessing the behaviour of a particular section or condition, following the integration of the MATLAB model with OPAL-RT, allowing real-time excitation using the OPAL-RT OP4510 real-time simulator.

Real-time simulation case study results confirmed the grid-representing import data source block to be an effective tool for recreating specific POC testing conditions, in addition to relaying previously recorded grid data effectively for RPP behavioural studies. Case studies testing the ability of the voltage- and frequency validation subsystem to track POC conditions accurately, confirmed them to be capable of effective POC assessment, leading to an appropriate response in line with grid-code requirements. This involved the subsystems keeping simulated RPPs connected while within the continuous operating region, allowing the RPP to ride through disturbances within the ride-through region, and to disconnect when outside the grid-code ride-through requirement boundaries. Controlling the simulated RPP according to grid-code voltage- and frequency requirements furthermore allowed assessment of the RPP support response, for which simulation results showed the test RPP to react effectively and to support the grid within its design limitations for all case studies performed. The developed testbed therefore succeeded in achieving its intended purpose, through the case studies having been shown to be capable of producing accurate and meaningful results when implemented as RPP grid-integration behavioural studies tool.

### **7.3 Study contributions**

The study developed a South African grid-code-guided RPP control testbed for the purpose of performing tailored renewable grid-integration studies in South Africa. This is significant since, from what was known, no such tool yet existed, despite the importance of performing comprehensive tailored renewable energy integration studies to ensure the success of renewable energy integration projects. To allow tailored simulations to be performed, the testbed's design incorporates a means of importing grid-measured data, replacing the more commonly used static simulation circuit design, thus allowing simulated conditions to be tailored and recreated easily. Furthermore, the testbed took a novel approach to the control strategy of simulated RPPs, implementing South African RPP-grid-code voltage- and frequency requirements according to which simulated RPPs are operated. Finally, the model is integrated with OPAL-RT, allowing real-time simulations to be performed, improving on the accuracy which can be achieved by standard simulation models. These testbed design attributes allow accurate real-time simulation results to be produced when implemented to study grid-code-imposed RPP strains, and the effect of disconnecting RPPs on the grid. Such studies then form part of the research needed to ensure that planned renewable generation additions have the desired effect, strengthening South Africa's grid and improving the reliability of supply.

### **7.4 Limitations of the study**

- The availability of up-to-date renewable energy grid-integration statistics in South Africa, which, for this study, was limited to 2019 figures.
- The lack of measured South African grid data to import and replay during testbed testing.
- The available software versions used which, for this study, were limited to MATLAB R2015b, and RT-LAB v11.3.1.34.
- The active grid-code-guided control abilities included in the testbed's design, limited to voltage and frequency for this study.

### **7.5 Recommendations for future work**

- Studying and forecasting the effects of decreasing inertia on South Africa's grid characteristics, and fault response, to maintain a balance where the loss of grid inertia does not compromise renewable integration goals.
- Conducting a study on the theoretical limits for renewable energy integration in South Africa, taking into consideration the South African grid, and its associated challenges.
- Expanding the developed real-time simulation testbed potentially to include active monitoring of additional grid-code parameters.

- Illustrating the abilities of the renewable testbed using local South African grid-recorded data of past events, which the study did not manage to obtain, leading to the use of another grid's recorded event data for Case studies 8 and 9.
- Comparing the results obtained from the real-time simulations to those of a MATLAB-only simulation, noting if, how, and why results differ.
- Comparing the demands put on RPPs by South African grid conditions, to those of other countries.

## **7.6 Closing summary**

In response to South Africa's ambiguous future renewable energy integration goals, this study set out to develop a real-time simulation testbed tailored to South African grid-code requirements, capable of performing RPP grid-integration behavioural studies. Using South Africa's RPP grid-code requirements as a guide, the testbed, and testbed testing procedures were developed. The POC support response observed of the RPP, alongside the validated control abilities of the voltage- and frequency-validation subsystems to operate simulated RPPs in line with their respective grid-code voltage- and frequency requirements, showed the developed testbed to be capable of accurate and efficient simulations. Effectively, this then showed the ability of the developed testbed to perform RPP grid-integration behavioural studies in line with South African grid-code requirements, thus achieving the goal of this study through the testbed's design. The research and testbed developed hope to encourage future renewable grid-integration studies, promoting the successful integration of planned renewable integration. This, in turn, should assist South Africa's currently strained electrical grid, to achieve the desired grid stability, and to supply reliability once again.



## REFERENCES

- Asmine, M., Brochu, J., Fortmann, J., Gagnon, R., Kazachkov, Y., Langlois, C.E., Larose, C., Muljadi, E., MacDowell, J., Pourbeik, P. and Seman, S.A. 2010. Model validation for wind turbine generator models. *IEEE Transactions on Power Systems*, 26(3), pp 1769–1782. doi: 10.1109/TPWRS.2010.2092794.
- Ateba, B. B. and Prinsloo, J.J. 2019. 'Strategic management for electricity supply sustainability in South Africa', *Utilities Policy*. Elsevier, 56(October 2018), pp. 92–103. doi: 10.1016/j.jup.2018.10.010.
- Australian Energy Market Operator. 2017. *Black System South Australia 28 September 2016*. Australia. Available at: [http://www.aemo.com.au/-/media/Files/Electricity/NEM/Market\\_Notices\\_and\\_Events/Power\\_System\\_Incident\\_Reports/2017/Integrated-Final-Report-SA-Black-System-28-September-2016.pdf](http://www.aemo.com.au/-/media/Files/Electricity/NEM/Market_Notices_and_Events/Power_System_Incident_Reports/2017/Integrated-Final-Report-SA-Black-System-28-September-2016.pdf).
- Ayamolowo, O. J., Manditereza, P. T. and Kusakana, K. 2022. South Africa power reforms: The path to a dominant renewable energy-sourced grid, *Energy Reports*. Elsevier, 8, pp 1208–1215. doi: 10.1016/j.egy.2021.11.100.
- Barradas, S. (2019) 'Medupi power station project, South Africa', *Engineering News*, February. Available at: <https://www.engineeringnews.co.za/print-version/medupi-power-station-project-south-africa-2019-02-08>.
- Barrows, C.P., Katz, J.R., Cochran, J.M., Maclaurin, G.J., Marollano, M.C., Gabis, M.G., Reyes, N.C., Munoz, K.J., Jesus, C.D., Asedillo, N. and Binayug, J. 2018. Greening the grid: Solar and wind grid integration study for the Luzon-Visayas system of the Philippines', *Alternatives Journal*, 27(4), pp. 1–113. doi: <https://doi.org/10.2172/1418740>.
- Bélanger, J., Venne, P. and Member, S. 2010. The what, where and why of real-time simulation, *Planet Rt*, pp 37–49. Available at: [http://www.ecadtools.com.au/documents-opal/L00161\\_0436.pdf](http://www.ecadtools.com.au/documents-opal/L00161_0436.pdf).
- Bello, M., Smit, R., Carter-Brown, C. and Davidson, I.E. 2013, July. Power planning for renewable energy grid integration-Case study of South Africa. In *2013 IEEE Power & Energy Society General Meeting* (pp. 1-5). IEEE pp. 1–5. doi: 10.1109/PESMG.2013.6672904.
- Bertrand-Vasseur, A. and Berthelot, J. M. 2017. *Renewables 2017 Analysis and Forecast to 2022 Executive Summary*, International Energy Agency (IEA). Available at: <https://www.iea.org/Textbase/npsum/renew2017MRSsum.pdf>.
- Bian, D., Kuzlu, M., Pipattanasomporn, M., Rahman, S. and Wu, Y. 2015, July. Real-time co-simulation platform using OPAL-RT and OPNET for analyzing smart grid performance. In *2015 IEEE Power & Energy Society General Meeting* (pp 1–5). doi: 10.1109/PESGM.2015.7286238
- Buraimoh, E. and Davidson, I. E. 2020. Overview of fault ride-through requirements for photovoltaic grid integration, design and grid code compliance, *9th International Conference on Renewable Energy Research and Applications, ICRERA 2020*, pp. 332–336. doi: 10.1109/ICRERA49962.2020.9242914.
- Buraimoh, E. and Davidson, I. E. 2022. Laboratory procedure for real-time simulation experiment of renewable energy systems on OPAL-RT digital simulator, in *10th IEEE International Conference on Smart Grid*, (pp 221–226).
- Campbell, R. 2018. South Africa should not be over-reliant on renewable energy for its future electricity needs, *Creamer Media's Engineering News*, December. Available at: [https://www.engineeringnews.co.za/article/south-africa-should-not-be-over-reliant-on-renewable-energy-for-its-future-electricity-needs-2018-12-06/rep\\_id:4136](https://www.engineeringnews.co.za/article/south-africa-should-not-be-over-reliant-on-renewable-energy-for-its-future-electricity-needs-2018-12-06/rep_id:4136).

Cliffe Dekker Hofmeyr. 2019. The Integrated Resource Plan 2019: A promising future roadmap for generation capacity in South Africa, *Energy Alert*. Available at: <https://www.cliffedekkerhofmeyr.com/en/news/publications/2019/Corporate/energy-alert-22-october-The-Integrated-Resource-Plan-2019-A-promising-future-roadmap-for-generation-capacity-in-South-Africa.html> (Accessed: 2 December 2019).

Cochran, J., Bird, L., Heeter, J. and Arent, D.J. 2012. *Integrating Variable Renewable Energy in Electric Power Markets : Summary for Policymakers*. United States. Available at: <https://www.nrel.gov/docs/fy12osti/53730.pdf>.

CSIR Energy Centre 2018. Statistics of utility-scale solar PV, wind and CSP in South Africa in 2017. Pretoria: Council for Scientific and Industrial Research, p. 8. Available at: <https://www.csir.co.za/sites/default/files/Documents/Statistics of RE in SA in 2017 - CSIR - FINAL.pdf>.

D'Sa, A. 2005. 'Integrated resource planning (IRP) and power sector reform in developing countries', *Energy Policy*, 33(10), pp. 1271–1285. doi: 10.1016/j.enpol.2003.12.003.

Department of Energy. 2011. *Integrated Resource Plan for Electricity 2010–2030*, 2(March), p. 78. doi: 10.1016/j.wneu.2010.05.012.

Department of Energy. 2018. *Draft Integrated Resource Plan 2018*. Pretoria. Available at: <http://www.energy.gov.za/IRP/irp-update-draft-report2018/IRP-Update-2018-Draft-for-Comments.pdf>.

Department of Energy and Department of National Treasury. 2018. *Independent Power Producers Procurement Programme (IPPPP), An Overview*. Pretoria. Available at: <https://www.google.com/url?sa=t&rct=j&q=&esrc=s&source=web&cd=11&ved=2ahUKEwiE9c7pronjAhURSxUIHRgFAQ8QFjAKegQIAxAC&url=https%3A%2F%2Fwww.ipp-projects.co.za%2FPublications%2FGetPublicationFile%3Ffileid%3D71515393-218c-e811-9489-2c59e59ac9cd%26fileName%3D20>.

Department of Mineral Resources and Energy. 2019. *Integrated Resource Plan 2019*. Department of Energy Republic of South Africa, pp. 8–98. Available at: <http://www.energy.gov.za/IRP/2019/IRP-2019.pdf>.

Department of Minerals and Energy. 1998. *White Paper on the Energy Policy of the Republic of South Africa*. Pretoria. Available at: [http://www.energy.gov.za/files/policies/whitepaper\\_energypolicy\\_1998.pdf](http://www.energy.gov.za/files/policies/whitepaper_energypolicy_1998.pdf).

Department of Minerals and Energy. 2003. *White Paper on Renewable Energy*. Pretoria. Available at: [https://unfccc.int/files/meetings/seminar/application/pdf/sem\\_sup1\\_south\\_africa.pdf](https://unfccc.int/files/meetings/seminar/application/pdf/sem_sup1_south_africa.pdf).

Department of Minerals and Energy. 2011. *National Climate Change Response White Paper*. Pretoria. Available at: [https://www.environment.gov.za/sites/default/files/legislations/national\\_climatechange\\_response\\_whitepaper.pdf](https://www.environment.gov.za/sites/default/files/legislations/national_climatechange_response_whitepaper.pdf).

El-Azab, R. and Amin, A. 2015. Optimal solar plant site selection, *Conference Proceedings - IEEE SOUTHEASTCON*. IEEE, 2015-June(June), pp. 1–6. doi: 10.1109/SECON.2015.7132992.

Eskom (2009) *Southern Africa grid map*, *Eskom Holdings Limited Annual Report*. Available at: [http://www.financialresults.co.za/eskom\\_ar2009/ar\\_2009/downloads/01\\_profile.pdf](http://www.financialresults.co.za/eskom_ar2009/ar_2009/downloads/01_profile.pdf).

Eskom. 2015a. *SERE WIND FARM*. Available at: <http://www.eskom.co.za/AboutElectricity/FactsFigures/Documents/RW0000SereWindFarmRev1>.

pdf.

Eskom. 2015b. Sere wind farm project. Western Cape: Eskom. Available at: <http://www.eskom.co.za/AboutElectricity/RenewableEnergy/Pages/SereWindFarm.aspx>.

Eskom. 2016. *Transmission development plan 2016–2025*. Pretoria. Available at: <http://www.eskom.co.za/Whatweredoing/TransmissionDevelopmentPlan/Documents/TransDevPlan2016-2025Brochure.pdf>.

Eskom. 2017. *Ingula pumped storage scheme, peaking power stations*. Available at: <http://www.eskom.co.za/Whatweredoing/ElectricityGeneration/PowerStations/Peaking/Pages/Ingula.aspx> (Accessed: 25 June 2019).

Eskom. 2018. *Eskom Integrated Report 2018*, (March), p. 80. doi: [https://doi.org/10.1163/2210-7975\\_hrd-9885-20180026](https://doi.org/10.1163/2210-7975_hrd-9885-20180026).

Eskom. 2019a. *Camden Power Station, Eskom heritage*. Available at: <http://www.eskom.co.za/sites/heritage/Pages/Camden.aspx>.

Eskom. 2019b. *Eskom Transmission Development Plan 2019 to 2028 (Public Version), Transmission Development Plan*. Pretoria. Available at: <http://www.eskom.co.za/Whatweredoing/TransmissionDevelopmentPlan/Documents/2019-2028PublicTDPReport1.pdf>.

Esko. 2019c. *Grootvlei Power Station, Eskom Power Stations*. doi: <https://doi.org/10.1063/1.4984567>.

Eskom. 2019d. *Komati Power Station, Eskom Power Stations*. Available at: [http://www.eskom.co.za/Whatweredoing/ElectricityGeneration/PowerStations/Pages/Komati\\_Power\\_Station.aspx](http://www.eskom.co.za/Whatweredoing/ElectricityGeneration/PowerStations/Pages/Komati_Power_Station.aspx).

Eskom generation division. 2019. *Eskom Power Stations*. Pretoria: Eskom, p. 1. doi: [https://doi.org/10.1016/s1359-6128\(05\)00671-3](https://doi.org/10.1016/s1359-6128(05)00671-3).

Eskom holdings limited. 2008. *Eskom Annual Report 2008*. Pretoria. Available at: [https://financialresults.co.za/eskom\\_ar2008/ar\\_2008/downloads/eskom\\_ar2008.pdf](https://financialresults.co.za/eskom_ar2008/ar_2008/downloads/eskom_ar2008.pdf).

Etxegarai, A., Eguia, P., Torres, E., Buigues, G. and Iturregi, A. 2017. Current procedures and practices on grid code compliance verification of renewable power generation, *Renewable and Sustainable Energy Reviews*. Elsevier, 71(January 2017), pp. 191–202. doi: 10.1016/j.rser.2016.12.051.

Faraz, T. 2012. Benefits of concentrating solar power over solar photovoltaic for power generation in Bangladesh, *2nd International Conference on the Developments in Renewable Energy Technology (ICDRET 2012)*. IEEE, pp. 1–5. Available at: <https://ieeexplore-ieee.org/libproxy.cput.ac.za/document/6153444>.

Generation Communication. 2011. Eskom's generation plant mix. Pretoria: Eskom, pp. 1–3. Available at: <http://www.eskom.co.za/OurCompany/SustainableDevelopment/ClimateChangeCOP17/Documents/GenerationMix.pdf>.

Global Energy Network Institute. 2016. *Energy Summary: South-Africa*. South Africa: GENI. Available at: [http://www.geni.org/globalenergy/library/national\\_energy\\_grid/south-africa/index.shtml](http://www.geni.org/globalenergy/library/national_energy_grid/south-africa/index.shtml).

Global Wind Energy Council. 2017. *Global Installed Wind Power Capacity*. Global statistics. Available at: <https://gwec.net/wp-content/uploads/2018/04/Global-Installed-Wind-Power->

Capacity-MW—Regional-Distribution-1.jpg.

GLOBELEQ. 2020. Jeffreys Bay Wind Farm. Jeffreys Bay. Available at: <https://jeffreysbaywindfarm.co.za/>.

Grobbelaar, S. S. and Uriona, M. 2018. Learning curves in the wind and solar sectors in South Africa, *2018 IEEE PES/IAS PowerAfrica, PowerAfrica 2018*. IEEE, pp. 463–467. doi: 10.1109/PowerAfrica.2018.8520990.

Gu, H. 2016. Maximum instantaneous renewable energy integration of power grids, *Proceedings of the 2016 Australasian Universities Power Engineering Conference, AUPEC 2016*. IEEE, pp. 1–5. doi: 10.1109/AUPEC.2016.7749368.

Gupta, R. 2017a. *First Falls Hydroelectric Station*. Eastern Cape. Available at: <http://globalenergyobservatory.org/geoid/3180>.

Gupta, R. 2017b. *Ncora Hydroelectric Power Station SA*. Eastern Cape. Available at: <http://globalenergyobservatory.org/geoid/4449>.

Gupta, R. 2017c. *Second Falls Hydroelectric Station SA*. Eastern Cape. Available at: <http://globalenergyobservatory.org/geoid/5304>.

Huang, Y. W., Kittner, N. and Kammen, D. M. 2019. ASEAN grid flexibility: Preparedness for grid integration of renewable energy, *Energy Policy*. Elsevier, 128 (August 2018), pp. 711–726. doi: 10.1016/j.enpol.2019.01.025.

International Energy Agency. 2017). *Solar energy, Renewables*. Available at: <https://www.iea.org/topics/renewables/solar/> (Accessed: 12 June 2019).

Jain, S. and Jain, P. K. 2017. The rise of renewable energy implementation in South Africa, *Energy Procedia*. 143, pp. 721–726. doi: 10.1016/j.egypro.2017.12.752.

Kemal, M.S., Pedersen, R., Iov, F. and Olsen, R. 2017. DiSC-OPAL: A Simulation framework for real-time assessment of distribution grids, *2017 Workshop on Modeling and Simulation of Cyber-Physical Energy Systems (MSCPES)*, pp. 1–5. doi: <https://doi.org/10.1109/mscpes.2017.8064541>.

Knorr, K., Zimmermann, B., Bofinger, S., Gerlach, A.K., Bischof-Niemz, T. and Mushwana, C. 2016. *Wind and solar PV resource aggregation study for South Africa*. Pretoria, South Africa: Council for Scientific and Industrial Research.

Li, Y., Shi, W., Zhang, X. and Tang, W. 2016. Renewable energy generation power in the loop real time simulation platform research, In *2016 19th International Conference on Electrical Machines and Systems (ICEMS)*. The Institute of Electrical Engineers of Japan, pp. 1–3. Available at: <https://ieeexplore-ieee-org.libproxy.cput.ac.za/document/7837493>.

Liu, Y., Yu, R., Zhang, L., Jiang, D., Chen, N. and Zhao, D., 2018, October. Research on short-circuit currents calculation method considering dynamic reactive power support of renewable energy systems. In *2018 2nd IEEE Conference on Energy Internet and Energy System Integration (EI2)* (pp. 1-9). IEEE. doi: 10.1109/EI2.2018.8582215.

Lucas, A. 2017. Confected conflict in the wake of the South Australian blackout: Diversionary strategies and policy failure in Australia's energy sector, *Energy Research & Social Science*. Elsevier, 29(May), pp. 149–159. doi: 10.1016/j.erss.2017.05.015.

Luna, E. G., Manrique, R. F. and Bocanegra, E. L. P. 2018. Monitoring and control system using ETAP real-time on generation plant emulation using OPAL-RT, *2018 IEEE ANDESCON, ANDESCON 2018 - Conference Proceedings*. IEEE, pp. 1–6. doi:

10.1109/ANDESCON.2018.8564653.

Mainstream Renewable Power. 2016. Noupoot wind farm. Northern Cape. Available at: <https://noupootwind.co.za/noupoot-wind-farm/overview/>.

Mainstream Renewable Power. 2017a. KHOBAB wind farm. Northern Cape. Available at: <https://khobabwind.co.za/>.

Mainstream Renewable Power. 2017b. Loeriesfontein wind farm. Northern Cape. Available at: <https://loeriesfonteinwind.co.za/loeriesfontein-wind-farm/overview/>.

Mainstream Renewable Power. 2018a. Kangnas wind farm. Northern Cape. Available at: <https://kangnaswind.co.za/kangnas-wind-farm/overview/>.

Mainstream Renewable Power. 2018b. Perdekraal East wind farm. Western Cape. Available at: <https://perdekraaleastwind.co.za/perdekraal-wind-farm/overview/>.

Mararakanye, N. and Bekker, B. 2019. Renewable energy integration impacts within the context of generator type, penetration level and grid characteristics, *Renewable and Sustainable Energy Reviews*. Elsevier, 108(April 2019), pp. 441–451. doi: 10.1016/j.rser.2019.03.045.

MathWorks. 2017. *MathWorks Help Center: Frequency (Phasor), Help Center*. Available at: <https://www.mathworks.com/help/phymod/sps/powersys/ref/frequencyphasor.html> (Accessed: 15 December 2021).

MathWorks. 2020. *Grid code compliance for Renewable Resource Integration, File Exchange*. Available at: <https://www.mathworks.com/matlabcentral/fileexchange/71071-grid-code-compliance-for-renewable-resource-integration> (Accessed: 13 November 2020).

MathWorks. 2021a. *Introducing the Phasor Simulation Method, MathWorks Help Center*. Available at: <https://www.mathworks.com/help/phymod/sps/powersys/ug/introducing-the-phasor-simulation-method.html> (Accessed: 13 May 2021).

MathWorks. 2021b. *Simulink Solver, MathWorks Help Center*. Available at: <https://www.mathworks.com/help/simulink/gui/solver.html> (Accessed: 13 May 2021).

Merabet, A., Tawfique, K.A., Islam, M.A., Enebeli, S. and Beguenane, R. 2014, December. Wind turbine emulator using OPAL-RT real-time HIL/RCP laboratory. In *2014 26th International Conference on Microelectronics (ICM)* (pp. 192-195). IEEE. doi: 10.1109/ICM.2014.7071839.

Mulaudzi, S. K. and Bull, S. 2016. An assessment of the potential of solar photovoltaic (PV) application in South Africa', *IREC 2016 - 7th International Renewable Energy Congress*. IEEE, pp. 1–6. doi: 10.1109/IREC.2016.7478917.

Naicker, P. and Thopil, G. A. 2019. A framework for sustainable utility scale renewable energy selection in South Africa, *Journal of Cleaner Production*. Elsevier, 224, pp. 637–650. doi: 10.1016/j.jclepro.2019.03.257.

National Energy Regulator of South Africa (NERSA). 2012. *Electricity Supply Statistics for South Africa 2012*. doi: <https://doi.org/10.1787/data-00462-en>.

National Energy Regulator of South Africa.(NERSA) 2016. *Grid connection code for renewable power plants (RPPs) connected to the electrical transmission system or the distribution system in South Africa*. doi: <https://doi.org/10.1109/powerafrica.2017.7991291>.

National Energy Regulator of South Africa.(NERSA). 2019. Grid connection code for renewable power plants connected to the electricity transmission system or the distribution system in South

Africa'. Eskom Transmission Division. Available at: National Planning Commission. 2011.

National Development Plan 2030 *Executive Summary*.

[https://www.gov.za/sites/default/files/Executive\\_Summary-NDP\\_2030\\_-\\_Our\\_future\\_-\\_make\\_it\\_work.pdf](https://www.gov.za/sites/default/files/Executive_Summary-NDP_2030_-_Our_future_-_make_it_work.pdf).

Newbery, D. and Eberhard, A. 2008. South African network infrastructure review : Electricity' *Paper prepared for National Treasury and the Department of Public Enterprises Government of South Africa*, 2. Available at: <http://www.gsb.uct.ac.za/files/SAElectricityPaper08.pdf>.

Nhlapo, B. and Awodele, K. 2020. Review and comparison of the South African grid code requirements for wind generation with the European countries' grid codes, *2020 International SAUPEC/RobMech/PRASA Conference, SAUPEC/RobMech/PRASA 2020*. IEEE, pp. 1–6. doi: 10.1109/SAUPEC/RobMech/PRASA48453.2020.9041080.

Noureen, S. S., Roy, V. and Bayne, S. B. 2018. An overall study of a real-time simulator and application of RT-LAB using MATLAB SimPowerSystems, *2017 IEEE Green Energy and Smart Systems Conference, IGESSC 2017*, 2017-Novem, pp. 1–5. doi: 10.1109/IGESC.2017.8283453.

OPAL-RT Technologies (n.d.) *RT-LAB Online Courses, Video Tutorials*. Available at: [https://www.opal-rt.com/opal\\_tutorial/preparing-simulink-model-real-time-execution/](https://www.opal-rt.com/opal_tutorial/preparing-simulink-model-real-time-execution/) (Accessed: 7 May 2021).

Oyewo, A.S., Aghahosseini, A., Ram, M., Lohrmann, A. and Breyer, C. 2019. Pathway towards achieving 100% renewable electricity by 2050 for South Africa. *Solar Energy*, 191, pp.549-565. doi: 10.1016/j.solener.2019.09.039.

Papathanassiou, S. and Tsili, M. 2009. A review of grid code technical requirements for wind farms, *IET Renewable Power Generation*, 3(March 2009), pp. 308–332. doi: 10.1049/iet-rpg.2008.0070.

Paquin, J.N., Moyen, J., Dumur, G. and Lapointe, V. 2007, October. Real-time and off-line simulation of a detailed wind farm model connected to a multi-bus network. In *2007 IEEE Canada Electrical Power Conference* (pp. 145-152). IEEE. doi: 10.1109/EPC.2007.4520321

Power Africa. 2018. *South Africa Energy Sector Overview*. Available at: [https://www.usaid.gov/sites/default/files/documents/1860/South\\_Africa\\_-\\_November\\_2018\\_Country\\_Fact\\_Sheet.pdf](https://www.usaid.gov/sites/default/files/documents/1860/South_Africa_-_November_2018_Country_Fact_Sheet.pdf).

Prinsloo, L. and Burkhardt, P. 2019. Eskom's Ingula hydro-power plant running at 25% below capacity, *BusinessDay*, 27 March, p. 1. Available at: <https://www.businesslive.co.za/bd/national/2019-03-27-eskoms-ingula-hydro-power-plant-running-at-25-below-capacity/>.

RSA Department of Energy. 2018. *2018 South African Energy Sector Report*. Edited by K. Ratshomo. Pretoria: Department of Energy. doi: <https://doi.org/10.2172/1430268>.

SABC News. 2019. Kusile Power Station's Unit 3 produces its first power. SABC, p. 1. Available at: <http://www.sabcnews.com/sabcnews/kusile-power-stations-unit-3-produces-its-first-power/>.

Sewchurran, S. and Davidson, I. 2016. Guiding principles for grid code compliance of large utility scale renewable power plant integration onto South Africa's transmission/distribution networks, *2016 IEEE International Conference on Renewable Energy Research and Applications*, 5. doi: <https://doi-org.libproxy.cput.ac.za/10.1109/ICRERA.2016.7884392>.

Sewchurran, S. and Davidson, I. E. 2017. Introduction to the South African renewable energy grid code version 2.9 requirements (Part II - Grid code technical requirements), *2017 IEEE AFRICON: Science, Technology and Innovation for Africa, AFRICON 2017*, pp. 1225–1230. doi:

10.1109/AFRCON.2017.8095657.

Sharma, A. and Sharma, M. 2018. Power & energy optimization in solar photovoltaic and concentrated solar power systems, *Asia-Pacific Power and Energy Engineering Conference, APPEEC*, 2017-Novem, pp. 1–6. doi: 10.1109/APPEEC.2017.8308973.

Siemens. 2011. Siemens wind turbine SWT-2.3-108, The new productivity benchmark. Hamburg, Germany: Siemens. Available at: [https://www.usbr.gov/lc/region/g2000/envdocs/MohaveCountyWindFarm/Plan\\_of\\_Development/Attachment\\_2 - Siemens Wind Turbine SWT-2.3-108\\_EN\\_508.pdf](https://www.usbr.gov/lc/region/g2000/envdocs/MohaveCountyWindFarm/Plan_of_Development/Attachment_2_-_Siemens_Wind_Turbine_SWT-2.3-108_EN_508.pdf).

Singh, S.K., Padhy, B.P., Chakrabarti, S., Singh, S.N., Kolwalkar, A. and Kelapure, S.M. 2014, December. Development of dynamic test cases in OPAL-RT real-time power system simulator. In *2014 18th National Power Systems Conference (NPSC)* (pp. 1-6). doi: 10.1109/NPSC.2014.7103856

Sourcewatch. 2011. Kusile Power Station. Sourcewatch. Available at: [https://www.sourcewatch.org/index.php/Kusile\\_Power\\_Station](https://www.sourcewatch.org/index.php/Kusile_Power_Station).

Sreedevi, J., Meera, K.S., Ravichandran, S., Santhanakumar, R. and Sumathi, T. 2016, November. Grid stability with large wind power integration-a case study. In *2016 IEEE Region 10 Conference (TENCON)* (pp. 571–575). IEEE.

Statistics South Africa. 2018. *Electricity generated and available for distribution (Preliminary)*. Pretoria. Available at: <http://www.statssa.gov.za/publications/P4141/P4141October2018.pdf>.

TimesLive. 2019. Eskom's Medupi Unit 3 achieves commercial operation status, *29 June 2019*, 29 June. Available at: <https://www.timeslive.co.za/news/south-africa/2019-06-29-eskoms-medupi-unit-3-achieves-commercial-operation-status/>.

Wang, W., Zhu, Y., Liu, C., Dong, P., Li, B., Li, Y., He, F. and Zhang, Y. 2019. An implementation technology of electromagnetic transient real-time simulation for large-scale grid based on HYPERSIM, In *2018 International Conference on Power System Technology, POWERCON 2018 - Proceedings*. IEEE, pp. 167–172. doi: 10.1109/POWERCON.2018.8602121.

Windpower Engineering & Development. 2020. Turbine model: SWT-2.3-108 onshore. Available at: <https://www.windpowerengineering.com/turbine/siemens-swt-2-3-108-onshore/>.

Wright, J. G., Tuson, P. M. and Van Coller, J. M. 2012. Studies for wind energy facility grid code compliance in South Africa, In *IEEE Power and Energy Society Conference and Exposition in Africa: Intelligent Grid Integration of Renewable Energy Resources, PowerAfrica 2012*. IEEE. doi: 10.1109/PowerAfrica.2012.6498619.

Wu, B., Lang, Y., Zargari, N. and Kouro, S. 2011. *Power conversion and control of wind energy systems*. (Ed.) L. Hanzo. John Wiley

Yan, R., Saha, T.K., Modi, N., Masood, N.A. and Mosadeghy, M. 2015. The combined effects of high penetration of wind and PV on power system frequency response. *Applied Energy*, 145, pp.320-330. doi: 10.1016/j.apenergy.2015.02.044.

Yan, R., Saha, T. K. and Member, S. 2018. The anatomy of the 2016 South Australia blackout: A catastrophic event in a high renewable network, *IEEE Transactions on Power Systems*. IEEE, 33(5), pp. 5374–5388. doi: 10.1109/TPWRS.2018.2820150.

## APPENDICES

### Appendix A: Grid-code frequency requirements

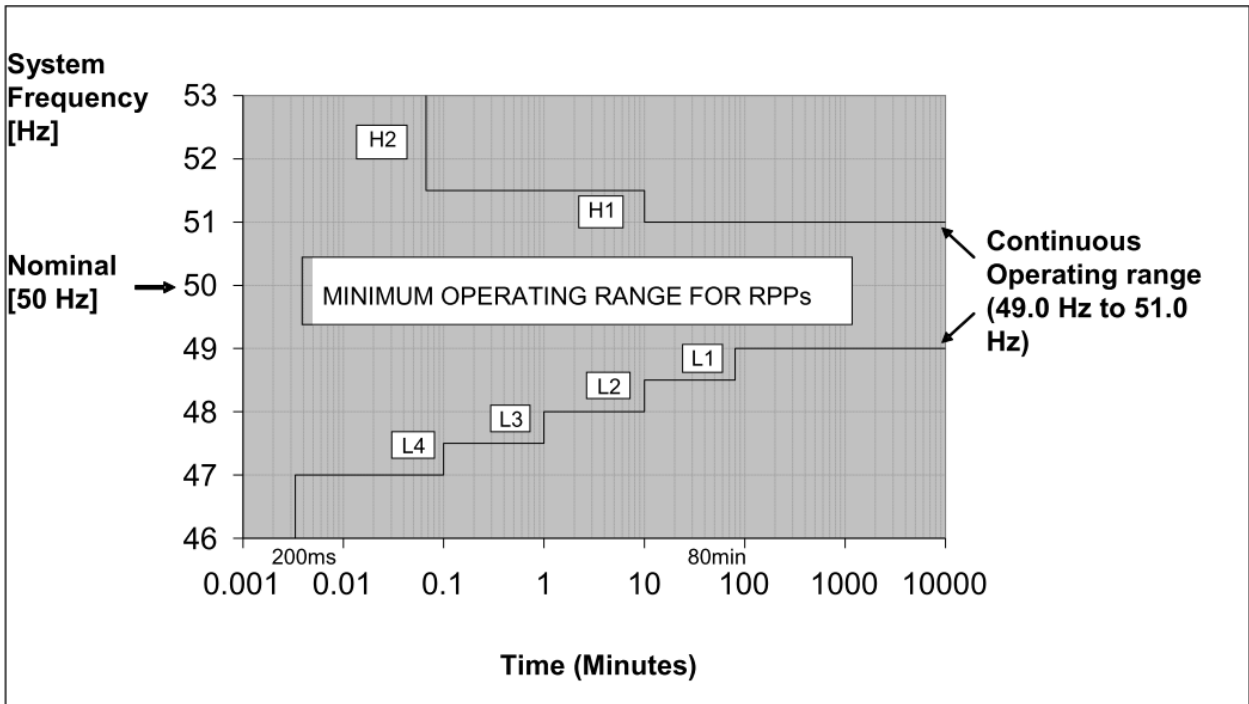


Figure 0.1: Minimum cumulative frequency operating range over a RPPs lifespan

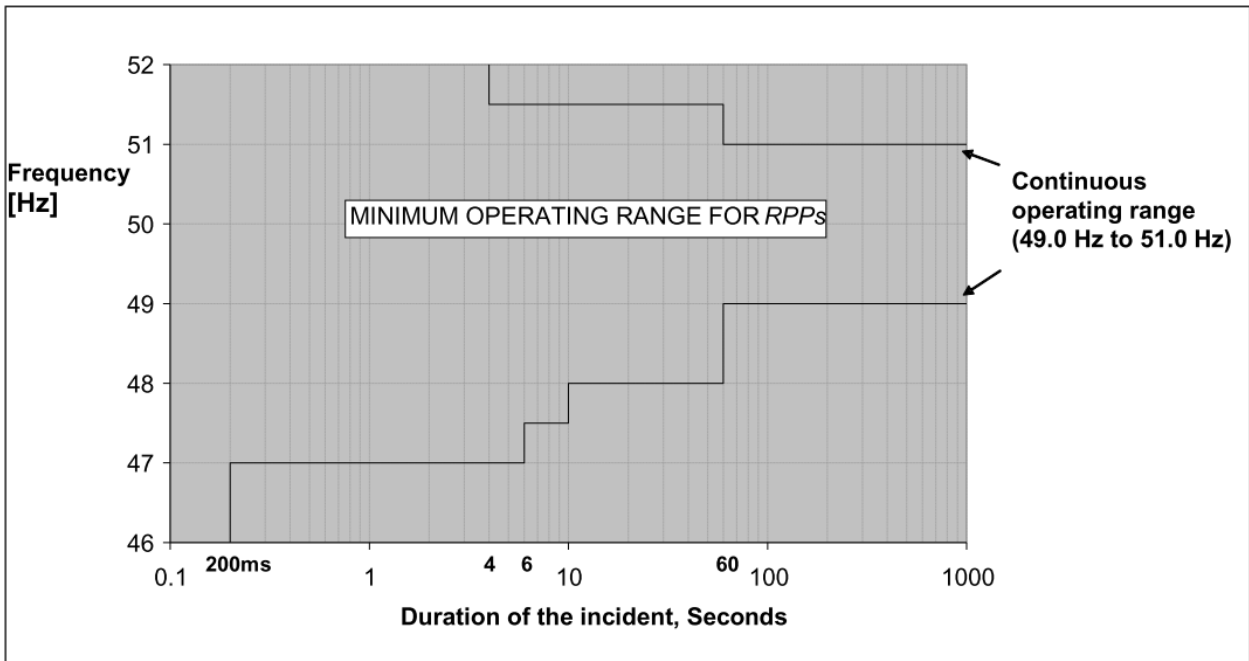


Figure 8.2: Minimum frequency operating range of a RPP during a frequency disturbance



## Appendix B: Grid-code voltage requirements

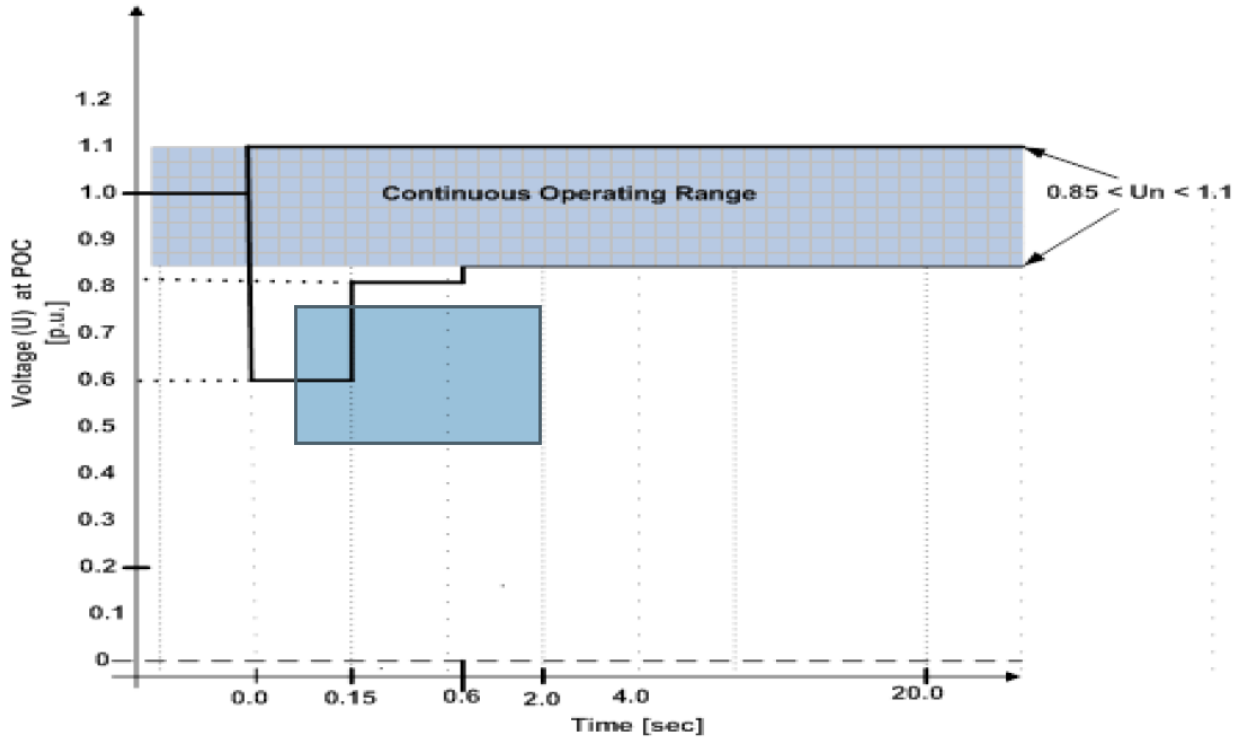


Figure 8.3: Voltage ride through requirements for Categories A1 and A2 RPPs

Table 8.1: Maximum disconnection times set for Categories A1 and A2 RPPs

Voltage range (at the POC)	Maximum trip time [Seconds]
$V < 50 \%$	0,2 s
$50 \% \leq V < 85 \%$	2 s
$85 \% \leq V \leq 110 \%$	Continuous operation
$110 \% < V < 120 \%$	2 s
$120 \% \leq V$	0,16 s

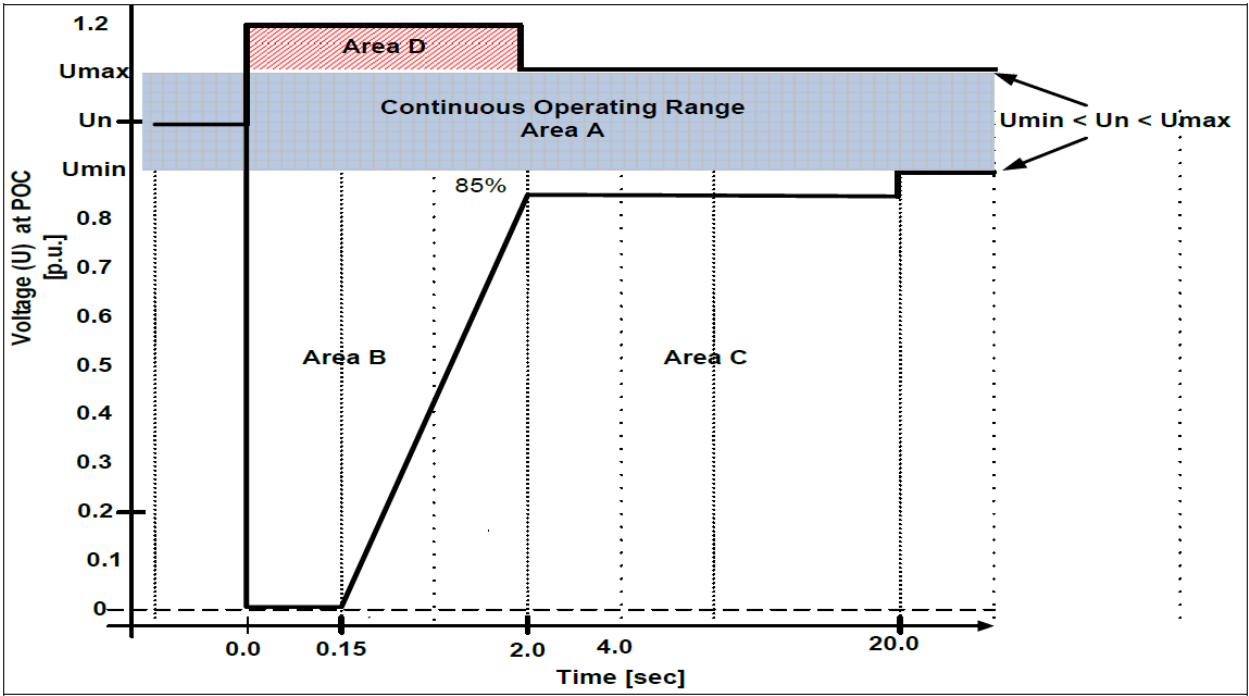


Figure 8.4: Voltage ride-through limits for non-synchronous machines of Categories A3, B, and C

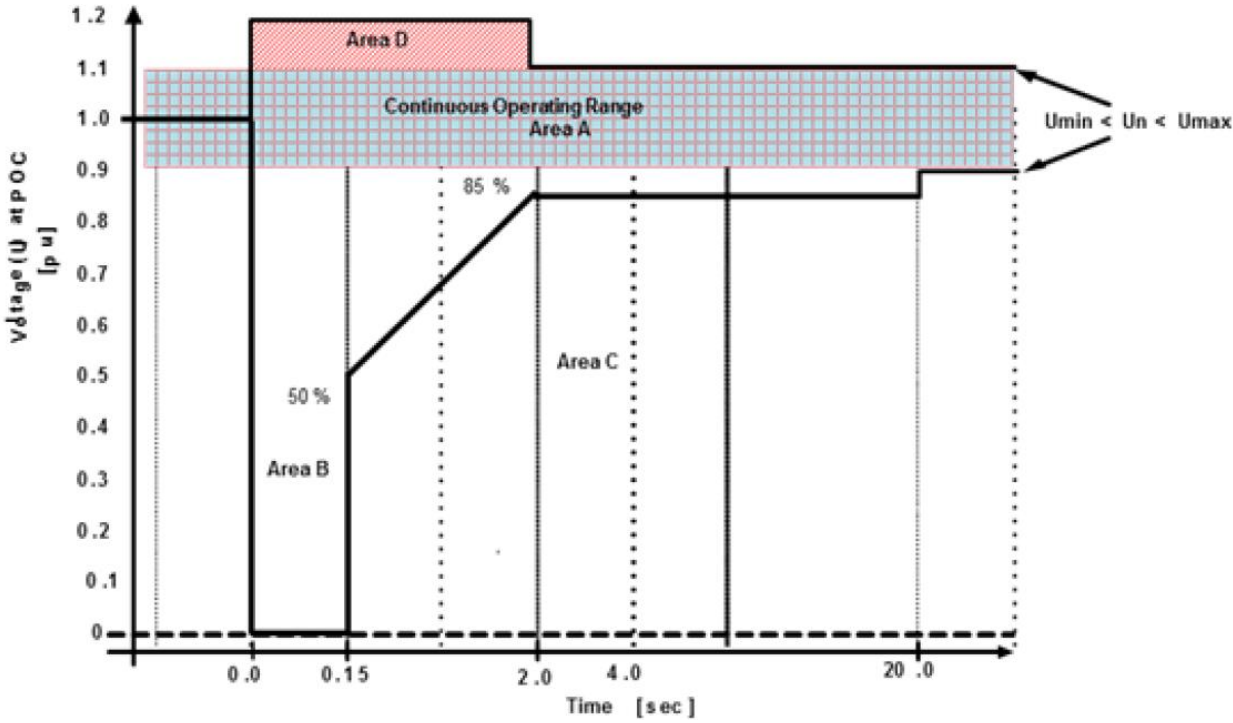


Figure 8.5: Voltage ride-through limits for synchronous machines of Categories B and C

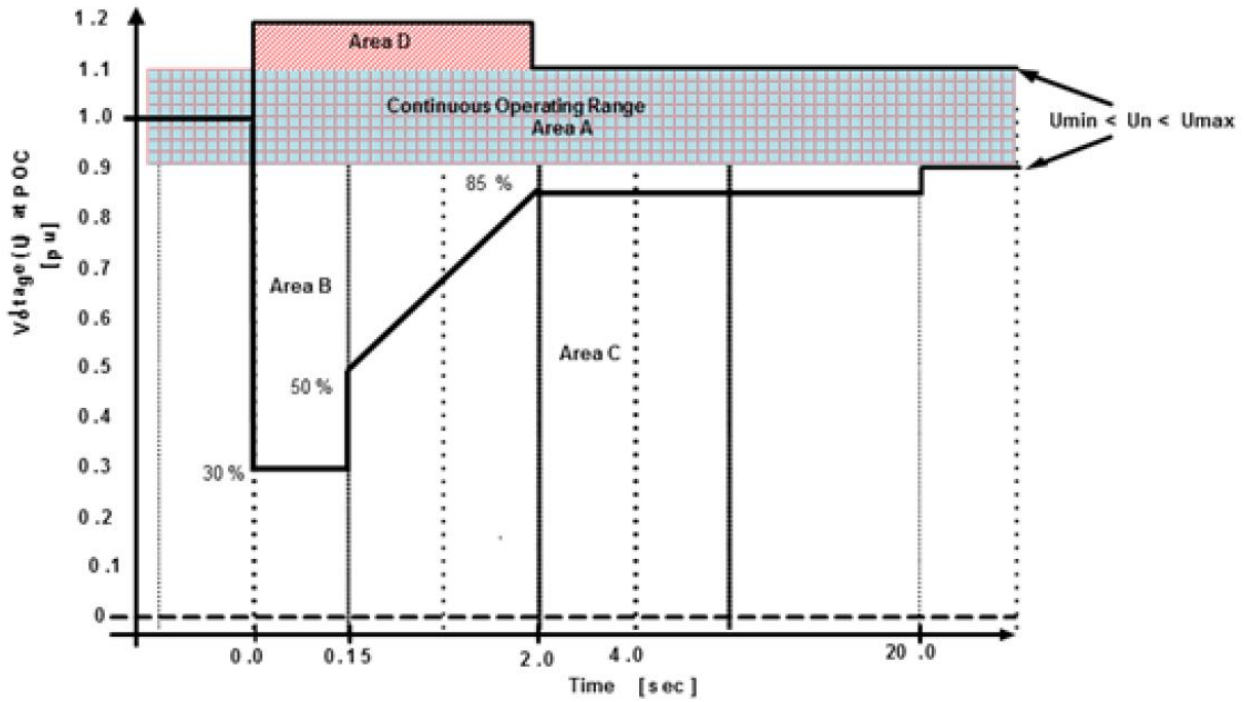


Figure 8.6: Voltage ride-through limits for synchronous machines of Category B during 3-phase faults

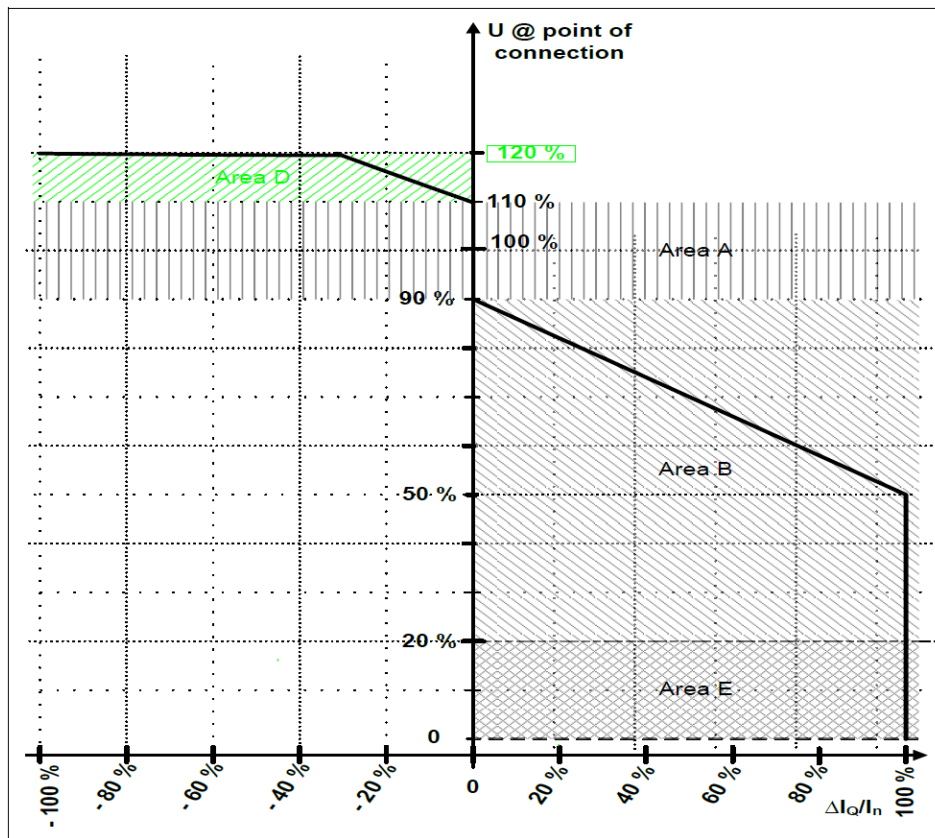


Figure 8.7: Reactive power (IQ) support requirements during voltage drops or peaks at the POC

## Appendix C: Grid-code power requirements

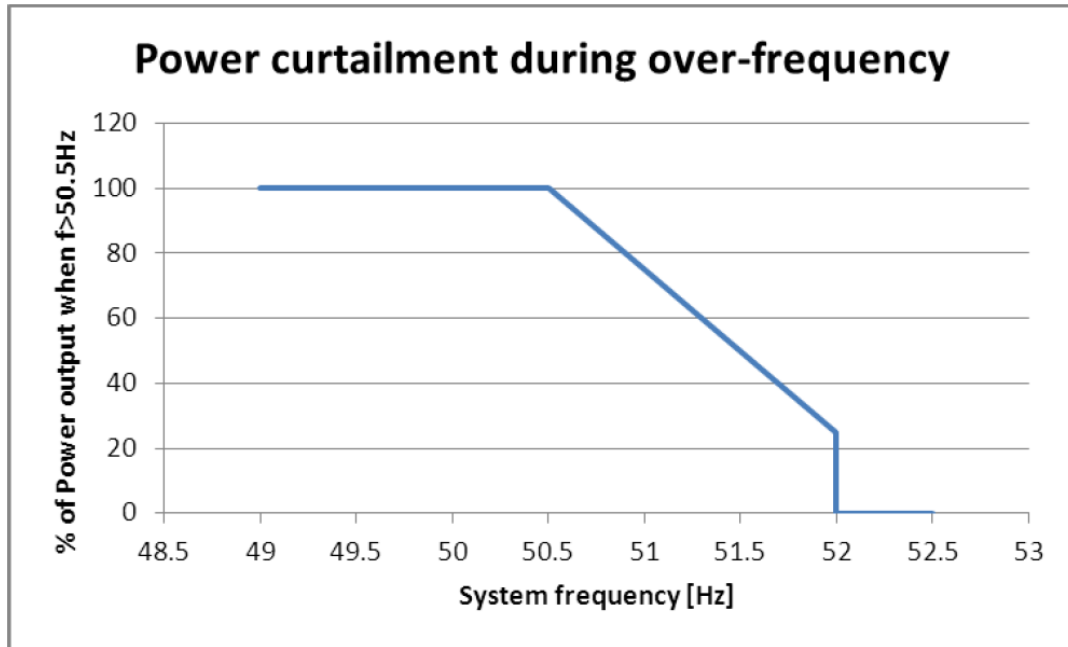


Figure 8.8: Power curtailment requirements for RPPs during over-frequency events

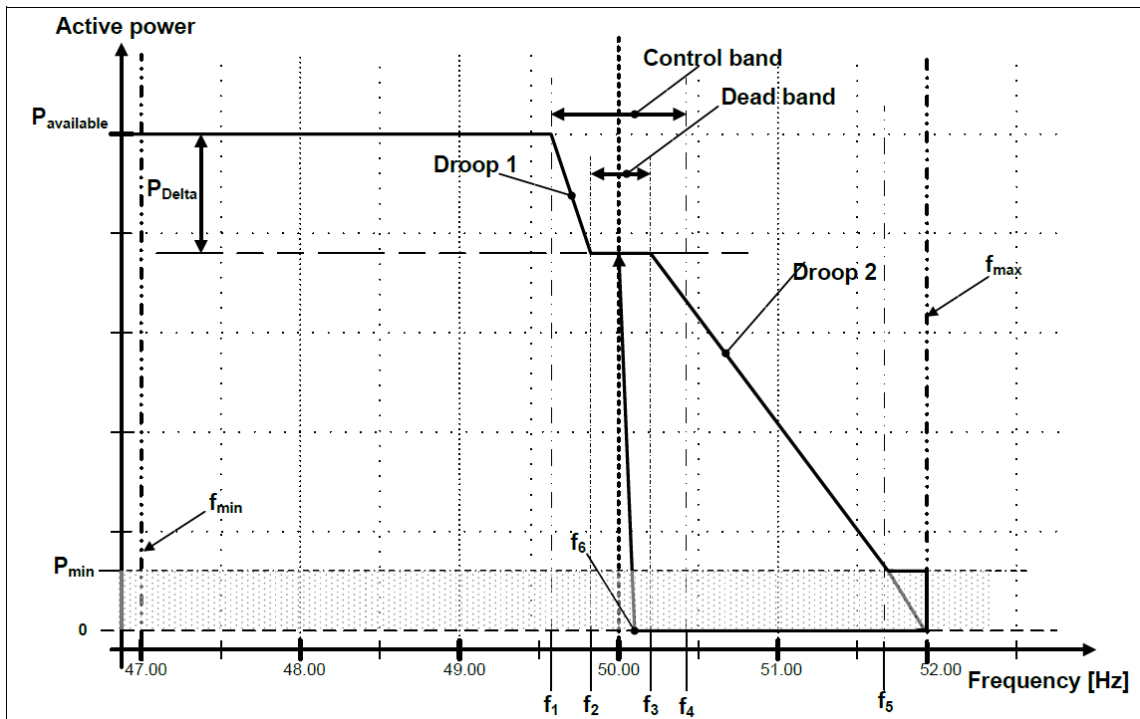


Figure 8.9: Category C RPP frequency response requirements

Table 8.2: Default frequency settings

<b>Parameter</b>	<b>Magnitude (Hz.)</b>
$f_{\min}$	47
$f_{\max}$	52
$f_1$	As agreed with SO
$f_2$	As agreed with SO
$f_3$	As agreed with SO
$f_4$	50.5
$f_5$	51.5
$f_6$	50.2

## Appendix D: Grid-code reactive power requirements

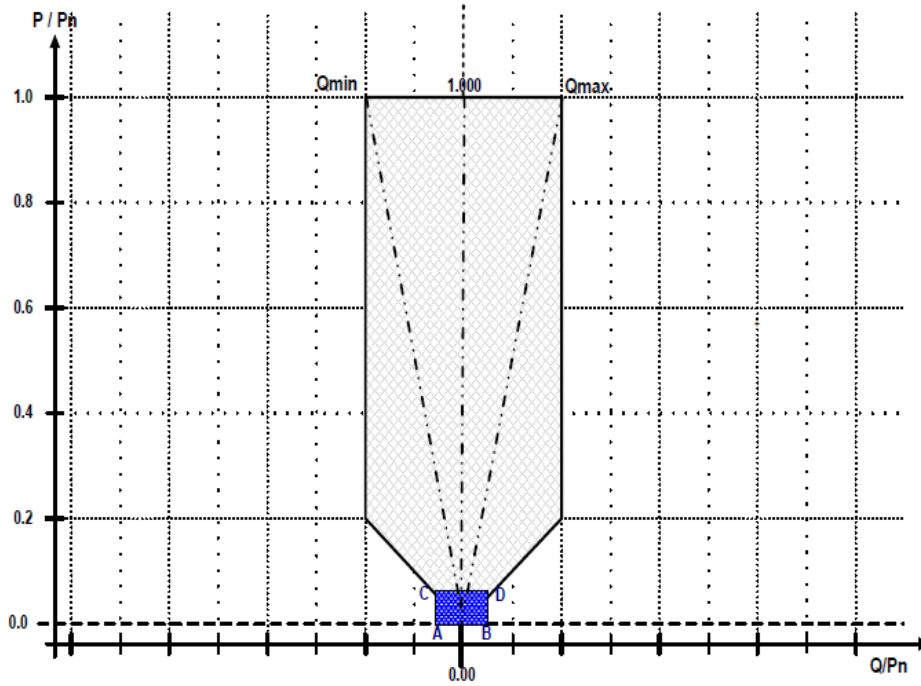


Figure 8.10: Category B RPP reactive power requirements at the POC

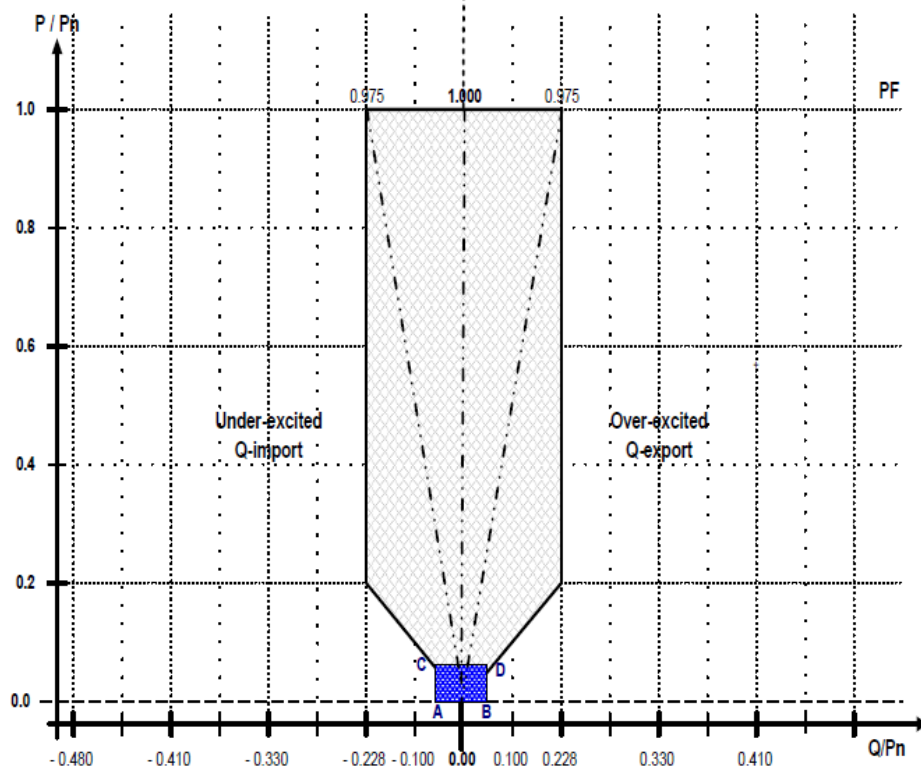


Figure 8.11: Category B RPP reactive power requirements at nominal voltage at POC

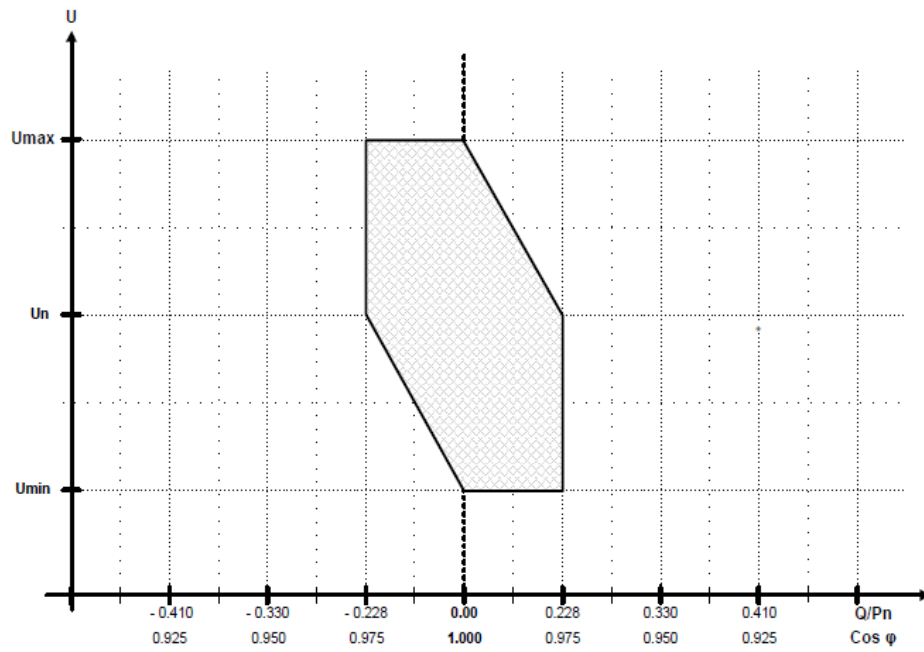


Figure 8.12: Reactive power and voltage control range requirements for Category B RPPs

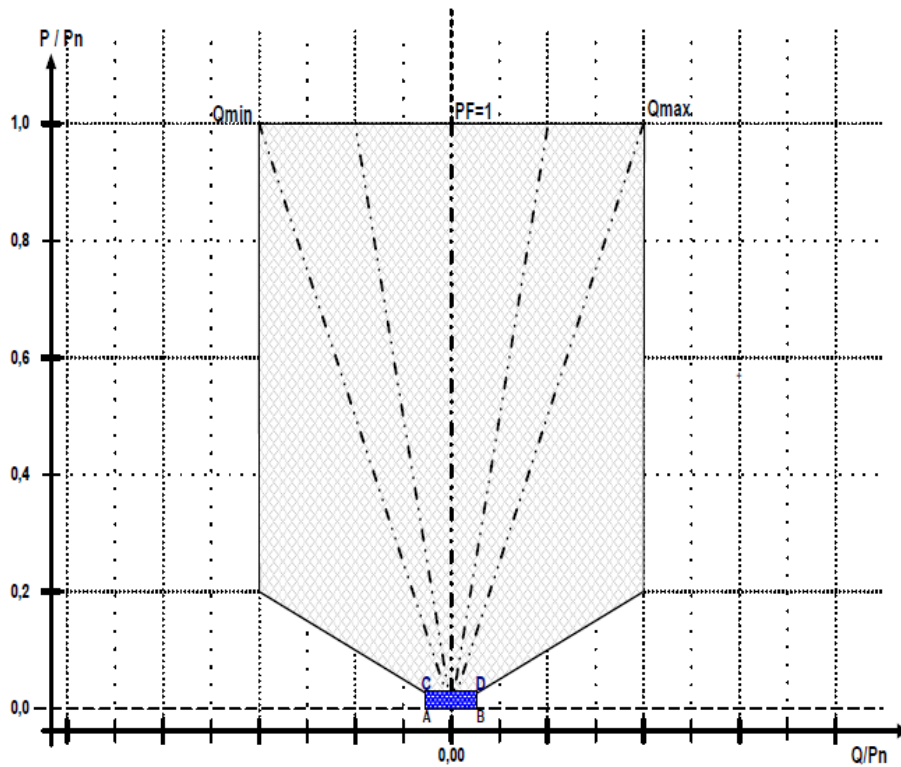


Figure 8.13: Category C reactive power requirements at POC

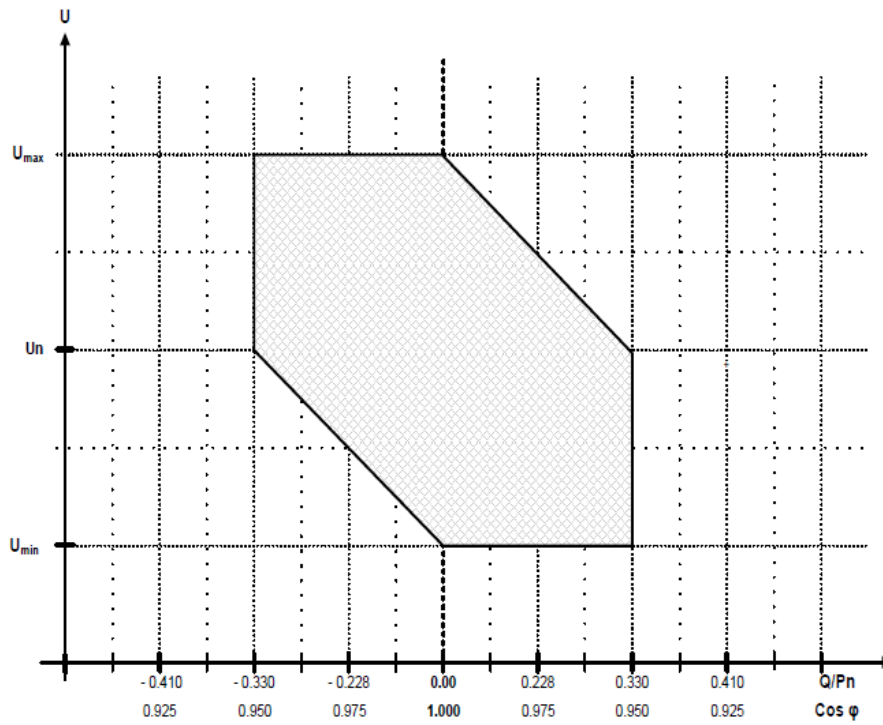


Figure 8.14: Reactive power and voltage control range for Category C RPPs



## Appendix E: Grid-code reactive power control requirements

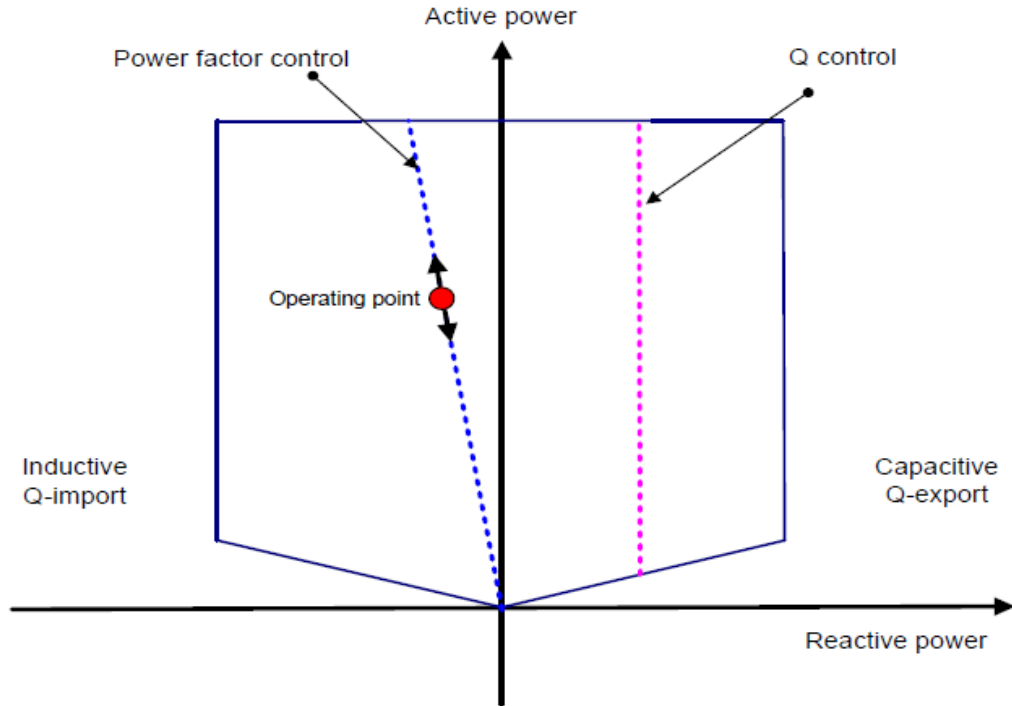


Figure 8.15: RPP reactive power control function requirements

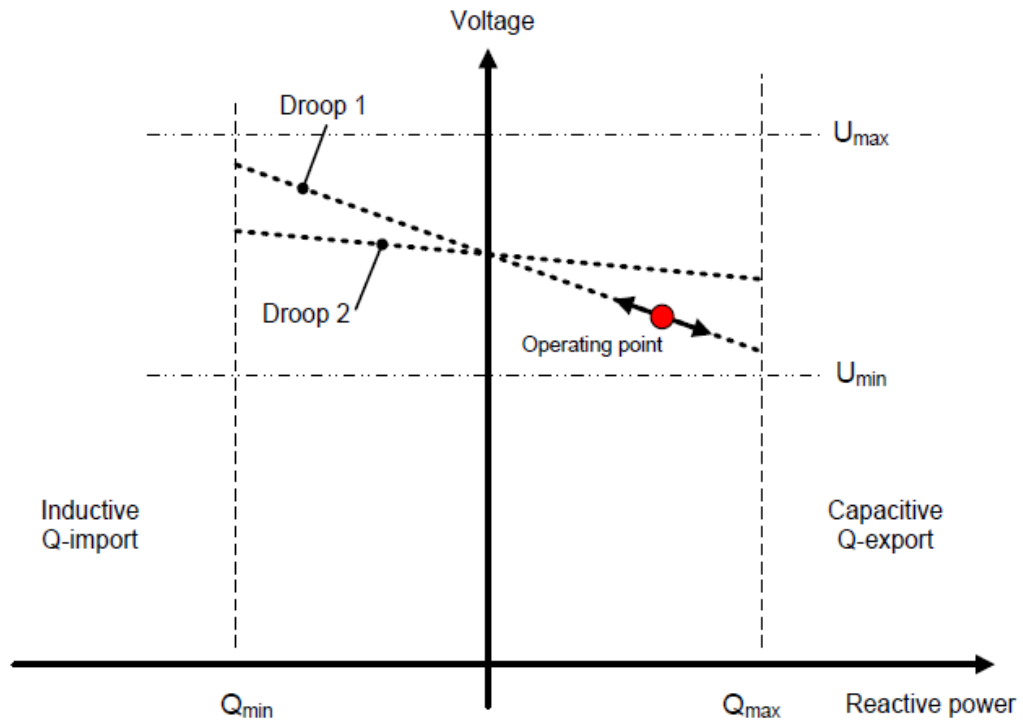


Figure 8.16: RPP voltage control requirements

## Appendix F: South African electrical grid map

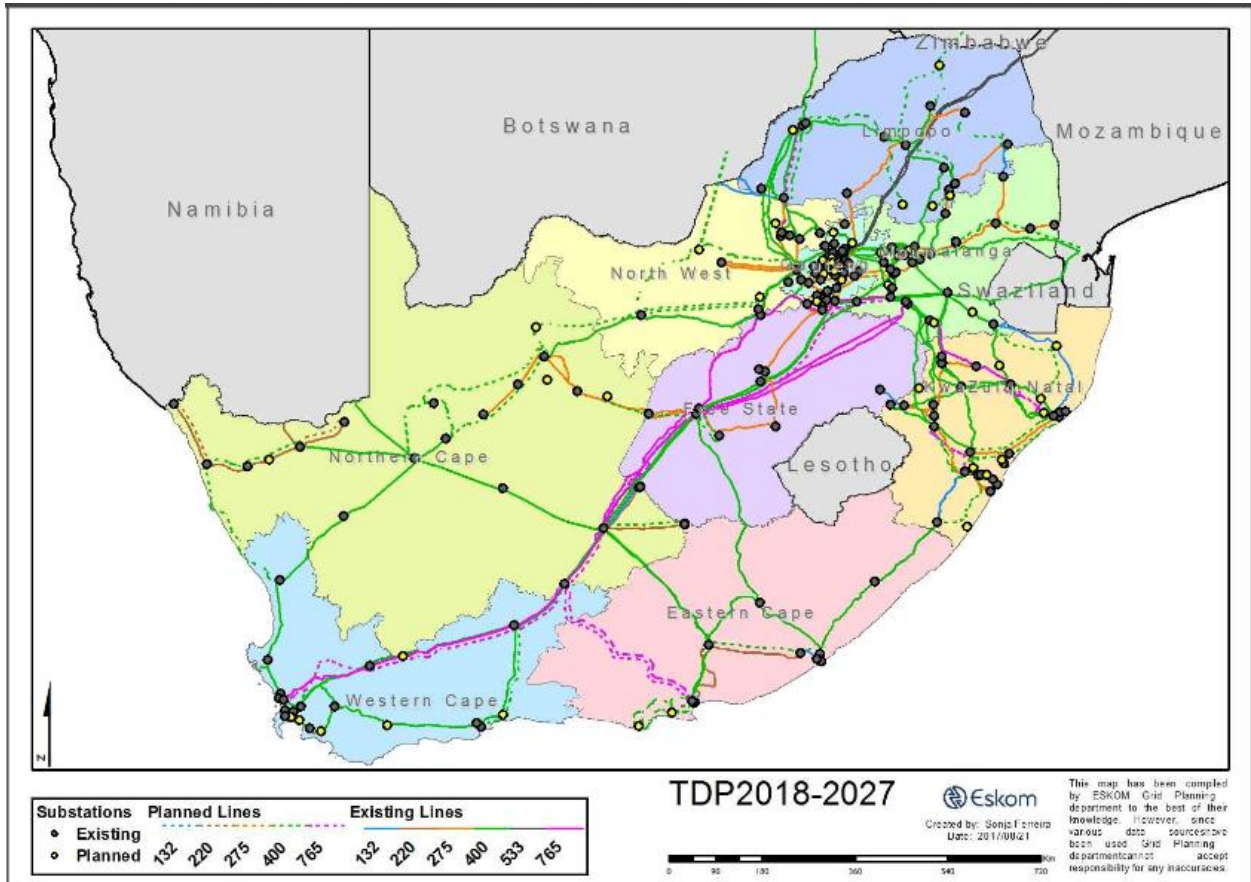


Figure 8.17: South Africa's existing and planned electrical network

## Appendix G: MATLAB Live script code

```
if (POC_voltage=="<11kV")
    Vn1=[0.85] % V normal lower limit
    Vnu=[1.1] % V normal upper limit

elseif (POC_voltage=="11/22/33/44kV")
    Vn1=[0.9] % V normal lower limit
    Vnu=[1.08] % V normal upper limit

elseif (POC_voltage=="66/88/132kV")
    Vn1=[0.9] % V normal lower limit
    Vnu=[1.0985] % V normal upper limit

else display "unknown parameter"
end

if (RPP_type=="Cat_A1,A2")
    T1=[0 0.15 0.15001 0.6 0.60001 25]; % Time breakpoints
    V1=[0.6 0.6 0.8 0.8 Vn1 Vn1]; % LVRT voltage boundaries
    T2=[0 25]; % Time breakpoints
    V2=[Vnu Vnu]; % HVRT voltage boundaries

elseif (RPP_type=="Cat_A3,B_non-sync")
    T1=[0 0.15 2 20 20.00001 25]; % Time breakpoints
    V1=[0 0 0.85 0.85 Vn1 Vn1]; % LVRT voltage boundaries
    T2=[0 25]; % Time breakpoints
    V2=[Vnu Vnu]; % HVRT voltage boundaries

elseif (RPP_type=="Cat_C_non-sync")
    T1=[0 0.15 2 20 20.00001 25]; % Time breakpoints
    V1=[0 0 0.85 0.85 Vn1 Vn1]; % LVRT voltage boundaries
    T2=[0 2 2.00001 25]; % Time breakpoints
    V2=[1.2 1.2 Vnu Vnu]; % HVRT voltage boundaries

elseif (RPP_type=="Cat_A3,B_sync")
    T1=[0 0.15 0.15001 2 20 20.00001 25]; % Time breakpoints
    V1=[0 0 0.5 0.85 0.85 Vn1 Vn1]; % LVRT voltage boundaries
    T2=[0 25]; % Time breakpoints
    V2=[Vnu Vnu]; % HVRT voltage boundaries

elseif (RPP_type=="Cat_C_sync")
    T1=[0 0.15 0.15001 2 20 20.00001 25]; % Time breakpoints
    V1=[0 0 0.5 0.85 0.85 Vn1 Vn1]; % LVRT voltage boundaries
    T2=[0 2 2.00001 25]; % Time breakpoints
    V2=[1.2 1.2 Vnu Vnu]; % HVRT voltage boundaries

elseif (RPP_type=="Cat_A3,B_sync_3-ph_fault")
    T1=[0 0.15 0.15001 2 20 20.00001 25]; % Time breakpoints
    V1=[0.3 0.3 0.5 0.85 0.85 Vn1 Vn1]; % LVRT voltage boundaries
    T2=[0 25]; % Time breakpoints
    V2=[Vnu Vnu]; % HVRT voltage boundaries
```

```
else display "unknown parameter"  
end  
  
plot(T1,V1,T2,V2);  
title('VRT requirements of selected RPP')  
xlabel('Time')  
ylabel('Voltage')  
legend('LVRT limit','HVRT limit')
```

## Appendix H: Editing Certificate



### Editing Certificate

Ricky Woods Academic Editing Services    Editing certificate

Cell: +27 (0)83 3126310

Email: [rickywoods604@gmail.com](mailto:rickywoods604@gmail.com)

To Whom It May Concern

CPUT

#### Editing of Doctoral thesis

I, Marietjie Alfreda Woods, hereby certify that I have completed the editing and correction of the thesis: **Development of a real-time testbed for renewable energy integration studies** by Gideon Daniel Joubert submitted in fulfilment of the requirements of the degree Doctor of Engineering in Electrical Engineering in the Faculty of Engineering at Cape Peninsula University of Technology, Bellville Campus.

I believe that the thesis meets with the grammatical and linguistic requirements for a document of this nature.

Name of Editor: Marietjie Alfreda (Ricky) Woods

Qualifications: BA (Hons) (Wits); Copy-editing and Proofreading (UCT); Editing Principles and Practice (UP); Accredited Text Editor (English) (PEG)

27 October 2022

A handwritten signature in black ink that reads "M. Woods".

Professional  
EDITORS  
Guild

**Ricky Woods**  
Accredited Text Editor (English)

Membership number: W001003  
Membership year: March 2022 to February 2023

083 312 6310  
[rickywoods604@gmail.com](mailto:rickywoods604@gmail.com)  
[www.rickywoods604.wxsite.com/website](http://www.rickywoods604.wxsite.com/website)

[www.editors.org.za](http://www.editors.org.za)

